

**NON-LINEAR FINITE ELEMENT ANALYSIS OF FRP-PRECAST CONCRETE  
SANDWICH PANELS**

A Dissertation

Presented in Partial Fulfillment of the Requirements for the

Degree of Doctor of Philosophy

with a

Major in Civil Engineering

in the

College of Graduate Studies

University of Idaho

by

Paul M. Hopkins

Major Professor: An Chen, Ph.D., P.E.

Committee Members: Richard Nielsen, Ph.D., P.E.; Krista Brown, Ph.D., P.E.;  
Pizhong Qiao, Ph.D., P.E.

Department Administrator: Richard Nielsen, Ph.D., P.E.

June 2015

## AUTHORIZATION TO SUBMIT DISSERTATION

This dissertation of Paul M. Hopkins, submitted for the degree of Doctor of Philosophy with a major in Civil Engineering and titled “Non-Linear Finite Element Analysis of FRP-Precast Concrete Sandwich Panels,” has been reviewed by in final form. Permission, as indicated by the signatures and dates given below, is now granted to submit final copies to the College of Graduate Studies for approval.

Major Professor \_\_\_\_\_ Date: \_\_\_\_\_  
An Chen, Ph.D.

Committee  
Members \_\_\_\_\_ Date: \_\_\_\_\_  
Richard Nielsen, Ph.D.

\_\_\_\_\_ Date: \_\_\_\_\_  
Krista Brown, Ph.D.

\_\_\_\_\_ Date: \_\_\_\_\_  
Pizhong Qiao, Ph.D.

Department  
Administrator \_\_\_\_\_ Date: \_\_\_\_\_  
Richard Nielsen, Ph.D.

## ABSTRACT

Precast insulated concrete sandwich panels have been used with proven success in commercial building application as wall elements to provide both vertical and lateral strength and thermal and environmental protection. Various configurations and materials have been used to provide certain degrees of strength, thermal resistance and composite action. The mechanics of the sandwich panel rely on the transfer of compressive and tensile forces due to flexure via shear through the web connectors. These web connectors have varied from steel wire trusses to carbon fiber composite grid trusses to solid concrete zones. For optimum thermal performance the connectors not providing a thermal bridge are best suited. For optimum strength and stiffness performance the shear connectors that create the highest degree of composite action and anchorage in the concrete zones shall be used. Furthermore, if the insulated concrete sandwich panels can be better understood, developed and tested in the horizontal application rather than as a wall element, they can be used for roof and possibly floor applications. This will provide environment and thermal resistance and required strength and stiffness.

This study investigates the design and testing of several scaled test sandwich panel configurations using solid web FRP plate shear connectors. The stiffness, strength and degree of composite action for each set of panels is calculated and compared and finally 2 full scale test panels are developed and tested. Along with testing and calculations, numerical modeling or finite element analysis is employed to show correlation between the test results for future development of an analytical model. Precast concrete sandwich panel engineering performance varying depending on the degree of composite action of its constituent materials and strength of properties. Employing a nonlinear numerical solver that can capture the quasi-static response of the panels under flexural loading is valuable and desirable for future development.

These test panels, both scaled and full-scale show adequate results for strength, stiffness and degree of composite action to justify further development and research into their use as roof or floor structural support members. Long term creep effects have also been investigated in this study, however further creep studies are warranted and recommended. Finally, these panels are not limited to the use of residential and commercial application; rather they have the potential as suitable candidates for structures intended to provide blast and/or accidental explosion protection.

# VITA

Paul M. Hopkins, P.E., S.E.

E-mail: [paulhopkinsm@gmail.com](mailto:paulhopkinsm@gmail.com) Phone: (267) 324-4830

## Professional Preparation

Drexel University, Philadelphia, PA	Civil Engineering	B.S., 2000
	Architectural Engineering	B.S., 2000
Arizona State University, Tempe, AZ	Civil Engineering (Structural)	M.S., 2004

## Appointments

- Vice President/Regional Office Manager, TD&H Engineering, Media, PA 2015
- Structural Analysis Engineer IV, Boeing Company, BDS, Philadelphia, PA 2013
- Principal Engineer, Hopkins Structural Design Solutions, LLC, Lewiston, ID 2010
- Regional Office Manager, TD&H Engineering, Lewiston, ID 2007
- Engineer/Scientist II, The Boeing Company, IDS, Mesa, AZ 2005
- Design Engineer, E.I.T., Paragon Structural Design, Phoenix, AZ 2004
- Graduate Research Assistant, Arizona State University, Tempe, AZ 2002
- Associate Engineer, E.I.T., Worley Parsons, Reading, PA 2000
- Senior Technician, Schnabel Engineering Associates, West Chester, PA 1998

## Professional Registrations

- Registered Professional Engineer (PE) in Civil Engineering, CA, AZ, ID, MD, NM, NJ, OR, PA, & WA
- Registered Structural Engineer (SE) in WA, ID and AZ

## Area of Expertise

Seismic evaluations, historic building renovation and evaluation, structural evaluation, inspection and retrofit. Advanced linear and non-linear static and dynamic finite element analysis for stress and fatigue of metal and composite parts and components utilizing Abaqus and Solidworks. Building design with steel, wood, masonry, concrete, precast concrete & composite materials.

## Publications

1. Chen, A., Norris, T., Hopkins, P., Yossef, M. (2015) "Experimental Investigation and Finite Element Analysis of Flexural Behavior of Insulated Concrete Sandwich Panels With FRP Plate Shear Connectors". Engineering Structures.

2. Hopkins, P., Brown, K., Yossef, M. & Chen, A. (2014). "The Effect of Degree of Composite Action on Flexural Behavior of Precast Concrete Sandwich Panels". CICE 2014, 7<sup>th</sup> International Conference on FRP Composites in Civil Engineering, 8/21/2014.
3. Hopkins, P., Norris, T., Pena, N. & Chen, A. (2014). "Development of FRP Plate Shear Connector for Insulated Concrete Sandwich Panels". CICE 2014, 7<sup>th</sup> International Conference on FRP Composites in Civil Engineering, 8/21/2014.
4. Smith, F. A. & Hopkins, P. M., (2006). "Nonlinear Internal Loads Modeling". AHS Forum 62, 5/11/2006

### **Patents**

NA

### **Synergistic Activities**

- Member of American Society of Civil Engineers (ASCE)
  - Committee Member Aerospace Division (ASD), Advanced Materials and Structures
  - Member of Philadelphia SEI Chapter.
- Member of American Society for Composites (ASC)
- Member of American Institute of Steel Construction (AISC)
- Member of American Concrete Institute (ACI)
- Member of Delaware Valley of Structural Engineers (DVASE)
- Member of Structural Engineers Association of Pennsylvania (SEAOP)

### **Collaborators & Other Affiliations**

- Practitioner Advisor (2008-2013), American Society of Civil Engineers, University of Idaho Student Chapter

### **Academia**

- Temporary Lecturer (2008-2013), University of Idaho, Civil Engineering Department
  - Statics, Theory of Structures, Economics, Reinforced Concrete Design, Steel Design
- Adjunct Professor (2013-Present), Widener University, Civil Engineering Department
  - Structural Mechanics, Structural Dynamics, Structural Analysis II, Steel Design

## ACKNOWLEDGEMENTS

I would like to thank the following individuals, groups and organizations for their support and assistance in the completion of this study:

- Dr. Krista M. Brown, P.E. who initially gave me a chance to “break” a panel.
- Dr. An Chen, P.E. & Dr. Richard Nielsen for their continued support, guidance and optimism.
- Dr. Pizhong Qiao for participating on my committee.
- Financial support from Higher Education Research Council (HERC), Idaho State Board of Education
- Technical support from Missouri Structural Composites, LLC.
- Material donation from Crane Composites, Inc.
- Material donation and testing support from Central Pre-Mix Prestress, Co., Spokane, WA.
- The CE 441: Reinforced Concrete Students – Fall 2012, University of Idaho, for their help in the production and testing of several initial scaled test specimens.
- Nicholas Pena, Thomas Norris and Mostafa Yossef for their assistance in developing the tests, performing analysis and documentation as part of their thesis requirements.
- Special acknowledgement to my wife Katie and my sons Branden, Jayden & Sean for their encouragement and support. Without their love and devotion, this would not have been completed.

## **DEDICATION**

I would like to dedicate this work to my father, Paul J. Hopkins, who would not only have been proud of this accomplishment, but more so knowing I always remained a father first and a student second. Thank you to my wife Katie, my sons Branden, Jayden and Sean for their patience and support while this was completed. Thank you to my mother, family and friends for their continuous support and encouragement.

## TABLE OF CONTENTS

<b>AUTHORIZATION TO SUBMIT DISSERTATION .....</b>	<b>ii</b>
<b>ABSTRACT .....</b>	<b>iii</b>
<b>VITA.....</b>	<b>iv</b>
<b>ACKNOWLEDGEMENTS.....</b>	<b>vi</b>
<b>DEDICATION.....</b>	<b>vii</b>
<b>NOTATION.....</b>	<b>xvii</b>
<b>ABBREVIATIONS .....</b>	<b>xviii</b>
<b>CHAPTER 1: INTRODUCTION.....</b>	<b>1</b>
1.1 PROBLEM STATEMENT .....	1
1.2 OVERVIEW OF RESEARCH PROGRAM TO DEVELOP FPCS PANELS .....	6
1.3 RESEARCH SIGNIFICANCE .....	10
<b>CHAPTER 2: LITERATURE REVIEW.....</b>	<b>12</b>
2.1 INTRODUCTION.....	12
2.2 SUPPORTIVE RESEARCH.....	12
2.2.1 VARIATIONS IN TEST PANEL CONSTRUCTION .....	14
2.2.2 VARIATIONS IN TESTING PERFORMED.....	15
2.2.3 FINITE ELEMENT ANALYSIS .....	15
2.2.4 PRECAST PANELS WITH COMPOSITE MATERIALS .....	16
2.3 WYTHE CONNECTORS.....	17
2.4 COMPOSITE BONDING WITH CONCRETE .....	18
2.5 PERCENTAGE OF COMPOSITE ACTION IN PANEL.....	19
2.5.1 NONCOMPOSITE ACTION .....	20
2.5.2 FULLY COMPOSITE ACTION .....	20
2.5.3 PARTIALLY COMPOSITE ACTION.....	21
2.6 BLAST RESISTANCE OF CONCRETE SANDWICH PANELS .....	21
2.7 LITERATURE REVIEW CONCLUSIONS.....	22
<b>CHAPTER 3: BENDING BEHAVIOR OF PRECAST CONCRETE SANDWICH PANELS WITH CFRP SHEAR GRID.....</b>	<b>24</b>
3.1 INTRODUCTION.....	24
3.2 EXPERIMENTAL INVESTIGATION .....	24
3.3 MATERIALS.....	25
3.4 FULL SCALE TESTING .....	28
3.5 DISCUSSIONS AND RECOMMENDATIONS.....	33

**CHAPTER 4: FINITE ELEMENT ANALYSIS OF FRP-PRECAST CONCRETE**

<b>SANDWICH PANELS.....</b>	<b>34</b>
4.1 INTRODUCTION.....	34
4.2 ANALYTIC MODEL .....	34
4.3 FINITE ELEMENT ANALYSIS.....	37
4.3.1 MATERIAL PROPERTIES.....	37
4.3.2 CONCRETE DAMAGED PLASTICITY MODEL .....	44
4.3.3 ELEMENT TYPES.....	63
4.4 EXPERIMENTAL INVESTIGATION .....	63
4.4.1 FABRICATION OF TEST SPECIMENS .....	63
4.4.2 TESTING OF THE PANELS .....	65
4.4.3 SCALED TEST PANELS.....	68
4.4.3 FULL SCALE TEST PANELS.....	80
4.5 TEST RESULTS VS. ANALYTICAL AND FEA PREDICTIONS .....	88
4.5.1 SOLID SCALED TEST PANEL .....	89
4.5.2 SCALED SANDWICH TEST PANEL .....	94
4.5.3 FULL SCALE SANDWICH TEST PANEL .....	107
4.6 DEGREE OF COMPOSITE ACTION .....	112
4.6.1 LOAD-DEFLECTION METHOD.....	113
4.6.2 STRAIN DISTRIBUTION METHOD .....	117
4.7 DESIGN CONSIDERATIONS .....	128
4.8 CONCLUDING REMARKS.....	130
<b>CHAPTER 5: CREEP BEHAVIOR OF FRP-PRECAST CONCRETE SANDWICH PANELS.....</b>	<b>131</b>
5.1 INTRODUCTION.....	131
5.2 EXPERIMENTAL DATA.....	131
5.3 ANALYTIC MODELS.....	135
5.3 EXPERIMENTAL INVESTIGATION .....	138
5.4 FINITE ELEMENT ANALYSIS.....	143
5.5 TEST RESULTS VS. ANALYTICAL AND FE PREDICTIONS .....	146
5.6 CREEP SUMMARY.....	148
<b>CHAPTER 6: BLAST RESISTANCE OF FRP-PRECAST CONCRETE SANDWICH</b>	
<b>PANELS.....</b>	<b>150</b>
6.1 INTRODUCTION.....	150
6.2 BLAST LOADING.....	151

6.2.1 COMPUTATION OF BLAST PRESSURE USING HEMISPHERICAL DETONATION GRAPH .....	155
6.2.2 COMPUTATION USING IDEALIZED BLAST PRESSURE WAVE FORMULAS ...	156
6.3 FINITE ELEMENT ANALYSIS .....	157
6.3.1 FEA BLAST LOADING MODEL VALIDATION .....	157
6.3.2 FEA BLAST MODEL FOR FPCS PANEL .....	162
6.4 BLAST ANALYSIS CONCLUSION .....	170
<b>CHAPTER 7: APPLICATION OF FRP-PRECAST CONCRETE SANDWICH ROOF PANELS .....</b>	<b>172</b>
7.1 RESIDENTIAL .....	172
7.2 INDUSTRIAL & COMMERCIAL .....	173
7.3 MILITARY .....	173
<b>CHAPTER 8: CONCLUSIONS AND RECOMMENDATIONS .....</b>	<b>174</b>
8.1 ABBREVIATED SUMMARY .....	174
8.2 DETAILED SUMMARY .....	175
<b>REFERENCES .....</b>	<b>177</b>
<b>APPENDIX .....</b>	<b>181</b>
<b>APPENDIX A – EPS INSULATION .....</b>	<b>181</b>
<b>APPENDIX B – ANALYTICAL CALCULATIONS FOR FULL SCALE PANEL .....</b>	<b>185</b>
<b>APPENDIX C – C-GRID© INFORMATION FROM MANUFACTURER .....</b>	<b>189</b>
<b>APPENDIX D – ANALYTICAL CALCULATIONS SOLID 10” CONCRETE PANEL .....</b>	<b>192</b>
<b>APPENDIX E – FINITE ELEMENT ANALYSIS PROCEDURE .....</b>	<b>196</b>

## LIST OF FIGURES

Figure 1 – Typical green roof construction.....	2
Figure 2 – Simplified example of sandwich panel with FRP plate.....	2
Figure 3 – Simplified example of sandwich panel with FRP shear connectors.....	2
Figure 4 – Green roof residential construction.....	5
Figure 5 – Concrete panel construction configurations.....	8
Figure 6 – Initial slab testing comparisons.....	9
Figure 7 – Linear range DCA comparison.....	10
Figure 8 – FRP truss wythe connectors.....	18
Figure 9 – Stress distribution of a noncomposite panel.....	20
Figure 10 – Stress distribution of a fully composite panel.....	21
Figure 11 – Stress distribution of a partial composite panel.....	21
Figure 12 – Typical Cross Section of Composite Panel.....	25
Figure 13 – C-Grid Mechanical Properties from Blue Ridge Design, Inc.....	26
Figure 14 – Composite Panel Production Prior to Pour.....	27
Figure 15 – C-Grid Materials and Ties Used in Production.....	27
Figure 16 - Test Panel Setup.....	28
Figure 17 – Final Load Placement.....	29
Figure 18 – Load deflection curve for test panel.....	30
Figure 19 – Top Layer of Longitudinal Pre-stressing Strand Splitting Failure.....	31
Figure 20 – Uniform and Symmetrical Bottom Transverse Cracks.....	32
Figure 21 – Test vs. Analytical Results for Cracking.....	32
Figure 22 – 10 inch solid concrete panel.....	34
Figure 23 – Compressive strength of concrete samples.....	38
Figure 24 – Concrete compressive test data.....	39
Figure 25 – Stress/Strain data for various reinforcing steel (Ref. Lowes, 1995) <sup>[37]</sup> .....	41
Figure 26 – True stress-strain properties of ASTM A615 Gr. 60 steel.....	42
Figure 27 – Response of concrete to uniaxial loading in compression (ABAQUS 2013).....	47
Figure 28 – Compression stiffness recovery parameter, $w_c$ (ABAQUS 2013).....	49
Figure 29 – Compressive inelastic strain definition of compression hardening (ABAQUS 2013)....	50
Figure 30 – Yield surface of deviatoric plan (ABAQUS 2013).....	51
Figure 31 – Yield surface in plane stress (ABAQUS 2013).....	51
Figure 32 – Compressive stress-strain relationship in ABAQUS.....	53
Figure 33 – Theoretical compressive stress strain curve for 4,120 psi concrete.....	55

Figure 34 – Theoretical vs. cylinder test results of compressive strain/strain values .....	57
Figure 35 – Response of concrete to uniaxial loading in tension (ABAQUS 2013).....	58
Figure 36 – Cracking strain definition of tension stiffening (ABAQUS 2013) .....	59
Figure 37 – Noyal and Rasheed’s (2006) tension stiffening model .....	60
Figure 38 – Modified tension stiffening model for ABAQUS.....	60
Figure 39 – Tensile stiffening model for the 4,120 psi concrete.....	61
Figure 40 – Wooden concrete form.....	64
Figure 41 – Typical FRP shear connector geometry .....	65
Figure 42 – Four-point bending setup .....	65
Figure 43 – Actual four-point bending test .....	66
Figure 44 – Three point bending setup.....	66
Figure 45 – Actual three-point bending test.....	66
Figure 46 – 10 in. solid concrete panel (108SOL10L3PTNOFRPS1) .....	68
Figure 47 – 10 in. sandwich panel with discrete connectors (108DIS10L4PTNOFRPS2).....	69
Figure 48 – 10 in. sandwich panel with segmental connectors (108SEGUP10L3PTNOFRPS2).....	69
Figure 49 – 10 in. sandwich panel with segmental connectors (108SEGUP10L3PTNOFRPS1).....	70
Figure 50 – 10 in. sandwich panel with continuous connectors (108CON10L3PTNOFRPS1) .....	70
Figure 51 – 10 in. sandwich panel with segmental connectors and FRP plates (108SEG10L3PTFRPS1) .....	71
Figure 52 - 10 in. sandwich panel with continuous connectors and FRP plates (108CON10L3PTFRPS1) .....	71
Figure 53 – FPCS scaled test panel with top and side FRP plates <sup>[44]</sup> .....	72
Figure 54 – Splitting tensile test specimen.....	73
Figure 55 – Stress-strain plot for splitting tensile test specimen.....	74
Figure 56 – 8 in. panel with inverted segmental connector and FPCS (108SEGDN8L3PTFPCSS1) 75	
Figure 57 – Load displacement graph for 8 in. FPCS panel (108SEGDN8L3PTFPCSS1).....	75
Figure 58 – 10 in. FRP sandwich panel (108SEGDN10L3PTFPCSS1) in testing apparatus.....	76
Figure 59 – 10 in. Segmental FRP panel with top and side FRP plates.....	77
Figure 60 - Load displacement graph for 10 in. FPCS 108SEGDN10L3PTFPCSS1 <sup>[44]</sup> .....	77
Figure 61 – FPCS panel comparison <sup>[44]</sup> .....	79
Figure 62 – Adjusted FPCS panel comparison <sup>[44]</sup> .....	80
Figure 63 – 8 in. full scale test panel.....	82
Figure 64 – 10 in. full scale test panel .....	83
Figure 65 – Full scale FPCS panel insulation, rebar and strain gages <sup>[44]</sup> .....	84

Figure 66 – Full scale FPCS first concrete lift pour <sup>[44]</sup> .....	85
Figure 67 – Cured and stripped full-scale FPCS specimens <sup>[44]</sup> .....	85
Figure 68 – Full-scale FPCS loading diagram <sup>[44]</sup> .....	86
Figure 69 – Full-scale FPCS panel in testing apparatus <sup>[44]</sup> .....	86
Figure 70 – 8” Full-scale FPCS load-deflection curve.....	87
Figure 71 – 10” Full-scale FPCS load-deflection curve.....	87
Figure 72 – 10 inch solid concrete panel construction.....	89
Figure 73 – FEA measured support reaction versus step time for 108SOL10L3PTNOFRPS1.....	90
Figure 74 – 108SOL10L3PTNOFRPS1 Damage Tension FEM Plots .....	91
Figure 75 – 108SOL10L3PTNOFRPS1 Damage Tension FEM Plots (Bottom).....	92
Figure 76 – 10 inch solid concrete panel FEA vs. Test results .....	93
Figure 77 – 10 inch sandwich panel with discrete connectors, 108DIS10L4PTNOFRPS2 .....	94
Figure 78 - FEA tension damage 108DIS10L4PTNOFRPS2 .....	96
Figure 79 – FEA tension damage, panel bottom, 108DIS10L4PTNOFRPS2 .....	97
Figure 80 – FEA deflection plots, U2, 108DIS10L4PTNOFRPS2.....	98
Figure 81 – FEA measured support reaction versus step time for 108DIS10L4PTNOFRPS2.....	99
Figure 82 – 10 inch sandwich panel with discrete connectors FEA vs. Test .....	100
Figure 83 – 10 inch sandwich panel with segmental connectors .....	101
Figure 84 – 10 inch sandwich panel with segmental connectors FEA vs. Test results .....	101
Figure 85 – 10 inch sandwich panel with segmental connector construction .....	102
Figure 86 – 10 inch sandwich panel with segmental connector FEA vs. Test.....	102
Figure 87 – 10 inch sandwich panel with continuous connectors construction .....	103
Figure 88 – 10 inch sandwich panel with continuous connectors FEA vs. Test.....	103
Figure 89 - 10 inch sandwich panel with continuous connectors and FRP top plate .....	104
Figure 90 – 10 inch sandwich panel with continuous connectors FEA vs. Test.....	104
Figure 91 – 10 inch sandwich panel with segmental down connectors FRP top/side plate (FPCS). 105	
Figure 92 – 10 in FPCS FEA vs test and non-FPCS .....	105
Figure 93 – Scaled test panel FEA summary plot .....	106
Figure 94 – Full scale test FPCS panel with segmental connectors .....	107
Figure 95 - FEA deflection plots, U2, 10 inch FRPCS full scale panel.....	108
Figure 96 – FEA tension damage side view plots, Dt, 10 inch FRPCS full scale panel.....	109
Figure 97 – FEA tension damage bottom view plots, Dt, 10 inch FRPCS full scale panel .....	110
Figure 98 – FEA tension damage top view plots, Dt, 10 inch FRPCS full scale panel .....	111
Figure 99 – 10 inch FRPCS full scale panel FEA vs. Test .....	112

Figure 100 – Solid slab test panel strain distribution .....	118
Figure 101 – Solid slab FEA strain distribution ( $\epsilon_{11}$ ).....	118
Figure 102 – Solid slab FEA strain distribution plot ( $\epsilon_{11}$ ) .....	119
Figure 103 – Solid slab FEA panel rebar strain vs. test results.....	120
Figure 104 – Discrete connector test panel strain distribution.....	120
Figure 105 – Discrete connector FEA panel strain distribution.....	121
Figure 106 – Segmental connector test panel strain distribution .....	121
Figure 107 – Segmental connector test panel strain distribution .....	122
Figure 108 – Continuous connector test panel strain distribution.....	123
Figure 109 – Continuous connector FEA panel strain distribution.....	123
Figure 110 – FPCS Segmental 10” FEA panel strain distribution.....	124
Figure 111 – FPCS Segmental 10” Full Scale FEA panel Strain Distribution .....	124
Figure 112 – FEA DCA vs. Load comparison .....	128
Figure 113 – Partial composite section vs. solid panel section.....	129
Figure 114 – 8 inch creep test panel with FRP top & side plates (FPCS).....	132
Figure 115 – 10 inch creep test panel with FRP top & side plates (FPCS).....	133
Figure 116 – 10 inch creep test panel with no FRP plate.....	133
Figure 117 – 10 inch solid creep test panel.....	134
Figure 118 – ACI multiplier for long term deflection (ACI 318, Figure R9.5.2.5) .....	136
Figure 119 – Analytical creep deflection, ACI 318 .....	137
Figure 120 – Creep test loading diagram .....	138
Figure 121 – Creep test set up for 10” FPCS panel .....	138
Figure 122 – Creep test panel set up for 8” FPCS, 10” sandwich and 10” solid panel.....	139
Figure 123 – Creep deflection vs. time, Norris <sup>[44]</sup> .....	140
Figure 124 – Quarter point deflection vs. time, Norris (2014).....	141
Figure 125 – Quarter point deflection vs. time, no initial deflection .....	142
Figure 126 – Secondary creep comparisons.....	143
Figure 127 – 10 in. solid concrete creep test panel 4 deflection .....	146
Figure 128 – 10 in. FPCS sandwich creep test panel 2 deflection .....	147
Figure 129 – Estimated long term creep effects for 10” FPCS panel .....	148
Figure 130 – Facility terrorist attack, (FEMA 426) .....	151
Figure 131 – Typical blast pressure wave (Hinman, 2003) .....	152
Figure 132 – Idealized blast pulse versus time .....	152
Figure 133 – Positive phase air blast parameters for hemispherical TNT Detonation, Surface .....	154

Figure 134 – Negative pressure parameters for hemi-spherical blast <sup>[26]</sup> .....	155
Figure 135 – Blast parameters from ATBlast program.....	156
Figure 136 – Reinforcing steel layout in plan view <sup>[51]</sup> .....	158
Figure 137 – Cross section of panel and loading direction <sup>[51]</sup> .....	158
Figure 138 – Boundary conditions of FEA (a) vertical support, (b) back face, (c) pressure loading face <sup>[51]</sup> .....	159
Figure 139 – Recreation of blast pressure vs. time plots .....	159
Figure 140 – FEA comparisons with experimental.....	160
Figure 141 – Experimental and FEA results from Thiagarajan et. al. <sup>[51]</sup> .....	161
Figure 142 – ABAQUS FEA plots using Damaged Plasticity Model .....	161
Figure 143 – Blast loading diagram for solid concrete panel .....	162
Figure 144 – Solid panel construction details .....	162
Figure 145 – Blast loading diagram for FPCS panel .....	163
Figure 146 – Segmental FPCS panel construction details .....	163
Figure 147 – Finite element analysis model of 10” solid panel 108SOL10L3PTNOFRPS1 .....	164
Figure 148 – Blast interaction properties in Abaqus.....	165
Figure 149 – 10” Solid panel blast loading tension damage .....	166
Figure 150 – Deflection versus time for 10” solid concrete panel under blast loading .....	167
Figure 151 - 10” FPCS panel blast loading tension damage.....	168
Figure 152 - Deflection versus time for 10” FPCS panel under blast loading.....	169
Figure 153 – Deflection versus time for 10” FPCS panel and 10” solid panel under blast loading .	170
Figure 154 – Blast load sandwich panel 108SEGUP10L3PTNOFRPS2.....	171
Figure 155 – Deflection vs. time for 10” sandwich panel and 10” solid panel under blast loading .	171
Figure 156 – Sunberg house, Pass Christian, Mississippi (Hurricane Katrina) .....	172
Figure 157 – Abaqus CAE model tree .....	197
Figure 158 – Entire assembly modeled in Abaqus.....	198
Figure 159 – 108SEGUP10L3PTFRPS1 Parts .....	199
Figure 160 – ASTM A615 reinforcing steel material properties .....	200
Figure 161 – Concrete 4,120 psi material properties .....	201
Figure 162 – Concrete Damaged Plasticity constants .....	202
Figure 163 – Concrete compression damage .....	203
Figure 164 – Concrete tension damage.....	204
Figure 165 – EPS Insulation material properties .....	205
Figure 166 – Rebar sections are assigned as stringers .....	208

## LIST OF TABLES

Table 1 – Summary of test panel construction type literature review .....	14
Table 2 – Summary of test panel testing .....	15
Table 3 – DCA equation summary .....	19
Table 4 – Test panel load and deflection data .....	29
Table 5 – Analytical results for 10 inch solid concrete panel .....	36
Table 6 – Material properties for insulation .....	37
Table 7 – Material properties for concrete .....	38
Table 8 – Material properties for reinforcing steel .....	42
Table 9 – ASTM A615 Gr. 60 reinforcing steel nonlinear material properties .....	43
Table 10 – FRP material properties .....	44
Table 11 – Hsu and Hsu numerical compression stress-strain model .....	54
Table 12 – Damaged plasticity values for 4,120 psi concrete .....	56
Table 13 – Concrete damaged plasticity model for tension stiffening .....	62
Table 14 – FEA element types .....	63
Table 15 – Test panel nomenclature key plan summary .....	67
Table 16 – FPCS scaled test panel construction details .....	72
Table 17 – Compressive strength of FPCS panels <sup>[44]</sup> .....	72
Table 18 – FPCS panels ultimate load summary <sup>[44]</sup> .....	78
Table 19 – FPCS panels failure mode summary <sup>[44]</sup> .....	78
Table 20 – Full scale FPCS panel construction details <sup>[44]</sup> .....	80
Table 21 – Compressive strength of full-scale test panel cylinders <sup>[44]</sup> .....	84
Table 22 – Full scale FPCS ultimate load summary .....	88
Table 23 – Initial load vs. deflection test values for all specimens .....	114
Table 24 – DCA load deflection method summary .....	117
Table 25 – Degree of composite action (DCA) – strain distribution method .....	127
Table 26 – DCA load displacement vs. strain distribution methods based on test data .....	127
Table 27 – Creep test block weights .....	134
Table 28 – ACI load duration multipliers .....	136
Table 29 – ACI sustained load factors and deflections .....	137
Table 30 – 10” solid panel deflection calculations .....	141

## NOTATION

$a$ = depth of equiv. rect. stress block $A_s$ = area of mild-steel reinforcement $d_c$ = compressive damage parameter $d_t$ = tension damage parameter $E$ = Young's Modulus $E_c$ = modulus of elasticity of concrete $E_o$ = initial tangential modulus $f_c$ = concrete compressive design strength $f_{pu}$ = stress in prestressed reinforcement $f_r$ = modulus of rupture of concrete $F_{ys}$ = yield stress of steel $F_u$ = tensile strength $I_{cr}$ = cracking moment of inertia $M_{cr}$ = cracking moment $P_{cr}$ = cracking service load WWF = welded wire fabric $\beta$ = shape parameter $\varepsilon_c$ = compressive strain $\varepsilon_t$ = tensile strain $\tilde{\varepsilon}_t^{ck}$ = tensile cracking strain $\tilde{\varepsilon}_t^{pl}$ = tensile plastic strain $\varepsilon_{ot}^{el}$ = elastic tensile strain-undamaged mat'l $\varepsilon_o$ = concrete strain at peak stress $\lambda$ = normal weight concrete factor $\nu_c$ = Poisson's ratio of concrete $\nu_s$ = Poisson's ratio of steel $\rho_c$ = mass density of concrete $\rho_s$ = mass density of steel $\sigma_c$ = compressive stress in concrete	$\sigma_{cu}$ = concrete 28 day compressive strength $\sigma_t$ = tensile stress in concrete $\sigma_{to}$ = maximum tensile strength in concrete
---	---

## ABBREVIATIONS

ACI	=	American Concrete Institute
ASTM	=	American Society for Testing and Materials
CFRP	=	Carbon-Fiber Reinforced Polymer
DCA	=	Degree of composite action
EPS	=	Expanded Polystyrene
FEA	=	Finite Element Analysis
FEM	=	Finite Element Model
FPCS	=	FRP-Confined Precast Concrete Sandwich
FRP	=	Fiber-Reinforced Polymer
GFRP	=	Glass fiber reinforced polymer
IBC	=	International Building Code
RVE	=	Representative Volume Element
XPS	=	Extruded Polystyrene

# CHAPTER 1: INTRODUCTION

## 1.1 PROBLEM STATEMENT

Most sandwich panels are comprised of two outer concrete wythes and an interior polystyrene or polyurethane insulation layer. These outer concrete wythes are connected to one another with some form of shear or panel connector, whether it's a proprietary or conventional system. There also is temperature reinforcing steel usually in the form of welded wire fabric and/or prestressing strand to help with lifting and moving the panel.

It has not been documented or verified when the first sandwich panels were incorporated in structures; however it is estimated to be around the 1960's. In the 1970's there was a large demand for energy efficient building construction that increased the demand and popularity of these panels. Then in the 2000's renewed demand for energy efficient and sustainable building products brought these panels back to the forefront of precast building construction. The typical design and installation of concrete sandwich panels configures the panels to span vertically from foundation to roof and/or floor diaphragm. In some cases the sandwich panels are used as a spandrel panel connecting vertical column elements over opening in the wall system. The panels are designed today to provide axial, shear, in-plane bending strength, and out-of-plane bending strength. The panels are required to be built with enough strength to be manufactured, lifted out of the forming bed, mobilized to the construction site, lifted in place, support gravity axial loads and wind and seismic out-of-plane loads.

With new improvements and desire to have green construction and sustainable building design, these panels could also be used in roof systems to provide in-plane diaphragm shear, out-of-plane bending, insulation and membrane protection against the environment. A bending test was conducted by the author on a sandwich panel which was originally constructed as a vertical wall element. The test results showed promise that the panel could be used as a horizontal structural element. The outline and summary of the investigation is shown in Chapter 3 of this report. Following this proof-of-concept test, extensive research has been carried out to develop an innovative sandwich roof panel. These panels when placed in the horizontal configuration rather than the typical vertical wall application can provide strength, weather resistance and insulation similar to the conventional concrete green roof system shown in Figure 1. Precast/prestressed concrete insulated sandwich panels will be referred to as sandwich panels or simply panels in this dissertation.

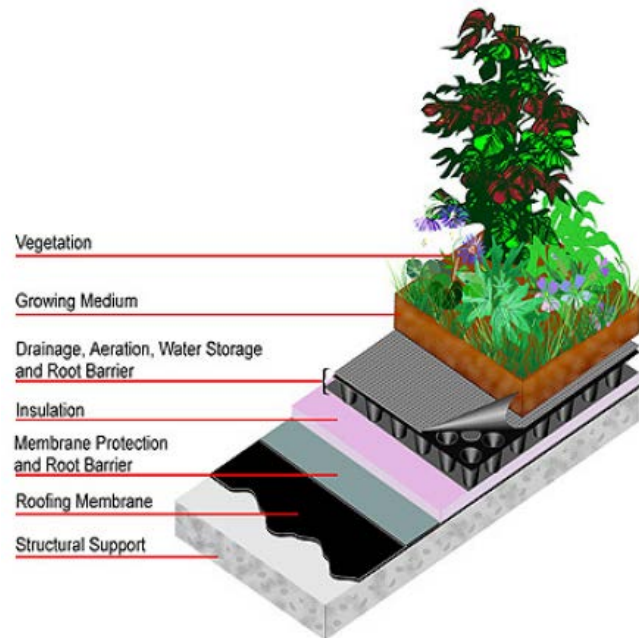


**Figure 1 – Typical green roof construction**

The intended typical configuration of the sandwich panel will have a top exterior plate comprised of fiber-reinforced polymer (FRP) as shown in Figure 2.

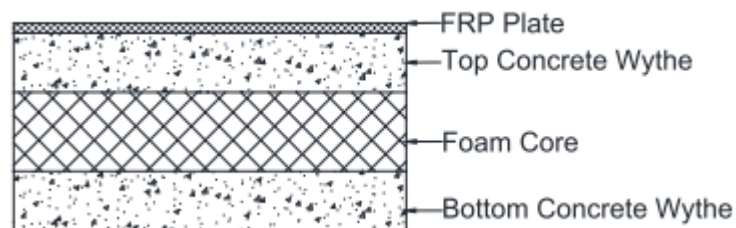


**Figure 2 – Simplified example of sandwich panel with FRP plate**

The panels will have various configurations of FRP shear connectors connecting the top concrete wythe to the bottom concrete wythe as shown in Figure 2. The FRP shear connectors configuration that produces the highest strength and flexural stiffness and the highest degree of composite action (DCA) will be promoted to future research, testing and production.



**Figure 3 – Simplified example of sandwich panel with FRP shear connectors**

The insulation foam core is located in the center wythe of the panel and the exterior FRP plate will be anchored or bonded to the concrete outer wythes in order to develop composite action. FRP shear

connectors will be mechanically anchored to the outer concrete wythes through the use of reinforcing steel and concrete interlocking. Other forms of mechanical shear transfer such as solid zones of concrete, commercially available mechanical ties and/or proprietary composite ties such as C-Grid® will not be used in this study to develop composite action through the depth of the panel. The insulation used in the panel can either be expanded polystyrene (EPS) or extruded polystyrene (XPS) and in this study EPS was used. Although solid zones of concrete provide the most reliable form of full-composite action, the thermal bridge that it creates is counterproductive in the intended use of the panel. The top concrete wythe in this study will be studied with and without primary flexural steel reinforcement due to the presence of the FRP plate, which is intended to provide flexural strength. The top and bottom concrete wythes will be anchored together with FRP shear connectors which provide mechanical shear transfer. The bottom concrete wythes shall have primary longitudinal steel reinforcement for strength and serviceability. Transverse steel reinforcement will be added for control of shrinkage and temperature effects.

These panels are called FRP-Confined Precast Concrete Sandwich (FPCS) panels. The FPCS panels are believed to be good candidates for both residential and commercial applications, however they could also be used for industrial and military/government applications to resist explosion and/or blast events. A brief study is included in this report to show the advantages of the FPCS panel when used as a roof element to resist blast loading when compared to a solid reinforced concrete panel.

Finally advantages in the use of this FPCS design will include increased production time with no concrete stripping required and no top wythe reinforcement required. The panels will be energy efficient and when used in roof applications they will provide the insulation and the roofing membrane in one single installation. More specifically the FPCS panel will provide the following advantages:

**(1) Energy Efficient:** Similar to precast sandwich wall panel, FPCS panels have a better thermal efficiency from the foam core. Precast insulated wall panels have been identified to be one of the most structural efficient systems in terms of low material consumption and high thermal efficient systems. Bush and Stine (1994)<sup>[16]</sup> stated that the use of insulated precast wall panels can increase the thermal efficiency of concrete sandwich panels nearly 30 percent over that of a stud wall system. These thermally efficient systems can save nearly 20 percent in energy cost compared to framed walls (Gleich 2007)<sup>[1]</sup>. Insulated concrete sandwich wall panels with polystyrene cores can exhibit R-values of up to 30 in comparison to a stud wall system with an R-value of 5 to 10 (Christian &

Kosny 1999)<sup>1</sup>. With the additional FRP layer, it is expected that FPCS panels will have better thermal capacity than precast sandwich wall panels. FRP has a thermal resistance R value of about 3.3 F-ft<sup>2</sup>-hr/Btu-in, which is comparable to EPS (average R-value of 3.8 F-ft<sup>2</sup>-hr/Btu-in) typically used for sandwich wall panel.

**(2) Reduced Weight and Higher Strength:** FPCS panels can also provide a lighter system which is critical for the construction industry and seismic design. It has been reported that precast sandwich wall panels can achieve equivalent strength to a solid panel yet consume nearly half the concrete material. It is expected that FPCS panels can have higher capacity than the sandwich wall panel, since FRP plate can provide a confining effect to the concrete, which can increase the concrete flexural strength.

**(3) Reduced Cost:** The cost reduction comes from a) the reduced concrete material as indicated above; b) elimination of water membrane, which costs about \$1.2-\$1.8/ft<sup>2</sup>, and insulation layer, which costs about \$1.2-\$1.6/ft<sup>2</sup> ([www.howewyse.com](http://www.howewyse.com)); and c) elimination of the reinforcement for top concrete wythe. The added cost from FRP plate can be offset by these cost reductions.

**(4) Reduced Overall Roof Depth:** Due to the elimination of the water membrane and insulation layers, the overall depth of the roof can be reduced. When installing precast structural products on the roofs or floors of a building they usually come in the form of precast single or double tees, inverted tee beams with hollow core plank or other structural members that have a large depth to them to achieve adequate strength and stiffness. One primary advantage to using a concrete sandwich panel roof or floor system is the ability to build structures with low floor-to-roof heights. This leaves more architectural and mechanical plenum space for the building, which is sometimes critical to meeting zoning requirements by the building authorities.

There are various forms of green roof construction, including various structural materials and support systems. The residential home built in Salmon, ID, in 2006, Figure 4, utilized insulated concrete forms for wall construction then post and steel beam system for support of hollowcore plank roof. The hollowcore plank then had to be grouted, a topping slab added, insulation, water proof membrane, bituminous damproofing, then top soil. Although the construction was quick and the building is simple to construct, additional steps were included for the insulation and water proof membrane. Furthermore the steel beam system and the hollow core system acted non-compositely to

create an adequate structural roofing system, that in turn took up space in the ceiling cavity and then again with the support posts.



**Figure 4 – Green roof residential construction**

Other green-roof systems include steel with steel deck, wood, cast-in-place concrete and precast structures. The common attribute for green roof systems are sufficient insulation, even with soil topping to negate a condensation effect from the potential thermal gradient, and an adequate water proofing membrane to protect against water intrusion.

**(5) Fast Construction:** FPCS panels provide a quick and efficient construction system when construction costs are critical or the job site is subjected to harsh construction environments. Panels can be cast in a controlled environment ensuring structural quality, and then placed in the field with less labor than in-situ roofs.

(6) **Water Resistant:** FRP has excellent water resistance property. For FPCS panels, since FRP and concrete are an integral part, the water resistance is expected to be better than an in-situ roof with traditional water membrane.

(7) **Durable:** For FPCS panels, concrete can effectively resist cracking due to the confining effect from FRP plate. Even if concrete cracks for any other reason, the effect is less significant due to the protection from the FRP plate above. Therefore, it is expected that the FPCS roof can have a longer life span than a traditional roof.

## **1.2 OVERVIEW OF RESEARCH PROGRAM TO DEVELOP FPCS PANELS**

The research team involved with this dissertation, including the author, intends to develop and test both scaled and full-scale precast concrete sandwich panels to be used for green-roof applications. The panel must be able to span long distances of greater than or equal to 16 feet, support engineered green roof soil or up to three feet of top soil, and have incorporated within the construction of the panel a composite material exterior membrane that will both serve as moisture barrier and flexural strength. Further objectives of this study are to develop fiber-reinforced polymer (FRP) shear connectors, which can be easily cut from commercially available FRP plates, and study their effects on the flexural behavior of insulated concrete sandwich panels. A finite element (FE) analysis model shall be developed for each test panel to determine if a numerical approach can be used to determine the strength and deflections of the panel. Creep testing shall be performed on the panels to study the long term loading effects of the sandwich panels and finally a brief blast analysis study will be conducted to compare the baseline solid concrete panel to one of the FRP concrete sandwich panels tested in this study.

### **In summary the following shall be performed:**

1. Develop FRP shear connectors and several concrete sandwich panel configurations to compare strength, stiffness and degree of composite action (DCA).
2. Test the scaled and full scale test panels in a static setting.
3. Conduct a creep test on both solid concrete panels and sandwich FRP concrete panels to study long term effects.

4. Create innovative dynamic FE models for sandwich panels with soft core to determine the accuracy of numerical analysis in designing future sandwich panels.
5. Create and FE model to predict the creep behavior
6. Perform a blast numerical analysis on (1) solid concrete panel and (1) FRP concrete sandwich panel.
7. Propose design guidelines.
8. Determine the commercial application of these panels.

In parallel to this dissertation, items 1 through 3 have been addressed in the thesis by Norris<sup>[44]</sup>. Figure 5 shows the organization of the sandwich panels that were constructed and tested. The solid concrete panel is the baseline or reference panel and from there we have 3 main types of sandwich panels which then are segregated into with and without FRP plates. With this order of development and testing we have created a reliable set of data for the various configurations that we feel will be most common and useful. Then with validation of a FEA model, we can perform parametric studies and determine if any other arrangements shall be considered.

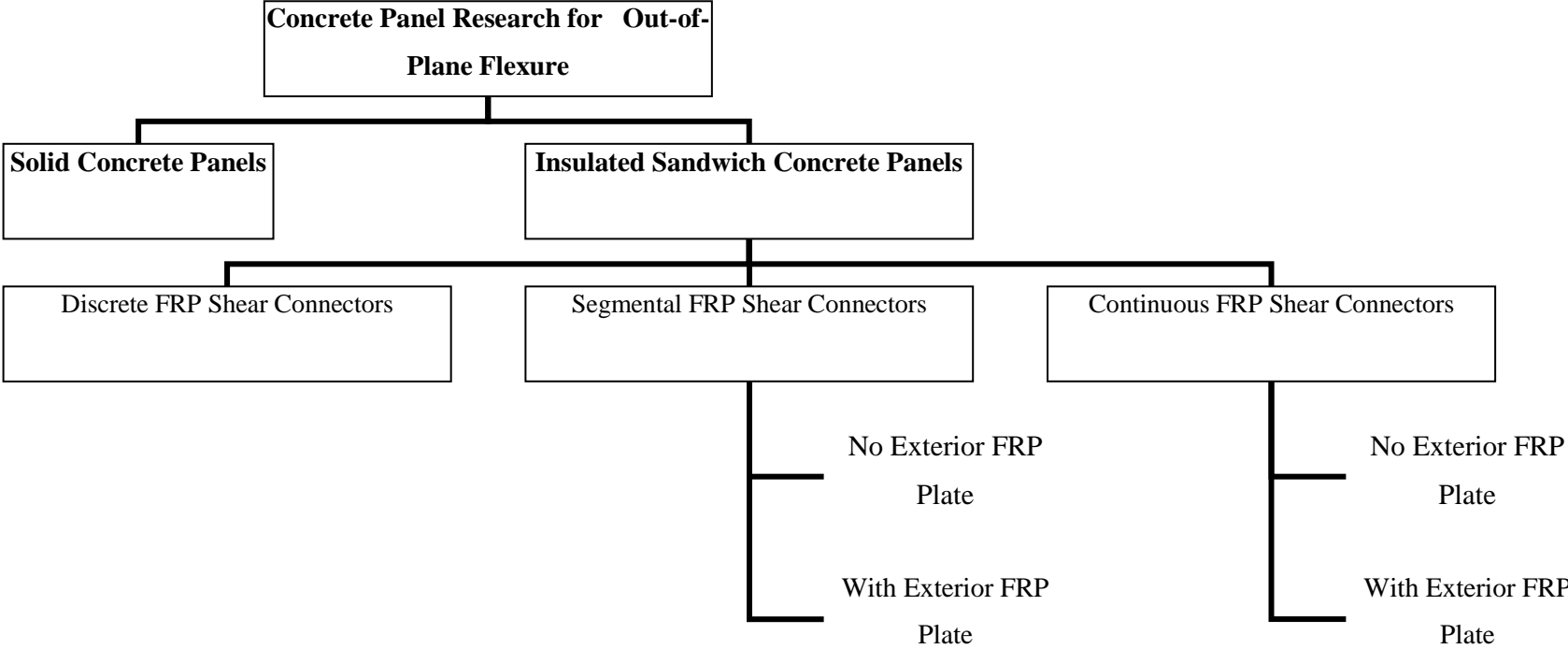


**Figure 5 – Concrete panel construction configurations**

The shear connectors are fabricated by cutting patterns from commercially available FRP composite products. Several different configurations of the shear connectors in the sandwich panels were compared with the baseline solid concrete panel test results to determine the DCA and flexural strength and stiffness capability. The first set of (8) concrete scaled test panels are shown in Figure 5 which were comprised of a set of solid panels and sandwich panels, then within the sandwich panel group discrete FRP, segmental FRP and continuous FRP connectors were incorporated. The load versus deflection comparison of the panels is shown in Figure 6. Further test results are presented later in this study and in the thesis submitted by Tom Norris<sup>[44]</sup>. Panels were also tested in select cases with and without exterior FRP plates on the concrete top and side surfaces. These types of solid web shear connectors are in contrast to the to other forms of precast concrete sandwich panel connectors such as glass fiber reinforced polymer (GFRP) truss ties, steel wire ties, and carbon fiber truss girds. Solid concrete zones in some cases have also been used to develop higher composite action between the concrete wythes, however thermal bridging occurs when this method is used, negating the intended effect of the insulation layer.

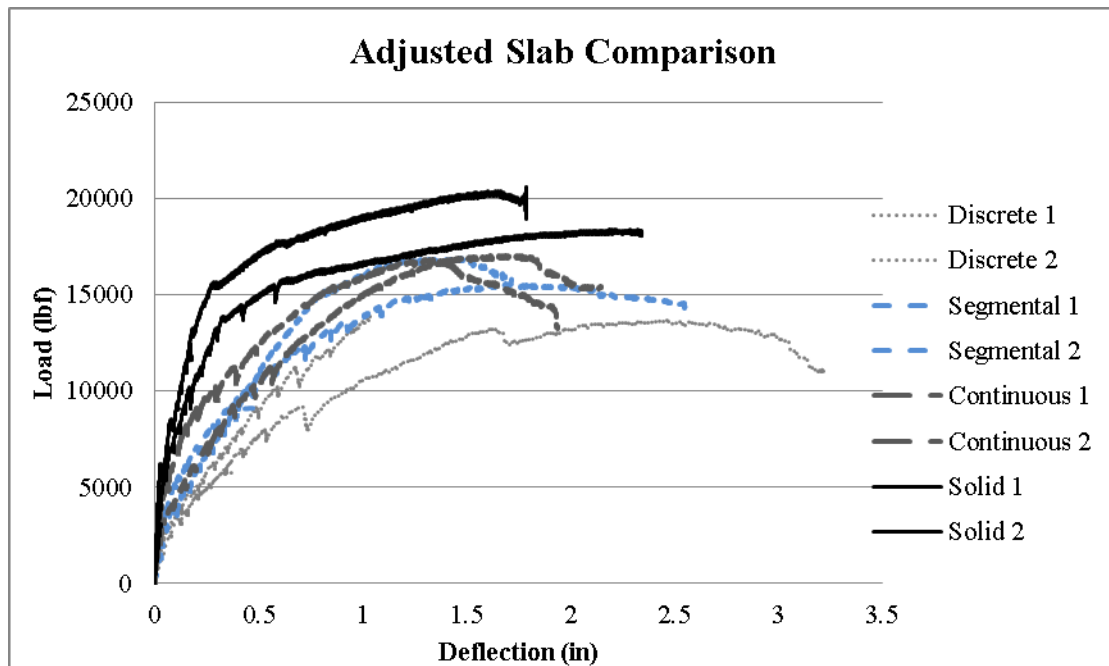


Figure 6 – Initial slab testing comparisons

A brief overview of the (8) scaled test panels load versus deflection in the linear-elastic range is shown in Figure 7 and right away it is clear the continuous and segmental FRP connectors provide superior DCA values when compared to the discrete FRP connectors. Considering solid slab is 100% composite or DCA, it can be shown in Figure 7 that the continuous FRP connectors, although do not provide 100% of DCA, achieve the highest values.

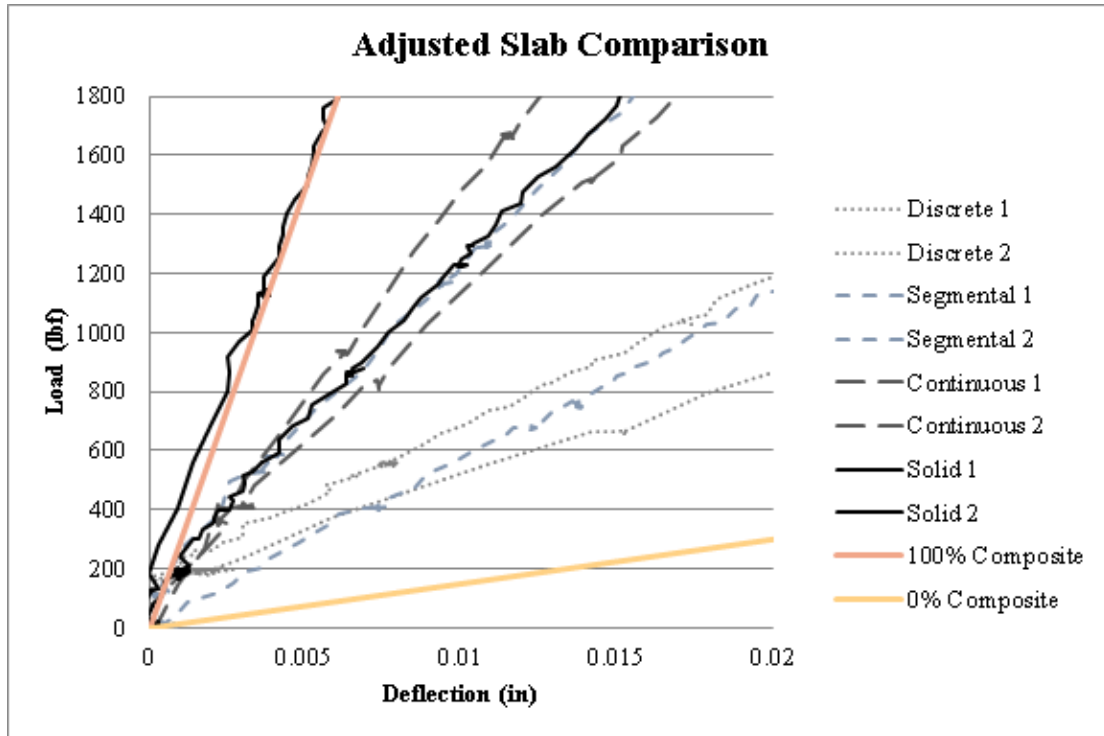


Figure 7 – Linear range DCA comparison

### 1.3 RESEARCH SIGNIFICANCE

The most accurate and confident way to determine the strength of these precast concrete sandwich panels is to test them for static and cyclic loading. These tests are costly and time consuming, so naturally it would be better to speed up the iterative design cycle and have the ability to use finite element analysis to determine the maximum strength, deflection and failure mechanisms. Furthermore, it has been found that this numerical analysis problem cannot be completely solved by a static linear model since the failure of the panel in itself is a quasi-static mechanism. The linear static finite element analysis model seems to present better results at the initial portion of the loading, however the dynamic quasi-static analysis model provides better post-cracking results which are useful to predict failures. The flexibility of the shear connectors also proposes problems with solving the numerical problem and once again a quasi-static FEA model is better suited for this structural system. As the applications for these panels expanded to blast resistant structures, this type of dynamic versus static model is necessary in order to model that type of response and therefore it's an appropriate adjustment.

Therefore, the primary research significance to this study is the creation of quasi-static FE models using ABAQUS<sup>®</sup> numerical explicit solver, which is a commercially available program. Damage plasticity models that have been developed and tested by other researchers in the past<sup>[28][39][23][54]</sup>, where used as starting points for this FE study, however explicit analysis was applied in the numerical solver to capture more of the quasi-static effects of the concrete damage. Good correlation is shown between the FE model and the test results and furthermore the FE analysis shows excellent damage results and areas of concern as the panels undergo flexural behavior. These models can be used to predict flexural strength and deflection when loaded and if warranted, cyclic loading can be applied.

Creep analysis has also been included in this study to provide insight on the long term effects of the panels when positioned horizontally and loaded in out-of-plane bending. There were no available commercial solvers or routines for analyzing creep effects in concrete sandwich panels and this study includes a subroutine program to be used in ABAQUS for the creep analysis of these types of panels.

Concrete is a common building material utilized in construction for the protection and/or mitigation for blast explosions, whether terroristic or accidental. The Unified Facilities Criteria (UFC)<sup>[52]</sup> was initially established in the 1960's and focused primarily on concrete as a blast protective building structure. Since then other materials have been studied, tested and documented in the UFC 3-340-02 to provide engineers other resources from which to choose from when considering blast protection. However precast concrete sandwich panels are not mentioned as a primary building load carrying and blast resisting material. There is mention of using precast concrete panels along with a steel frame and solid precast concrete building materials as a standalone structure. The limitation recommended by the report is that precast concrete building material be used for low pressure levels 1 to 2 psi and limited to single-story buildings. The primary focus of this research study is not on blast design and mitigation effects. However the author feels that the precast concrete sandwich panels tested to offer both blast resting strength along with the desired energy efficiency in one product. A brief numerical analysis shall be performed with no test data backup to present some useful comparisons. Perhaps future studies could show this to be a suitable and desirable building material for these applications.

## **CHAPTER 2: LITERATURE REVIEW**

### **2.1 INTRODUCTION**

The focus of this study is to develop concrete sandwich panels with FRP shear connectors to support live and dead out of plane loading which may include green roof loading. Further goals of this study are to determine the degree of composite action of the panels and how they compare to solid reinforced concrete structures. In the case of the insulated sandwich panel the substitution of the insulation for the concrete reduces weight while providing necessary thermal resistance values. In this literature review the focus was primarily on the strength of the panels, the sensitivity to variations in construction types and methods, variations in insulation and recommended use of the panel. Until recently, within the last 10-20 years, little experimentation has been performed on panels with an outer composite membrane in the form of FRP materials. Rather most of the available research was focused in the composite internal action of the concrete wythes and the wythe ties. The existing DCA research is valuable and will be utilized in this study. The material and configuration of the shear connectors in this study are unique, and although existing concrete wythe connectors will be mentioned, their application will not be utilized. Finite element model research that is available for the nonlinear numerical analysis of the concrete panels is valuable and there is plenty of available methods and documentation. This study shall utilize an explicit analysis to capture the quasi static phenomena, which will be unique to other FE models. The creep and blast sections of this study are unique to these types of panels. Although there does exist plenty of blast analysis research for concrete structures, especially since 2001, little of that is specific to insulated concrete sandwich panels. Furthermore creep is a special case to this study and the industry lacks concrete creep data. Analytical creep models have been developed by many researchers and through ACI, however once again there is little available research when it comes to creep studies for insulated concrete panels.

### **2.2 SUPPORTIVE RESEARCH**

Earlier research in the 1990's by Bush & Wu (1998)<sup>[14]</sup> and Bush & Stine (1994)<sup>[16]</sup> investigated concrete sandwich panels with metal truss connectors. The panels were placed in the horizontal position and tested as semi-composite sandwich panels where bending stress and deflection predictions were verified with testing and finite element analysis models. They found that insulation provided additional paths of shear resistance in the testing and the testing results were not fully

captured by the FE model or the closed form solution. Bush, et al.<sup>[14]</sup> also concluded longer panels provided higher composite action while shorter panels behaved more non-composite.

The composite sandwich panels, in reality, are neither fully composite nor fully non-composite and the percentage of composite action will depend on the phase of loading, whether in the early elastic range or the later inelastic nonlinear range. The degree of composite action is sensitive to the type of construction and how and where the wythe ties are incorporated. A much larger unknown is the interference effect between the concrete and the insulation and the type of insulation used. Salmon, et al (1997)<sup>[49]</sup> stated that the bond between the insulation layer and that of the concrete will deteriorate over time and not provide sufficient strength over the life of the panel. This is an important concept when considering creep in a panel under horizontal construction applications with primarily out-of-plane bending. In most of Salmon's research, the load-displacement graphs showed that the stiffness values tend to drop dramatically when the bond between the insulation and the concrete is released. This is generally true for all insulated concrete sandwich panels and foam core composite sandwich panels in general. It's not a mechanical bond between the insulation and outer wythes, therefore slippage will occur at some point during the life or loading of the panel.

Furthermore Pessicki & Mylynarczyk (2003)<sup>[47]</sup> in the 2000's used "off-the-shelf" wythe connectors and compared that to using just concrete and insulation which utilized solid concrete zones to develop composite action in out-of-plane bending. Pessicki & Lee (2007)<sup>[34]</sup> tested three-wythe panels that had insulation in two layers and then concrete in three layers, however this three-wythe panel resulted in the same section thickness. The insulation and the concrete were alternated so that the concrete had no direct path from the exterior face to the interior face and thus the thermal bridge was broken. This three-wythe panel was superior to the two-wythe panels with mechanical ties and provided longer spans and higher degree of composite action. The disadvantage to the three-wythe panel was the cost and labor involved in building the panel. Pessicki in their research developed and provided suitable properties for use in the FEM of the insulation and guidance on the development of the FEM for incorporation of the pre-strand forces. Pessicki, et al. recommends the use of solid concrete zones in the panel to develop full composite action as the most reliable method. Otherwise, in order to develop full composite action, achieve longer spans and higher loading, the mechanical wythe ties and insulation used must be carefully selected and designed to verify that full composite action is being achieved.

The research presented in this dissertation will focus on the development of mechanical connectors using commercially available FRP composites. The PCI Committee on the State of the Art of Precast/Prestressed Concrete Sandwich Wall Panels<sup>[45][46]</sup> provides a thorough list of what is available for the design of these panels, details on the construction of the panels, and research findings on the influence of the construction types and materials used. There is however differences of opinion embedded in this PCI committee report. The PCI committee report provides a list of materials such as insulation and the mechanical wythe ties and steps to construct these panels. Energy, fire and composite action performance calculations examples are also provided in the committee report. The PCI Committee does not lean one way or another towards an adopted or recommended design practice. It is up to the designer to determine the specific situation of the panel's use and the responsibility of the professional engineer to ensure the panel will achieve desired performance.

### 2.2.1 VARIATIONS IN TEST PANEL CONSTRUCTION

There are several examples of test panel construction variation in order to determine the more effective and better performing sandwich panel. The construction types range from two-wythe panels to three-wythe panels, solid concrete zone ties, CFRP composite wythe ties, steel truss wythe ties and others. Table 1 provides a brief summary of some of the variations in past concrete sandwich panel construction that has been research and tested.

**Table 1 – Summary of test panel construction type literature review**

<b>Reference</b>	<b>Construction Type</b>	<b>Remarks</b>
Bush & Stine <sup>[16]</sup> 1994	Two-wythe sandwich wall panel tested for flexure only.	Fatigue testing over 55,000 cycles.
Lee & Pessicki <sup>[35]</sup> 2008	Three-Wythe Sandwich Wall Panel	Solid concrete zones with M-ties
Frankl, Lucier, Hassan & Rizkalla <sup>[21]</sup> 2011	Two-wythe sandwich wall panel with CFRP shear grids	Panel tested with gravity and lateral loads in testing frame. Reverse cyclic loading.

### 2.2.2 VARIATIONS IN TESTING PERFORMED

With the development and evolution of better performing precast concrete sandwich panels came the experimental backbone known as testing. Table 2 provides a summary of various important testing configurations performed by researchers in recent years.

**Table 2 – Summary of test panel testing**

Reference	Testing Type	Remarks
Bush & Stine <sup>[16]</sup> 1994	Static Flexural and Fatigue Cyclic Third Point Loading Truss girder push out test	Lateral flexural results proved to be better than expected. Fatigue test was unique.
Lee & Pessiki <sup>(35)</sup> 2007	Three-wythe panel configurations. Static flexural test only.	Use of prestressing strands. Recommendations to reduce transverse bending. Three-wythe panels behave with high degree of composite action with longer spans.

### 2.2.3 FINITE ELEMENT ANALYSIS

Finite element analysis is a common numerical analysis tool used to help predict failure modes and load patterns for structures that cannot always be extensively tested. Most of the research sources cited in this report do contain actual testing and finite element analysis correlation. Some of the earlier finite element analysis models developed by Bush and Wu<sup>(14)</sup> used solid elements to represent the concrete wythes and insulation materials while truss elements were used for the shear ties. The FEM results provided conservative values and sensitivity analyses were conducted to determine the primary cause in the variation from test data to the FEM results. Finite element models were also developed for two-wythe and three-wythe concrete sandwich panels and incorporated prestress transfer forces as shown in Jun Lee and Pessiki's work<sup>(34)(35)</sup>. The results presented in those two papers are limited to the fully bonded insulation to concrete wythe configurations and the linear FEA model. Guidance is provided by Lee & Pessiki on the modeling techniques, load transfer for prestress forces and boundary conditions; however no further mention on the nonlinear quasi-static numerical analysis approach that is the focus in this report.

In recent years there has been advancement in computing technology and numerical modeling tools for non-linear finite element analysis of reinforced concrete structures. Benayoune., et. al.<sup>[14]</sup> used a commercially available software program known as LUSAS and showed reasonable estimation of the experimental load-deflection curve. The LUSAS program used the finite element analysis model developed by Jefferson<sup>[29]</sup>.

In a more related topic to this study, in 2011 Henin et. al.<sup>[24]</sup> built and tested precast concrete sandwich panels with GFRP truss ties between concrete wythes for floor and roof applications and developed a FEA model using shell elements for the concrete and bar elements for the truss ties and compared service level results to the test data. There was no mention in this paper about ultimate loading FEA using a non-linear approach nor was it stated which FEA package was utilized.

#### **2.2.4 PRECAST PANELS WITH COMPOSITE MATERIALS**

Most research in precast concrete sandwich panels prior to the year 2000 used metal ties and grid structures to connect the concrete wythes together. In the mid to late 2000's to 2010's, the use of FRP composite shear ties with glass fiber and carbon fiber materials were being utilized. This is because the FRP connectors reduce the thermal bridging effect between concrete wythes that is common when metal connectors such as trusses are used. Using FRP exterior plates is not a common application for precast concrete sandwich panels. The intention in this research study is to determine if there is any strength increase to the panels flexural resistance by using exterior bonded FRP plates. One of the latest and most successful sandwich panel research studies using composite materials as a constituent material is the precast, prestressed concrete sandwich wall panel with CFRP shear grid connectors tested and published in the Spring 2011 PCI Journal by Frankl, et al<sup>(21)</sup>. Here the panels were configured as vertical wall elements and had both gravity and lateral loading applied to them. The panels showed high degrees of composite action using the CFRP grid shear connectors; however the degree of composite action varied with the quantity and configuration of the shear grid connectors. The use of composite materials is proving to be both a benefit for thermal resistance and strength in flexural towards complete composite action of the assembly.

## 2.3 WYTHE CONNECTORS

There are a number of various wythe connectors on the market today both proprietary and non-proprietary. From research review it appears that no specific wythe shear connector, including no connector at all or the use of solid zones of concrete, has been established as the industry preferred design. Wythe connectors can provide tensile strength when lifting the concrete panel out of the form bed and in fully- or partially-composite type walls they are used to resist in-plane shear caused by out-of-plane flexure. Panels may use solid zones of concrete or the mechanical wythe connectors to provide composite action to ensure this composite mechanism. This dissertation will focus on the analysis and research of composite and partially composite panels and exclude any design studies on non-composite panels.

Several common shear connectors used in concrete sandwich panel construction are shown in Figure 8 a specifically the C-Grid©, P-24 Delta Tie and M-Ties are included. The FRP shear connectors developed and tested in this study most nearly resemble the P-24 Delt Tie which is the glass reinforced fiber truss tie all the way to the left in Figure 8. It primarily uses interlocking with concrete as its bond strength to develop the composite action.

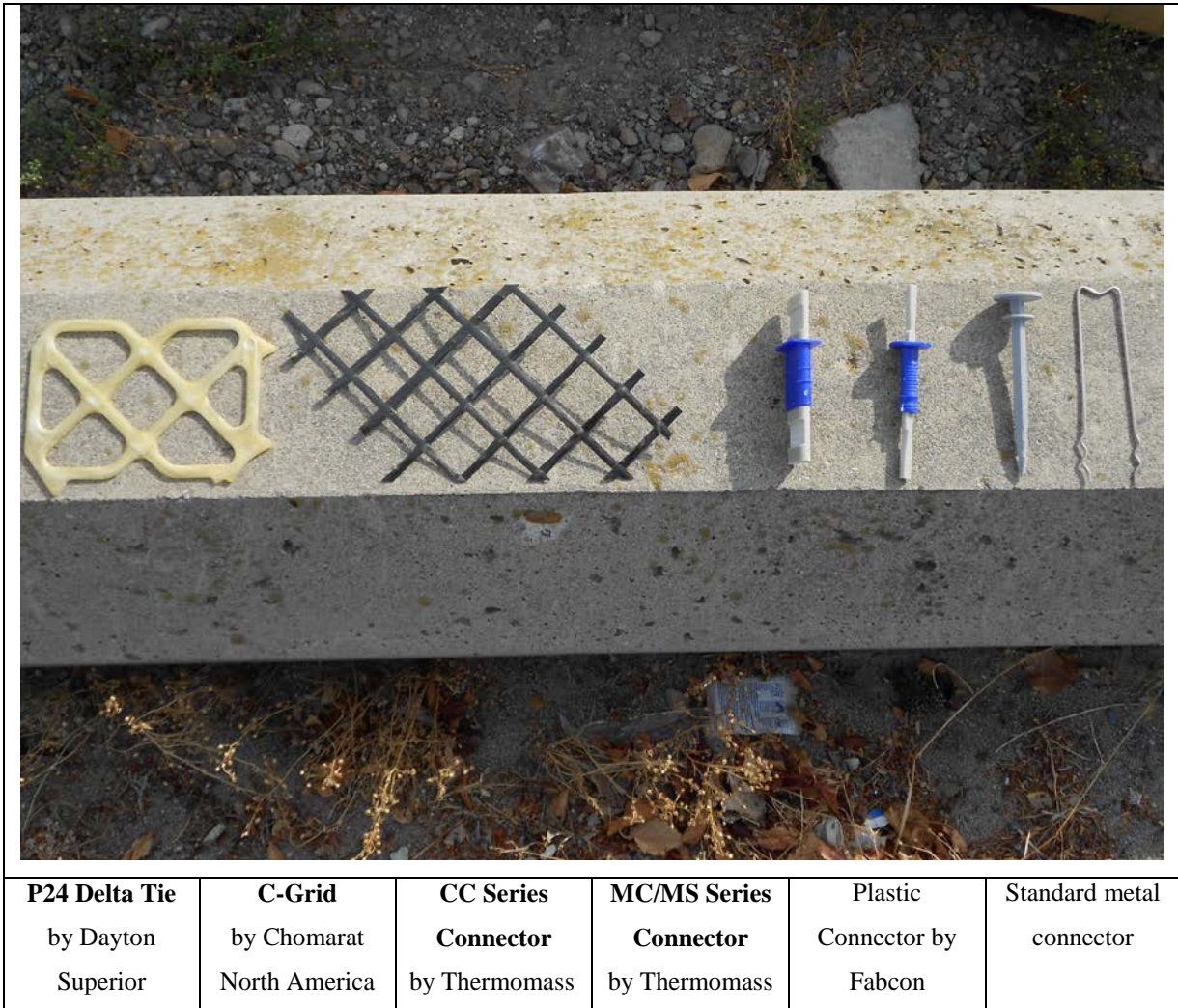


Figure 8 – FRP truss wythe connectors

## 2.4 COMPOSITE BONDING WITH CONCRETE

The internal shear ties whether they be metal trusses, M-Ties, P-24 Delta Ties, CFRP or FRP composite grids or webs almost exclusively rely on mechanical bond with the concrete wythes. Just as with deformed reinforcing steel, there is some degree of chemical or friction at the surface of the two components, however once under even small amount of load will debond due to Poisson's effect and thus the remaining bond is the mechanical interlocking. With composite ties such as those shown in Figure 8, the open webs allow for concrete to flow through during fabrication and that provides the mechanical bond. The better the bond that can be provided, the higher the degree of composite action in the panel can be obtained. Further in this study, various types of mechanical interlocking shall be displayed in an attempt to capture the most efficient structural behavior and the highest degree of composite action.

## 2.5 PERCENTAGE OF COMPOSITE ACTION IN PANEL

The percentage of composite action that a sandwich panel can exhibit is an important engineering design parameter. In some cases the panel can be conservatively considered noncomposite and only one of the outer wythes is used for the axial and flexural load carrying capacity. In many cases the sandwich panel which contains a concrete wythe on each side connected with some form of shear tie will exhibit a percentage of composite. Successful sandwich panel design and construction depends on the correlation between the structural behavior of the panel and the intended design.<sup>[45]</sup> There have been several variations in the calculation of the degree or percent of composite action, composite moment and/or composite flexural stiffness.

Bush and Stine<sup>[16]</sup> used the calculated moments from the panel by using the section modulus and the average strain difference and determined the following formula for percent composite moment:

$$M_{com} = \frac{[M_{ext} - (M_{tw} + M_{bw})]}{M_{ext}} \times 100 \quad [16]$$

where

$M_{com}$  = percent of composite moment

$M_{ext}$  = external moment at midspan of panel,  $wl^2/8$

$M_{tw,bw}$  = internal noncomposite moment on top or bottom wythe =  $SE_c\varepsilon$

$S$  = section modulus of single uncracked wythe

$E_c$  = modulus of elasticity of concrete

$\varepsilon$  = average strain difference at outer faces of wythe, as determined from test data

**Table 3 – DCA equation summary**

Reference	DCA Equation
Bush & Stine <sup>[16]</sup> 1994	$M_{com} = \frac{[M_{ext} - (M_{tw} + M_{bw})]}{M_{ext}} \times 100$
Pessicki & Lee <sup>[35]</sup>	$\kappa = \frac{I_{exp} - I_{nc}}{I_c - I_{nc}} (100)$
Frankl, Lucier, Hassan & Rizkalla <sup>[21]</sup>	$k = \frac{\Delta_{noncomposite} - \Delta_{experimental}}{\Delta_{noncomposite} - \Delta_{composite}} (100)$

### 2.5.1 NONCOMPOSITE ACTION

In precast concrete sandwich panel analysis, design and construction noncomposite panels are considered to have two wythes of concrete minimum that do not act dependent on one another. Usually in these types of designs there is a larger structural concrete wythe that provides all of the structural integrity and the nonstructural wythe is the exterior and thinner weathering layer.

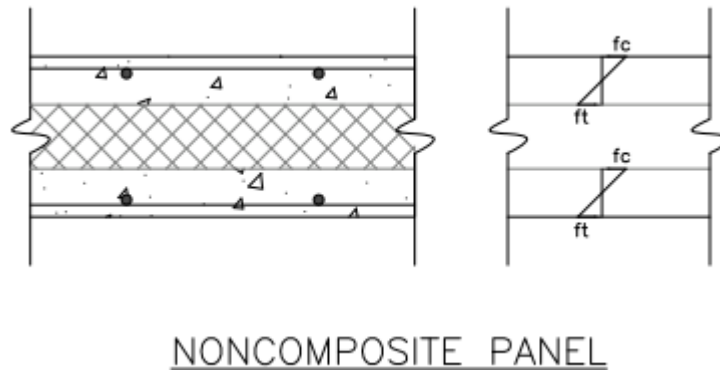
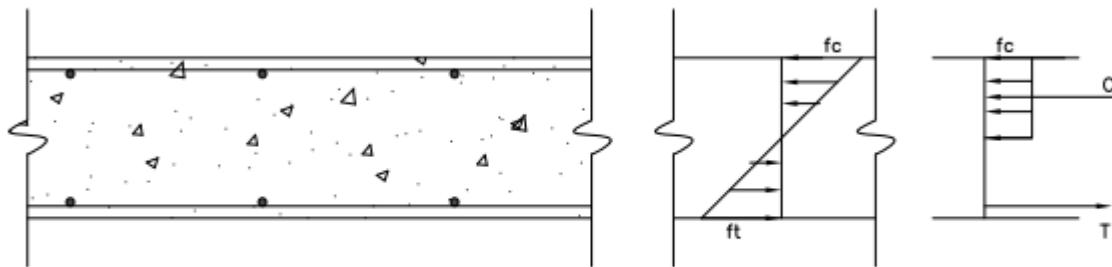


**Figure 9 – Stress distribution of a noncomposite panel**

### 2.5.2 FULLY COMPOSITE ACTION

Full composite action is defined as when the two outer wythes act in unison to provide flexural strength in the panel. The shear ties between the wythes must be designed and constructed so that there is full shear transfer between outer wythes. The baseline full composite concrete panel would be one with sufficient reinforcing steel and no insulation layer as shown in Figure 10. The stress distribution in this type of panel due to flexural forces will have the ideal linear change from compressive stress at one extreme fiber to tensile stress at the opposite extreme fiber. However, even then, ACI has defined equivalent stress balance equations that allow the tension side to be supported by the reinforcing steel and then on the compression side the combination of the concrete and steel is used to develop a resulting compressive force. At different stages of the loading of the panel, it will be either be more fully composite or become partially composite. The purposes of this study the reinforced concrete panel shall be considered the baseline fully composite panel.



### FULL COMPOSITE PANEL

Figure 10 – Stress distribution of a fully composite panel

### 2.5.3 PARTIALLY COMPOSITE ACTION

Partial composite action will have the insulation layer in the sandwich panel and the two outer wythes will be connected with shear ties. The design does provide some degree of composite action, however when compared to the solid concrete panel, it will not be considered fully composite. The advantage is the insulation layer provides the thermal barrier required in the building construction, the thermal bridge is severed if composite shear ties are utilized, and there is less concrete used due to the insulation layer which helps with shipping, erection and other design considerations. One type of configuration and the stress distribution for a partial composite panel is shown in Figure 11.

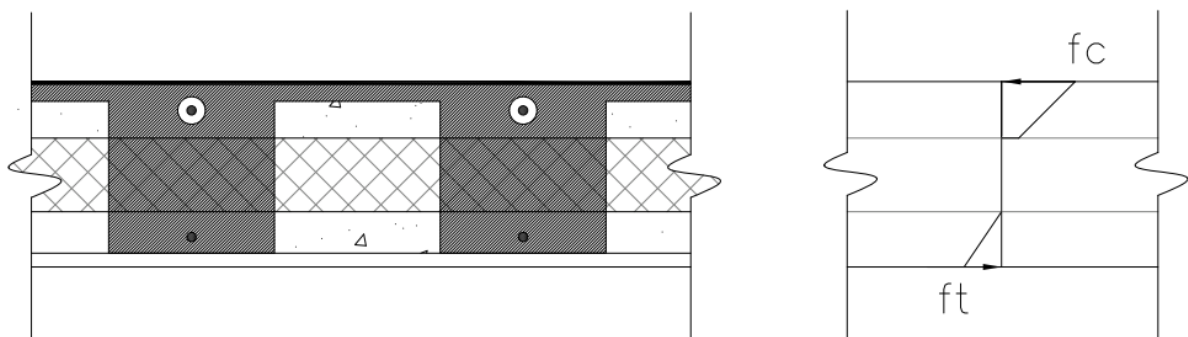


Figure 11 – Stress distribution of a partial composite panel

### 2.6 BLAST RESISTANCE OF CONCRETE SANDWICH PANELS

As previously mentioned, reinforced concrete has been extensively researched, tested and used as a building material for blast resistance since the 1960's. Quantitative research and testing has been developed over the past several decades to provide engineers blast load parameters and methods for

calculating dynamic response of structural elements.<sup>(52)</sup> What is lacking in the UFC 3-340-02 manual is any extensive design guidelines or research on sandwich panels used a load bearing structural component that also can provide blast protection. It is the opinion of this author that precast concrete sandwich panels provide both the required insulation properties and load carrying capacity and should be further studied and tested to determine the suitability for these panels to be used as blast mitigation and blast resistant structures. The panels are comprised of laced components of FRP shear ties and reinforcing steel to maintain fragment control. Integrity of the concrete between top and bottom withes is maintained with the FRP shear ties and the panel can provide better ductility and energy dissipation than actual solid concrete. All of these statements are based on limited experimental test data containing static test specimens; however experience gained from the static testing and reviewing the finite element analysis leads to confidence in further developing these design function.

## 2.7 LITERATURE REVIEW CONCLUSIONS

Existing available research for insulated concrete panels has been collected and studied and will be used, when applicable, to further develop the conclusions in this report. Existing equations and methods for determining the degree of composite action shall be utilized and the available methods and documentation for performing nonlinear finite element analysis on concrete structures. Unlike past researchers such as Pessicki<sup>[34][35]</sup>, Bush<sup>[14][16]</sup>, Frankl<sup>[21]</sup>, this study shall utilize FRP plates as shear connectors cut from commercially available products and also develop exterior membrane FRP plate applications utilized for both strength and durability. Unlike open web trusses, these FRP plates shall be solid with holes for concrete and reinforcing steel anchorage in order to develop better mechanical bonds and higher degree of composite action.

Dating back to the 1970's there have been nonlinear concrete numerical models developed<sup>[24]</sup> based on crack growth theory, and these early concepts have been improved with subsequent research<sup>[43][28][54]</sup> to what is current used today as Damaged Plasticity in Concrete in ABAQUS. The FE models presented in this study have used these models and numerical theories and by executing an explicit analysis in this study rather than an implicit analysis, the results show good correlation with excellent insight.

Analytical creep models for concrete are available and there appears to be several documented equations and power law models for concrete materials. There is lack of available research for numerical modeling and subroutine programs in ABAQUS for concrete structures and the focus in this study shall be to provide a starting point for this subroutine.

# **CHAPTER 3: BENDING BEHAVIOR OF PRECAST CONCRETE SANDWICH PANELS WITH CFRP SHEAR GRID**

## **3.1 INTRODUCTION**

The test and analysis results presented in this section are to provide the reader and understanding of the background to the research that is the focus of this dissertation. The test panel presented in this chapter was originally constructed for use as a vertical wall element. The panel was tested in out-of-plane flexure and the results showed promise that the panel could be used as a horizontal structural element. The shear connectors used in this panel are proprietary and fully tested engineering properties could not be obtained from the manufacturer. The only properties that were provided were the Poisson's Ratio, Material Density, Young's Modulus and ultimate tensile strength. A nonlinear finite element analysis model will require the stress strain distribution of the material in a standard tensile test. Therefore the results presented are to show how a typical sandwich panel , when subjected to flexural out-of-plane loading, can provide suitable deflection and strength requirements.

## **3.2 EXPERIMENTAL INVESTIGATION**

Central Pre-Mix Prestress Co. had in September, 2011 a composite precast concrete panel that was tested by the author, with the assistance of the manufacturing facility, to failure. This particular panel was rejected on site by an architect and bore no known defects or problems. The panel was constructed as shown in Figure 12 and in accordance with ACI and PCI specifications. The panel was approximately 10'x23'x0'-10" and it presented a unique opportunity to the author to test a full scale precast concrete panel while developing a finite element analysis model to be used in future design work.

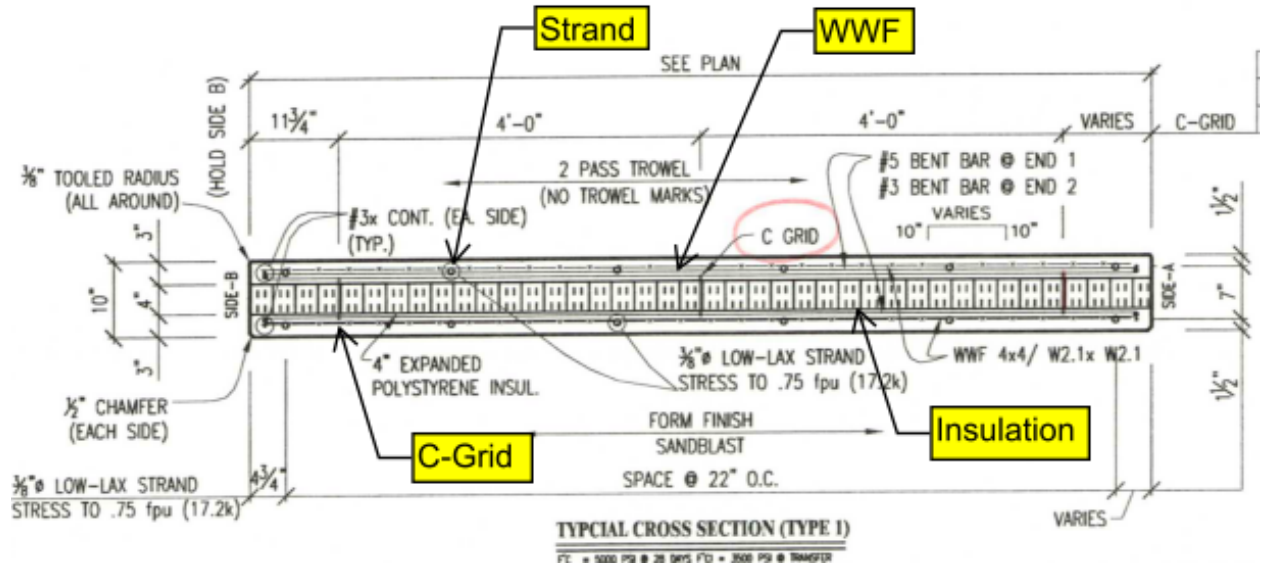


Figure 12 – Typical Cross Section of Composite Panel

### 3.3 MATERIALS

The composite concrete and insulated panel is comprised of (2) 3-inch reinforced concrete panels, (1) 4-inch polystyrene insulated interior panel and (3) rows of C-Grid CFRP. At first, the FE model in this study utilized all properties with exception to the insulation. Other documented research<sup>[16][34][35]</sup> shows that the insulation plays a small role in the initial stages of flexural loading by providing additional composite action strength. Then the frictional bond breaks between the concrete and insulation wythe and slippage occurs. The modeling results presented at the NW SEA conference in 2011<sup>[27]</sup> had a FE model with no insulation materials. The latest FE model did however include the insulation plus all constituent materials such as every wire truss grid and the prestress strand. Both of these models are presented here in this report.

The engineering properties for the proprietary material C-Grid which is a CFRP thin truss structure is shown in Figure 13.

Table 1: C-GRID mechanical properties

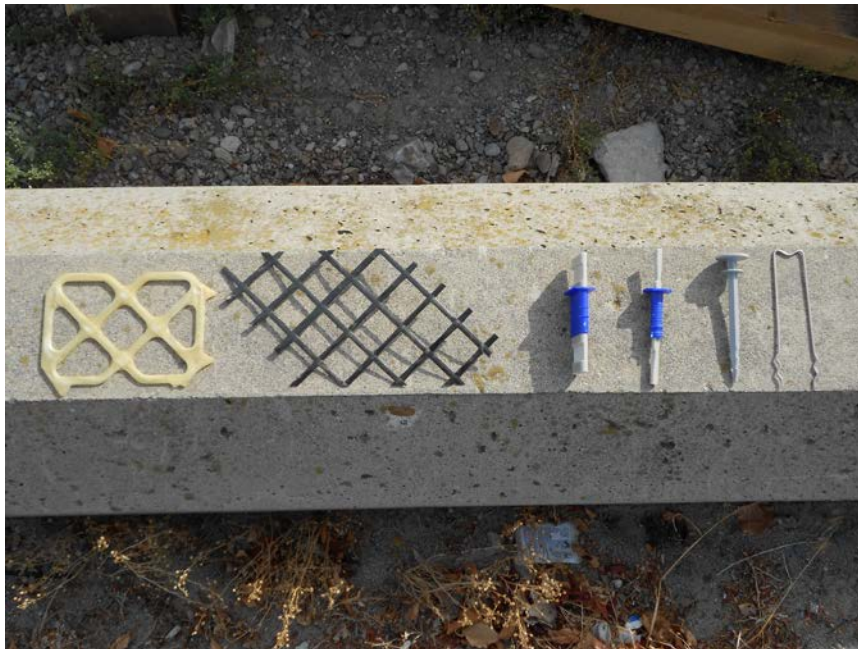
C-GRID Type	Longitudinal Properties				Transverse Properties			
	$A_{C-GRID}$ in <sup>2</sup> /ft (mm <sup>2</sup> /m)	$f_{y,C-GRID}$ ksi/ft (GPa/m)	$E_{C-GRID}$ ksi (GPa)	$\epsilon_{f_y,C-GRID}$ %	$A_{C-GRID}$ in <sup>2</sup> /ft (mm <sup>2</sup> /m)	$f_{y,C-GRID}$ ksi/ft (GPa/m)	$E_{C-GRID}$ ksi (GPa)	$\epsilon_{f_y,C-GRID}$ %
C100 – 3.54 × 3.54	0.019390 (41.04)	290 (2.00)	30,800 (205)	0.94	0.019390 (41.04)	290 (2.00)	30,800 (205)	0.94
C50 – 3.54 × 4.0	0.009695 (20.52)	290 (2.00)	30,800 (205)	0.94	0.008580 (18.16)	255 (1.76)	27,000 (180)	0.94
C50 – 2.36 × 4.0	0.014542 (30.78)	290 (2.00)	30,800 (205)	0.94	0.008580 (18.16)	255 (1.76)	27,000 (180)	0.94
C50 – 2.95 × 2.95	0.011634 (24.63)	290 (2.00)	30,800 (205)	0.94	0.011634 (24.63)	255 (1.76)	27,000 (180)	0.94
C50 – 2.36 × 2.36	0.014542 (30.78)	290 (2.00)	30,800 (205)	0.94	0.014542 (30.78)	255 (1.76)	27,000 (180)	0.94
C50 – 1.8 × 1.6	0.019390 (41.04)	290 (2.00)	38,000 (253)	0.76	0.021450 (45.40)	255 (1.76)	27,000 (180)	0.76
C50 – $\emptyset$ × 2.7	-	-	-	-	0.012711 (26.91)	255 (1.76)	27,000 (180)	0.94
C50 – $\emptyset$ × 4.0	-	-	-	-	0.008580 (18.16)	255 (1.76)	27,000 (180)	0.94
C25 – $\emptyset$ × 2.7	-	-	-	-	0.007461 (15.76)	325 (2.24)	34,600 (231)	0.94
C12 – 1.5 × 1.5	0.005728 (12.12)	325 (2.24)	25,000 (167)	1.3	0.005728 (12.12)	325 (2.24)	27,000 (180)	1.2

Figure 13 – C-Grid Mechanical Properties from Blue Ridge Design, Inc.

The precast insulated panel is assembled on a flat horizontal bed as shown in Figure 14. The materials are assembled prior to the pour and the prestressing strand is stressed. For this particular panel C-Grid was installed between the concrete wythes to create some degree of composite action. Based on the vendor's website the C-Grid is supposed to place at certain distances or spacing to achieve a certain degree of composite action. The C-Grid is merely placed in the form and the concrete, when poured, shall interlock between openings in the C-Grid truss elements. Other research has shown that when using the wire trusses or in this case C-Grid trusses, concrete paste will creep up into the insulation layer creating further complexities at that interface which will be hard to model numerically. Other panels may use similar forms of wythe ties such as the P-24 Delta ties and the M-Tie by Dayton Superior. Some of these other ties are shown in Figure 15.



**Figure 14 – Composite Panel Production Prior to Pour**



**Figure 15 – C-Grid Materials and Ties Used in Production**

### 3.4 FULL SCALE TESTING

The test panel was laid down flatwise and supported on two 6x6 wood blocks as shown in Figure 16. The loading applied consisted of precast concrete ecology blocks each weighing approximately 3,400 lbs.

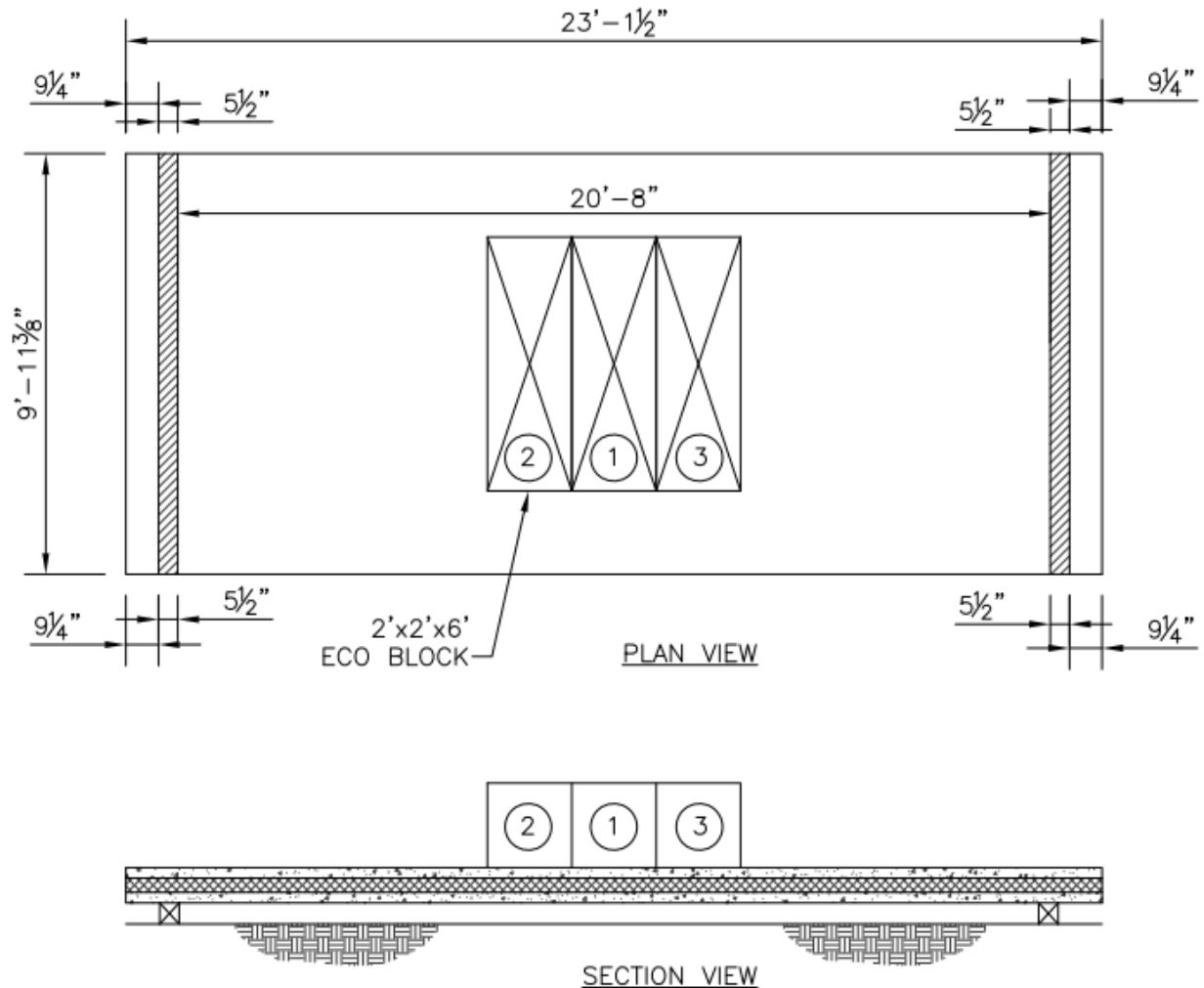


**Figure 16 - Test Panel Setup**

Using a hydraulic load test cell would have been ideal, however was not within the scope of the budget nor readily available. Instead the blocks were carefully and strategically placed on the panel as shown in Figure 17, one by one with an approximate 10 minute time gap between block placement. Deflection and load recordings were taken between each block added. Both survey equipment measurement and a dial gauge was used for deflection recordings. The blocks were later weighed individually to obtain their exact weight.



**Figure 17 – Final Load Placement**

The data was recorded as shown in Table 4 and the total load placed on the panel was 21,100 lbs. The final deflection at the end of the test when all 7 blocks were added was 1.5625". The load was left in place for 4 days and the deflection increased to 2.75" when a final measurement was recorded. Then the blocks were removed and the panel was placed upright for inspection. Following release of the blocks the panel rebounded to a deflection of 1.375", which means it recovered approximately 1.375" of elastic deflection and retained 1.375" of plastic or permanent deflection. The Summary of the loading, deflections and an equivalent pressure load is shown in Table 4. The service moment is derived by back-calculating the flexural moment from the deflection and corresponding load and it does include the self-weight of the panel. The service pressure is the applied load divided by the entire area of the panel.

If the deflection criteria of an acceptable roof panel is  $L/360$  and the panel is approximately 23 feet in span length, then the critical service deflection value is approximately 0.76 inches. From Table 4 the 5 block added created a deflection of approximately 0.625 inches, which corresponds to  $L/440$ , and the service pressure load can be deduced to 70.0 psf. If this panel were to be installed in a southern U.S. climate region where the snow load is typically 10 psf minimum and the roof live load is 20 psf, then the panel could theoretically support an additional 50 psf of soil or green roof loading.

**Table 4 – Test panel load and deflection data**

Date	Blocks	Block Weight (lbs)	delta (in)	Difference (in)	Deflection (in)	Load (lbs)	Service Moment M (kip-ft)	Service Pressure Load (psf)
9/2/2011	none	0	0		0.0000	0	39.4	0.0
	1	3400	1/16	1/16	0.0625	3400	56.8	14.8
	2	3400	2/16	1/16	0.1250	6800	74.2	29.6
	3	3450	4/16	2/16	0.2500	10250	91.9	44.6
	4	3400	7/16	3/16	0.4375	13650	109.4	59.3
	5	2440	10/16	3/16	0.6250	16090	121.9	70.0
	6	2570	1 2/16	8/16	1.1250	18660	135.0	81.1
	7	2440	1 9/16	7/16	1.5625	21100	147.5	91.7
9/6/2011			2 12/16	1 3/16	2.7500	21100	147.5	91.7
9/9/2011			1 6/16	1 6/16	1.3750	0	39.4	0.0

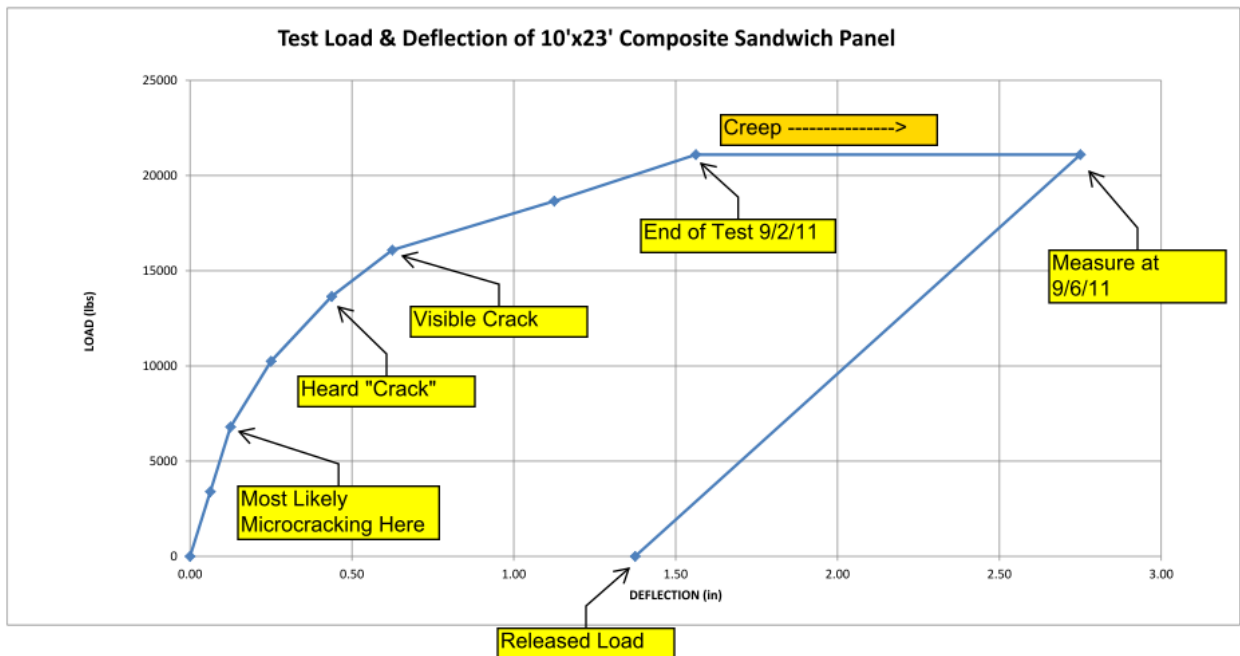


Figure 18 – Load deflection curve for test panel

The test data was plotted and a Load vs. Deflection curve was created as shown in Figure 18. The curve jumps up quickly due to the large and heavy blocks added to the panel, nevertheless a linear and nonlinear curve can be recognized. Each node on the curve represents a block added to the panel and then in the case of the creep the load was sustained. Up to about block 2 the curve is linear and the concrete is most likely uncracked. Then it is assumed micocracking has begun as the curve begins to go nonlinear. We heard a crack at block 4 and the visible cracks were seen at block 5. Refer to the chart in Table 4 for accumulated weight as blocks were added. The completion of the loading was at 21,100 lbs and concluded on 9/2/11. The load was left in place and then the deflection was recorded again on 9/6/11; however complete failure still had not occurred. The load was released and final plastic deformation was recorded.

The concrete wythes definitely cracked and the concrete in the top wythe began to have tensile splitting failures due to the over loading of the concrete by the radial tensile forces developed outward from the press-stress strand. This phenomenon is shown in Figure 19. The tensile stresses radiating outward from the prestress strand cause the splitting tensile crack to develop in the concrete. These types of cracks are difficult to predict and to simulate in a FE program. The engineer must be mindful of this type of possible failure not just when design a precast panel, but also when placing post-installed anchors in concrete which have been known to cause similar affects.



**Figure 19 – Top Layer of Longitudinal Pre-stressing Strand Splitting Failure**

The bottom concrete wythe had near uniform and symmetrical transverse cracks as shown in Figure 20. These cracks were most likely the ones that we heard during the test. We never did hear nor confirm that we heard popping of the anchorage of the C-Grid and it is unknown if that ever occurred.

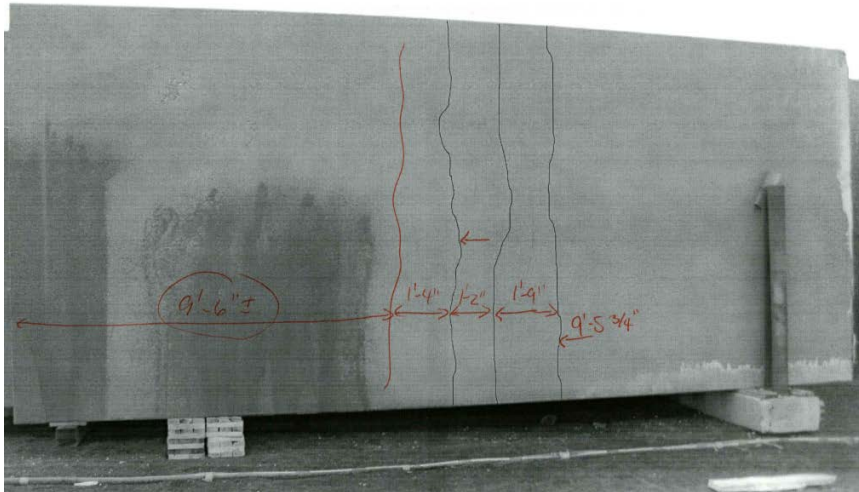


**Figure 20 – Uniform and Symmetrical Bottom Transverse Cracks**

Although a strain gage was not placed on the panel and recordings were not taken to determine composite action, it is believed that the C-Grid was acting compositely with the concrete wythes. Complete failure never occurred and the concrete was cracked; therefore the continuous transfer of tension to compression forces in the bending section of the panel was maintained by the C-Grid. Other research<sup>[34]</sup> shows that the polystyrene insulation would also have provided additional shear resistance in transferring those compression and tension coupling forces.

<h2>Test vs. Analytical</h2>	
<u>Analytical Results</u>	
Cracking Moment of Inertia:	$I_{cr} = 220 \text{ in}^4$
Cracking Moment:	$M_{cr} = 111 \text{ kip-ft}$
Cracking Service Load:	$P_{cr} = 8.8 \text{ kips (Btwn Block 2 and 3)}$
<u>Test Results</u>	
Cracking Moment:	$M_{cr} \sim 90 \text{ kip-ft}$
Cracking Service Load:	$P_{cr} = \text{Between Block 2 and 3} \sim 9\text{K}$

**Figure 21 – Test vs. Analytical Results for Cracking**

The ultimate strength design calculations are difficult to determine due to the nonlinear nature of the panel under cracking loads, however up to the onset of cracking is fairly easy to determine since it's still in the linear range of the material. Figure 21 shows the comparison between the analytical

calculations and the test results with good correlation. These calculations are shown in further detail in Appendix B. When reviewing the values in Figure 18, it shows that between block 2 and 3 the curve becomes nonlinear. Therefore the critical cracking service load ( $P_{cr}$ ) is approximately 9 kips, which correlates to a cracking moment ( $M_{cr}$ ) of about 90 kip-ft. To check this value by hand the cracking moment is determined from ACI 318 Eqn. 9-9 as follows:

$$M_{cr} = \frac{f_r I_{gt}}{h - y_t}$$

Where,  $I_{gt}$  is the transformed gross moment of inertia,  $f_r$  is the modulus of rupture,  $h$  is the depth of the beam section and  $y_t$  is the centroid distance measured from the top. The critical cracking load ( $P_{cr}$ ) is then back-calculated from the critical moment by using classical simply supported beam equations. These checks are used to verify the FE model up to a certain point on the load versus deflection curve. After the curve begins to experience some non-linearity the remainder of the flexural strength shall be determined by using a nonlinear finite element analysis.

### 3.5 DISCUSSIONS AND RECOMMENDATIONS

The 10"x10'x23' precast concrete sandwich panel was produced per ACI and PCI specifications to be used as a wall element for a building application. The panel was rejected for architectural reasons and tested at the Central Pre-Mix Prestress plant in Spokane, WA in September 2011 under the supervision of the author. The testing confirmed that the panel could sustain significant out-of-plane loading and when considering a typical roof live load of 20 psf, the panel could support an additional 30 psf and still be within service deflection criterion per ACI and IBC.

The test results have set the stage for further sandwich panel testing and development and the creation of a new composite panel using solid FRP shear web connectors as will be shown in the following section. Since the composite shear grid connectors in this particular panel are proprietary, no further work or conclusions shall be made on their capabilities and degree of composite action.

Future work for these types of complicated panels is to determine the influence on the strength and stiffness the prestress strands provide. Furthermore the friction between the insulation and the concrete could be studied and finally parametric studies on the use of different shear connector types and configurations.

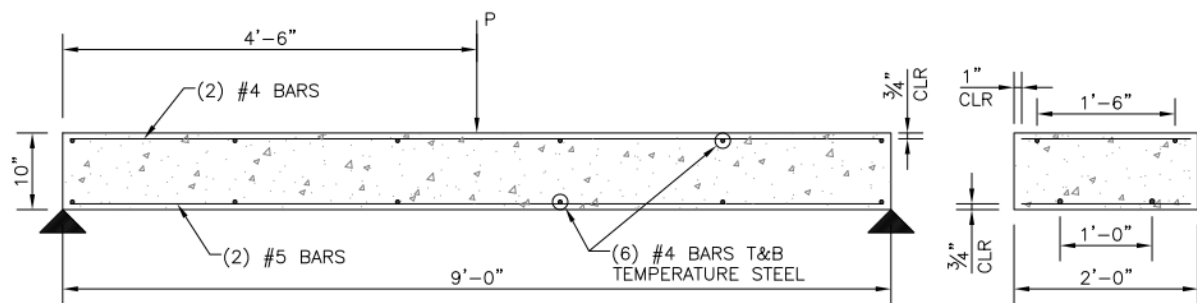
## CHAPTER 4: FINITE ELEMENT ANALYSIS OF FRP- PRECAST CONCRETE SANDWICH PANELS

### 4.1 INTRODUCTION

A set of 10" x 2'-0" x 9'-0" scaled sandwich panels were developed and tested with various configurations of FRP shear connectors. The organization chart for these panels is shown in Figure 5. Two full scale 2'-0" wide by 16'-0" long test panels were also developed and tested based on results from the scaled test panels. These test panels were used to determine the effect the type and configuration of the FRP shear connectors had on the stiffness and strength of concrete sandwich panel type construction. In this chapter, the test panels were numerically modeled using the commercial finite element analysis software package ABAQUS<sup>[1]</sup>. This allowed for nonlinear numerical models to be used to study the post-cracking effects of the concrete sandwich panels and determine modes of failure. In particular, the FEA models utilized the DAMAGED PLASTICITY function in ABAQUS which accounts for the loss in stiffness of the elements in compression and tension when limiting cracking and crushing strains are exceeded.

### 4.2 ANALYTIC MODEL

The finite element analysis results will be compared with the test results and conventional analytic hand calculation models as prescribed by ACI 318<sup>[4]</sup>. The construction, loading and boundary conditions of the 10 inch solid concrete panel are shown in Figure 22. The panel is 10 inches deep, 24 inches wide and simply supported at 9 feet.



**108SOL10L3PTNOFRPS1**

GROUP 1 AND 2 (DO NOT SCALE)

**Figure 22 – 10 inch solid concrete panel**

The panel is subjected to 3-point bending with a concentrated load at the mid span of the beam. The panel will be analyzed as a flexural member. The flexural strength, service and factored moments, the deflection and the deflection limit, all per ACI 318 requirements, are shown in Table 5. Only the solid concrete panel's strength and stiffness was calculated per ACI 318 formulas, as the sandwich panels become cumbersome and difficult to obtain accurate values of strength and deflection per conventional formulas. There are limitations even when determining the full strength of the solid concrete panel when using ACI formulas alone as can be shown in Figure 76. In this figure the test results, the FEA results and the ACI 318 results are shown and compared on one graph. The ACI strength plot does not capture the post-cracking nonlinear strength of the reinforced concrete member.

Table 5 – Analytical results for 10 inch solid concrete panel

Solid Concrete 10 inch scale test panel							
108SOL10L3PTNOFRPS1							
Span =	9	ft					
Height =	10	inches					
Width =	24	inches					
Point Load	Service Moment	Selfweight Moment	Total Service	Total Factored	Flexural Strength	Service	ACI Limit
P (kips)	$M_L$ (kip-ft)	$M_{sw}$ (kip-ft)	Moment	Moment	Moment	Deflection	L/480
			M (kip-ft)	$M_u$ (kip-ft)	$\phi M_n$ (kip-ft)	$\Delta$ (in)	
1	2.25	2.53	4.78	6.64	24.8	0.0002397	0.225
2	4.5	2.53	7.03	10.24	24.8	0.001069	0.225
3	6.75	2.53	9.28	13.84	24.8	0.003129	0.225
4	9	2.53	11.53	17.44	24.8	0.007167	0.225
5	11.25	2.53	13.78	21.04	24.8	0.014	0.225
6	13.5	2.53	16.03	24.64	24.8	0.024	0.225
7	15.75	2.53	18.28	28.24	24.8	0.038	0.225
8	18	2.53	20.53	31.84	24.8	0.056	0.225
9	20.25	2.53	22.78	35.44	24.8	0.078	0.225
10	22.5	2.53	25.03	39.04	24.8	0.103	0.225
11	24.75	2.53	27.28	42.64	24.8	0.13	0.225
12	27	2.53	29.53	46.24	24.8	0.16	0.225
13	29.25	2.53	31.78	49.84	24.8	0.19	0.225
14	31.5	2.53	34.03	53.44	24.8	0.222	0.225
15	33.75	2.53	36.28	57.04	24.8	0.254	0.225
16	36	2.53	38.53	60.64	24.8	0.287	0.225
17	38.25	2.53	40.78	64.24	24.8	0.319	0.225
18	40.5	2.53	43.03	67.84	24.8	0.351	0.225
19	42.75	2.53	45.28	71.44	24.8	0.382	0.225
20	45	2.53	47.53	75.04	24.8	0.413	0.225

In Table 5 the total service flexural moment ( $M$ ) and the factored flexural moment ( $M_u$ ) are derived using the formulas and load combinations in ACI 318. The governing load combination is  $1.2D+1.6L$ . The concrete panel's flexural capacity/strength ( $\phi M_n$ ) does not change and is approximately 24.8 kip-ft. Table 5 shows at which point the flexural capacity is no longer greater than the factored moment and that value occurs at approximately 6 kips of loading. It should be noted that the panel was tested to almost 20 kips of load and that is shown in Figure 76. Furthermore, if the limit on the deflection is taken to be  $L/480$  per ACI 318 Table 9.5(b) then the limit deflection for this span is 0.225 inches and that is analytically achieved at approximately 14 kips of load. The graph in Figure 76 shows that the concrete panel response is linear up to about 6-8 kips of load, then a bit more nonlinear to about 15 kips of load, where the curve tends to go more horizontal due to a high nonlinear response. The summary presented in this particular section is if the panel were designed per hand calculations alone based on ACI 318 formulas, the limitation would be

1/3 of what the panel is truly capable of. At 6,000 lbs of load the equivalent live load uniform pressure on the panel would be approximately 200 psf. At 10,000 lbs the approximate equivalent live load pressure is 300 psf, at 15,000 lbs it is 475 psf and at 20,000 lbs the approximate equivalent live load pressure is 600 psf. These numbers are presented to give a rough idea of the magnitude of the loading and the strength of the panel. Normal roof top loading is far less than 200 psf, however the span is only 9 feet so that needs to be taken into consideration.

The equations provided in Appendix D are included to document how the values in Table 5 were achieved. The calculations shown are for a 15,000 lb point load and all formulas are derived from the specification in ACI 318.

### 4.3 FINITE ELEMENT ANALYSIS

#### 4.3.1 MATERIAL PROPERTIES

In order to accurately simulate a concrete insulated sandwich test panel in the finite element analysis model, elastic and inelastic engineering properties are required for the concrete and steel components of the structure. These can be obtained through actual testing of representative samples of the test specimen, acquired by published data, or representative equations provided in published text books.

The EPS insulation was acquired by FMI EPS, LLC and the material specification data sheet is located in Appendix A. Table 6 shows the values used for the finite element analysis modeling in ABAQUS. Note that ABAQUS is a unit-less code and quantities must be specified in consistent format. The FEA models in this study used the United States' units of pounds, inches and seconds. Therefore the units of gravity in ABAQUS must be set to  $386.4 \text{ in/s}^2$ .

**Table 6 – Material properties for insulation**

<b>ASTM C578</b>	<b>Expanded Polystyrene</b>
Mass Density ( $\rho$ )	$2.059 \times 10^{-6} \text{ (lbf s}^2\text{)/in}^4$ (ABAQUS) $1.35 \text{ lb/ft}^3$ ( $22 \text{ kg/m}^3$ )
Young's Modulus (E)	340 psi
Poisson's Ratio ( $\nu$ )	0.3

Compressive strength tests were performed on (4) 6" x 12" concrete cylinders per ASTM C39 and the average compressive strength was calculated. Figure 23 shows the recorded strains for the

cylinder tests. The average compressive strength of the concrete was 4,120 psi with a standard deviation of 426 psi. Table 7 list the pertinent materials properties used for the analysis and strength calculations for the scale test panels.

**Table 7 – Material properties for concrete**

	<b>4120 psi Concrete</b>
Volume Density ( $\gamma$ )	150 lbf/ft <sup>3</sup>
Mass Density ( $\rho$ )	$2.246 \times 10^{-4}$ (lbf s <sup>2</sup> )/in <sup>4</sup>
Young's Modulus (E)	$3.795 \times 10^6$ psi
Poisson's Ratio ( $\nu$ )	0.15
Modulus of Rupture (fr)	412 psi

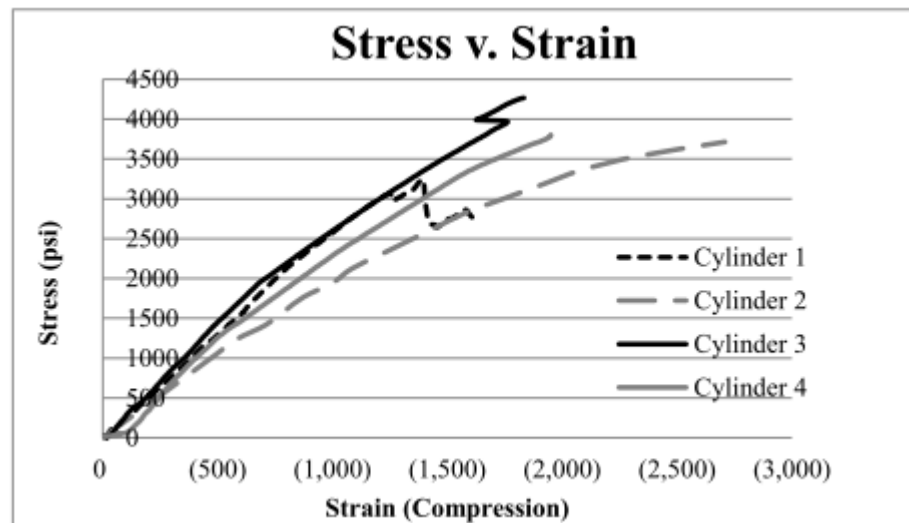


**Figure 23 – Compressive strength of concrete samples**

An example set of test data for one of the test cylinders is shown in Figure 24 where a 6" diameter by 12" tall concrete cylinder sample was obtained during the initial pour of the scaled test panels in November, 2012 and tested at the 28-day time interval at Washington State University testing labs. The cylinders were tested in accordance with ASTM C39 for compressive strength and the static modulus of elasticity and Poisson's ratio of the concrete in compression was obtained in accordance with ASTM C469/C469M-10 (2010).

Sample type (6"x 12" cylinder)	Date	12/13/2012		
Loading force (lbs.)	1st Reading	2nd Reading	Strain	Stress
0	0	0	0	0
5000	0.0005	0.001	4.16667E-05	176.8388
10000	0.002	0.002	8.33333E-05	353.6777
15000	0.003	0.003	0.000125	530.5165
20000	0.0035	0.004	0.000166667	707.3553
25000	0.005	0.005	0.000208333	884.1941
30000	0.006	0.006	0.00025	1061.033
35000	0.0075	0.007	0.000291667	1237.872
40000	0.0085	0.0085	0.000354167	1414.711
45000		0.0095	0.000395833	1591.549
50000		0.0105	0.0004375	1768.388
55000		0.012	0.0005	1945.227
60000		0.013	0.000541667	2122.066
65000		0.0145	0.000604167	2298.905
70000		0.016	0.000666667	2475.744
75000		0.0175	0.000729167	2652.582
80000		0.019	0.000791667	2829.421
85000		0.021	0.000875	3006.26
90000		0.023	0.000958333	3183.099
95000		0.025	0.001041667	3359.938
100000		0.028	0.001166667	3536.777
105000		0.0325	0.001354167	3713.615
<b>ASTM C469 Std Test Method for Static Modulus of Elasticity and Poisson's Ratio of Concrete</b>				
Length of Cylinder	12	in		
Diameter of Cylinder	6	in		
Ultimate load	106182	106182		
40% Ultimate load	42472.8	42472.8		
nearest 40% load S2	40000	40000		
40% Ultimate load strain E2	0.00035417	0.000354167		
5*10-5 strain load S1	5000	5000		
5*10-5 strain E1 (Reading/2/12)*	2.0833E-05	4.16667E-05		
Young's modulus(psi)	3713615.34	3961189.695		
Young's Modulus (final)	Ec =	3837403	psi	
Compressive Strength:	f'c =	3755.42	psi	

Figure 24 – Concrete compressive test data

In order to best represent the actual structure in the finite element model, the material properties of the structural elements should be attained prior to every discrete analysis. This is an unrealistic and difficult to task to accomplish each time an engineer wants to design a sandwich panel. Without test

data the estimated concrete material properties can be approximated by the following formulas derived by Mander<sup>[39]</sup>.

The analytical model of the concrete in compression can be best described by:

$$f_c = \frac{f'_{cc} x r}{r - 1 + x'} \quad (4-1)$$

where  $f'_{cc}$  = compressive strength of confined concrete.

$$x = \frac{\varepsilon_c}{\varepsilon_{cc}} \quad (4-2)$$

where  $\varepsilon_c$  = longitudinal compressive concrete strain

$$\varepsilon_{cc} = \varepsilon_{co} \left[ 1 + 5 \left( \frac{f'_{cc}}{f'_{co}} - 1 \right) \right] \quad (4-3)$$

generally  $\varepsilon_{co} = 0.002$  can be assumed, and

$$r = \frac{E_c}{E_c - E_{sec}} \quad (4-4)$$

where

$$E_c = 57,000 \sqrt{f'_{co}} \text{ psi} \quad (4-5)$$

Is the tangent modulus of elasticity of the concrete, and

$$E_{sec} = \frac{f'_{cc}}{\varepsilon_{cc}} \quad (4-6)$$

Although the formulas presented here by Mander<sup>[39]</sup> are for confined concrete only, therefore not a good representation of our test panel. Therefore another model for the concrete properties shall be investigated and use.

To represent the nonlinear material properties of the reinforcing steel we can use the model developed by Menegotto and Pinto<sup>[42]</sup>. The stress-strain properties of the reinforcing steel can be described by the following equation:

$$f_s = \frac{E_s \varepsilon_s}{\left[ 1 + \left( \frac{E_s \varepsilon_s}{f_y} \right)^{20} \right]^{0.05}} + (f_{su} - f_y) \left[ \left( \frac{l - (\varepsilon_{su} - \varepsilon_s)^p}{\varepsilon_{su} - \varepsilon_{sh}} \right)^{20p} + (\varepsilon_{su} - \varepsilon_s)^{20p} \right]^{0.05} \quad (4-7)$$

$$p = E_{sh} \left( \frac{\epsilon_{su} - \epsilon_{sh}}{f_{su} - f_y} \right) \quad (4-8)$$

However, using these formulas proved to be a bit cumbersome and instead a reference was found that contained reinforcing steel stress/strain data for several ASTM designations shown in Figure 25. Lowes<sup>[37]</sup> performed finite element analysis on reinforced concrete beam connections in bridge construction and had data for several grades of reinforcing steel. The ASTM A615 Gr. 60 steel is the closest designation to that which was used in all test panels at the University of Idaho from 2012 to 2013. The stress-strain curve was traced in Excel as shown in Figure 25 and then the engineering stress/strain curve plotted along with the true stress/strain curve is shown in Figure 26. ABAQUS uses the true stress/strain data in their constitutive equations.

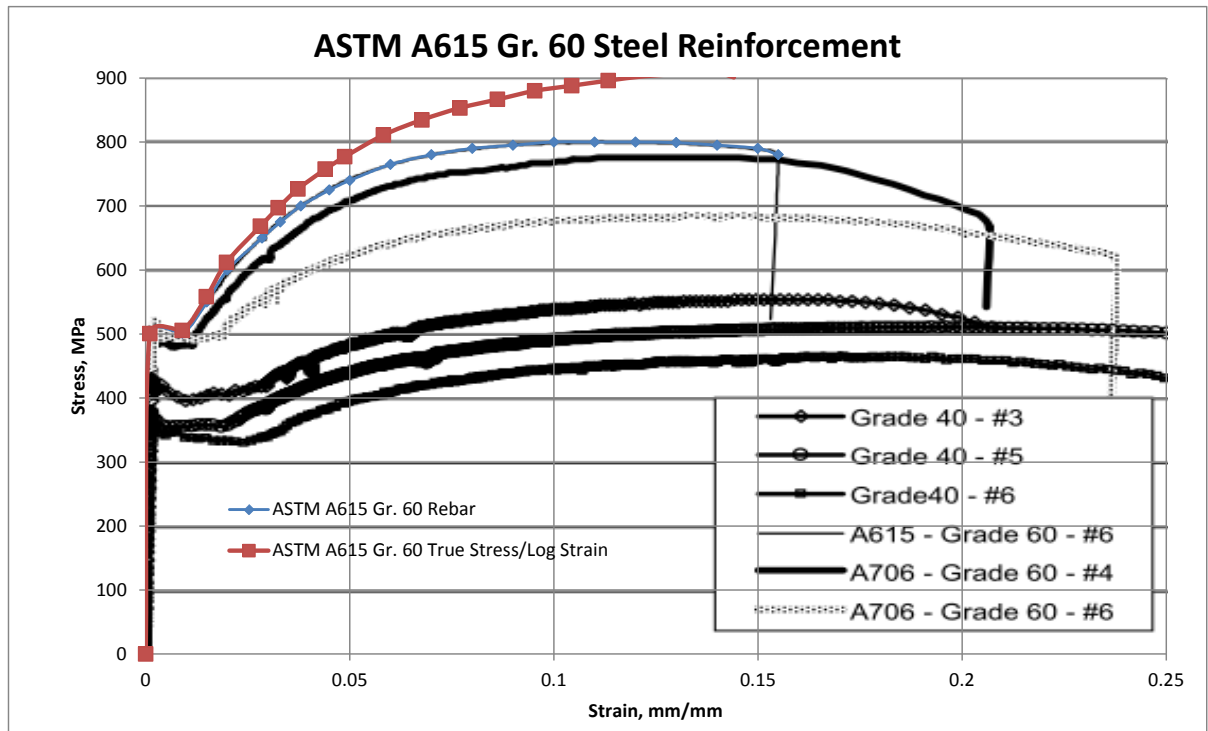


Figure 25 – Stress/Strain data for various reinforcing steel (Ref. Lowes, 1995)<sup>[37]</sup>

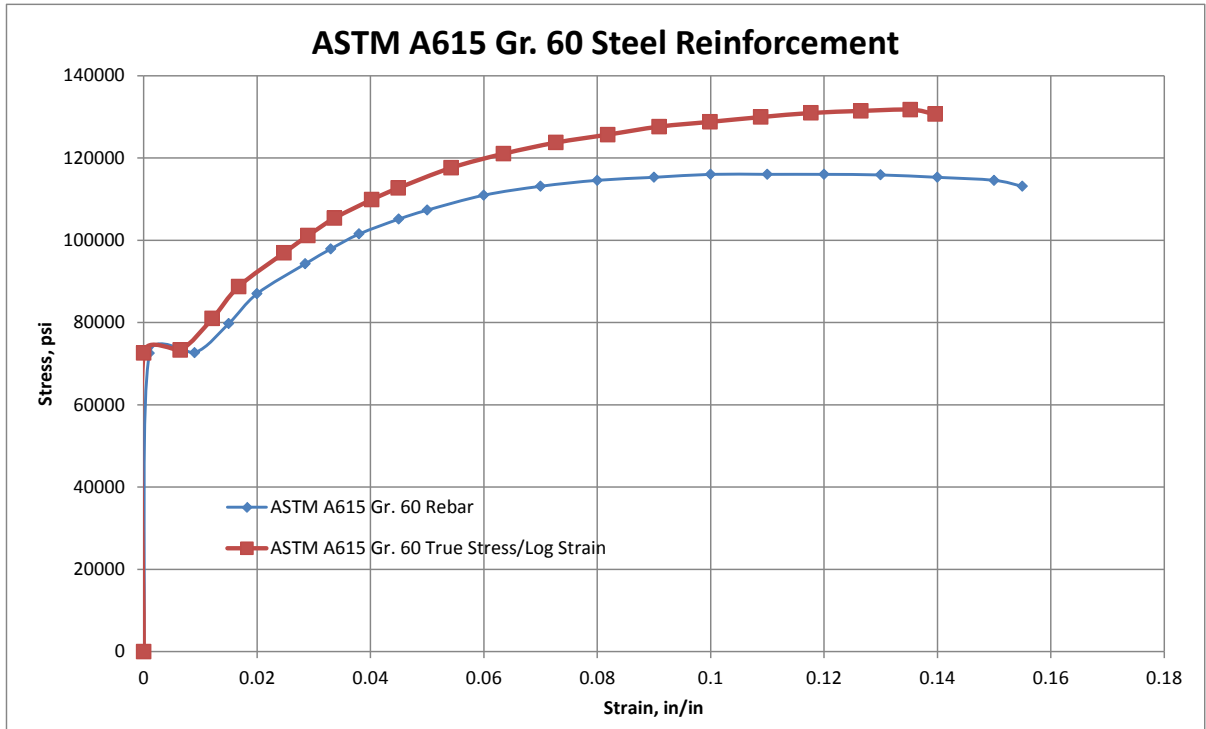


Figure 26 – True stress-strain properties of ASTM A615 Gr. 60 steel

Table 8 – Material properties for reinforcing steel

	ASTM A615 Gr. 60
Mass Density ( $\rho$ )	0.000783 (lbf s <sup>2</sup> )/in <sup>4</sup>
Young's Modulus (E)	29,000,000 psi
Poisson's Ratio ( $\nu$ )	0.3

ABAQUS material definition for metal plasticity is defined in Section 22.2.1 and the “true” stress (Cauchy stress) and logarithmic strain are used. The formulas for the true stress and logarithmic strain are as follows:

$$\sigma_{true} = \sigma_{nom} (1 + \epsilon_{nom}) \quad (4-9)$$

$$\epsilon_{ln}^{pl} = \ln(1 + \epsilon_{nom}) - \frac{\sigma_{true}}{E} \quad (4-10)$$

The values for the engineering stress and strain and true stress and logarithmic strain are shown in Table 9.

**Table 9 – ASTM A615 Gr. 60 reinforcing steel nonlinear material properties**

Eng Stress (psi)	Eng. Strain (%)	Eng Strain (in/in)	True Stress (psi)	Log Pl. Strain (in/in)
0	0	0	0	0
72519	0.1	0.001	72591.52	0
72664.04	0.9	0.009	73318.01	0.006432
79770.9	1.5	0.015	80967.46	0.012097
87022.8	2	0.02	88763.26	0.016742
94274.7	2.85	0.0285	96961.53	0.024758
97900.65	3.3	0.033	101131.4	0.02898
101526.6	3.8	0.038	105384.6	0.033662
105152.6	4.5	0.045	109884.4	0.040228
107328.1	5	0.05	112694.5	0.044904
110954.1	6	0.06	117611.3	0.054213
113129.6	7	0.07	121048.7	0.063485
114580	8	0.08	123746.4	0.072694
115305.2	9	0.09	125682.7	0.081844
116030.4	10	0.1	127633.4	0.090909
116030.4	11	0.11	128793.7	0.099919
116030.4	12	0.12	129954	0.108848
115885.4	13	0.13	130950.5	0.117702
115305.2	14	0.14	131447.9	0.126496
114580	15	0.15	131767	0.135218
113129.6	15.5	0.155	130664.7	0.139595

Table 10 provides the material properties for the FRP shear grid and exterior plates; both of which were provided by CRANE Composites.

Table 10 – FRP material properties

Typical Values			
Property	EATR .085"   2.2 mm		Test Method
Flexural Strength	33 x 10 <sup>3</sup> psi	228 MPa	ASTM - D790
Flexural Modulus	1.0 x 10 <sup>6</sup> psi	6895 MPa	ASTM - D790
Tensile Strength	45 x 10 <sup>3</sup> psi	310 MPa	ASTM - D638
Tensile Modulus	2.0 x 10 <sup>6</sup> psi	13790 MPa	ASTM - D638
Barcol Hardness	45	45	ASTM - D2583
Coefficient of Linear Thermal Expansion	0.8 x 10 <sup>-5</sup> in/in/°F	14 µm/m/°C	ASTM - D696
Thermal Conductivity	0.4 Btu-in/hr-ft <sup>2</sup> °F	5.0 cal-cm/hr-m <sup>2</sup> °C	ASTM - C177
Water Absorption	0.2%/24hrs@77°F	0.2%/24hrs@77°F	ASTM - D570
Specific Gravity	1.75	1.75	ASTM - D792

### 4.3.2 CONCRETE DAMAGED PLASTICITY MODEL

ABAQUS offers three modeling techniques for nonlinear concrete finite element analysis. The first model is called the concrete smeared cracking model, the second plastic analysis model is the concrete damaged plasticity model and the third model is the brittle cracking model.

#### Concrete Smeared Cracking Model

The concrete smeared cracking model was developed by ABAQUS through research work by Crisfield<sup>[19]</sup>, Hillerborg & Petersson<sup>[24]</sup> and Kupfer & Gerstle<sup>[32]</sup>. The model works best for monotonic loading for concrete beams where the compressive strength of the concrete material along with the corresponding plastic strain is incorporated into the analysis model material properties. The concrete smeared cracking model however is limited to use in the ABAQUS/Standard analysis method only, where this particular research study implores the use of an explicit analysis. The concrete smeared cracking model is also a more general model when describing the tensioning stiffening and compressive strain hardening effects of the concrete.

#### Brittle Cracking Model

The brittle cracking model relies heavily on the tensile damage created as the concrete begins to crack and does not account for any of the compressive strain failure mechanisms. If the mode of failure is primarily tensile cracking and the beam is shallow, such as a slab, this model would be an

appropriate model to use for the analysis. However, since there are compressive strain failure mechanisms and strength is influenced by the concrete crushing affect, it's best to use a model that incorporates both tensile and compressive failure modes.

### **Damaged Plasticity Model**

The third model that is available is the concrete damaged plasticity model which was used for the finite element modeling in this study as it incorporated both the compressive and tensile properties of the concrete material. The corresponding stiffness degradation values, or damage parameters, could also be used with the damaged plasticity model and this particular model takes into account tension stiffening. The concrete damaged plasticity model is best used for concrete specimens that would experience cyclic loading as the material properties allow for stiffness recovery as cracks close and open for both tensile and compressive values. This study does not perform cyclic loading, however it was also recommended by ABAQUS<sup>[1]</sup> to utilize this model for concrete flexural member analyses, which suits the study well. The most important benefit of this model is the use of quasi-static analysis and quasi-brittle materials. This is the specific reason for using the damaged plasticity model to take advantage of the quasi-static analysis using the explicit solver.

The concrete damaged plasticity model was developed by ABAQUS based on research by Lubliner et al<sup>[38]</sup> and Lee & Fenves<sup>[33]</sup>. Although the test panels in this study are not cyclically loaded, the capturing of stiffness degradation and damage to the concrete as the concrete either cracks in tension or crushes in compression is well defined and useful in the comparison of the FEA vs. Test data. This model is also best used for dynamically loaded concrete members, which supports the blast analysis techniques employed later in this study, see Chapter 6. Under the Damaged Plasticity model the concrete in tension and compression follow a linear elastic relationship until stress in the concrete elements reach the value of  $\sigma_{t0}$  and  $\sigma_{c0}$  which is the tensile failure stress and initial compressive yield stress respectively. The tensile failure stress  $\sigma_{t0}$  is the initialization of micro-cracking in the concrete. This is a useful analysis method that can be used to indicate micro cracking in the concrete, which is difficult to detect during a test or in a real structure. In both cases, following the onset of tensile failure stress or initial compressive yielding, strain softening in the concrete occurs and there is a numerical degradation that can be derived. The degradation of this stiffness is characterized by the variables in ABAQUS as  $d_t$  and  $d_c$  for tension and compression respectively. These degradation variables are a function of plastic strain, temperature and other inputted field variables as follows:

$$\text{Tension degradation: } d_t = d_t(\tilde{\varepsilon}_{ij}^p, \theta, f_i) \quad (0 \leq d_t \leq 1) \quad (4-11)$$

$$\text{Compression degradation: } d_c = d_c(\tilde{\varepsilon}_{cij}^p, \theta, f_i) \quad (0 \leq d_c \leq 1) \quad (4-12)$$

The total strain rate of the concrete is separated into the elastic strain rate and the plastic strain rate per the following equation:

$$\text{Strain rate: } \dot{\varepsilon}_{ij} = \dot{\varepsilon}_{ij}^e + \dot{\varepsilon}_{ij}^p \quad (4-13)$$

The elastic strain rate is denoted with the superscript “e” and the plastic strain rate is denoted with the superscript “p”. The model then uses the damage parameter “d”, which is a scalar value to determine the stress-strain relationship as follows

$$\sigma_{ij} = (1-d)D_{ijkl}^{el}(\varepsilon_{kl} - \varepsilon_{kl}^p) \quad (4-14)$$

where  $\sigma_{ij}$  is the stress in concrete in psi,  $D_{ijkl}^{el}$  is the initial (undamaged) stiffness of the concrete in psi and “d” is the scalar damage parameter or stiffness degradation value.  $\varepsilon_{kl}$  and  $\varepsilon_{kl}^p$  are the total and plastic strains respectively for the concrete material. ABAQUS uses the equivalent strain variables  $\varepsilon_{ij}^p$  and  $\varepsilon_{cij}^p$ , defined from uniaxial loading conditions, for the hardening of the material. For the uniaxial loading condition the stress-strain curve can be converted into stress versus plastic strain by consideration of the following equations

$$\sigma_{ij} = \sigma_{ij}(\tilde{\varepsilon}_{ij}^p, \tilde{\varepsilon}_{ij}^p, \theta, f_i) \quad (4-15)$$

$$\sigma_{cij} = \sigma_{cij}(\tilde{\varepsilon}_{cij}^p, \tilde{\varepsilon}_{cij}^p, \theta, f_i) \quad (4-16)$$

where  $\theta$  is the temperature and  $f_i$  accounts for other predefined variables. The subscripts “c” and “t” denote compression and tension respectively. The equivalent plastic strains can then be calculated based on the following equations

$$\tilde{\varepsilon}_{cij}^p = \int_0^t \dot{\tilde{\varepsilon}}_{cij}^p \quad (4-17)$$

$$\tilde{\varepsilon}_{ij}^p = \int_0^t \dot{\tilde{\varepsilon}}_{ij}^p \quad (4-18)$$

For a uniaxial loaded material the strain rates in tension and compression respectively are

$$\dot{\tilde{\varepsilon}}_{ij}^p = \dot{\tilde{\varepsilon}}_{t11}^p \quad (4-19)$$

$$\dot{\tilde{\varepsilon}}_{cij}^p = \dot{\tilde{\varepsilon}}_{c11}^p \quad (4-20)$$

The stress-strain behavior of the concrete specimen in uniaxial tension and compress is shown in Figure 35 and Figure 27 respectively.

### Compressive stress-strain behavior:

In absence of full stress strain test data for the concrete in compression, Hsu and Hsu<sup>[28]</sup> have developed a model to represent the stress strain response using only the maximum 28 day compressive strength of the concrete. The method is validated and tested for concrete specimens up to 9000 psi (62 MPa) compressive strength. The background to the concrete damaged plasticity compression model is briefly explained here as documented in ABAQUS<sup>[1]</sup> user's manual, then Hsu and Hsu's model is described and used.

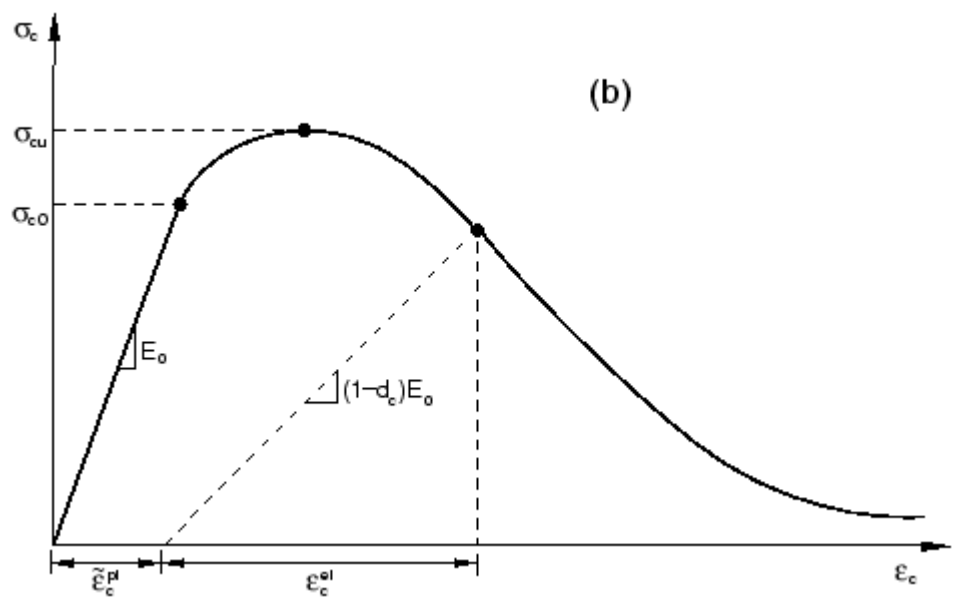


Figure 27 – Response of concrete to uniaxial loading in compression (ABAQUS 2013)

Cracks tend to propagate in the direction normal to the direction of stress. Cracks normally initiate in the direction of maximum shear stress then propagate in the direction of maximum principal stress. In the Figure 35 and Figure 27 the  $E_{0ijkl}$  is the initial or undamaged elastic stiffness of the material. The stress-strain relationship is then defined by ABAQUS per the following equations

$$\sigma_{ij} = (1 - d_t) E_{0ijkl} (\epsilon_{ij} - \tilde{\epsilon}_{ij}^p) \quad (4-21)$$

$$\sigma_{cij} = (1 - d_c) E_{0ijkl} (\epsilon_{cij} - \tilde{\epsilon}_{cij}^p) \quad (4-22)$$

When concrete nucleates a crack and the crack then propagates the load carrying capacity of the concrete is reduced due to the reduction in load carrying capacity of the area. The crack reduces the area capable of providing strength and this strength reduction needs to be accounted for in the

numerical model. The modulus of elasticity of the material, which is the essence of the numerical stiffness model, is also reduced as follows

$$E_{ijkl} = (1 - d)E_{0ijkl} \quad (4-23)$$

where the undamaged or initial modulus of elasticity of the concrete is defined as  $E_{0ijkl}$ . Since concrete can have degradation at any one time due to both tension and compression the damage parameter is determine as follows

$$(1 - d) = (1 - s_t d_t)(1 - s_c d_c) \quad 0 \leq s_t, s_c \leq 1 \quad (4-24)$$

where  $s_t$  and  $s_c$  are functions of the stress state and are introduced to represent stiffness recovery effects defined as

$$s_t = 1 - w_t r^*(\bar{\sigma}_{11}) \quad 0 \leq w_t \leq 1 \quad (4-25)$$

$$s_c = 1 - w_c (1 - r^*(\bar{\sigma}_{11})) \quad 0 \leq w_c \leq 1 \quad (4-26)$$

where,

$$r^*(\bar{\sigma}_{11}) = \begin{cases} 1 & \text{if } \sigma_{11} > 0 \\ 0 & \text{if } \sigma_{11} < 0 \end{cases} \quad (4-27)$$

The weighting factors  $w_t$  and  $w_c$  are material properties and control the recovery of the tensile and compressive stiffness as the load is reversed. The equivalent plastic strains are then determined as follows

$$\tilde{\epsilon}_{ij}^p = r^* \dot{\epsilon}_{11}^p \quad (4-28)$$

$$\tilde{\epsilon}_{ij}^p = -(1 - r^*) \dot{\epsilon}_{11}^p \quad (4-29)$$

The effect of the compression stiffness recovery factor  $w_c$  on the behavior of concrete is shown in Figure 28.

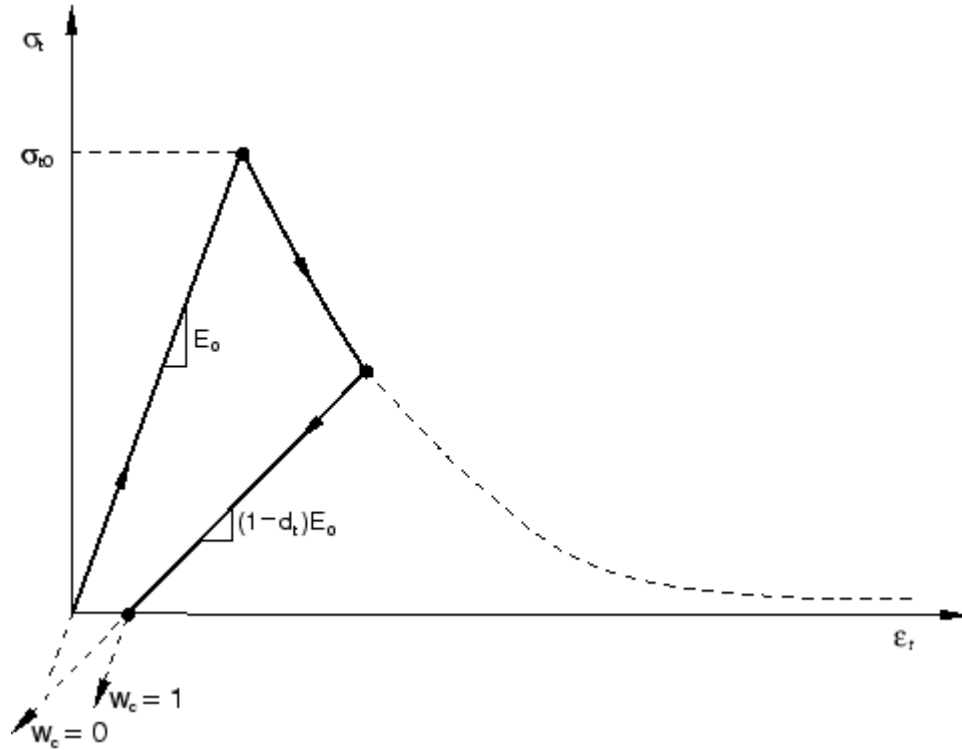
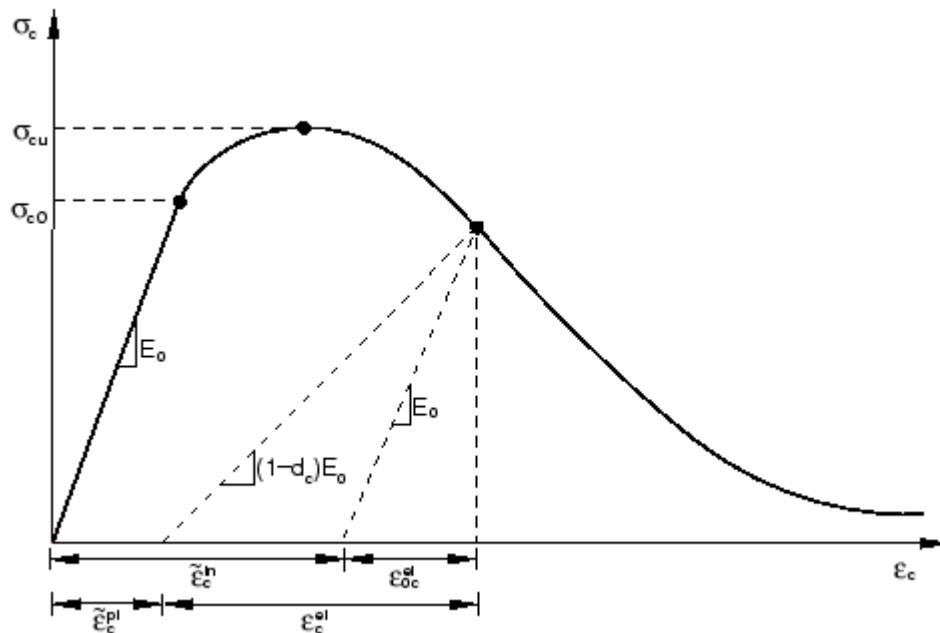


Figure 28 – Compression stiffness recovery parameter,  $w_c$  (ABAQUS 2013)

The separation of elastic, inelastic and total strain in the concrete material for tension is shown in Figure 36. The separation of elastic, inelastic and total strain in the concrete material for compression is shown in Figure 29.



**Figure 29 – Compressive inelastic strain definition of compression hardening (ABAQUS 2013)**

The yield criterion for the concrete damaged plasticity model was proposed by Lubliner et al<sup>[38]</sup> and takes into account modifications and input by Lee and Fenves<sup>[33]</sup>. Lee and Fenves modification accounts for the different strength evolution under tension and compression. The yield function is as follows:

$$F(\sigma_{ij}, \tilde{\varepsilon}_{ij}^p) = \frac{1}{(1-\alpha)} \left( q - 3\alpha + \beta(\tilde{\varepsilon}_{ij}^p) \left\langle \frac{\hat{\sigma}}{\hat{\sigma}_{\max}} \right\rangle - \gamma \left\langle \frac{\hat{\sigma}}{\hat{\sigma}_{\max}} \right\rangle \right) - \sigma_{cij}(\tilde{\varepsilon}_{cij}^p) \leq 0 \quad (4-30)$$

where  $\alpha$  and  $\gamma$  are dimensionless material constants. The effective hydrostatic pressure is defined as;

$$\bar{p}_{ij} = -\frac{\sigma_{ij} I_{ij}}{3} \quad (4-31)$$

The Von Mises equivalent effective stress is defined as;

$$q_{ij} = \sqrt{\frac{3}{2} S_{ij} S_{ij}} \quad (4-32)$$

And the deviatoric part of the effective stress is defined as;

$$S_{ij} = p_{ij} I_{ijkl} + \sigma_{ij} \quad (4-33)$$

The functions  $\alpha$  and  $\beta$  are derived from the following equations;

$$\beta(\tilde{\varepsilon}_{ij}^p) = \frac{\sigma_{cij}(\tilde{\varepsilon}_{cij}^p)}{\sigma_{tij}(\tilde{\varepsilon}_{tij}^p)} (1-\alpha) - (1+\alpha) \quad (4-34)$$

$$\alpha = \frac{\sigma_{b0} - \sigma_{c0}}{2\sigma_{b0} - \sigma_{c0}} \quad (4-35)$$

where,  $\sigma_{b0}$  and  $\sigma_{c0}$  are the initial equi-biaxial and uniaxial compressive yield stress. Experimentally

it is found that  $\frac{\sigma_{b0}}{\sigma_{c0}}$  ranges between 1.10 and 1.16 and  $\alpha$  from 0.08 to 0.12. The coefficient  $\gamma$  applies

for a stress state of triaxial compression. The yield surface obtained for deviatoric plane and in-plane stress formulations are shown in Figure 30 and Figure 31.

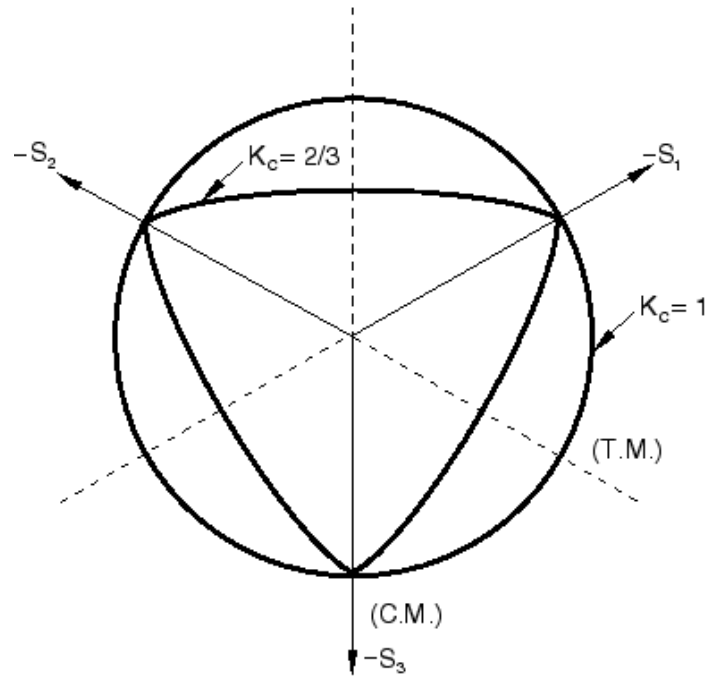


Figure 30 – Yield surface of deviatoric plan (ABAQUS 2013)

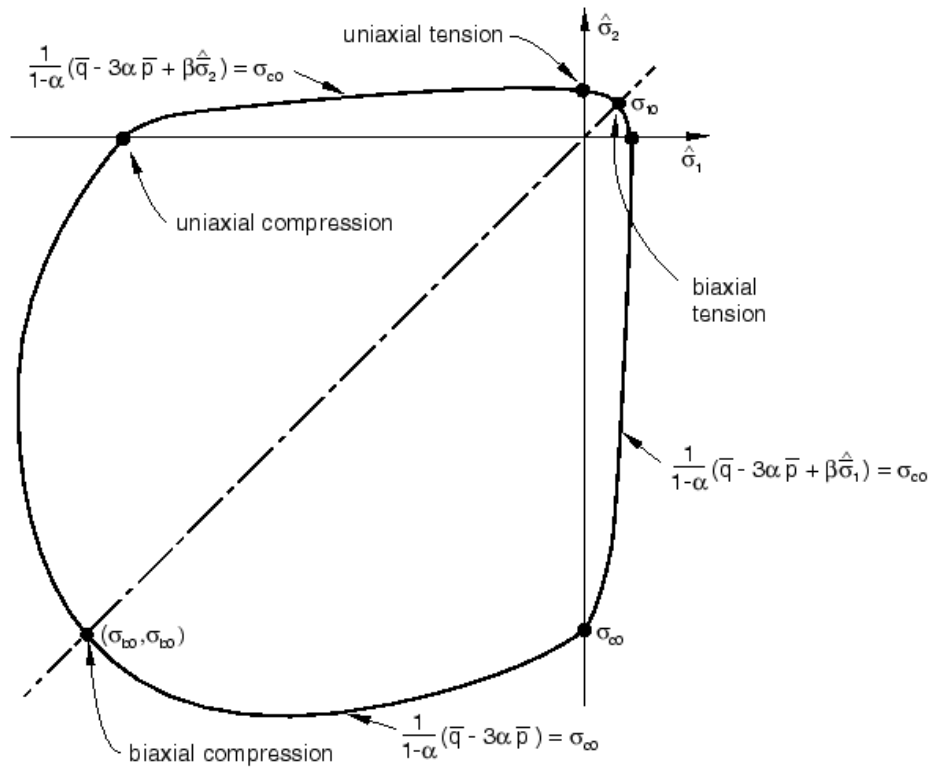


Figure 31 – Yield surface in plane stress (ABAQUS 2013)

The plastic-damage model assumes non-associated potential flow,

$$\dot{\varepsilon}_{ij}^p = \lambda \frac{\delta G(\bar{\sigma}_{ij})}{\delta \bar{\sigma}_{ij}} \quad (4-36)$$

The flow potential  $G$  chosen for this model is the Drucker-Prager hyperbolic function:

$$G = \sqrt{(\xi \sigma_{t0ij} \tan \psi)^2 + \bar{q}_{ij}^2} - \bar{p}_{ij} \tan \psi \quad (4-37)$$

where,  $\psi$  is the dilation angle measure in the p-q plane at high confining pressure;  $\sigma_{t0}$  is the uniaxial tensile stress at failure; and  $\xi$  is the eccentricity that defines the rate at which the function approaches the asymptote value.

When only the compressive strength of the concrete is known, Hsu and Hsu's model can be used to develop a stress-strain curve for the compressive material properties of the concrete. The model is used only to calculate the compressive stress values ( $\sigma_{cu}$ ) between the yield point (at  $0.5 \sigma_{cu}$ ) and the  $0.3\sigma_{cu}$  value per the following formula:

$$\text{Compressive Stress:} \quad \sigma_c = \left( \frac{\beta \left( \frac{\varepsilon_c}{\varepsilon_o} \right)}{\beta - 1 + \left( \frac{\varepsilon_c}{\varepsilon_o} \right)^\beta} \right) \sigma_{cu} \quad (4-38)$$

$$\text{Shape Parameter:} \quad \beta = \frac{1}{1 - \left[ \frac{\sigma_{cu}}{\varepsilon_o E_o} \right]} \quad (4-39)$$

Compressive Strength:  $\sigma_{cu}$  (28 days per ASTM C39)

$$\text{Strain at Peak Stress:} \quad \varepsilon_o = 8.9 \times 10^{-5} \sigma_{cu} + 2.114 \times 10^{-3} \quad (4-40)$$

$$\text{Initial Tangential Modulus:} \quad E_o = 1.2431 \times 10^2 \sigma_{cu} + 3.28312 \times 10^3 \quad (4-41)$$

Compressive Strain:  $\varepsilon_c$

Damage Parameter:  $d_c$

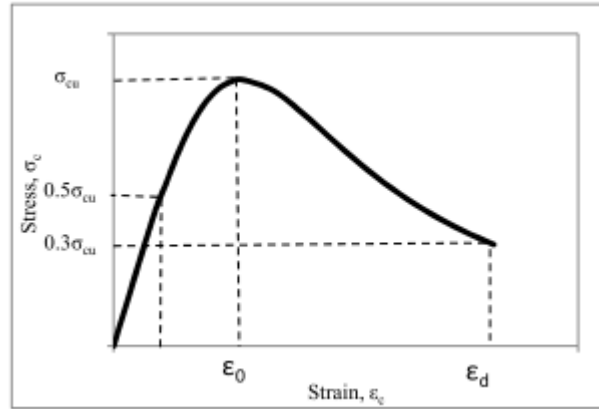


**Figure 32 – Compressive stress-strain relationship in ABAQUS**

For the concrete panel with an average 28-day compressive strength ( $\sigma_{cu}$ ) of 4,120 psi the initial tangential modulus of elasticity is:

Compressive Strength:  $\sigma_{cu} = 4,120 \text{ psi}$

Initial Tangential Modulus of Elasticity:  $E_o = 124.31(\sigma_{cu}) + 3,283 \text{ psi} = 3,795,277 \text{ psi}$

Strain at Peak Stress:  $\epsilon_o = 8.9 \times 10^{-5} (4,120 \text{ psi}) + 2.114 \times 10^{-3} = 0.002481 \text{ in/in}$

$\beta$ -Parameter: 
$$\beta = \frac{1}{1 - \left[ \frac{4120}{(0.002481)(3795277)} \right]} = 1.778112$$

The values for these calculations appropriate for the 4,120 psi concrete are shown in Table 11.

**Table 11 – Hsu and Hsu numerical compression stress-strain model**

Hsu and Hsu (1994) Numerical Compression Stress Strain Model				
<b>Maximum Compression Strength, <math>\sigma_{cu}</math></b>		4.12 <b>ksi</b>		
Output Values				
<b>Hsu</b>	<b>Initial Tangential Modulus, <math>E_0</math></b>			3795.2772 <b>ksi</b>
<b>Hsu</b>	<b>Strain at Peak Stress, <math>\epsilon_0</math></b>			0.00248068 <b>in/in</b>
<b>Hsu</b>	<b><math>\beta</math>-Parameter</b>			1.778111902 <b>unitless</b>
Total Strain		Compressive Stress Value		
0		0		0
0.000217		824		824
0.000467		1663.053579		1618.050493
0.000717	0.00025	2384.382119		2198.304431
0.000967	0.00025	2958.288172		2788.591509
0.001217	0.00025	3390.739168		3258.455353
0.001467	0.00025	3699.54347		3610.433171
0.001717	0.00025	3906.704136		3856.097125
0.001967	0.00025	4033.786023		4011.586745
0.002467	0.0005	4119.951766		4119.938036
0.002967	0.0005	4069.796734		4054.824915
0.003467	0.0005	3950.69143		3899.420226
0.003967	0.0005	3800.589433		3704.178648
0.004467	0.0005	3640.114311		3497.331857
0.004967	0.0005	3480.138338		3293.707984
0.005967	0.001	3180.66655		2920.78501
0.006967	0.001	2918.113086		2603.80051
0.007967	0.001	2691.961071		2338.896083
0.008967	0.001	2497.499152		2117.477977
0.009967	0.001	2329.558814		1931.197974
0.011967	0.002	2055.722369		1637.709593
0.013967	0.002	1842.844152		1418.741374
0.015967	0.002	1672.915447		1250.009753
0.017967	0.002	1534.156228		1116.397275
0.019967	0.002	1418.660274		1008.162431
0.022467	0.0025	1298.83896		898.8519069

Using these values the theoretical stress/strain curve can be plotted and is shown in Figure 33.

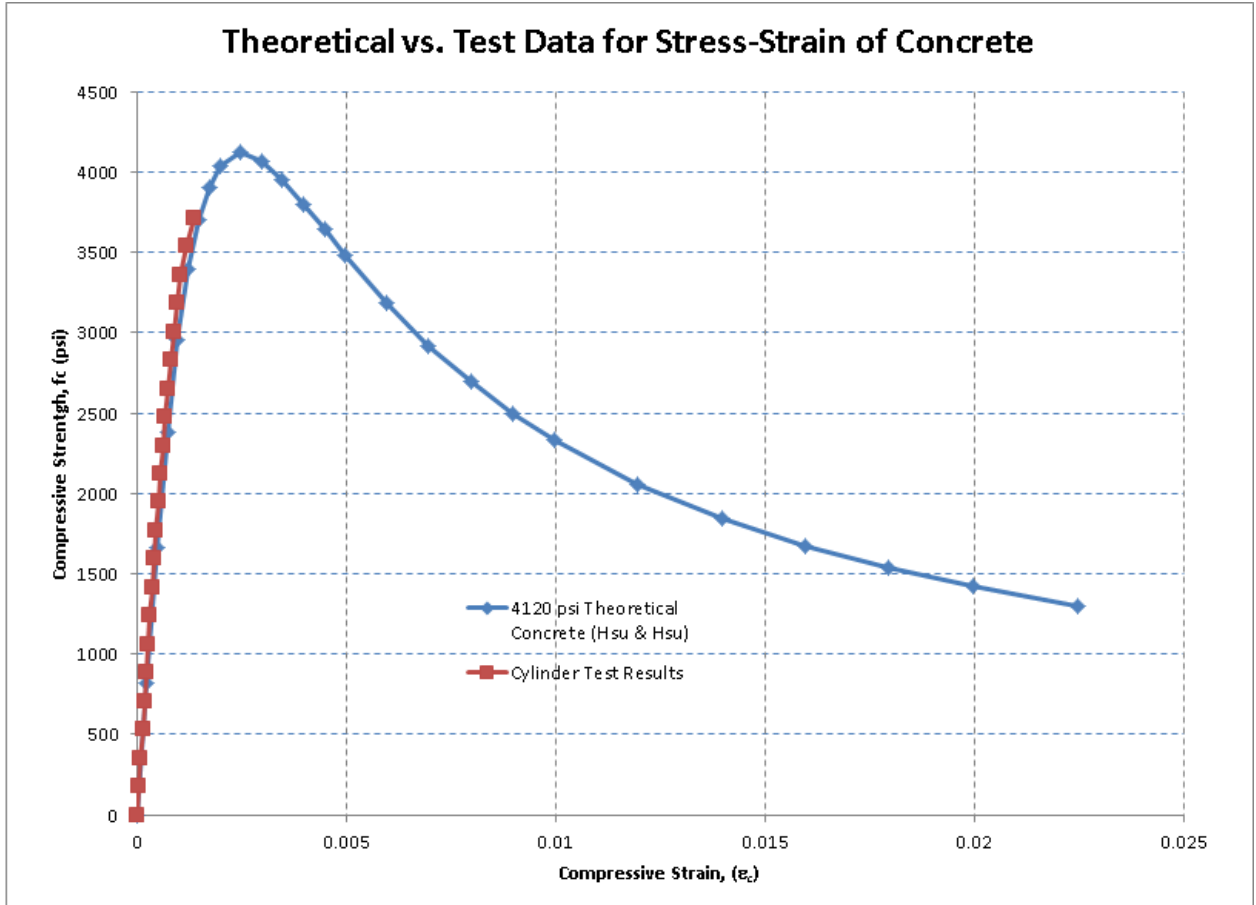


Figure 33 – Theoretical compressive stress strain curve for 4,120 psi concrete

The final compressive concrete damaged plasticity properties using the Hsu and Hsu model are shown in Table 12, which were incorporated into the ABAQUS FEA model.

Compressive Damage Parameter: 
$$d_c = 1 - \frac{\sigma_c}{\sigma_{c \max}} \quad (4-42)$$



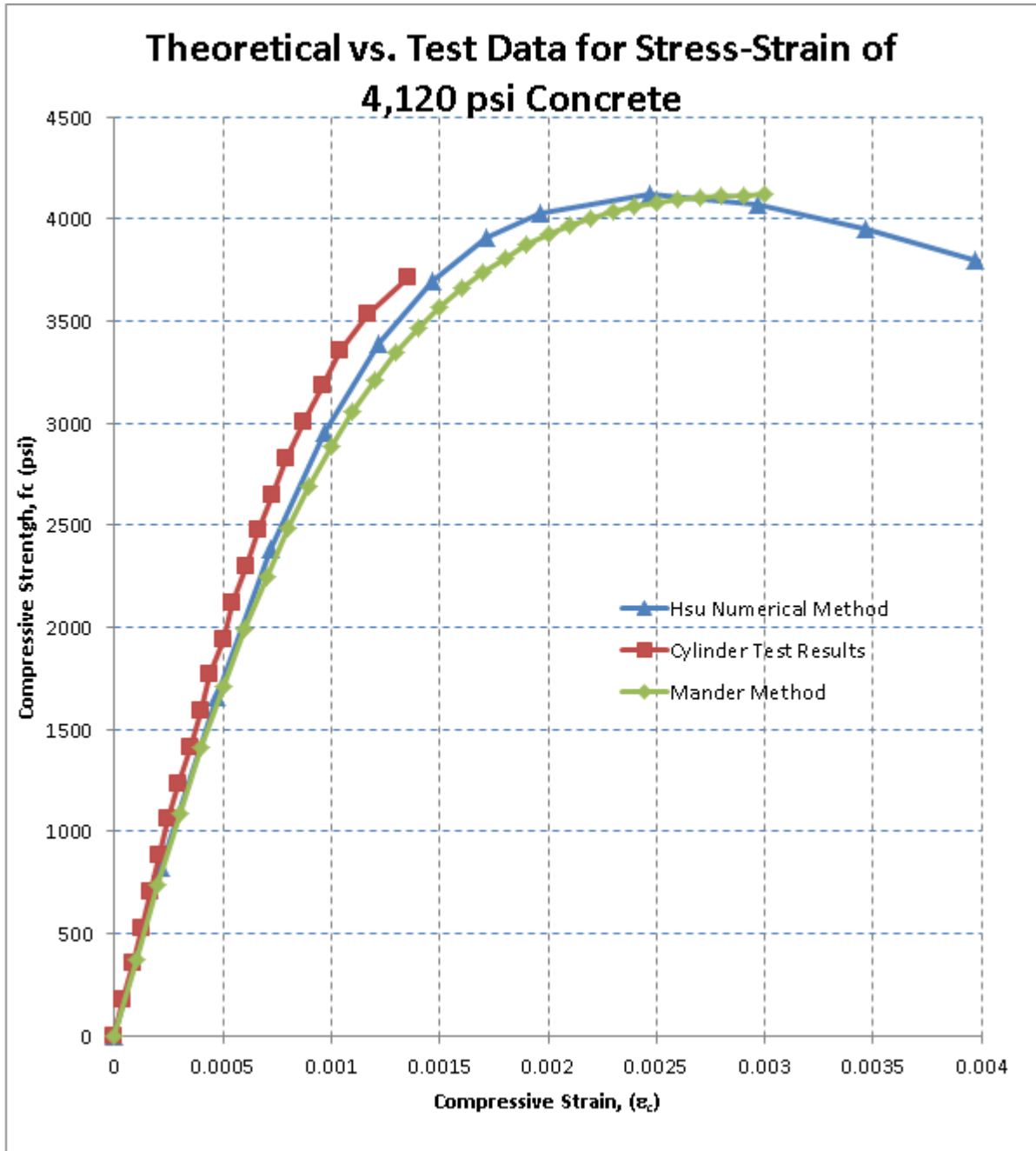


Figure 34 – Theoretical vs. cylinder test results of compressive strain/strain values

The Mander<sup>[39]</sup> method as previously described in Section 4.3.1 of this report is also plotted on the graph in Figure 34 for comparison. This model was not used for the compressive material properties in ABAQUS since the curve does not fully extend to the inelastic compressive strain definition of the model that is required for ABAQUS as shown in Figure 29. Mander's model is also for confined concrete, which is not applicable to the test panels.

### Tension stiffening behavior:

The concrete FEA model not only requires a good representation of the compressive material properties. It will also requires a robust tension stiffness behavior to account for the dramatic loss in tensile strength in the brittle concrete continuum. Figure 35 shows the general response of concrete to uniaxial loading in tension as documented in the ABAQUS user manual. It is not always possible to obtain the tensile properties from a concrete specimen and a good approximation is generally called for when performing engineering calculations and FEA modeling.

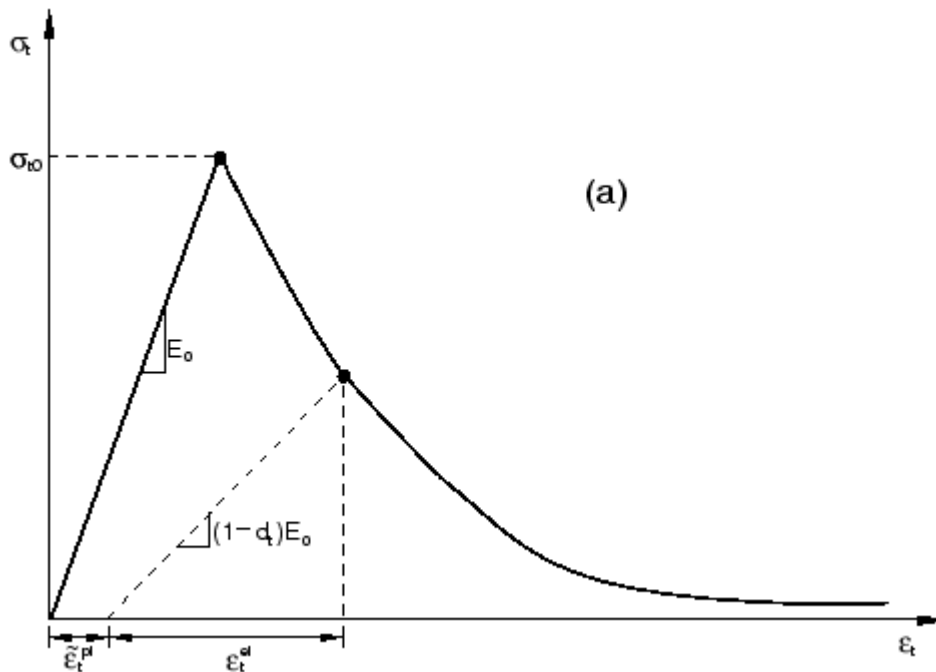


Figure 35 – Response of concrete to uniaxial loading in tension (ABAQUS 2013)

Wahalathantri, etal (2011) uses the Nayal and Rasheed (2006) tension stiffening model. This model accounts for tension stiffening, strain softening and the interaction between the reinforcing steel and the concrete. The user inputs are as follows:

Young's Modulus:	$E_0$
Tensile Stress:	$\sigma_t$
Cracking Strain:	$\tilde{\epsilon}_t^{ck}$
Damage Parameter:	$d_t$

The cracking strain is determined by subtracting the undamaged tensile strain ( $\epsilon_{ot}^{el}$ ) from the total strain component ( $\epsilon_t$ ) per the following equation:

$$\tilde{\varepsilon}_t^{ck} = \varepsilon_t - \varepsilon_{ot}^{el} \quad (4-43)$$

Where,  $\varepsilon_{ot}^{el} = \frac{\sigma_t}{E_o}$ , is the elastic strain corresponding to the undamaged material and  $\varepsilon_t$  = total tensile strain. The post-failure tensile stress relationship as defined in ABAQUS is shown in Figure 36.

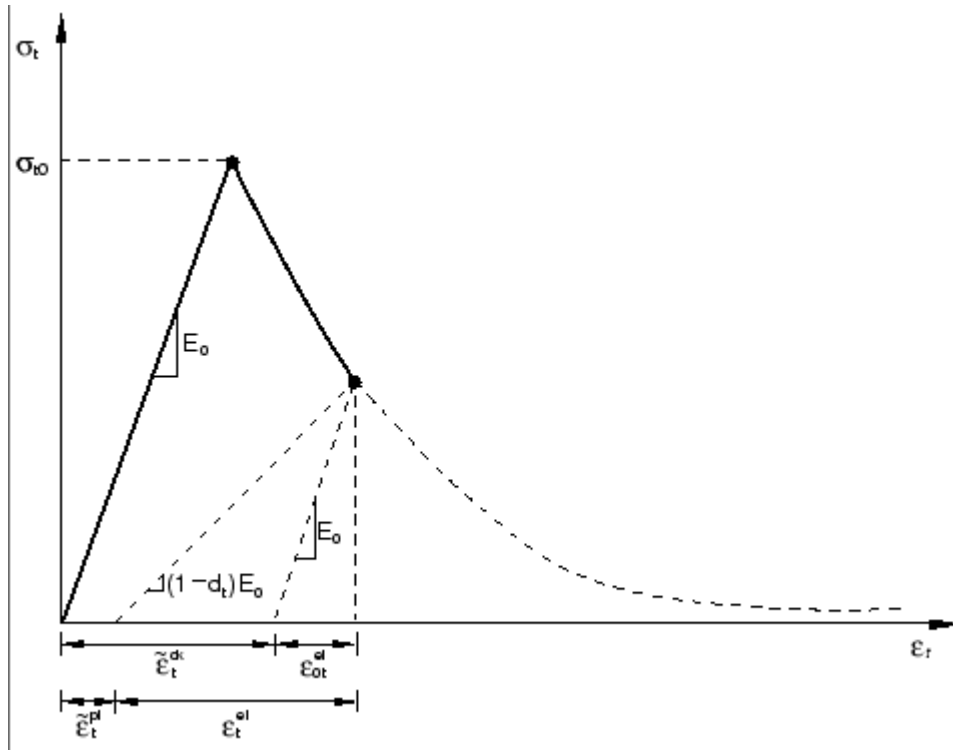
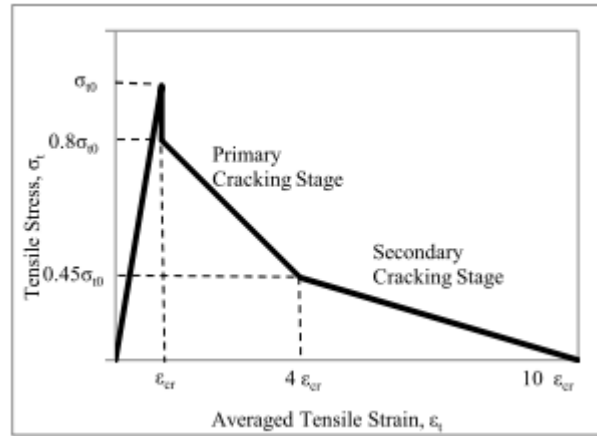


Figure 36 – Cracking strain definition of tension stiffening (ABAQUS 2013)

The tension stiffening model in ABAQUS was first developed by Gilbert and Warner (1978) and includes two distinct regions, the Primary Cracking Stage and the Secondary Cracking Stage as shown in Figure 36. The model is loaded to the tensile strength or modulus of rupture ( $f_r$ ) of the concrete, which is typically around 7-10% of the compressive strength of the concrete material.



**Figure 37 – Nayal and Rasheed's (2006) tension stiffening model**

Nayal and Rasheed (2006)<sup>[43]</sup> modified the Gilbert and Warner (1978)<sup>[23]</sup> tension stiffening curve as shown in Figure 37 to replace the curve with a single set of stiffening parameters that are applicable to the entire tensile zone. In order to create a more robust tension stiffening parameter and avoid runtime errors in ABAQUS, Wahalathantri, et al (2001)<sup>[54]</sup> modified Nayal's model to create the tension stiffening plot shown in Figure 38. The model is a bit cleaner and more robust and will be used here in this study to develop the tensile properties of the concrete material.

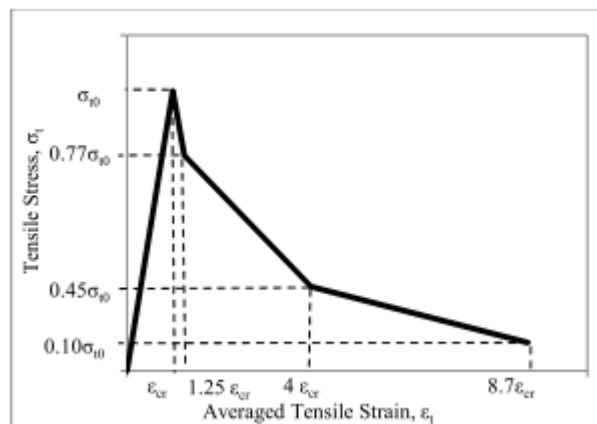


**Figure 38 – Modified tension stiffening model for ABAQUS**

For the scaled test panels in this study initially built and tested in 2012, only the compressive strength of the concrete was tested and recorded. No splitting tensile test was performed for the Phase I test panels. A set of 6" x 12" concrete cylinders were cast and then tested under compressive loading per ASTM C39 and the maximum average compressive strength recorded was 4,120 psi. The assumption that the tensile strength of the concrete is approximately 10% of the maximum compressive strength shall be employed in this study. This assumption is based on published data that the tensile strength of concrete typically falls within the range of 8 to 15% of the 28-day

compressive strength.<sup>[41][48]</sup> Therefore a specimen having a 28-day compressive strength ( $f'_c$ ) of 4,210 psi shall have a tensile strength ( $f_{ct}$ ) assumed to be 412 psi. The tensile parameters are:

Maximum Tensile Stress:  $\sigma_{to} = 412 \text{ psi}$

Initial Tangential Modulus of Elasticity:  $E_o = 124.31(\sigma_{cu}) + 3,283 \text{ psi} = 3,795,277 \text{ psi}$

This equation for the initial tangent modulus comes from Hsu and Hsu<sup>[28]</sup> numerical compression stress strain model and is also a good approximation to that which was derived at WSU in 2012 when the cylinders were tested and the modulus of elasticity was determined per ASTM C469,  $E_c = 3,837,403 \text{ psi}$ . The ACI 318 equation for calculating the modulus of elasticity is as follows:

$$E_c = 57,000 \cdot \sqrt{f'_c} = 57,000 \cdot \sqrt{4,120 \text{ psi}} = 3,658,671 \text{ psi} \quad \text{ACI 318}^{[4]}$$

The Young's Modulus of elasticity of the concrete determined by ASTM C469, Hsu and Hsu<sup>[28]</sup> equations and from ACI 318 are in close approximation with one another. To be consistent with the theoretical model of Hsu and Hsu we will use the derived formula for  $E_o$ . With the initial tangent modulus and the maximum tensile strength known, the critical tensile strain can be determined as follows:

Critical Tensile Strain:  $\varepsilon_{cr} = \frac{\sigma_{to}}{E_o} = \frac{412 \text{ psi}}{3,795,277 \text{ psi}} = 0.00010856 \text{ in/in}$

Using the equations for the critical points on the graph from Nashal & Rasheed's curve, Figure 38 the tension stiffening model is plotted for the 4,120 psi concrete and shown in Figure 39.

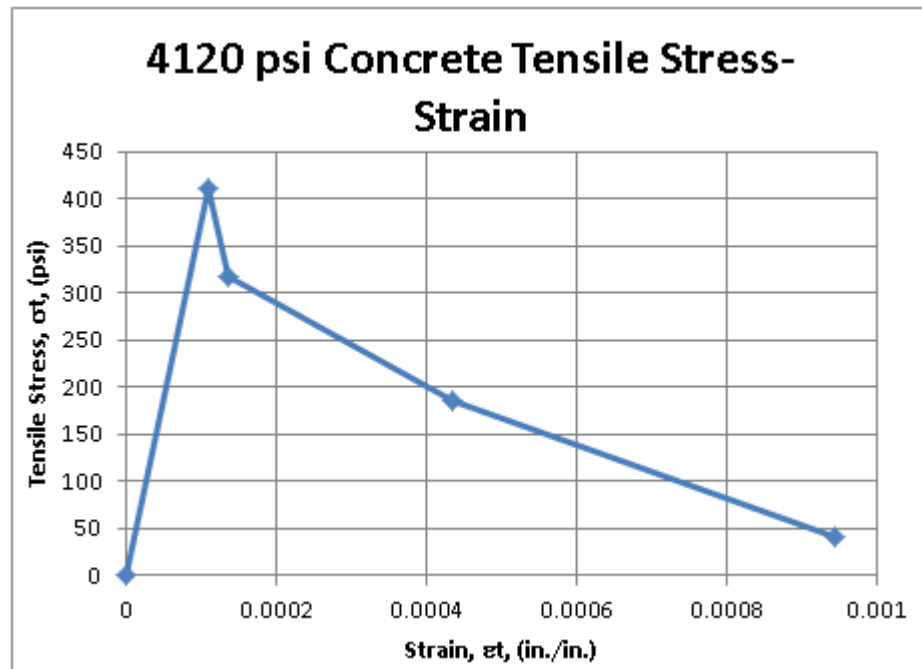


Figure 39 – Tensile stiffening model for the 4,120 psi concrete

The tensile stress ( $\sigma_t$ ) and the tensile strain ( $\varepsilon_t$ ) are shown in the graph in Figure 39. From here the cracking strain and damage parameter values are derived per the following equations:

$$\text{Cracking Strain:} \quad \tilde{\varepsilon}_t^{ck} = \varepsilon_t - \varepsilon_{ot}^{el} \quad (4-44)$$

$$\text{Damage Parameter:} \quad d_t = 1 - \frac{\sigma_{to}}{\sigma_t} \quad (4-45)$$

Both the compressive damage parameter  $d_c$  and the tension damage parameter  $d_t$  has been derived from the relationship between the Cauchy stress and the effective stress where the damage parameter is a scalar that represents the degradation between the two.

$$\sigma = (1 - d)\bar{\sigma}^{[1]} \quad (4-46)$$

**Table 13 – Concrete damaged plasticity model for tension stiffening**

Concrete Damaged Plasticity (Tension Stiffening)					
Tensile Behavior			Tension Damage		Check
Yield Stress	Eng. Strain	Cracking Strain	Damage Parameter	Cracking Strain	Plastic Strain
$\sigma_t$	$\varepsilon_t$	$\varepsilon_t^{ck}$	$d$	$\varepsilon_t^{ck}$	$\varepsilon_t^{pl}$
0	0	0.00000			0
412	0.000108556	0.00000	0.000	0.00000	0
317.24	0.000135695	0.00005	0.230	0.00005	2.71E-05
185.4	0.000434224	0.00039	0.550	0.00039	0.000326
41.2	0.000944437	0.00093	0.900	0.00093	0.000836

ABAQUS does incorporate a check to determine the validity of the accuracy of the tension stiffening curve by introducing a plastic strain calculation. The plastic strain ( $\tilde{\varepsilon}_t^{pl}$ ) can neither be negative nor decreasing as this will indicate an incorrect damage curve which will lead to an error message and the analysis will be aborted. The tensile plastic strain check is defined as:

$$\text{Tensile Plastic Strain:} \quad \tilde{\varepsilon}_t^{pl} = \tilde{\varepsilon}_t^{ck} - \frac{d_t}{(1 - d_t)} \frac{\sigma_t}{E_o} \quad (4-47)$$

### 4.3.3 ELEMENT TYPES

There are numerous types of elements that can be used in any ABAQUS finite element analysis model. The elements and their properties were tested for various configurations and types and the best suited elements are listed in Table 14. A thorough explanation of the FEA model has been provided in the Appendix.

**Table 14 – FEA element types**

<b>Material Component</b>	<b>Element Type</b>	<b>Comment</b>
Concrete	C3D8R	Linear hexahedral element with enhanced stiffness hourglass control and reduced integration
Insulation	C3D8R	Linear hexahedral element with enhanced stiffness hourglass control and reduced integration
Rebar	T3D2	Linear truss bar element
FRP Plate	S4R	Linear shell element
FRP Shear Connector	S4R	Linear shell element

## 4.4 EXPERIMENTAL INVESTIGATION

There were (12) initial scaled test panels fabricated and tested in the Fall of 2012. The undergraduate students, from CE 441: Reinforced Concrete Design, were an integral part of helping to fabricate these test panels. There was also another (2) scaled test panels constructed with FRP plate on the exterior top and sides of the panel and these are labeled as the FRP-confined precast concrete sandwich (FPCS) panels. These panels were tested in the Summer of 2013. Included in the initial scaled test panels were (2) solid reinforced concrete panels constructed and tested as control points or benchmark for the insulated sandwich panels.

### 4.4.1 FABRICATION OF TEST SPECIMENS

The thesis submitted by Thomas G. Norris<sup>[44]</sup> in 2014 contains a thorough description of the scaled-panel specimen fabrication, cure and testing. A brief summary is provided here for background information. The overall process is similar to any precast concrete product manufacturing technique.

The forms were constructed out of wood as shown in Figure 40 and then the rebar, insulation and FRP shear connectors were assembled.



**Figure 40 – Wooden concrete form**

The shear connectors for the sandwich panels were cut with hand tools and to represent the CAD detail shapes shown in Figure 41. The connectors were inserted through slots in the insulation into the voids that would be filled for the top and bottom wythe of the concrete. The larger holes (1 ½” diameter) in the Discrete Shear Connector are present to allow for concrete material to flow through the opening and create a better interlocking bond for the connector. This will help to achieve the higher degree of composite action and when performing the finite element analysis will be more representative to being “tied” to the concrete material.

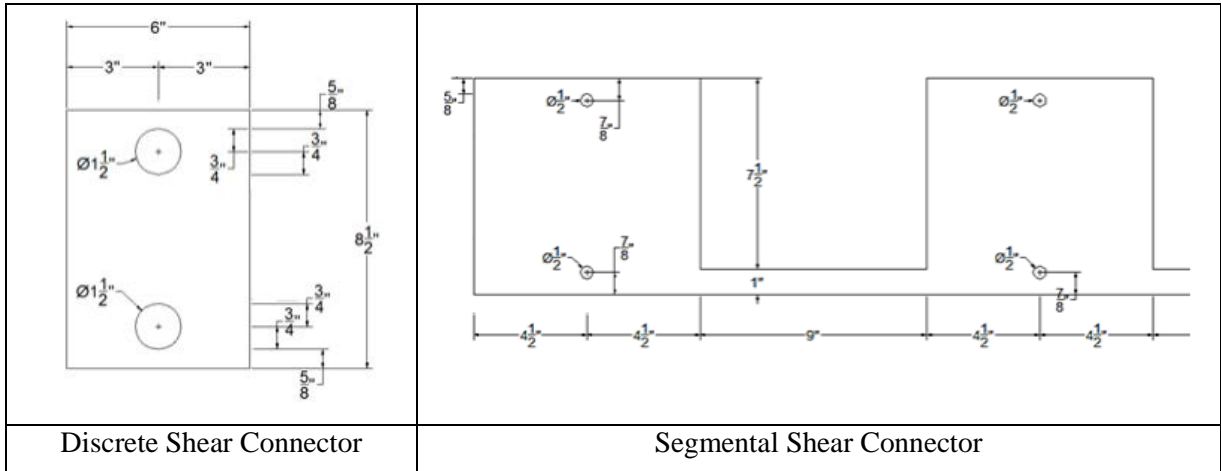


Figure 41 – Typical FRP shear connector geometry

The smaller 1/2" diameter holes in the segmental shear connectors are present to allow for transverse reinforcing steel to be inserted through the opening. Once again this will create a better mechanical bond between the FRP connectors and the concrete material and the representation in the finite element analysis model is more accurate.

#### 4.4.2 TESTING OF THE PANELS

The ideal testing situation is to have 4-point bending, shown in Figure 42 and Figure 43, so that there is a segment of zero shear forces and only pure flexural or moment forces for simply supported beams. Due to unexpected shear failures at the edge of the concrete panels between the foam core and solid zones, the remaining panels were switched from four-point bending to three-point bending, shown in Figure 44 and Figure 45.

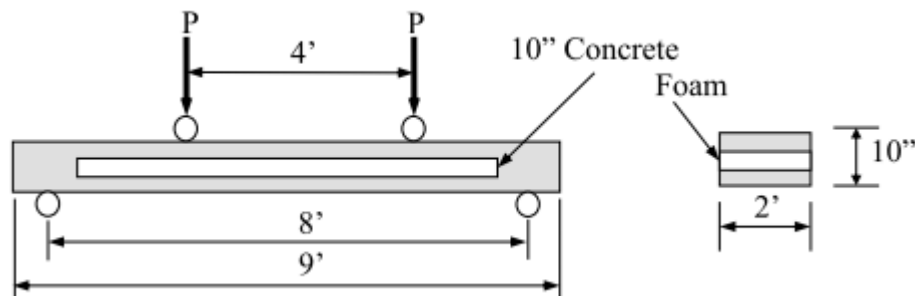


Figure 42 – Four-point bending setup



Figure 43 – Actual four-point bending test

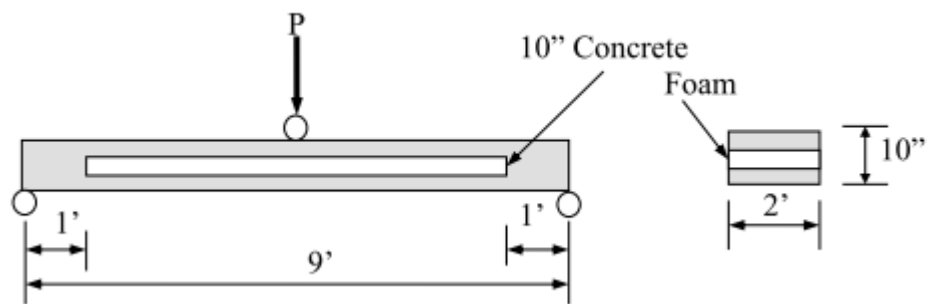


Figure 44 – Three point bending setup



Figure 45 – Actual three-point bending test

**Table 15 – Test panel nomenclature key plan summary**

Panel	Length (in)	Configuration	Shear Grid Layout	Thickness (in)	Type of Loading	FRP Plate	Support Locations	# of Panels	Comments	Note
108SOL10L3PTNOFRPS1	108	Solid	None	10	3 Point	No	Ends	2	Group 1 and 2 Spring 2012	
108DIS10L4PTNOFRPS2	108	3"+4"+3"	FRP-Discrete	10	4 Point	No	6" from ends	2	Group 3 and 12 Spring 2012	
108SEGUP10L3PTNOFRPS2	108	3"+4"+3"	FRP-Segmental	10	3 Point	No	6" from ends	1	Group 4 Spring 2012	
108SEGUP10L3PTNOFRPS1	108	3"+4"+3"	FRP-Segmental	10	3 Point	No	Ends	1	Group 5 Spring 2012	
108CON10L3PTNOFRPS1	108	3"+4"+3"	FRP-Continuous	10	3 Point	No	Ends	2	Group 6 & 7 Spring 2012	
108SEGUP10L3PTFRPS1	108	3"+4"+3"	FRP-Segmental	10	3 Point	Yes	Ends	2	Group 8 & 9 Spring 2012	
108CON10L3PTFRPS1	108	3"+4"+3"	FRP-Continuous	10	3 Point	Yes	Ends	2	Group 10 & 11 Spring 2012	
108SEGDN8L3PTFPCSS1	108	1"+4"+3"	FRP-Segmental	8	3 Point	Yes	Ends	2	Summer 2013	FPCS
108SEGDN10L3PTFPCSS1	108	3"+4"+3"	FRP-Segmental	10	3 Point	Yes	Ends	2	Summer 2013	FPCS

The following is a general description of the test panel nomenclature and ID's:

—      —      —      —      —      —  
**1      2      3      4      5      6**

**Digit 1: Length**

108 = 108 inches

**Digit 2: Cross Section**

SOL = Solid Panel

DIS = Discrete Connectors

SEG = Segmental Connectors

CON = Continuous Connectors

**Digit 3: Thickness**

10 = 10 inches

8 = 8 inches

**Digit 4: Loading Condition**

3PT = 3 Point Bending

4PT = 4 Point Bending

**Digit 5: FRP Exterior Plate?**

NOFRP = No

FRP = Yes (just top)

FPCS = Yes

**Digit 6: Support Condition**

S1 = Supported at ends

S2 = Supported 6" in from ends

#### 4.4.3 SCALED TEST PANELS

The following sections are the summary of the construction of the scaled test panels and the testing results for each of them.

##### Solid and Sandwich Scaled Test Panels:

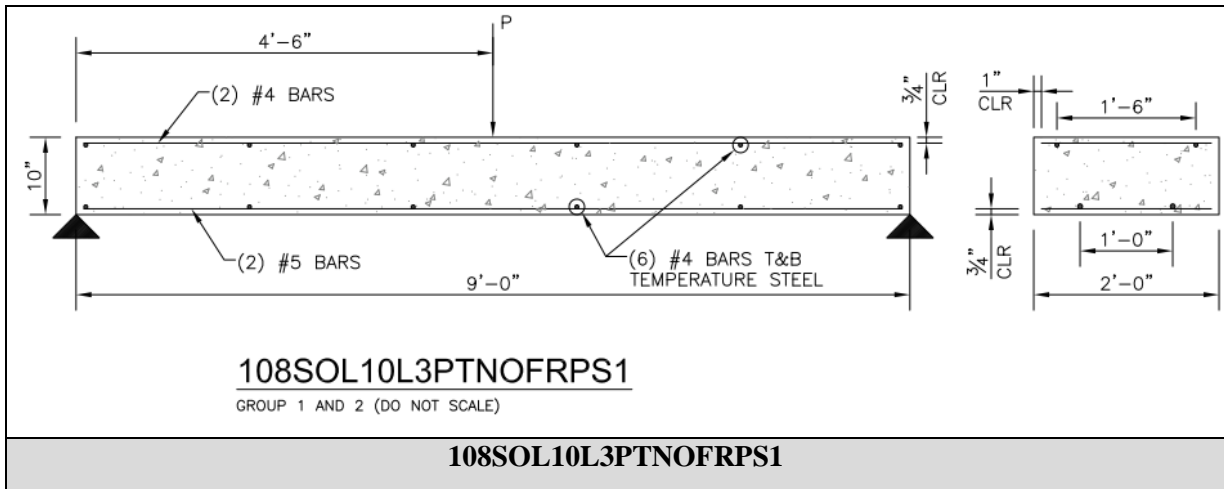
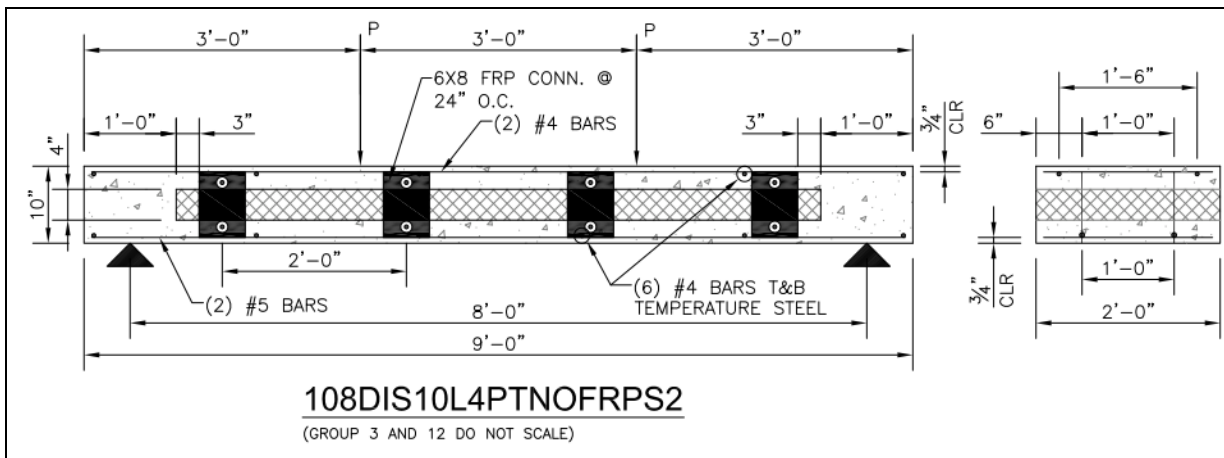
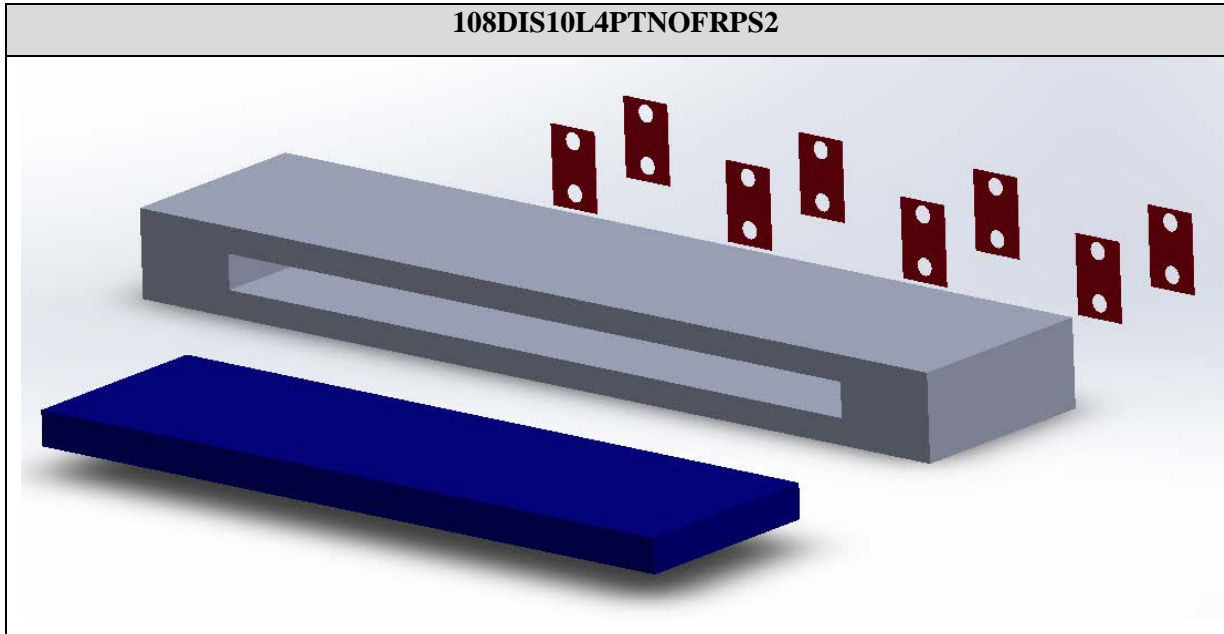


Figure 46 – 10 in. solid concrete panel (108SOL10L3PTNOFRPS1)

The control panel is the solid concrete panel reinforced with steel bars, top and bottom, longitudinal and transverse as shown in Figure 46. The various sandwich panels with discrete, segmental and continuous FRP shear connectors are shown in Figure 47 through to Figure 52. The discrete shear connectors shown in Figure 47 are comprised of 6"x8" FRP strips with 1.5" diameter holes for transverse reinforcing steel bars.





**Figure 47 – 10 in. sandwich panel with discrete connectors (108DIS10L4PTNOFRPS2)**

The segmental FRP shear connectors are shown in Figure 48 and Figure 49 where the difference in the test method was the location of the support points. In one case it was supported at approximately 8'-0" and then another case it was supported at 9'-0" like the other test panels. The segmental shear connectors were oriented in the upward position to provide continuous tensile strength support.

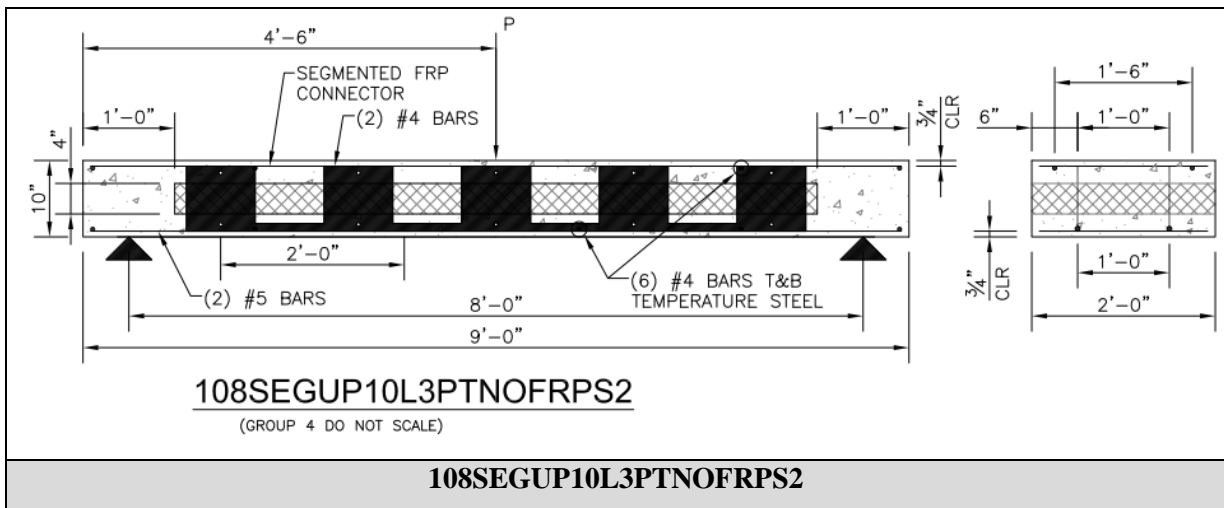


**Figure 48 – 10 in. sandwich panel with segmental connectors (108SEGUP10L3PTNOFRPS2)**

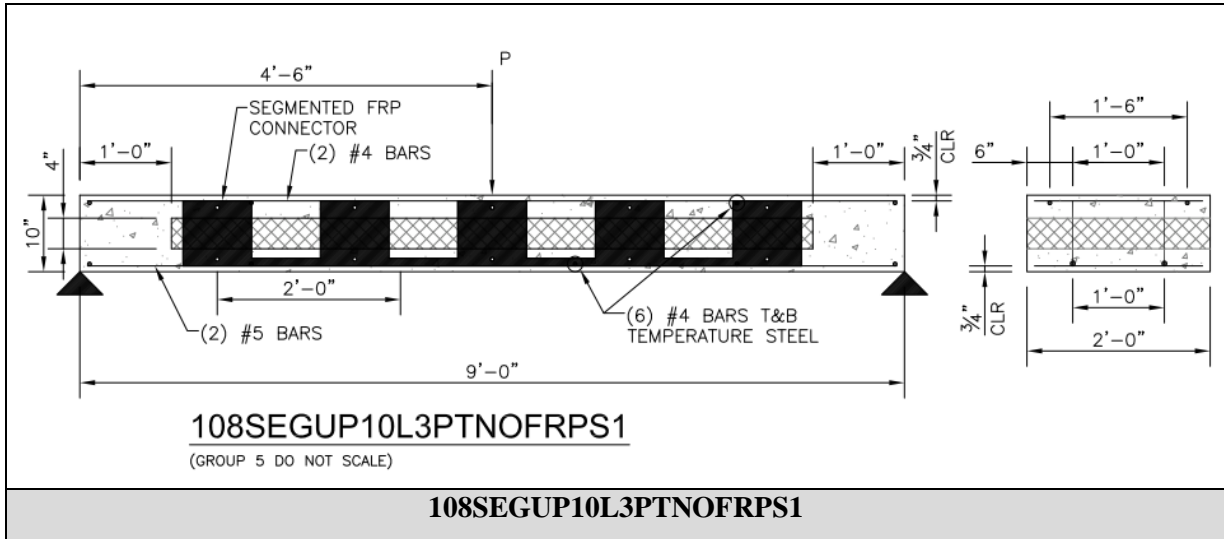


**Figure 49 – 10 in. sandwich panel with segmental connectors (108SEGUP10L3PTNOFRPS1)**

A continuous FRP shear connector was tested in the panel shown in Figure 50. Then another segmental FRP shear connector was used in the sandwich panel as shown in Figure 51, however in this case a FRP top plate was bonded to the concrete panel and the top longitudinal reinforcing bars were omitted.

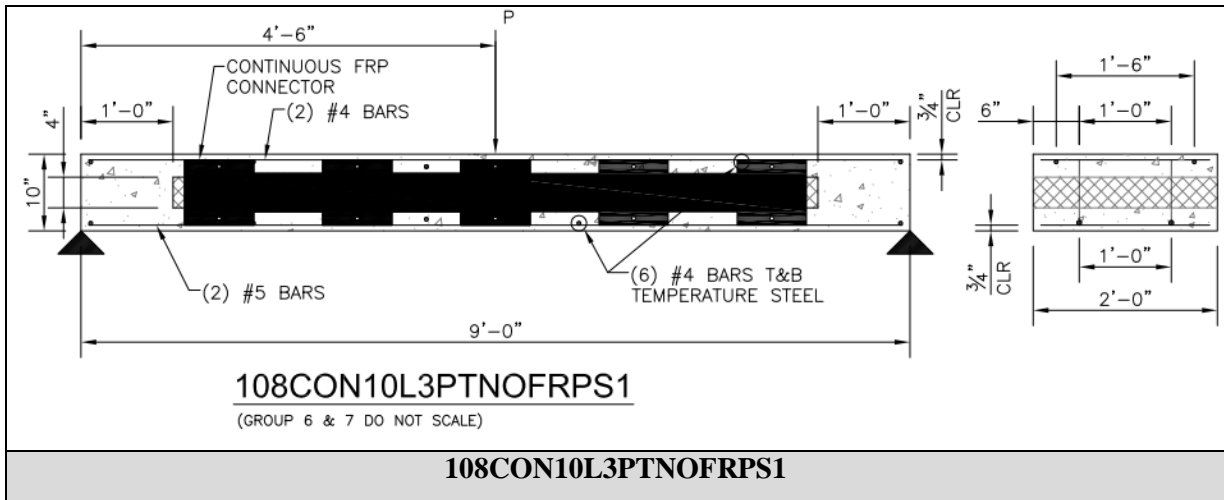


**Figure 50 – 10 in. sandwich panel with continuous connectors (108CON10L3PTNOFRPS1)**

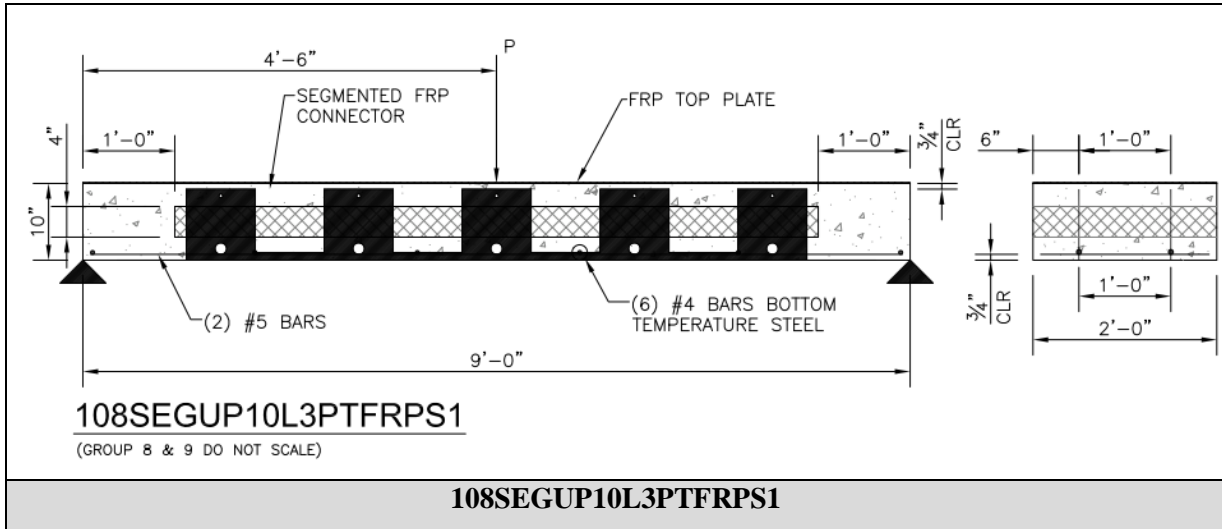


**Figure 51 – 10 in. sandwich panel with segmental connectors and FRP plates (108SEG10L3PTFRPS1)**

Similar to the segmental connector panel with on top longitudinal reinforcing steel, a sandwich panel with continuous FRP shear connectors was constructed with a FRP top plate bonded to the concrete surface and no top longitudinal reinforcing bars as shown in Figure 52.

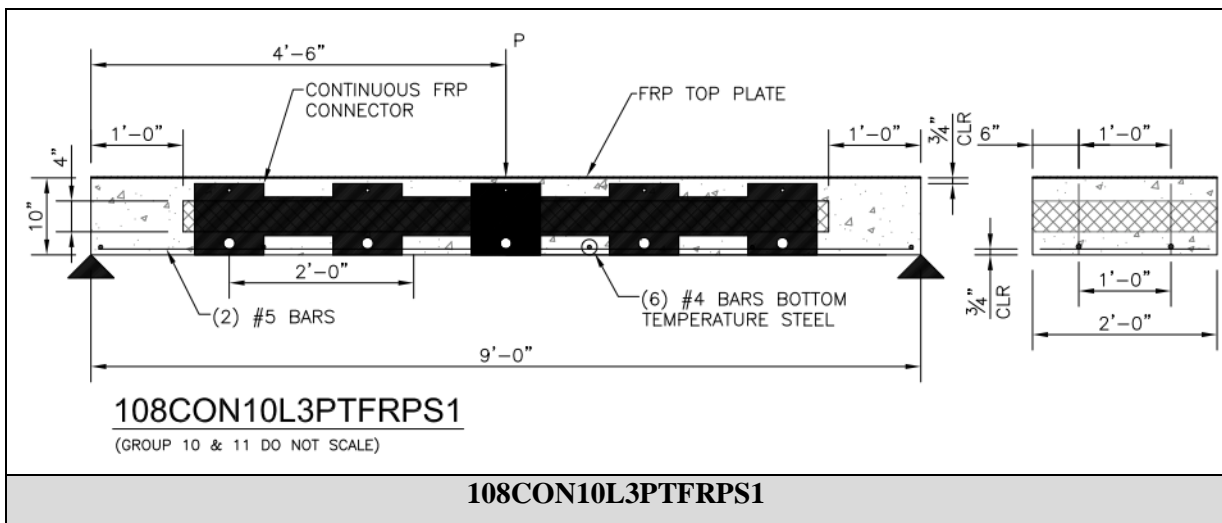


**Figure 52 - 10 in. sandwich panel with continuous connectors and FRP plates (108CON10L3PTFRPS1)**

### **FRP-Confined Precast Concrete Sandwich (FPCS) Panels:**

There were two panels constructed for each of the FPCS panels, two for the 8 inch deep panel and two for the 10 inch deep panel. The construction and configuration of each panel is shown in Figure 56 and Figure 59 respectively. The intent of the externally bonded top and side FRP plates to the concrete panel was to eliminate the need for the top layer of longitudinal reinforcement steel which is considered the compression steel in a flexural concrete beam/slab. All four FPCS test panels, two

each, were 2'-0" wide x 9'-0" long and they varied in depth as shown in the figures. Both groups of panels used segmental shear connectors; however these were inverted or pointed downward, opposite from those panels tested previously in Fall 2012. This configuration was used to aide in the absence of the compression steel reinforcement.

A generic cross section of the FPCS panel is shown in Figure 53 where the top concrete wythe varies from 8 inches to 10 inches for the two groups of specimens.

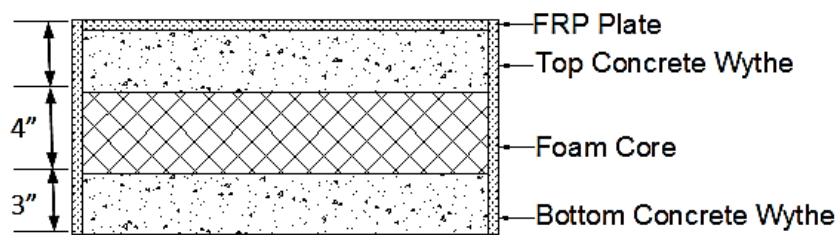


Figure 53 – FPCS scaled test panel with top and side FRP plates<sup>[44]</sup>

A summary of the construction details for the FPCS scaled test panels is shown in Table 16 which complement the construction drawings of the panels in Figure 56 and Figure 57.

Table 16 – FPCS scaled test panel construction details

Wythe Configuration	Compression Steel (#4 bars)	Tension Steel (#5 bars)	Top Temp. Steel (#4 bars)	Bottom Temp. Steel (#4 bars)	Load Conditions	Shear Connectors
3" - 4" - 3"	N/A	(2) @ 12" O.C.	N/A	(5) @ 18" O.C.	3-pt Bending	Segmental
	N/A	(2) @ 12" O.C.	N/A	(5) @ 18" O.C.	3-pt Bending	Segmental
1" - 4" - 3"	N/A	(2) @ 12" O.C.	N/A	(5) @ 18" O.C.	3-pt Bending	Segmental
	N/A	(2) @ 12" O.C.	N/A	(5) @ 18" O.C.	3-pt Bending	Segmental

Since these four FPCS panels were tested months after the original set of twelve scaled test panels the concrete properties were also tested again for the new batch. These new materials properties for the compressive strength are shown in Table 17.

Table 17 – Compressive strength of FPCS panels<sup>[44]</sup>

Specimen	10" FPCS Compressive Strength (psi)	8" FPCS Compressive Strength (psi)
Cylinder 1	4675	2787
Cylinder 2	4838	2818
Cylinder 3	4648	2968
Cylinder 4	5280	2687
<b>Average</b>	<b>4860.25</b>	<b>2815</b>

Likewise a splitting tensile test was performed per ASTM C496/C496M and the failure mode with strain gage is shown in Figure 54 and the plot of the stress/strain distribution is shown in Figure 55. The maximum tensile strength of the 4860 psi concrete is approximately 380 psi, which is 7.8% of the compressive strength. Typically the tensile strength of the concrete is approximately 7-10% of the compressive strength and this seems appropriate.



**Figure 54 – Splitting tensile test specimen**

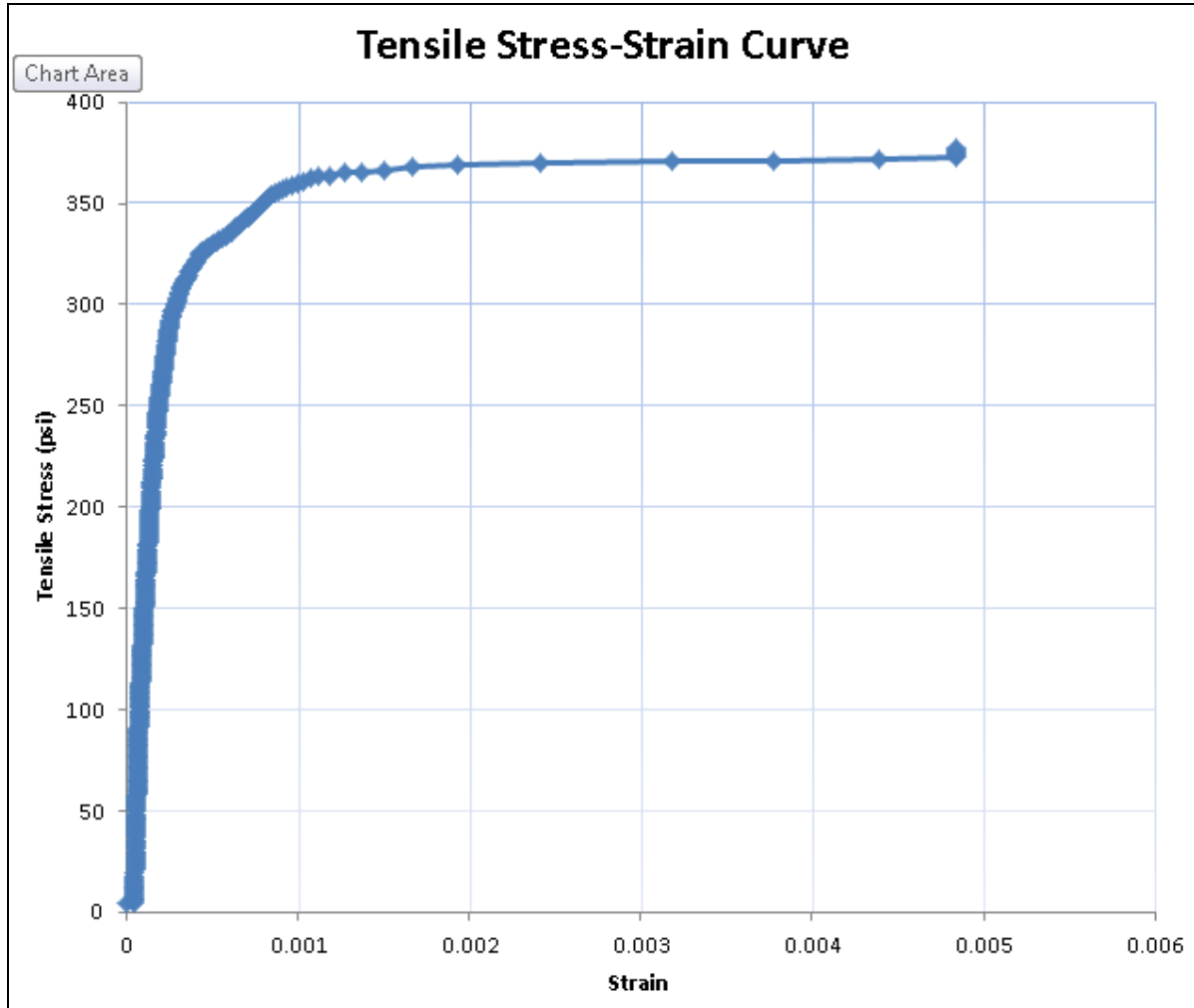


Figure 55 – Stress-strain plot for splitting tensile test specimen

The Phase I panels FEA model used the theoretical formulas by Hsu and Hsu to develop the Damaged Plasticity model. This is because the compressive strength of the concrete does not have a completed curve and then an approximation was used for the compressive and tensile data. To be consistent with Phase I, we use the 10% rule of thumb for the tensile strength of concrete with respect to the compressive strength and continue to use the theoretical model.

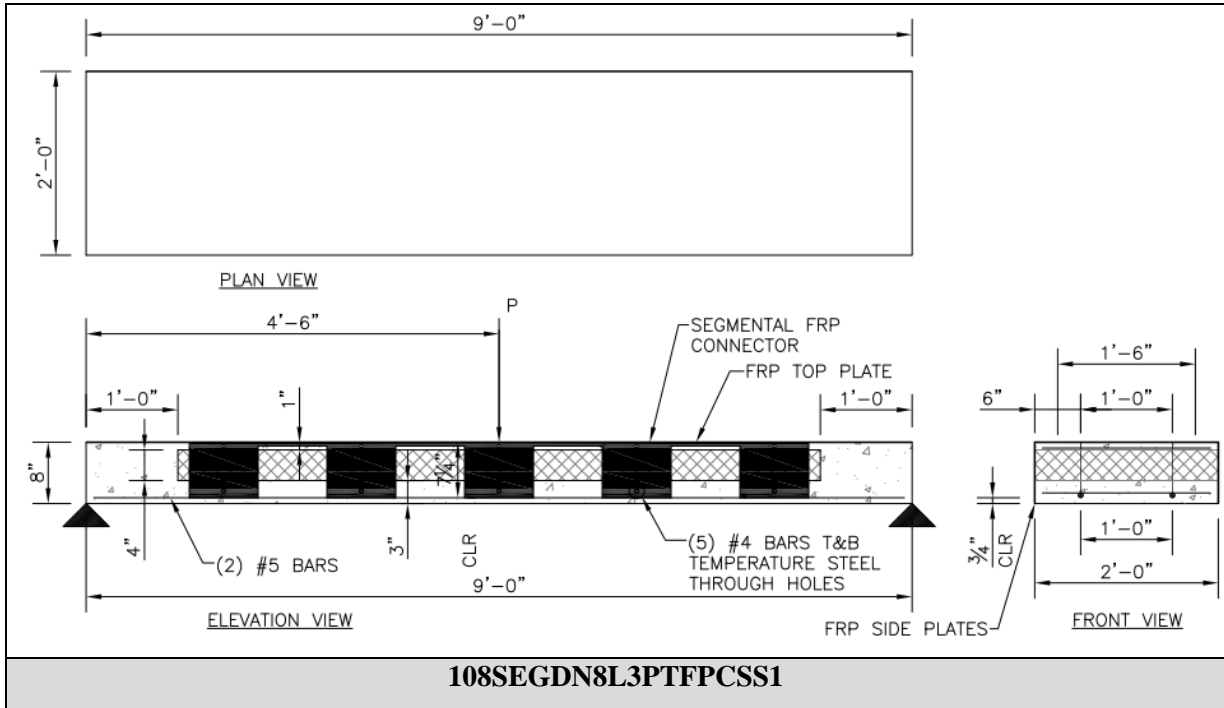


Figure 56 – 8 in. panel with inverted segmental connector and FPCS (108SEGDN8L3PTFPCSS1)

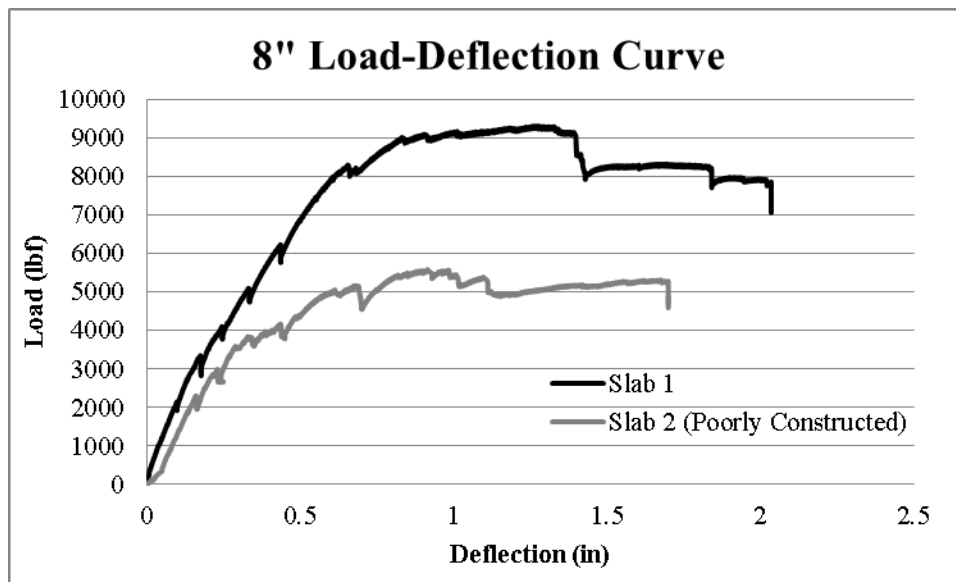


Figure 57 – Load displacement graph for 8 in. FPCS panel (108SEGDN8L3PTFPCSS1)

A picture of the FPCS test panel with the FRP top and side plates and secured in the test fixture is shown in Figure 58. The construction of the 10" FPCS panel is shown in Figure 59.



**Figure 58 – 10 in. FRP sandwich panel (108SEGDN10L3PTFFPCSS1) in testing apparatus**

A thorough description of the test set up, resin mixture, aggregate bonding and strain gage distribution is provided in Tom Norris' thesis document<sup>[44]</sup> and will not be repeated in this study.

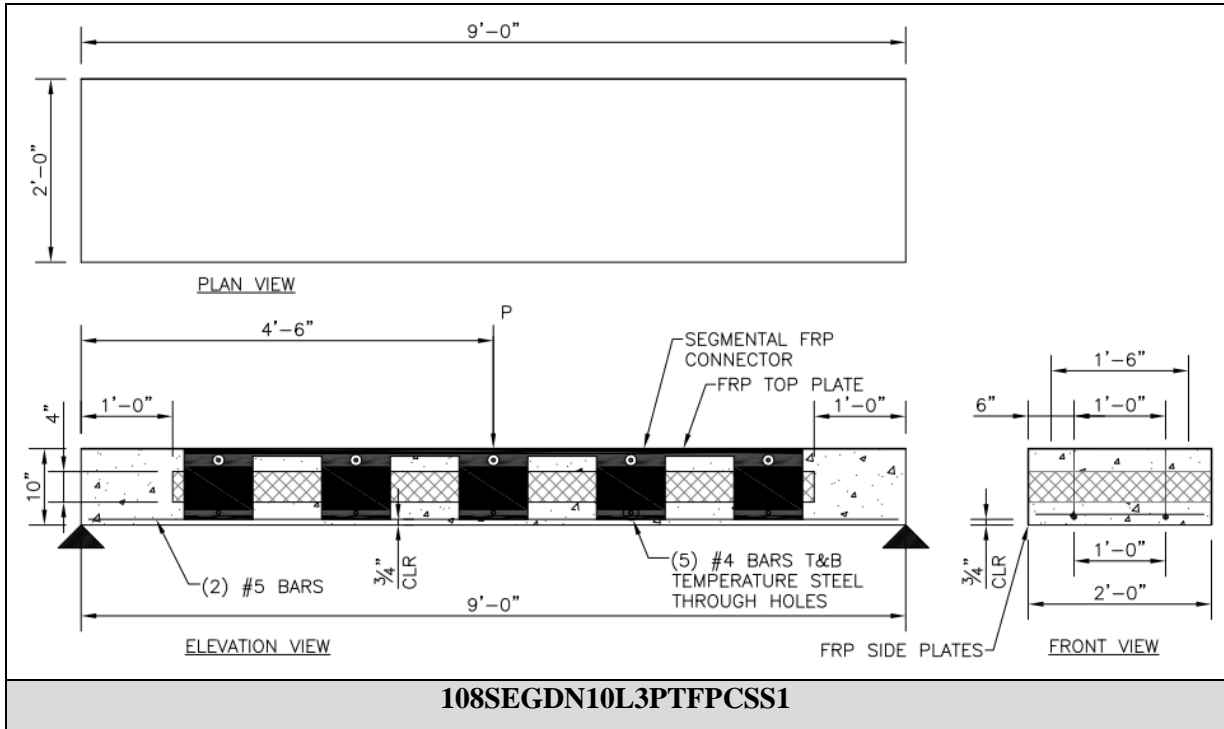


Figure 59 – 10 in. Segmental FRP panel with top and side FRP plates

The load-deflection curve for the (2) 10" FPCS panels were fairly consistent which made for a reliable data source as can be seen in Figure 60.

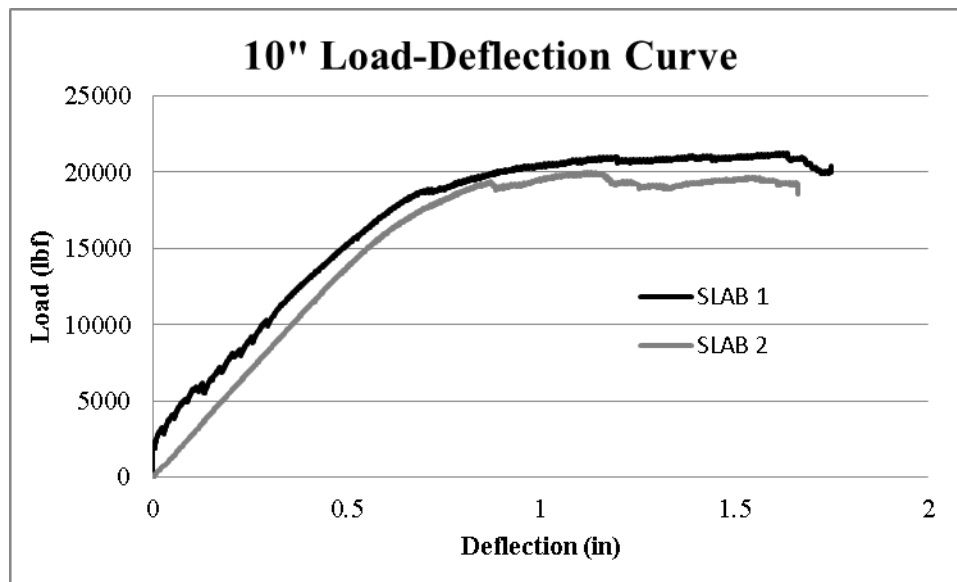


Figure 60 - Load displacement graph for 10 in. FPCS 108SEGDN10L3PTFPCSS1<sup>[44]</sup>

The summary for the (4) FPCS panels, the two 8 in. panel and the two 10 in. panel are shown in Table 18. The 8 in. panel is labeled as the 108SEGDN8L3PTFPCSS1 in the finite element analysis section while the 10 in. panel is labeled as 108SEGDN10L3PTFPCSS1.

**Table 18 – FPCS panels ultimate load summary<sup>[44]</sup>**

<b>Specimen Thickness</b>	<b>Effective Length (ft)</b>	<b>Bending Type</b>	<b>Moment Arm (ft)</b>	<b>Cracking Load (kip)</b>	<b>Cracking Moment (kip*ft)</b>	<b>Failure Load (kip)</b>	<b>Failure Moment (kip*ft)</b>	<b>Max Load Deflection (in)</b>
8"	9	3-pt	4.5	3	6.75	9.311	20.950	1.201
	9	3-pt	4.5	3	6.75	5.581	12.557	0.916
10"	9	3-pt	4.5	2	4.50	21.280	47.880	1.634
	9	3-pt	4.5	3	6.75	20.020	45.045	1.131

The 8 in. panel display inconsistent results as one of the panels had poor construction and lacked proper vibration and bonding of the concrete to the FPR plates. The 10 in. FPCS panel produced much higher flexural strength values. The summary for the failure modes is shown in

**Table 19 – FPCS panels failure mode summary<sup>[44]</sup>**

<b>Slab Thickness</b>	<b>Connector Type</b>	<b>Initial Failure Mode</b>	<b>Secondary Failure Mode</b>
8"	Segmental	Bending	Crushing/Insulation Rupture
	Segmental	Bending	FRP Debond/Insulation Rupture
10"	Segmental	Bending	FRP Debond
	Segmental	Bending	FRP Debond/Crushing

The two FPCS panels (8 in. and 10 in.), the solid concrete scaled test panel and the 10 in. sandwich panel with just FRP top plate load versus deflection curve is shown in Figure 61. The adjusted curves for two FPCS panels, along with the solid panel and the 10" FRP top plate only panel is shown in Figure 62.

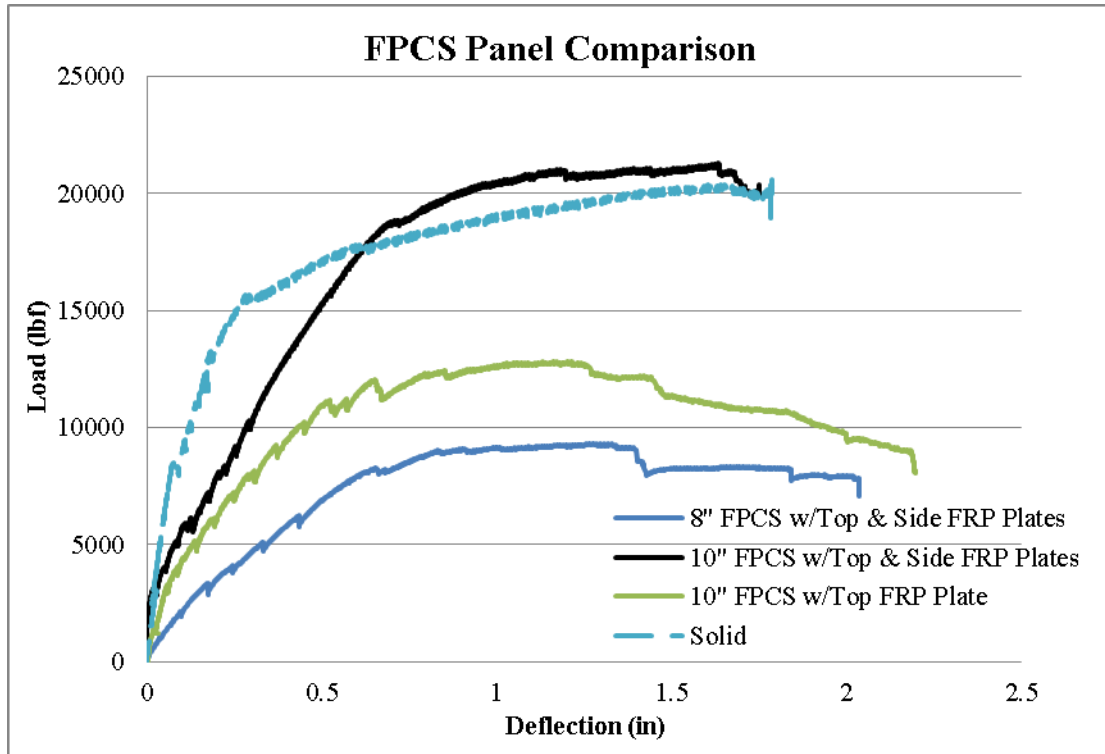


Figure 61 – FPCS panel comparison<sup>[44]</sup>

The solid concrete panel has the highest initial modulus of elasticity, however it does not provide the greatest load carrying capacity. The 10 in. FPCS panel exceeds 20,000 lbs of load carrying capacity with a reduced weight of approximately 40%.

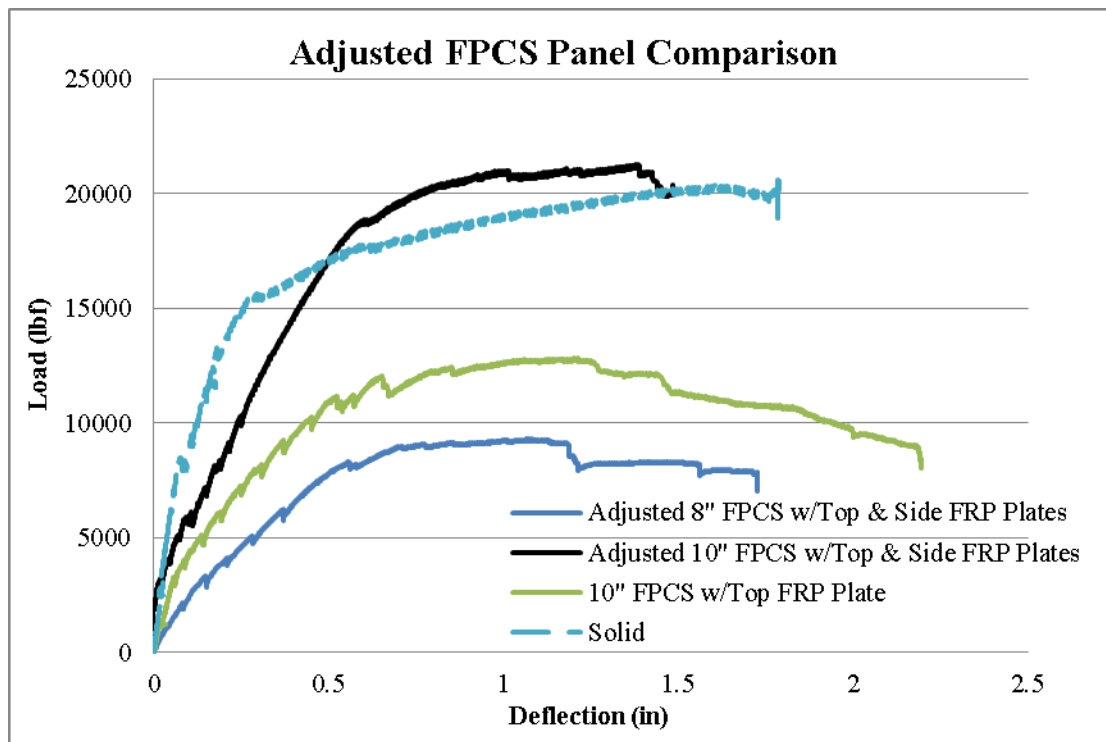


Figure 62 – Adjusted FPCS panel comparison<sup>[44]</sup>

#### 4.4.3 FULL SCALE TEST PANELS

##### Full Scale FRP-Confined Precast Concrete Sandwich (FPCS) Panels:

Following the construction and testing of (16) scaled test panels, (2) individual full-scale FPCS panels were constructed. Each panel is 16'-0" long and 2'-0" wide. One panel is 8 inches deep and the second panel is 10 inches deep. The construction of the panels is shown in Figure 63 and Figure 64 respectively. The panels use the same configuration of the scaled 8 in. and 10 in. FPCS panels previously constructed and tested. These two 16 foot long panels were also evaluated for strength, stiffness and DCA and a finite element analysis model was constructed to determine the correlation between numerical modeling and test results. The summary of the construction of the full scale test panels is shown in Table 20.

Table 20 – Full scale FPCS panel construction details<sup>[44]</sup>

FPCS Panel Thickness	Compression Steel (#4 bars)	Tension Steel (#5 bars)	Top Temp. Steel (#4 bars)	Bottom Temp. Steel (#4 bars)	Load Conditions	Shear Connectors	Length
8"	N/A	(2) @ 12" O.C.	N/A	(9) @ 18" O.C.	3-pt Bending	Segmental	16'
10"	N/A	(2) @ 12" O.C.	N/A	(9) @ 18" O.C.	3-pt Bending	Segmental	16'

The 8" FPCS full scale test panel is shown in Figure 63 and was constructed to determine if the FRP top plate and shear web connectors could provide enough strength to reduce the compressive zone of

the concrete panel. The effective of losing the concrete mass in the compression block zone will be an indicator as to how much strength it provides versus the FRP plate.

The 10 inch full scale test panel is similar to the 8 inch panel, however the top concrete wythe has the normal 3 inches. Both panels are without top longitudinal reinforcing steel.

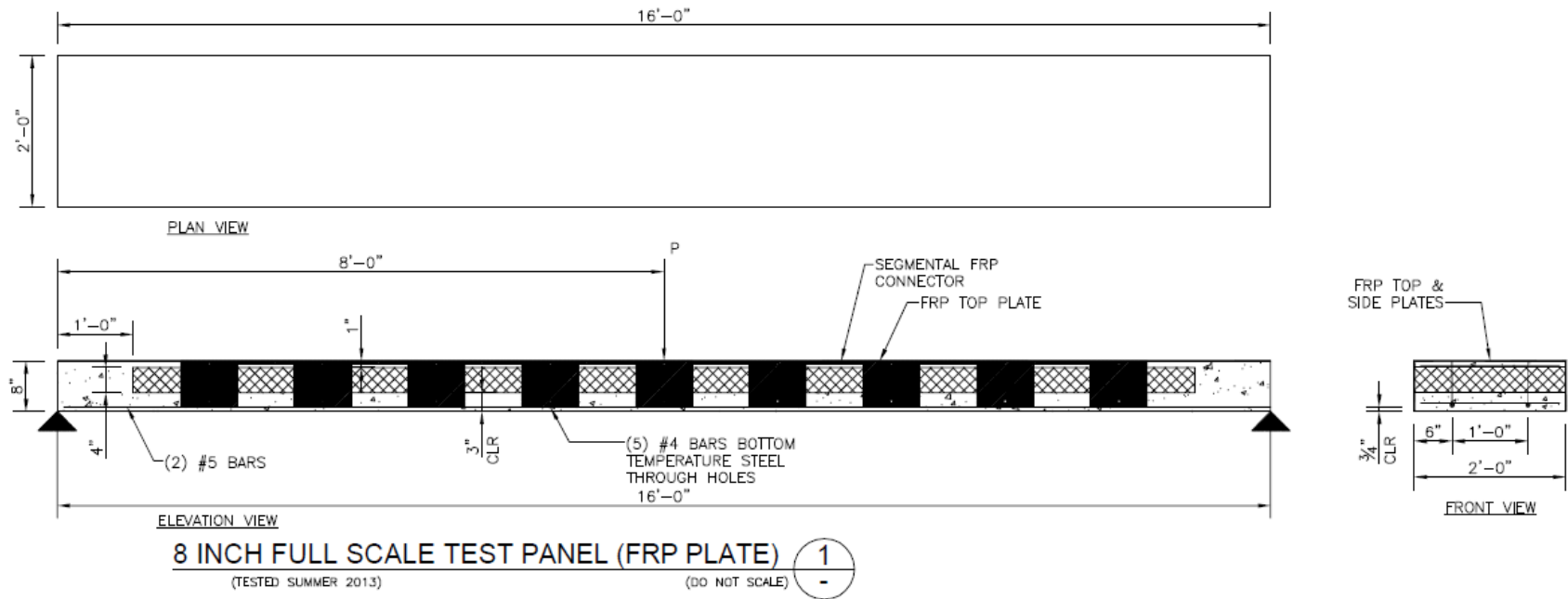


Figure 63 – 8 in. full scale test panel

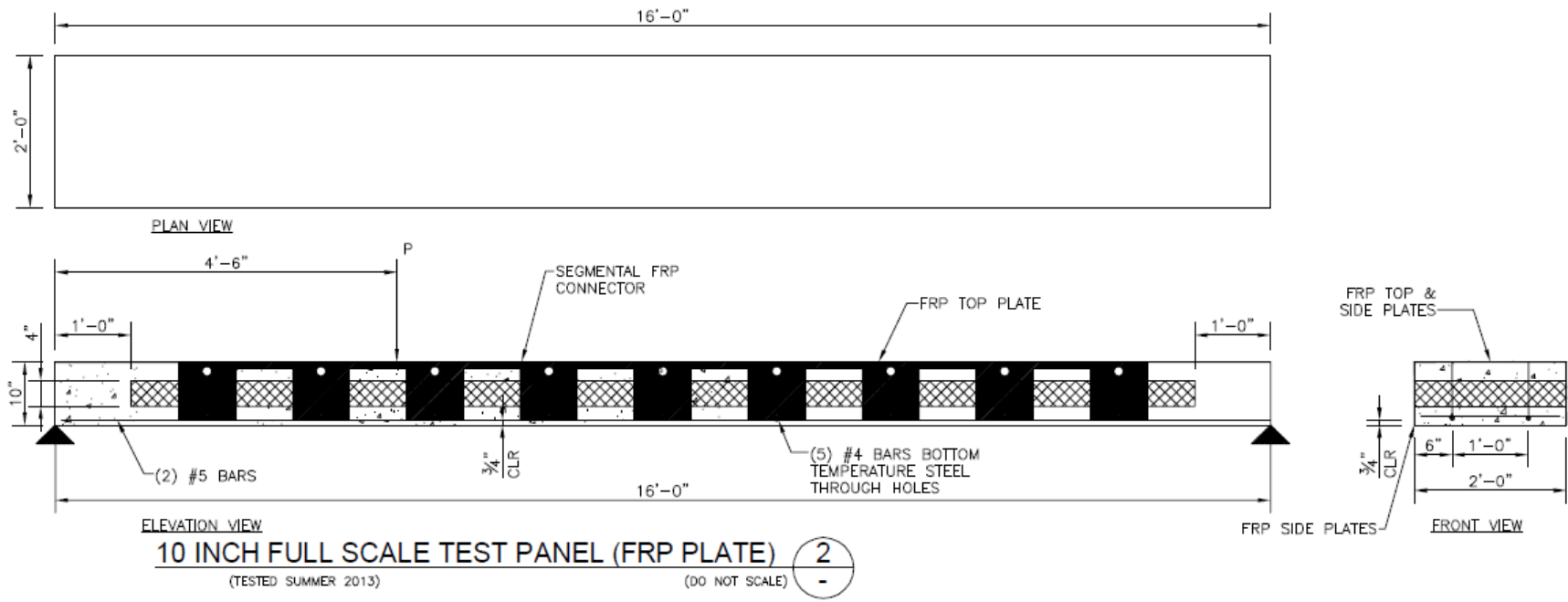


Figure 64 – 10 in. full scale test panel

The full scale FPCS panels were constructed and tested at a later date than the scaled FPCS panels and therefore a new batch of concrete was used and sample cylinders were tested. The 28-day compressive strength tested in accordance with ASTM C39 is shown in Table 21 and the average 28-day compressive strength of 4807 psi will be used for analytic calculations and finite element analysis modeling.

**Table 21 – Compressive strength of full-scale test panel cylinders<sup>[44]</sup>**

<b>Specimen</b>	<b>Compressive Strength (psi)</b>
Cylinder 1	4591
Cylinder 2	5003
Cylinder 3	4606
Cylinder 4	5030
<b>Average</b>	<b>4807.5</b>

The remaining material properties for steel, FRP and insulation remain the same as previously reported. A detailed description of the construction, cure and strain gage location for the full scale test panels can be found in Norris thesis<sup>[44]</sup>, however a few pictures of the construction details can be seen in Figure 65, Figure 66 and Figure 67. The FRP segmental shear connectors have transverse reinforcement steel inserted through the holes in the connectors for anchoring application as shown in Figure 65.



**Figure 65 – Full scale FPCS panel insulation, rebar and strain gages<sup>[44]</sup>**

The pea gravel aggregate that is glued to the FRP top plate is shown in Figure 66 while the first lift of the concrete pour is applied which comprises the top wythe of the specimen. The pea gravel was used to provide better mechanical bond of the FRP plate to the concrete.



**Figure 66 – Full scale FPCS first concrete lift pour<sup>[44]</sup>**

Finally the panels are cured and the forms are stripped which can be shown in Figure 67.



**Figure 67 – Cured and stripped full-scale FPCS specimens<sup>[44]</sup>**

The full-scale test panels were also loaded in 3 point bending, shown in Figure 68, to be consistent with prior testing methods. The previous scaled test panels had an effective length of 8 feet or 9 feet whereas the full-scale FPCS panels have an effective length of 16 feet.

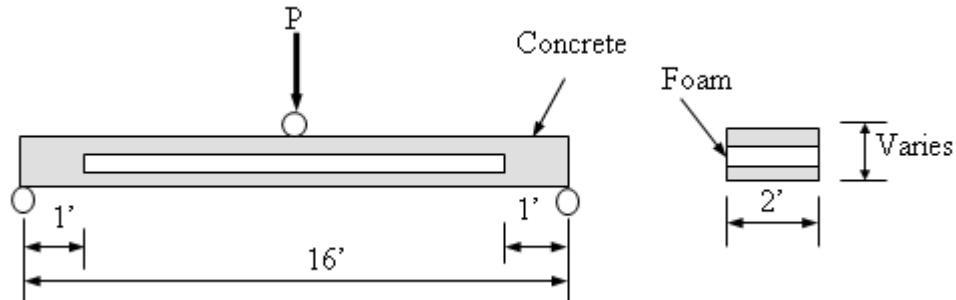


**Figure 68 – Full-scale FPCS loading diagram<sup>[44]</sup>**

The panel was carefully loaded in the testing apparatus as shown in Figure 69 and the inserted strain gages connected to the data collector. The panel was loaded to failure and measurements, pictures and failure modes were recorded during the test.



**Figure 69 – Full-scale FPCS panel in testing apparatus<sup>[44]</sup>**

The 8 inch panel exhibited a normal load-deflection curve for being a flexure-controlled specimen and this is shown in Figure 70. The maximum load was near 4,500 lbs and the corresponding deflection is 3.87" which is approximately  $L/50$ . The initial yielding load appears to be 3,000 lbs at approximately 1.0" and this correlates to  $L/192$ . If the panel were restricted to a  $L/360$  deflection criteria for live load, the limit deflection would be 0.53" and the limit load would be approximately 1,500 lbs.

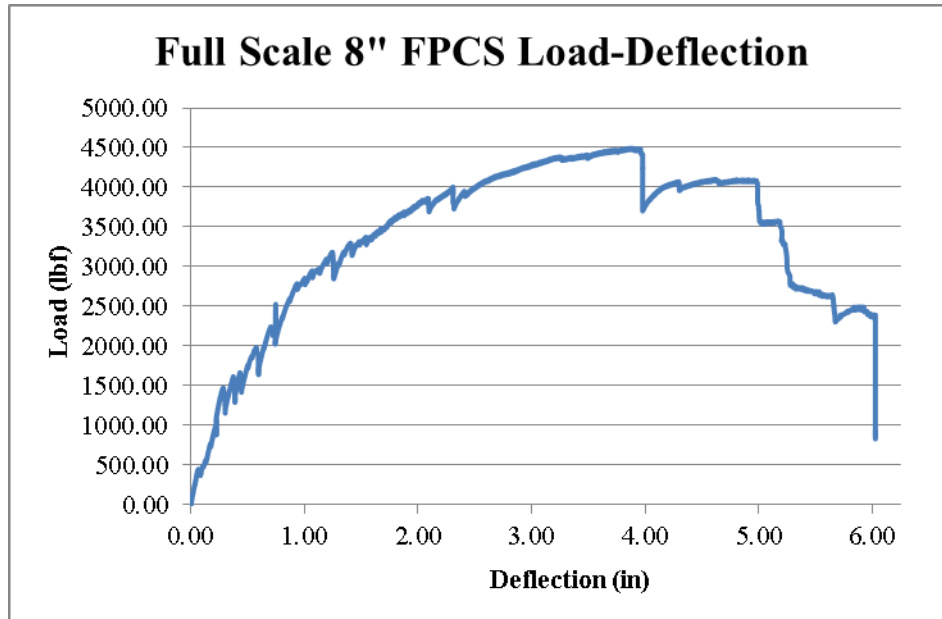


**Figure 70 – 8" Full-scale FPCS load-deflection curve**

Limiting the panel to a live load deflection criteria of  $L/360$  allows for plenty of reserve strength and factor of safety. Furthermore the panel is flexure-controlled and no brittle or sudden failure mechanisms exist near the limit load. Likewise with the 10 inch FPCS full scale panel the limit load at  $L/360$  deflection criteria is approximately 3,000 lbs, whereas the initial yielding load appears to be 9,000 lbs and the ultimate load is 9,500 lbs. These results are shown in Figure 71.

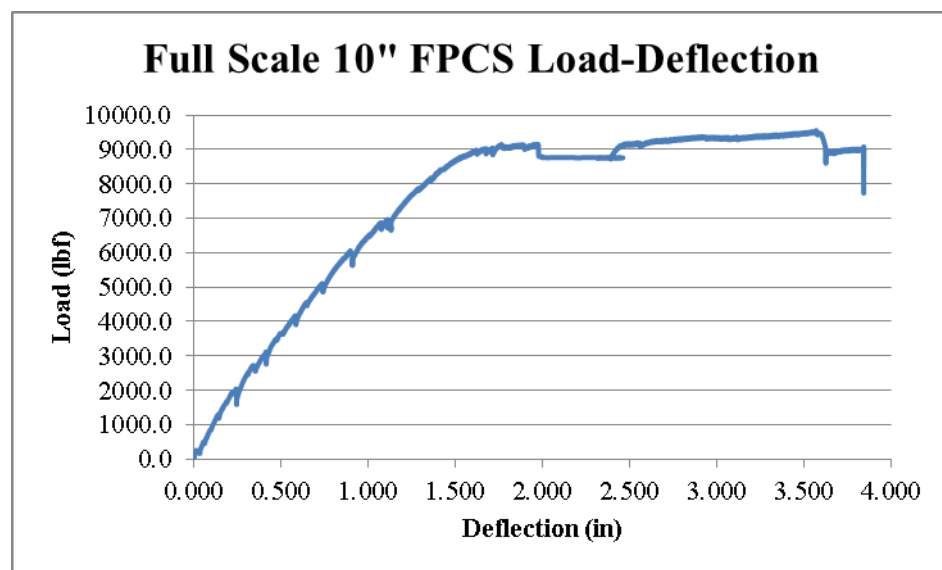


**Figure 71 – 10" Full-scale FPCS load-deflection curve**

The test results summary for the 8 inch and 10 inch full-scale FPCS panels are shown in Table 22. The 10 inch panel, as previously explained, has yield strength of 3 times that of the load at which most roof member deflection criteria exist. The approximate corresponding uniform live loading for the 8" and 10" panel with limiting deflection criteria of  $L/360$  is 40 psf and 80 psf respectively and the panels have proven to support up to 3 times that service load.

**Table 22 – Full scale FPCS ultimate load summary**

<b>Specimen Thickness</b>	<b>Effective Length (ft)</b>	<b>Bending Type</b>	<b>Moment Arm (ft)</b>	<b>Cracking Load (kip)</b>	<b>Cracking Moment (kip*ft)</b>	<b>Failure Load (kip)</b>	<b>Failure Moment (kip*ft)</b>	<b>Max Load Deflection (in)</b>
8"	16	3-pt	8	1	4.00	4.493	17.972	3.870
10"	16	3-pt	8	2	8.00	9.553	38.212	3.571

## **4.5 TEST RESULTS VS. ANALYTICAL AND FEA PREDICTIONS**

The following section shows the analysis results from a numerical study using ABAQUS© a commercially available finite element analysis software program. Unlike metals and some composite materials, concrete has a higher standard deviation with respect to engineering performance when subjected to flexural loads. Hundreds of analyses were performed on these panels using the following methodologies to determine the best approach for predicting strength and failure under flexural loading:

1. Linear Static general method with non-linear geometry
2. Linear Static RIKS method with non-linear geometry
3. Implicit Quasi-Static method with non-linear geometry
4. Explicit dynamic analysis method with non-linear geometry and amplitude load ramping.

As mentioned before, concrete beams and panels subjected to flexural loading experience quasi-static failure mechanisms as the concrete cracks and loads redistribute to the reinforced steel or other tension loading carry constituent materials. The Implicit Quasi-Static approach may seem to be the best suited for these models, however the Explicit Dynamic analysis provided the best insight to the overall failure and strength.

#### 4.5.1 SOLID SCALED TEST PANEL

The solid 10 inch concrete panel tested in the spring of 2012 (108SOL10DL3PTNOFRPS1) is shown in Figure 72. The panel has (2) No.5 rebars on the bottom longitudinal and (2) No. 4 rebars on the top longitudinal. There are some transverse No. 4 rebars for integrity and shrinkage control. The panel was loaded in 3-point bending with a single point load at midspan as shown in Figure 72.

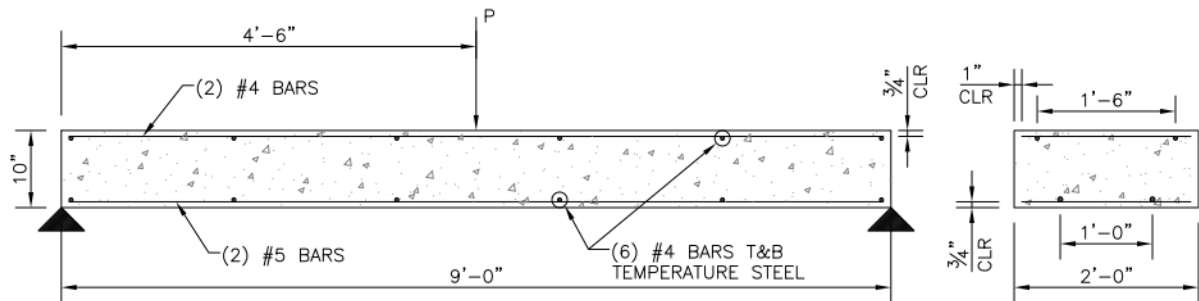


**Figure 72 – 10 inch solid concrete panel construction**

The results of the 10 inch solid concrete panel for load versus deflection are shown in Figure 76. The two solid blue lines are the Group 1 and Group 2 test panels performed at University of Idaho in the Spring of 2012. The panels were constructed in the University of Idaho lab under fair conditions. The dashed green line represents the calculations performed per the equations in ACI 318<sup>[4]</sup>. This line provides an upper bound and is near linear. The lower dashed red line is the finite element analysis results performed in ABAQUS for the 108SOL10L3PTNOFRPS1 analysis model. Using the damage concrete plasticity properties, the tension stiffening the nonlinear material properties of the reinforcing steel and an explicit quasi-static analysis the numerical solution was able to capture the earlier linear portion of the curve and the later nonlinear portion after the concrete is damaged due to cracking. This also takes into account the yielding of the steel reinforcement.

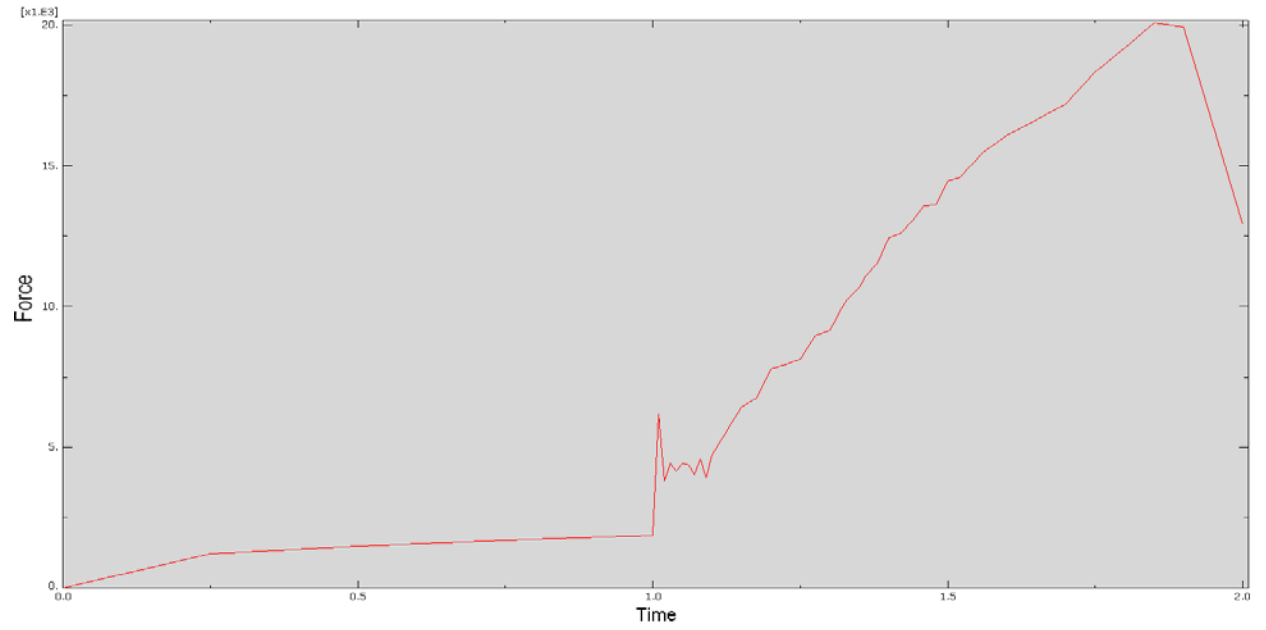


**Figure 73 – FEA measured support reaction versus step time for 108SOL10L3PTNOFRPS1**

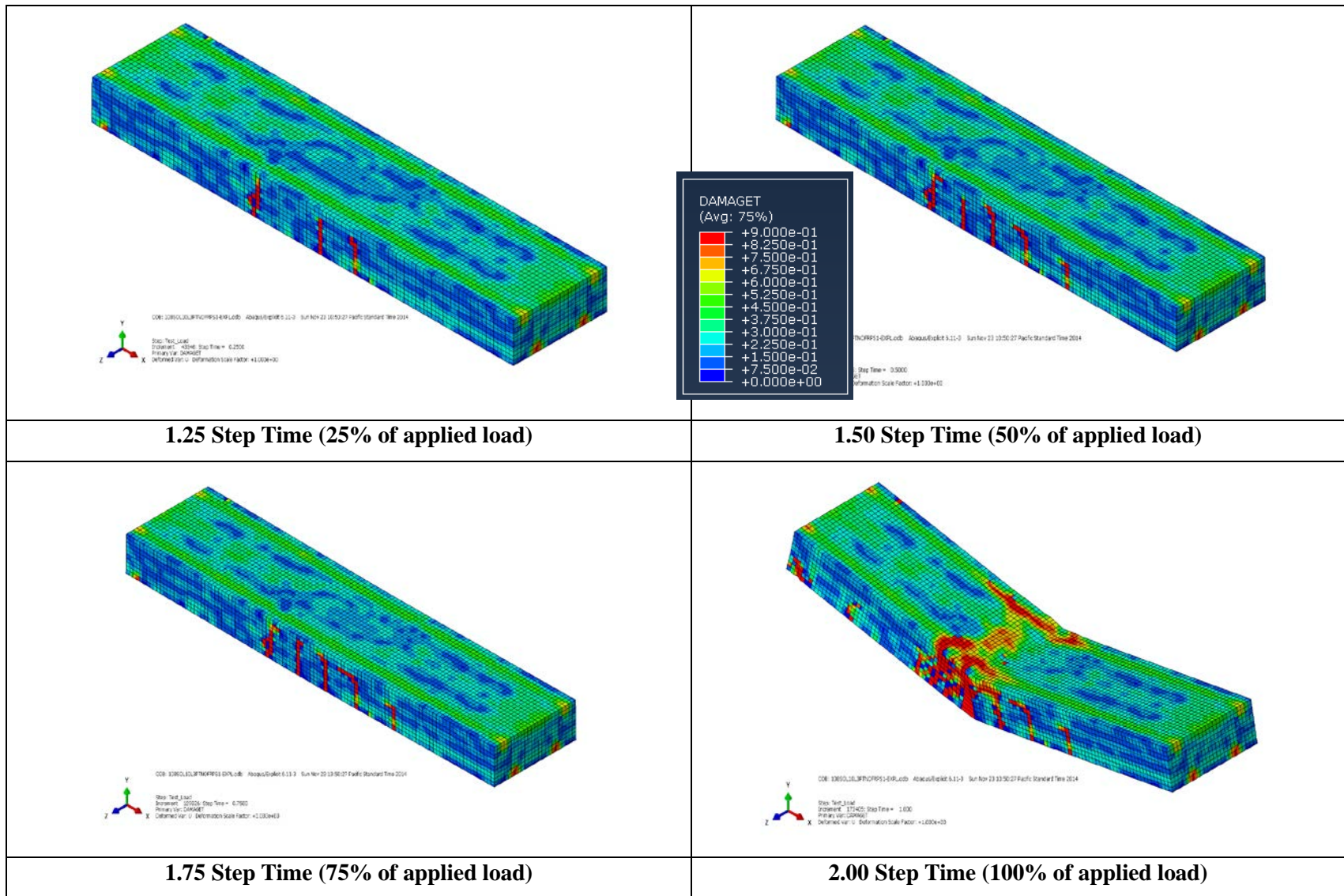


Figure 74 – 108SOL10L3PTNOFRPS1 Damage Tension FEM Plots

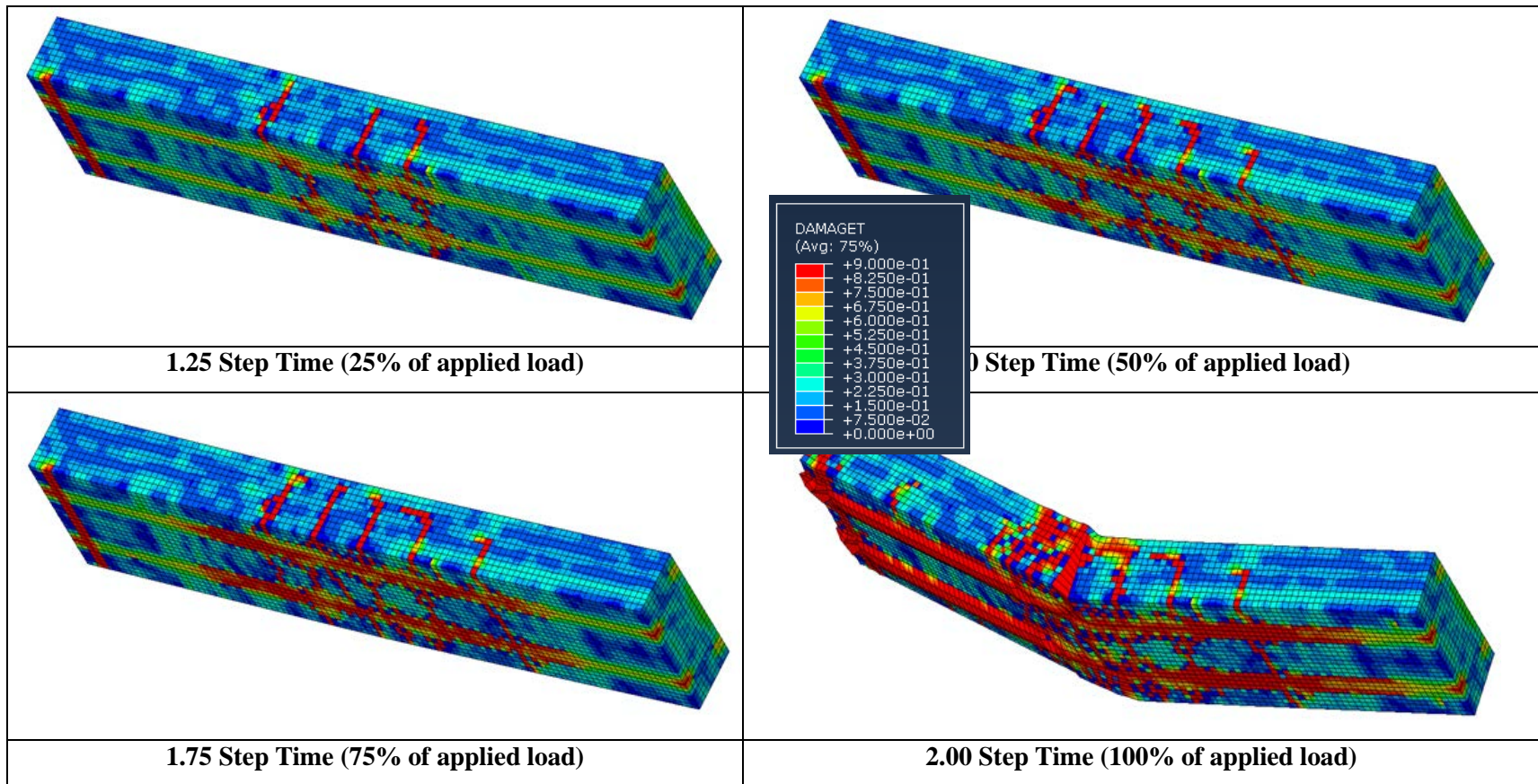
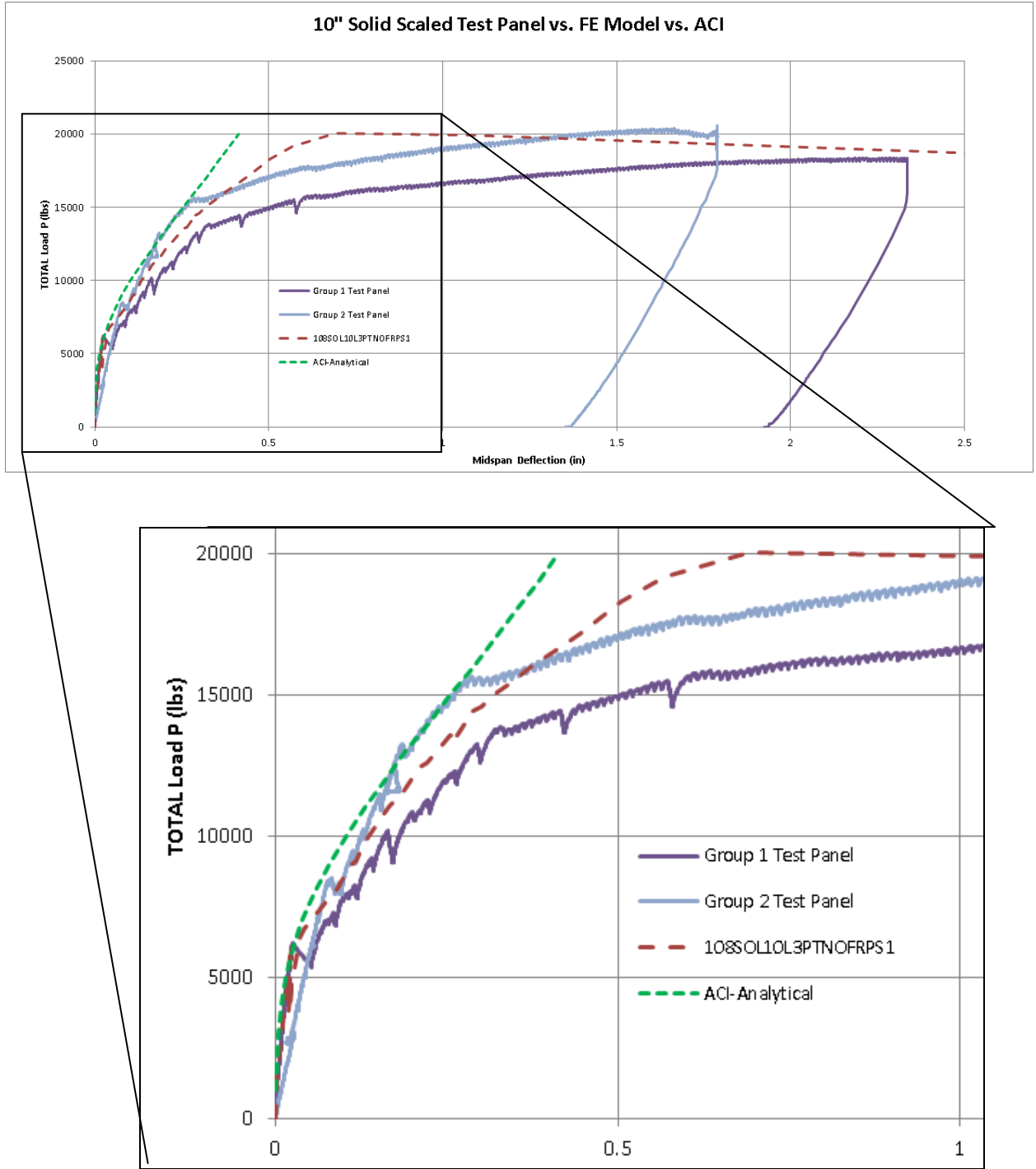


Figure 75 – 108SOL10L3PTNOFRPS1 Damage Tension FEM Plots (Bottom)



**Figure 76 – 10 inch solid concrete panel FEA vs. Test results**

In the initial regions of the curve for the 108SOL10L3PTNOFRPS1 FEA model there appears to be a bit of an up-and-down on the results around 10,000 lbs force and this is due to the way it is loaded in ABAQUS during the explicit analysis. The rate has to be controlled in order to not load it too quickly or too slowly. This is a case where it was loaded a bit too quickly in STEP 2 following the

selfweight load application in STEP 1 and a small amount of vibration occurs until it settles out and then resumes loading.

The ACI-318 formula for deflection of concrete beams is plotted in Figure 76. Per ACI-318, and its service limits, the design of the panel would be restricted to 6,000 lbs of load, which is only a fraction of the total strength of the panel. This allows for a suitable factor of safety in the design code.

#### 4.5.2 SCALED SANDWICH TEST PANEL

The next set of results presented in detail pertains to the sandwich panel with discrete FRP shear connectors. Another picture of the construction for this panel is shown in Figure 77 for depiction of the constituent materials and then following that are the FEA results for tension damage and deflection.

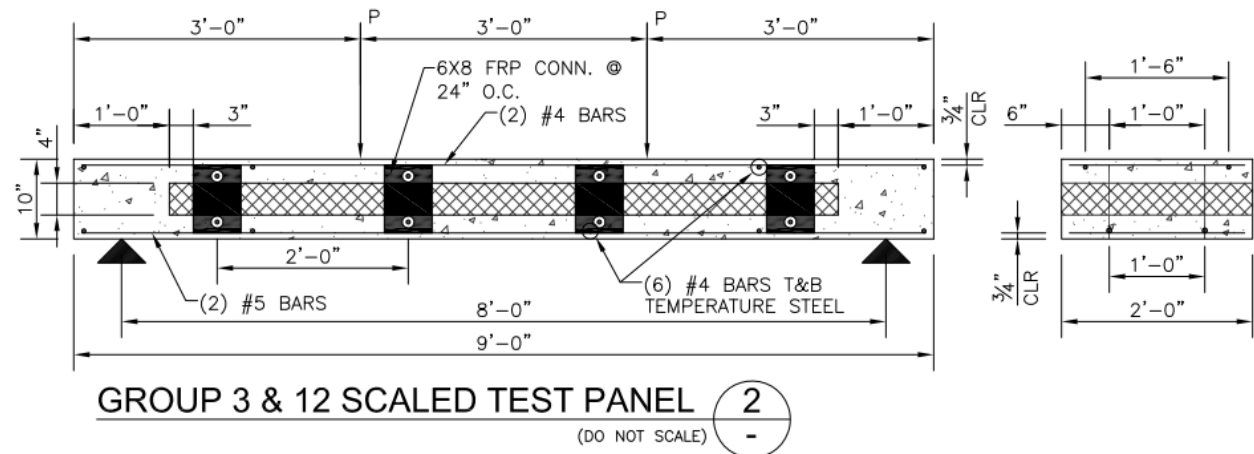


**Figure 77 – 10 inch sandwich panel with discrete connectors, 108DIS10L4PTNOFRPS2**

The tension damage plots on the top and bottom of the panel are shown in Figure 78 and Figure 79 respectively. These plots are good measure and indication of how the panel is deforming, cracking and failing. Other engineering measurements such as stress and deflection can be used to derive strength and stiffness values, however Tension Damage is highly valuable and the primary benefit to using the explicit analysis approach. The plots are summarized at  $\frac{1}{4}$  load point values, so at 25% of the load, 50% of the load and so on. What can be gathered from the plots is where the initial cracking occurs and where the panel experiences some load reversals or inflections as the stresses in the panels travel around the insulation layer. As the reinforcing steel is stress and exhibits tension

forces, the radial stresses from the reinforcing steel bar locations are also captured with this analysis method and this is another important aspect of determining the strength and failure of the panels.

The deflection plots shown in Figure 80 show the  $\frac{1}{4}$  load steps and deflection results and the distribution is not linear as can be seen and therefore indicates there is a level of DCA that changes as the load changes on the panel.

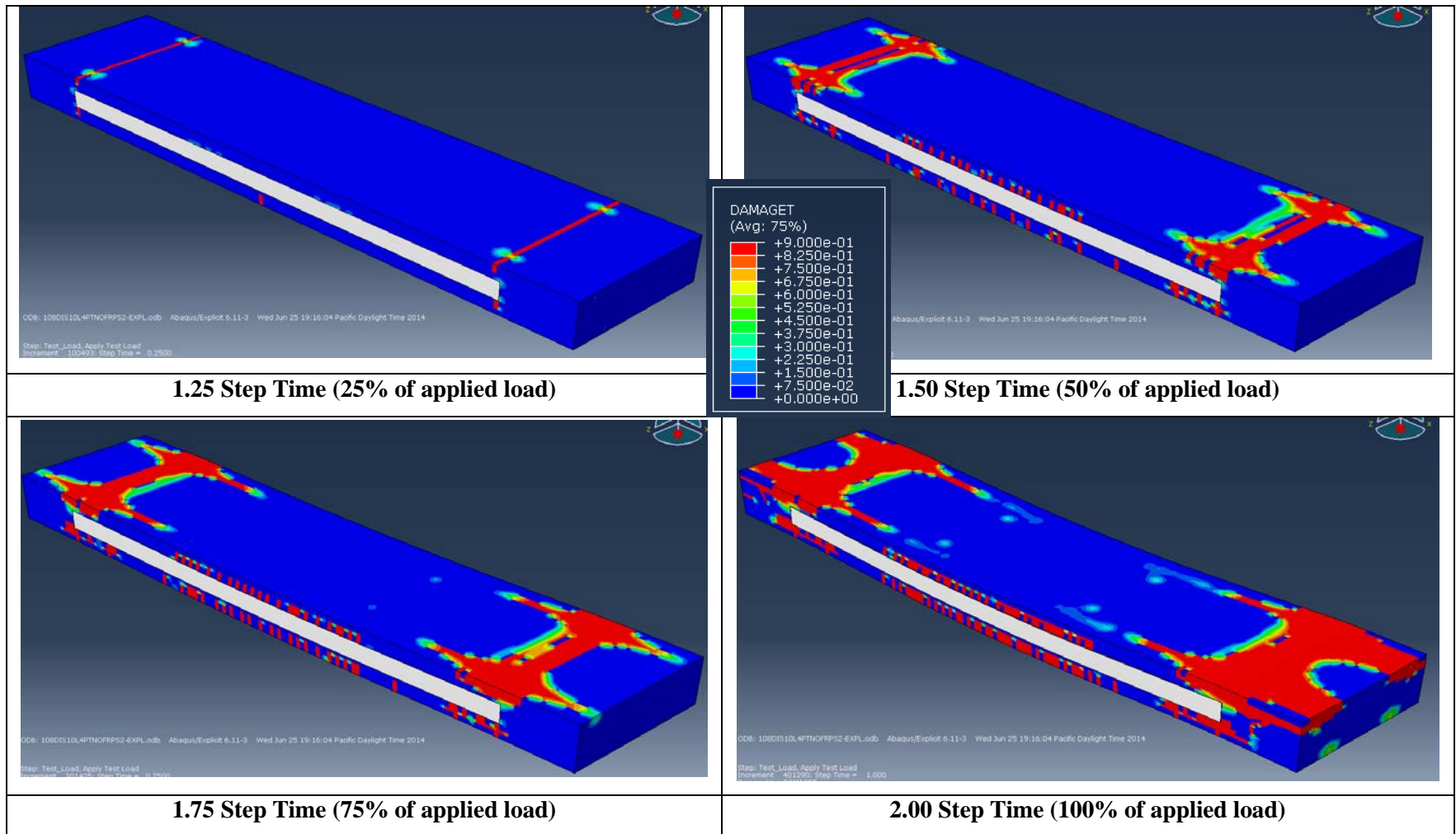


Figure 78 - FEA tension damage 108DIS10L4PTNOFRPS2

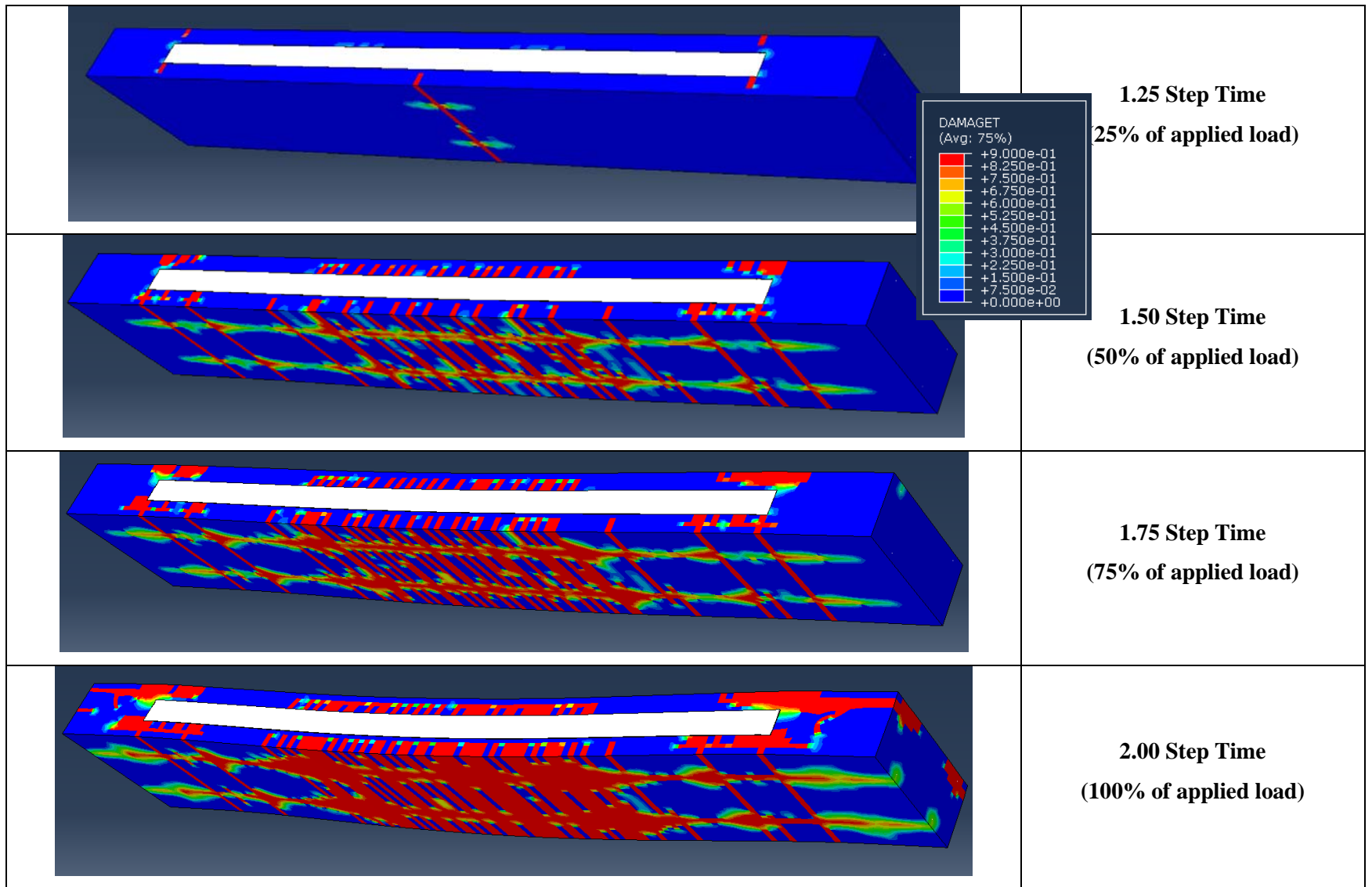
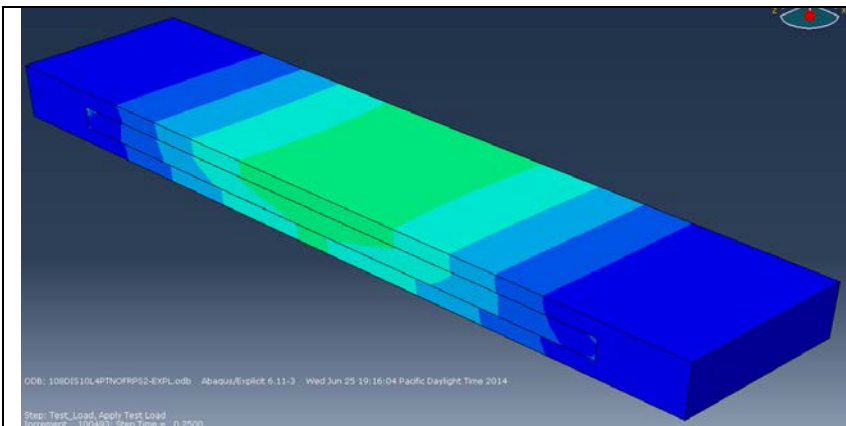
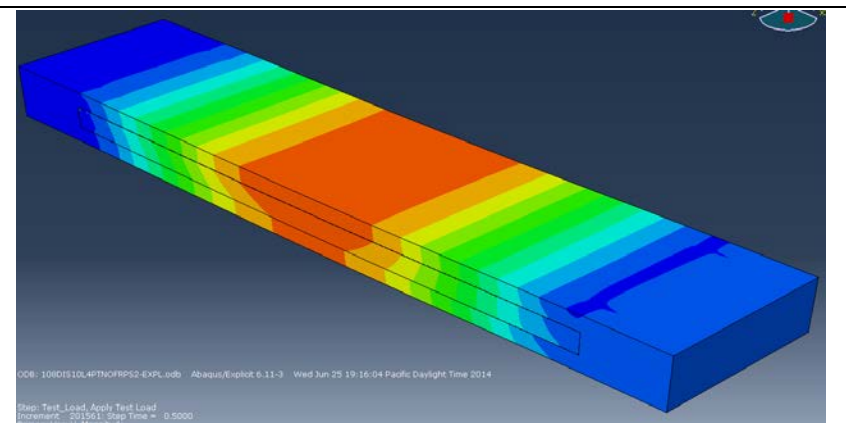


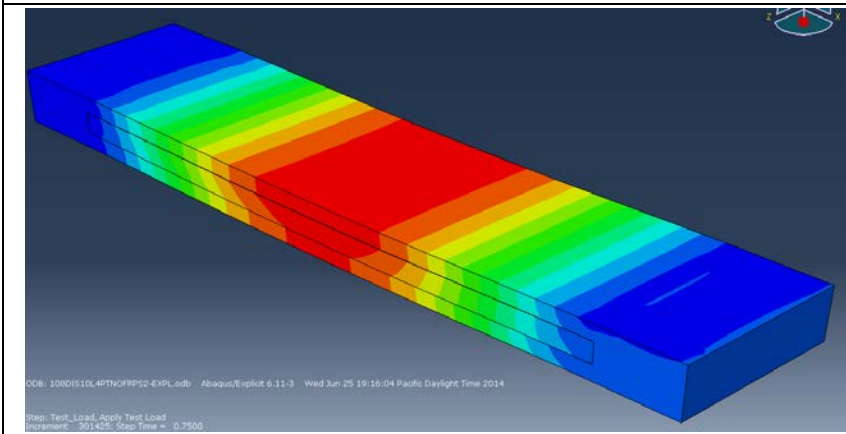
Figure 79 – FEA tension damage, panel bottom, 108DIS10L4PTNOFRPS2



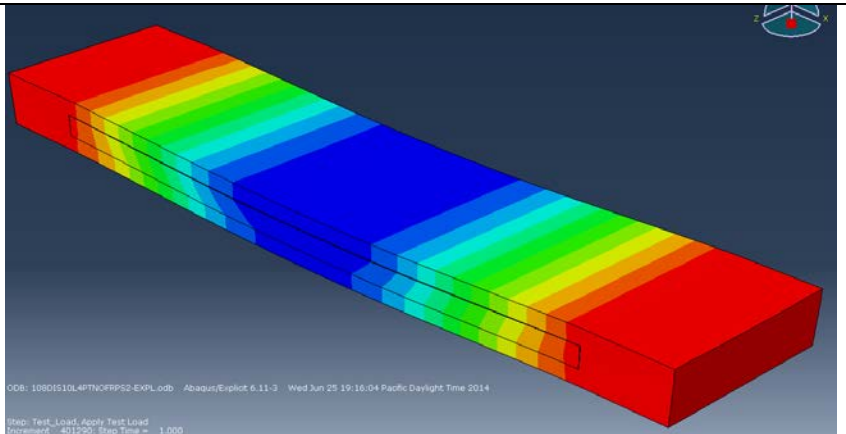
**1.25 Step Time (25% of applied load)**



**1.50 Step Time (50% of applied load)**



**1.75 Step Time (75% of applied load)**



**2.00 Step Time (100% of applied load)**

**Figure 80 – FEA deflection plots, U2, 108DIS10L4PTNOFRPS2**

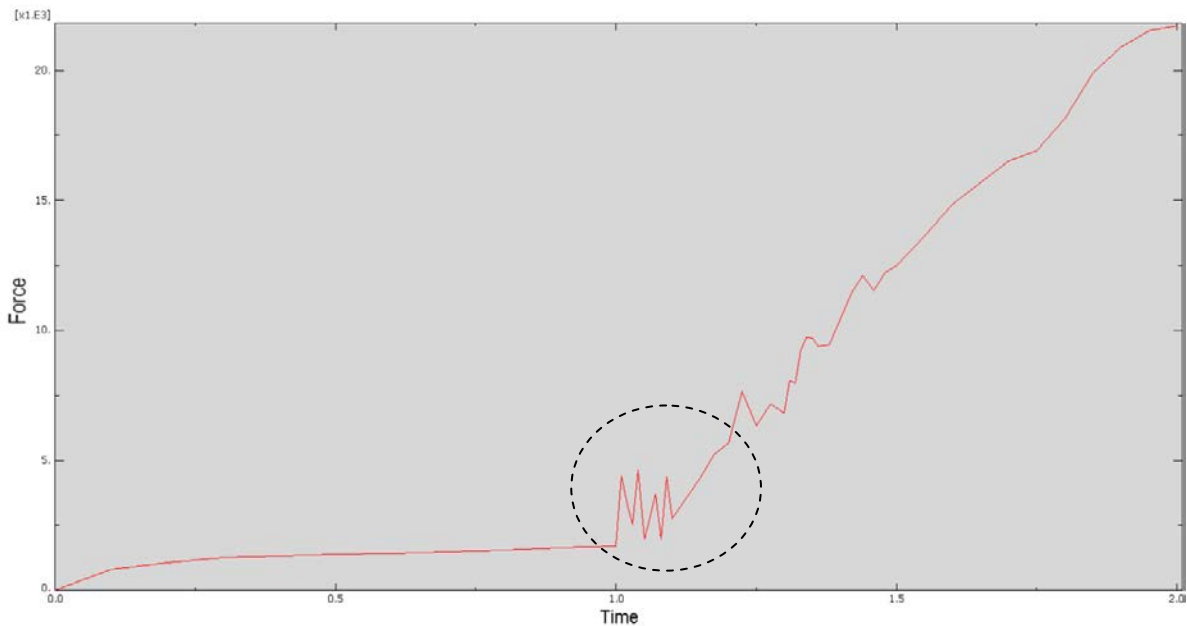


**Figure 81 – FEA measured support reaction versus step time for 108DIS10L4PTNOFRPS2**

In order to plot the load versus deflection the sum of the reaction forces in the vertical direction (RF2) versus the step time was used. This plot is shown in Figure 81. Step time 0 to 1.0 is the application of the selfweight to simulate the panel being supported in the test fixture with gravity loading only, but no test load applied. Step time 1.0 to 2.0 is the applied test load. Due to the explicit analysis the load is dynamically applied and therefore the panel has some vibration occurring until the load and ramping of the load smoothes out appropriately. This initial vibration or rebounding of load is shown by the dashed circled region and is most prevalent in the linear-elastic region of the loading. In order to eliminate the joggle in the force application, the amplitude of the loading needs to be adjusted, however overall the curve performs well and was not a major concern to get that initial load entirely accurate. By adjusting the load, the model will need to take longer to run, which may not be worth the computing time since this really only occurs near the linear-elastic region. See Appendix E, Step 8 for the amplitude of load versus time step. The amplitude is low compared to the time step in the beginning thereby reducing or slowing the load down as it first gets applied in the explicit analysis.

The applied loading result versus time shown in Figure 81 is represented with the load versus deflection curve in Figure 82, where the rebounding is represented by the jagged lines near the beginning of the load curve. As the curve and performance of the panel result in more non-linear

application, the explicit analysis is useful in determining the ultimate failure load, whereas a static linear analysis had difficult converging and solving that problem.

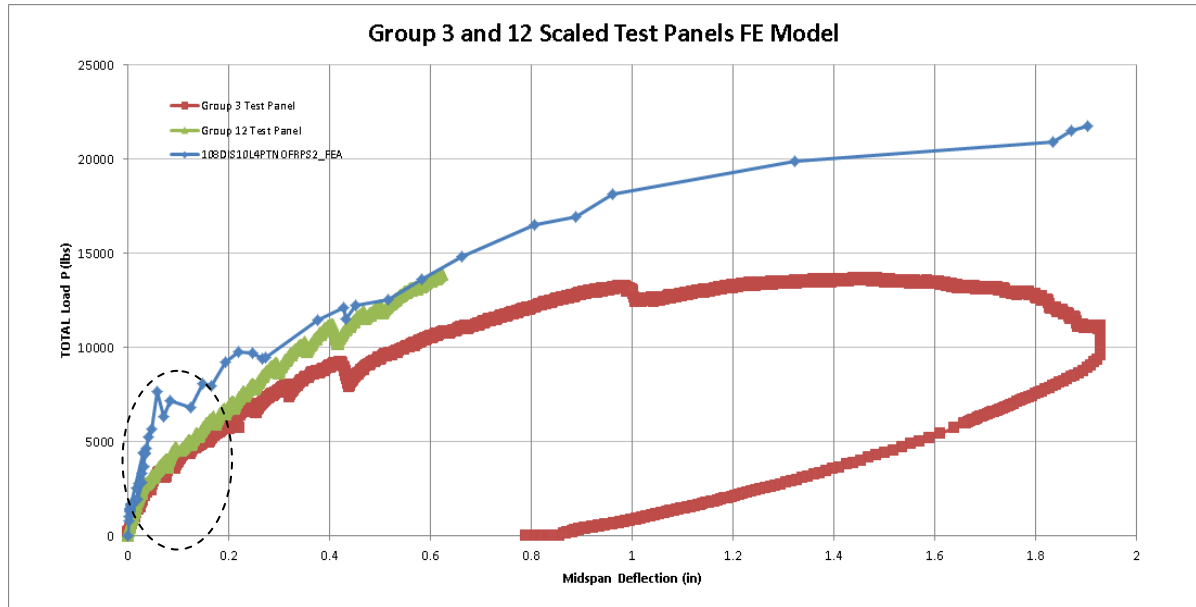


**Figure 82 – 10 inch sandwich panel with discrete connectors FEA vs. Test**

The early loading region shown in Figure 82 by the dashed circle could be omitted and the results from a linear static RIKS or linear static GENERAL FEA method could be used here. The curve beyond the dashed circle is useful information in determining the overall performance of the panel.

Further example of using the explicit quasi-static analysis approach is shown for the sandwich panel depicted in Figure 83 and the load versus deflection results in Figure 84. Although there is some bounciness with the early portion of the FEA curve, overall the FEA curve matches well with the test results, especially considering the non-linearity of the response.

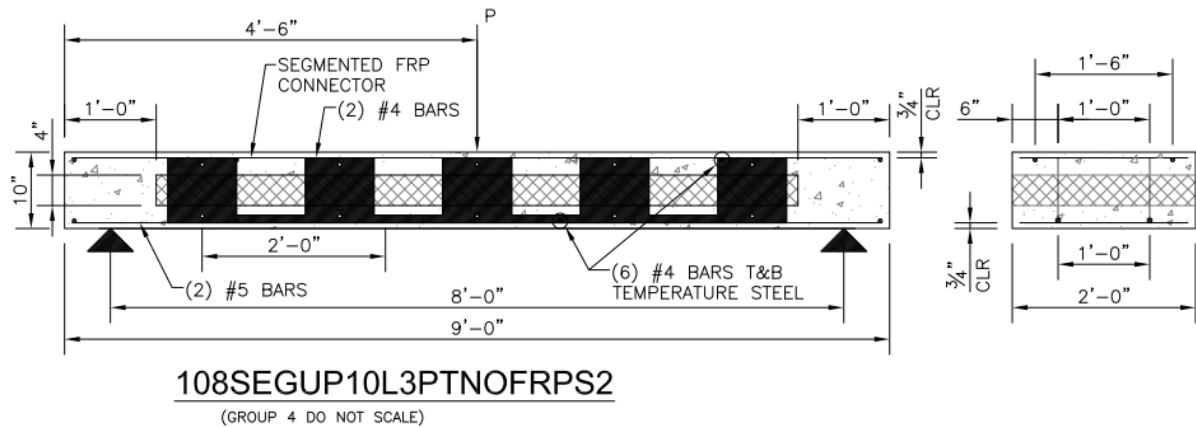


**Figure 83 – 10 inch sandwich panel with segmental connectors**

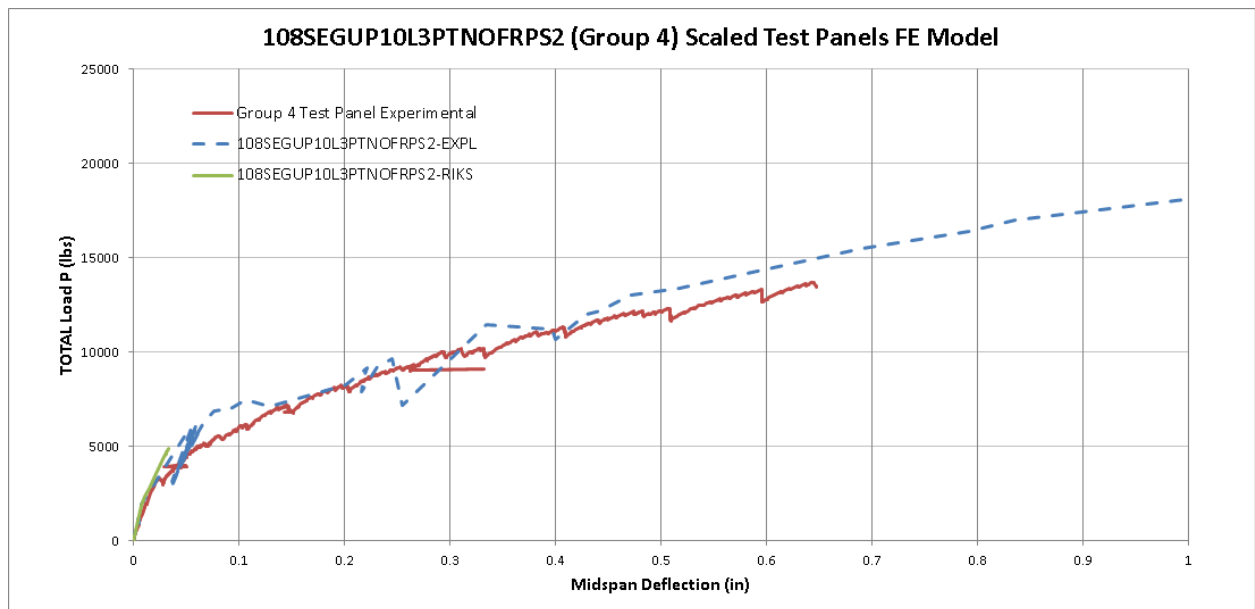
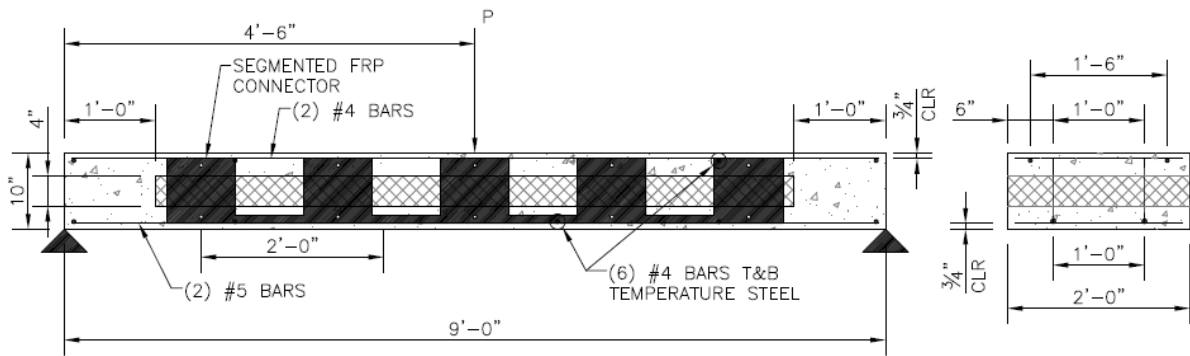


**Figure 84 – 10 inch sandwich panel with segmental connectors FEA vs. Test results**

The blue dashed line of the FEA curve shown in Figure 84 actually extends out past in an extrapolated format from the end test result curve. The test curve did not however reach back to zero which signifies an abrupt failure or other stoppage to the test. This could have been a sudden failure of the shear connectors and the concrete bond or a premature failure at the support locations.



**108SEGUP10L3PTNOFRPS1**

(GROUP 5 DO NOT SCALE)

**Figure 85 – 10 inch sandwich panel with segmental connector construction**

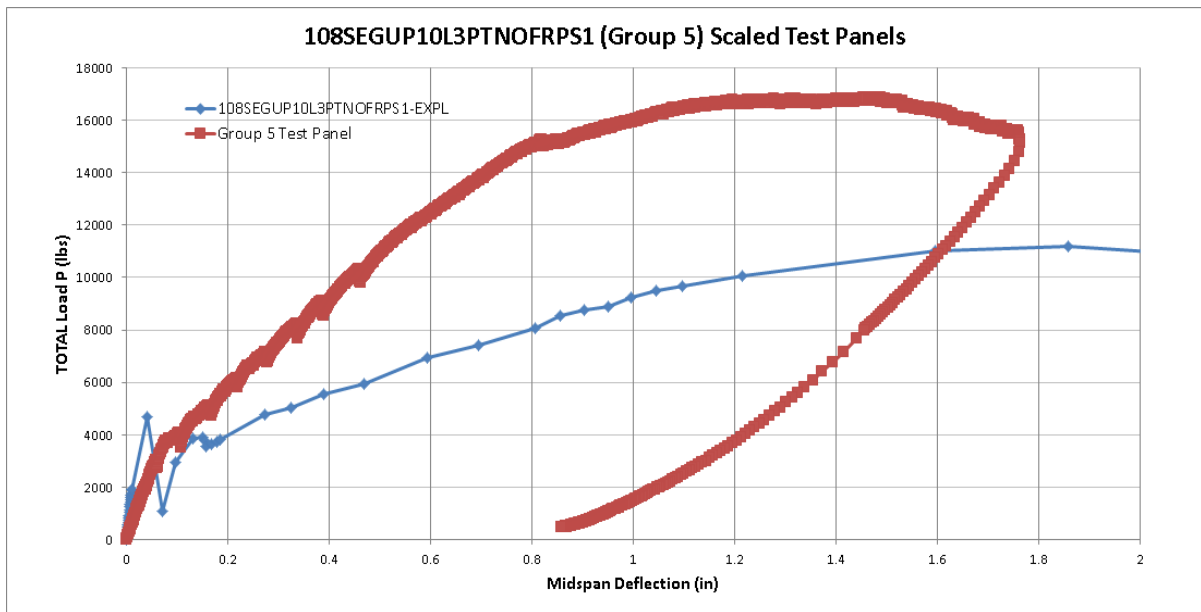


**Figure 86 – 10 inch sandwich panel with segmental connector FEA vs. Test**

The FEA model results when compared to the test results as shown in Figure 86 do not have good correlation in this particular model. The FEA model has been created as other the models and there is no explanation at this time as to why the test data and FEA results diverge. There could be a modeling error or there could be something else that is missing, however as these models are developed and used in future analyses, perhaps a more consistent methodology can be developed through experience.

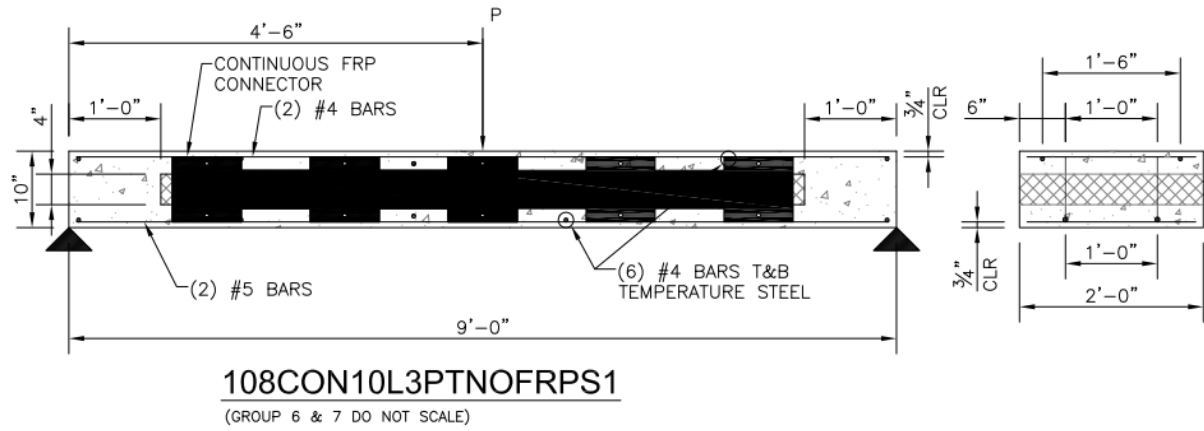


**Figure 87 – 10 inch sandwich panel with continuous connectors construction**

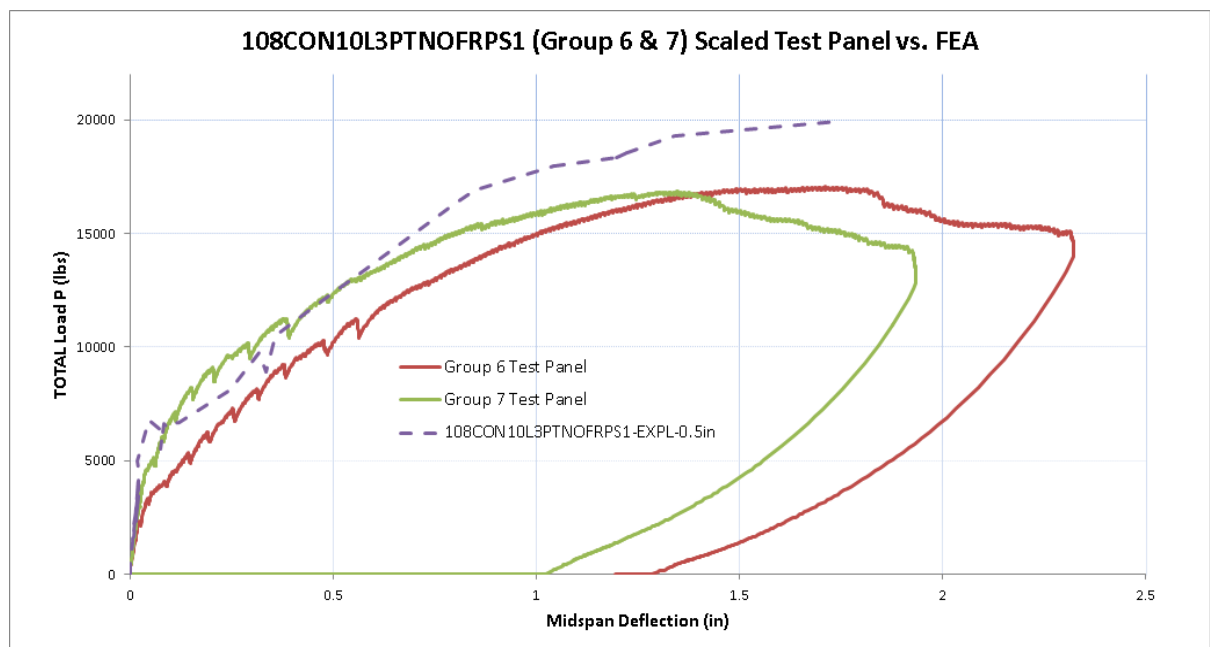
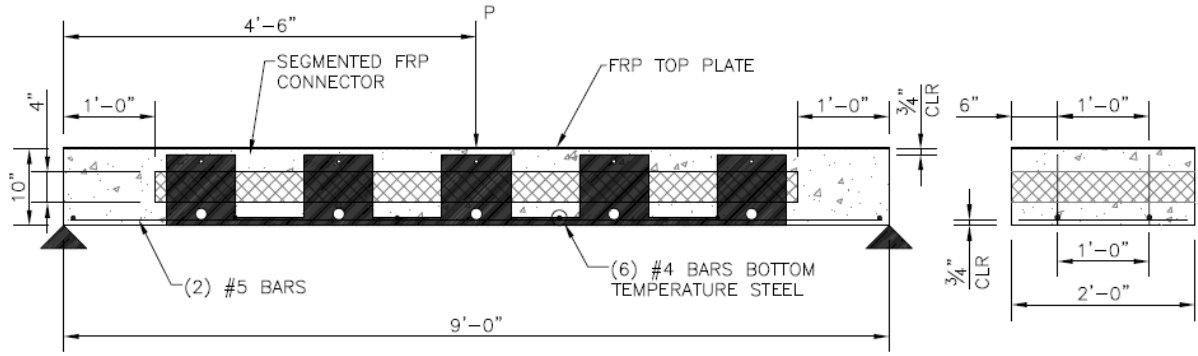


**Figure 88 – 10 inch sandwich panel with continuous connectors FEA vs. Test**



**108SEGUP10L3PTFRPS1**

(GROUP 8 & 9 DO NOT SCALE)

**Figure 89 - 10 inch sandwich panel with continuous connectors and FRP top plate**

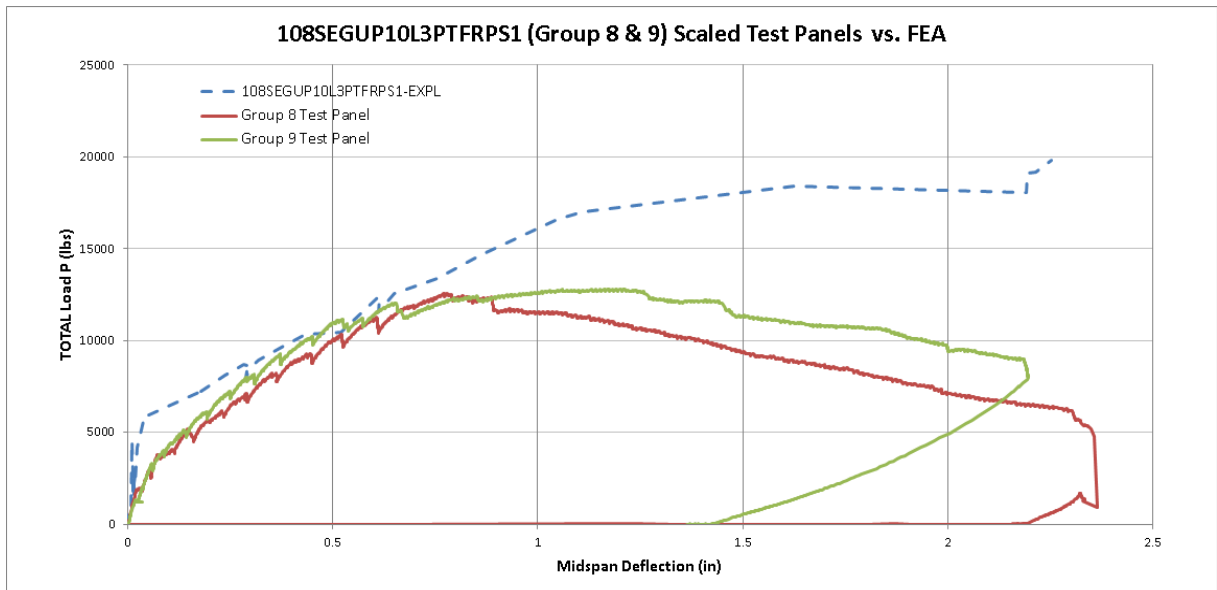


**Figure 90 – 10 inch sandwich panel with continuous connectors FEA vs. Test**

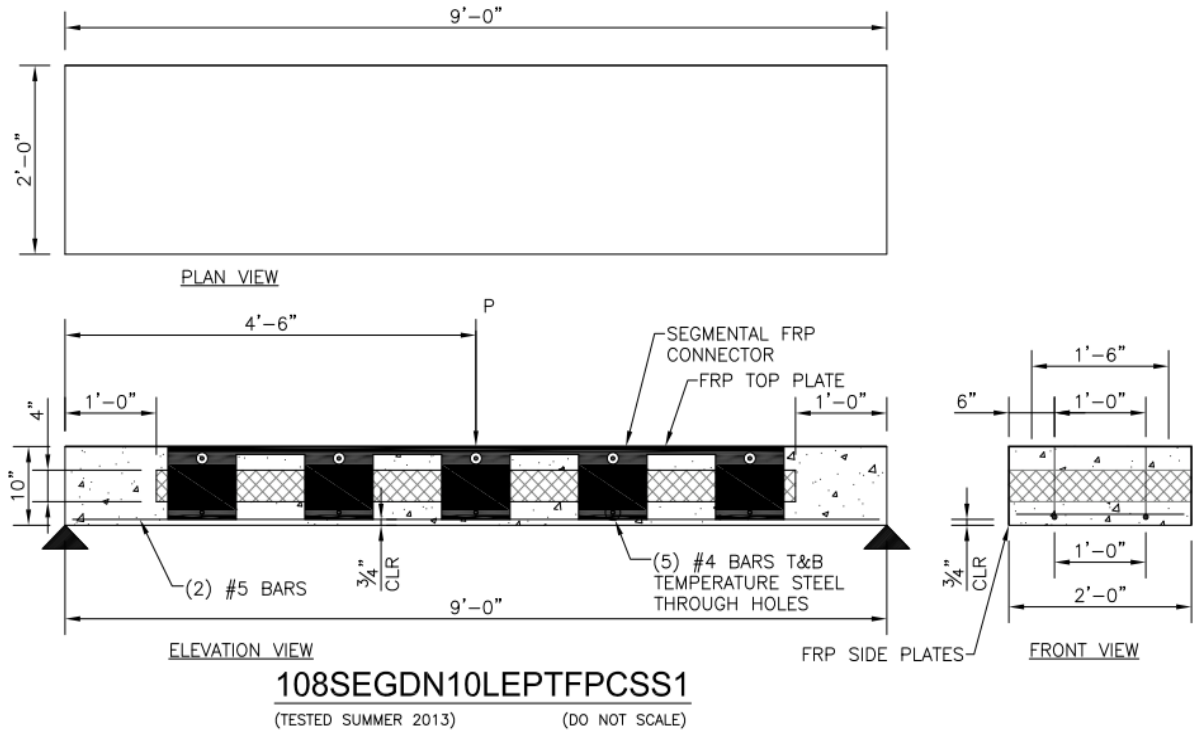


**Figure 91 – 10 inch sandwich panel with segmental down connectors FRP top/side plate (FPCS)**

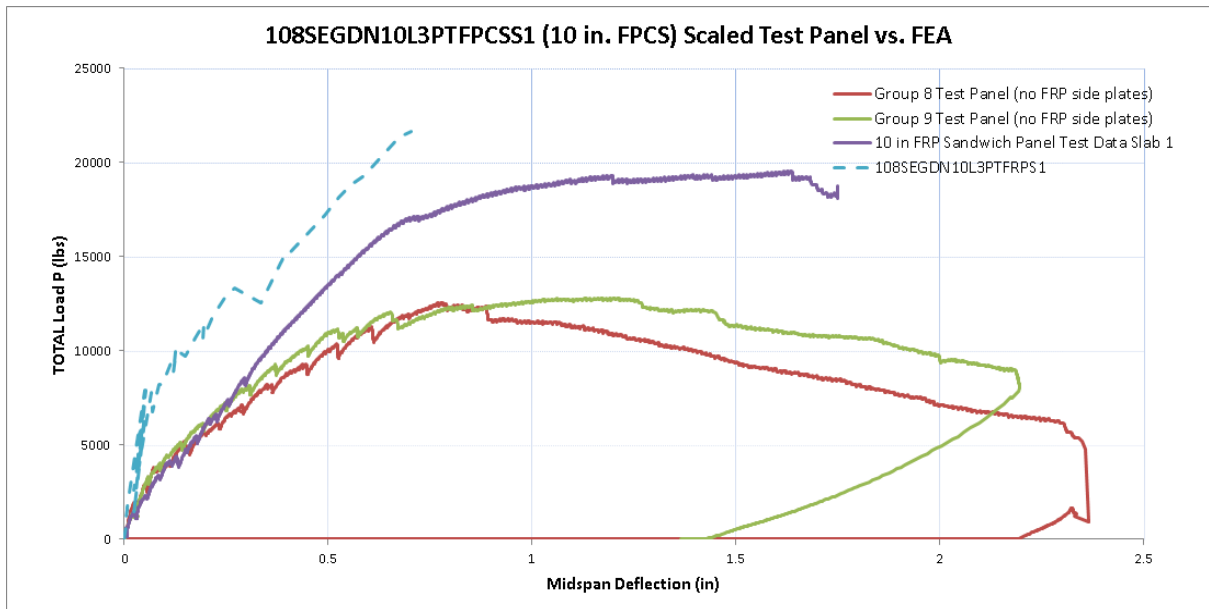


**Figure 92 – 10 in FPCS FEA vs test and non-FPCS**

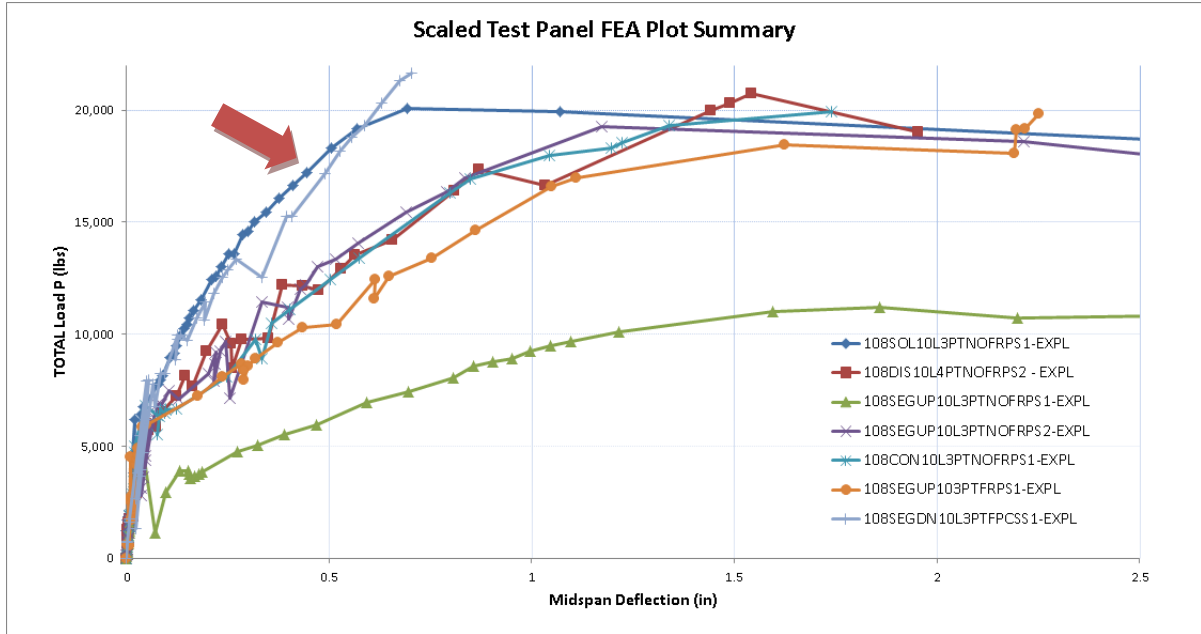


**Figure 93 – Scaled test panel FEA summary plot**

Several of the scaled test panel FEA plots are compared on the plot shown in Figure 93 – Scaled test panel FEA summary plot. The two curves with the stiffest response and nearly the highest strength value is the 10 inch solid reinforced panel and the 10 inch segmental connector down FPCS panel. Most of the other panels follow the same load-deflection response and there is one panel that performed poorly in the FEA model and shall be omitted for this discussion. It appears from these plots the confined FRP plate construction and no top longitudinal reinforcing steel performs adequately when compared to the solid reinforced panel and of course has the added insulation value and weight reduction.

### 4.5.3 FULL SCALE SANDWICH TEST PANEL

The FEA vs. test results are shown in the following pages and for reference and the construction of the 10” full-scale FPCS panel is shown in Figure 94. The primary goal is to construct a panel with the methodology researched in this report and have it span a suitable distance for typical building construction while supporting the required live loading.

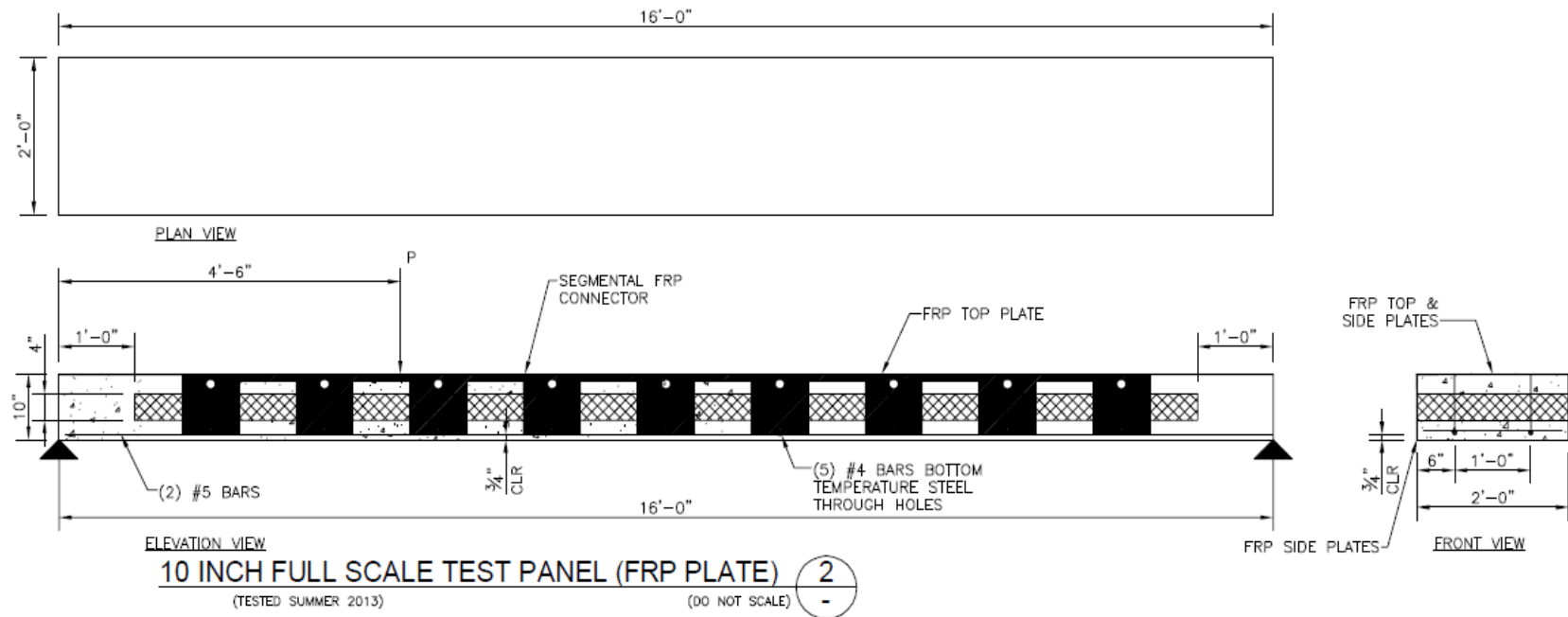


Figure 94 – Full scale test FPCS panel with segmental connectors

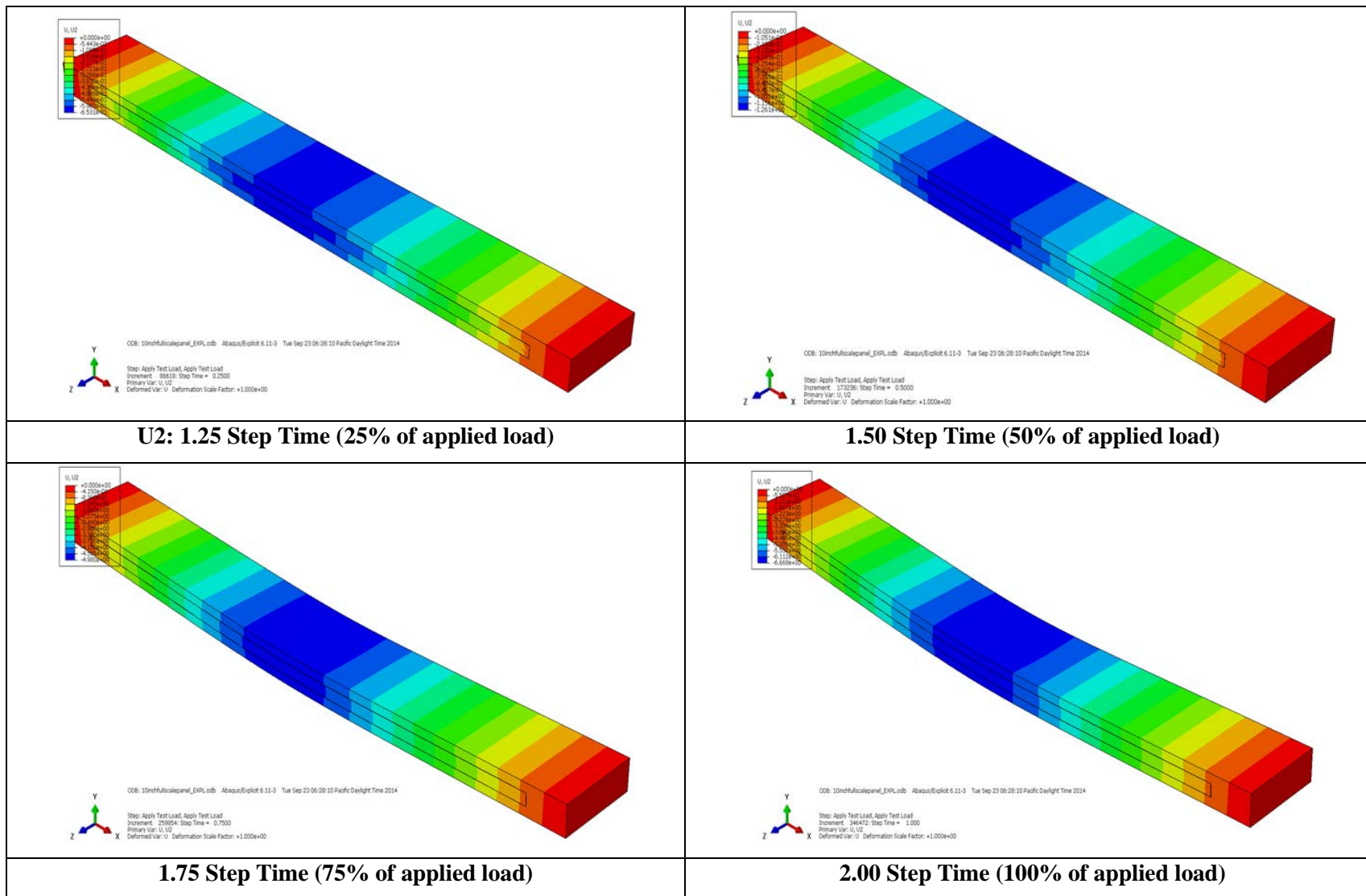


Figure 95 - FEA deflection plots, U2, 10 inch FRPCS full scale panel

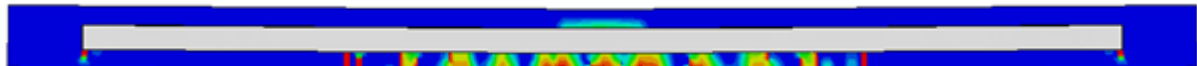
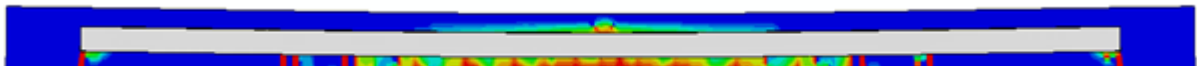
	<b>Dt: 1.10 Step Time (10% Load)</b>
	<b>Dt: 1.25 Step Time (25% Load)</b>
	<b>Dt: 1.50 Step Time (50% Load)</b>
	<b>Dt: 1.75 Step Time (75% Load)</b>
	<b>Dt: 2.00 Step Time (100% Load)</b>

Figure 96 – FEA tension damage side view plots, Dt, 10 inch FRPCS full scale panel

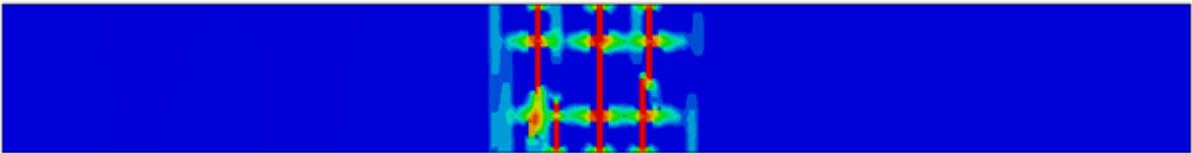
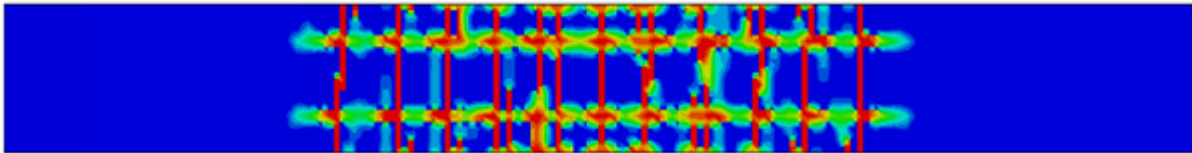
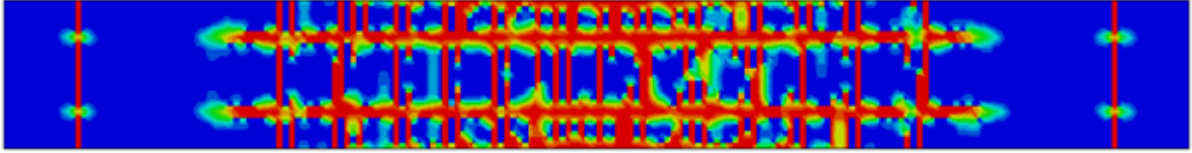
	<p><b>Dt: 1.10 Step Time (10% Load)</b></p>
	<p><b>Dt: 1.25 Step Time (25% Load)</b></p>
	<p><b>Dt: 1.50 Step Time (50% Load)</b></p>
	<p><b>Dt: 1.75 Step Time (75% Load)</b></p>
	<p><b>Dt: 2.00 Step Time (100% Load)</b></p>

Figure 97 – FEA tension damage bottom view plots, Dt, 10 inch FRPCS full scale panel

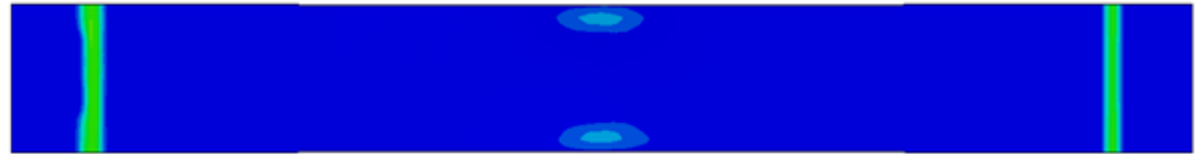
	<b>Dt: 1.10 Step Time (10% Load)</b>
	<b>Dt: 1.25 Step Time (25% Load)</b>
	<b>Dt: 1.50 Step Time (50% Load)</b>
	<b>Dt: 1.75 Step Time (75% Load)</b>
	<b>Dt: 2.00 Step Time (100% Load)</b>

Figure 98 – FEA tension damage top view plots, Dt, 10 inch FRPCS full scale panel

The two plots shown in Figure 99 are for the panel with both top and side FRP plates (red-dashed line) and the panel with just the top FRP plate (blue-dashed with dot line). Interesting to see here is the influence the FRP side plates have on the strength of the panel once the concrete starts to crack and the other tensile materials begin to carry more of the load. In the FEA model the FRP side plate is fully tied to the concrete model, which in reality the bond will break at some loading point and the pieces becoming non-composite. However when reviewing the results, for now we can assume the more realistic panel would have a load vs. deflection curve somewhere in between the two FEA results shown in Figure 99 which means we have good correlation in the non-linear region of the curve.

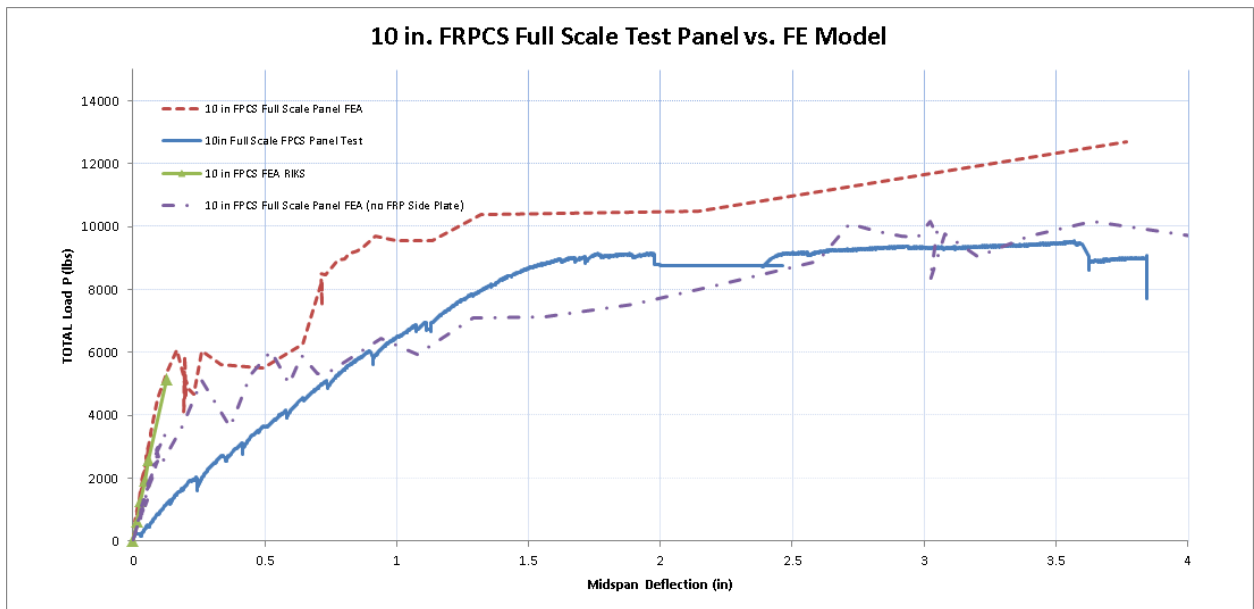


Figure 99 – 10 inch FRPCS full scale panel FEA vs. Test

## 4.6 DEGREE OF COMPOSITE ACTION

The degree of composite action for this research will be based on test data and finite element analysis data used to determine the flexural stiffness at the initial loading stages. The test data and degree of composite action for all test specimens is provided in greater detail in the thesis submitted by Tom Norris<sup>[44]</sup> and the summary of that data shall be presented here in this report for reference. The comparison of the sandwich panels to that of the solid panel is how the degree of composite action shall be determined.

#### 4.6.1 LOAD-DEFLECTION METHOD

The degree of composite action for the load-deflection method is determined per the following equation:

$$DCA = \frac{\left(\frac{1}{EI}\right)_{0\%} - \left(\frac{1}{EI}\right)_{Actual}}{\left(\frac{1}{EI}\right)_{0\%} - \left(\frac{1}{EI}\right)_{100\%}} (100\%)$$

where  $\left(\frac{1}{EI}\right)_{0\%}$  represents that of the sandwich panel if acting with 0% composite action or non-composite. For the noncomposite sandwich panel the top and bottom wythe moment of inertia is used as the summation of two individual sections in bending. The  $\left(\frac{1}{EI}\right)_{Actual}$  represents the value calculated for the slab from test results based on load and deflection at the initial stages of loading in the linear-elastic region. Finally the  $\left(\frac{1}{EI}\right)_{100\%}$  represents the value calculated for the solid slab control specimen, which is considered 100% composite. The deflection at the midspan for a simply supported beam with a concentrated load is:

$$\Delta = \frac{PL^3}{48EI}$$

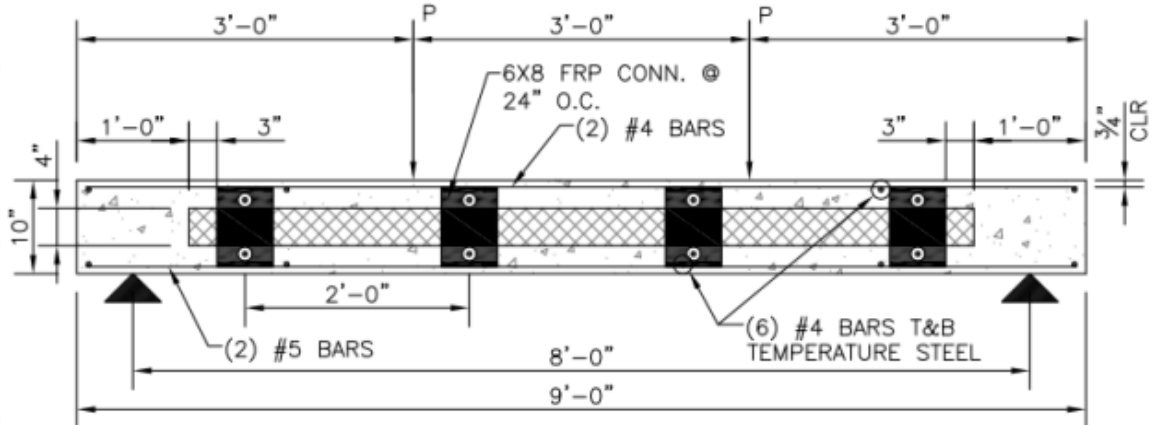
This deflection equation is used to determine the flexural rigidity  $\left(\frac{1}{EI}\right)_{Actual}$  of the test specimen at the linear-elastic loading stage. The value of P used in the calculation is in linear elastic range of 0-1400 lbs and the corresponding deflection at the value of P=1400 lbs is used to determine the slope P/Δ. The corresponding midspan deflections at a load of P=1,400 lbs is shown for all test specimens in Table 23.

Table 23 – Initial load vs. deflection test values for all specimens

<b>Load-Deflection Values by Phase</b>			
<b>Phase 1</b>			
<b>Specimen</b>	<b>Load (lb)</b>	<b><math>\Delta</math> (in)</b>	<b><math>\Delta_{\text{adjusted}}</math></b>
Solid Slab	1400	0.0027	-
		0.0113	-
Discrete Connectors (Adjusted)		0.0359	-
		0.0244	-
Segmented Connectors (Includes Adjustment)		0.0120	-
		0.0253	-
Continuous Connectors		0.0126	-
	0.0095	-	
<b>Phase 2.1</b>			
Segmental Connectors	1400	0.0152	-
		0.0271	-
Continuous Connectors		0.0151	-
		0.0112	-
<b>Phase 2.2</b>			
8" FPCS	1400	0.0597	0.0874
		0.1046	0.1531
10" FPCS		0.0176	0.0149
		0.0534	0.0452
<b>Phase 3</b>			
8" FPCS	1400	0.2700	0.2314
10" FPCS		0.1556	0.1333

The following calculations show the DCA for the first discrete shear connector test specimen (108DIS10L4PTNOFRPS2) considering analytical values for the solid concrete slab.

### Discrete Shear Connector DCA (Load-Displacement Method) Calculation:



### 108DIS10L4PTNOFRPS2

#### Analysis Information:

Concrete 28 day Compressive Strength:  $f'_c := 4120 \cdot \text{psi}$

Concrete Modulus of Elasticity (ACI 318):  $E_c := 57000 \cdot \sqrt{f'_c} \cdot \text{psi}$   $E_c = (3.659 \cdot 10^3) \text{ ksi}$

Simply Supported Beam Effective Length:  $L := 9 \cdot \text{ft}$

DCA Reference Load:  $P := 1400 \cdot \text{lb}$  (Constant)

Corresponding Mid Span Deflection:  $\Delta := 0.0359 \cdot \text{in}$

Panel Width:  $b := 24 \cdot \text{in}$  Wythe Height:  $h := 3 \cdot \text{in}$

Solid Panel Moment of Inertia Transformed considering rebar:  $I_{solid} := 2101.9 \cdot \text{in}^4$

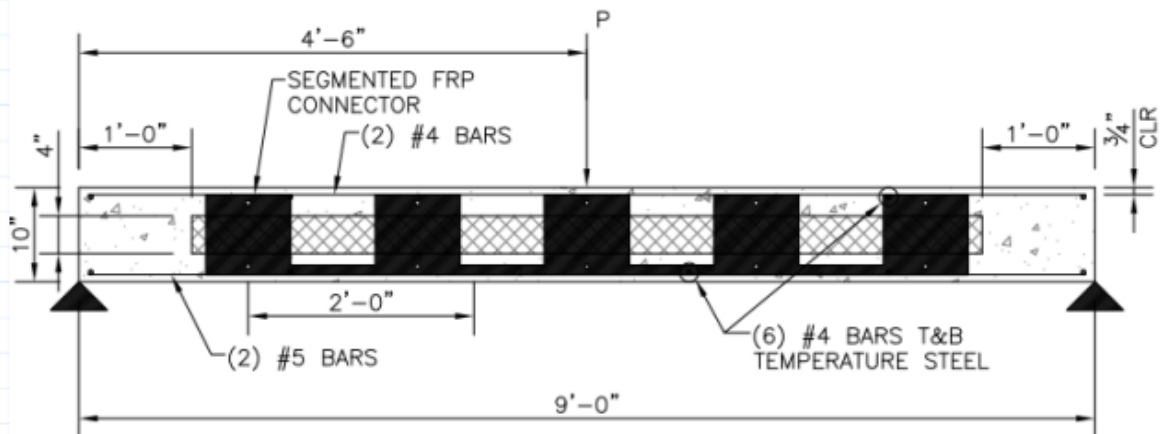
#### Specimen Moment of Inertia:

Solving for I:  $I_{actual} := \frac{P \cdot L^3}{\Delta \cdot 48 \cdot E_c}$   $I_{actual} = 279.7 \text{ in}^4$   
(test panel)

Moment of Inertia for fully non-composite specimen:  $I_{nc} := 2 \cdot \left( \frac{b \cdot h^3}{12} \right)$   $I_{nc} = 108 \text{ in}^4$

DCA:  $DCA := \frac{\left( \frac{1}{E_c \cdot I_{nc}} \right) - \left( \frac{1}{E_c \cdot I_{actual}} \right)}{\left( \frac{1}{E_c \cdot I_{nc}} \right) - \left( \frac{1}{E_c \cdot I_{solid}} \right)} \cdot (100\%)$   $DCA = 64.7\%$

### Segmental Shear Connector DCA (Load-Displacement Method) Calculation:



### 108SEG10L3PTNOFRPS1

#### Analysis Information:

Concrete 28 day Compressive Strength:  $f'_c := 4120 \cdot \text{psi}$

Concrete Modulus of Elasticity (ACI 318):  $E_c := 57000 \cdot \sqrt{f'_c} \cdot \text{psi}$      $E_c = (3.659 \cdot 10^3) \text{ ksi}$

Simply Supported Beam Effective Length:  $L := 9 \cdot \text{ft}$

DCA Reference Load:  $P := 1400 \cdot \text{lb}$     (Constant)

Corresponding Mid Span Deflection:  $\Delta := 0.0120 \cdot \text{in}$

Panel Width:  $b := 24 \cdot \text{in}$     Wythe Height:  $h := 3 \cdot \text{in}$

Solid Panel Moment of Inertia Transformed considering rebar:  $I_{solid} := 2101.9 \cdot \text{in}^4$

#### Specimen Moment of Inertia:

Solving for I:  
(test panel)  $I_{actual} := \frac{P}{\Delta} \cdot \frac{L^3}{48 \cdot E_c}$      $I_{actual} = 836.9 \text{ in}^4$

Moment of Inertia for fully  
non-composite specimen:  $I_{nc} := 2 \cdot \left( \frac{b \cdot h^3}{12} \right)$      $I_{nc} = 108 \text{ in}^4$

DCA:  $DCA := \frac{\left( \frac{1}{E_c \cdot I_{nc}} \right) - \left( \frac{1}{E_c \cdot I_{actual}} \right)}{\left( \frac{1}{E_c \cdot I_{nc}} \right) - \left( \frac{1}{E_c \cdot I_{solid}} \right)} \cdot (100\%)$      $DCA = 91.8\%$

The same procedure is used for the remaining test panels; however the moment of inertia from the solid test specimen is now used to determine the degree of composite action. In either case the

results are similar and the assumption of just using the analytical representation of the solid slab can be used in future calculations.

**Table 24 – DCA load deflection method summary**

<b>FEA DCA Calculations by Phase</b>						
<b>Phase 1</b>						
<b>Specimen</b>	<b>P/Δ</b>	<b>I</b>	<b>EI</b>	<b>1/EI</b>	<b>FEA DCA</b>	<b>TEST DCA</b>
Solid Slab	181913	1305	4774116424	2.09E-10	94.5%	100.0%
108SOL10L3PTNOFRPS1	0	0	0.0113	8.85E+01	-	90.5%
Discrete Connectors	82905	595	2175771465	4.60E-10	84.3%	63.2%
108DIS10L4PTNOFRPS2	0	0	0.02440317	4.10E+01	-	76.0%
Segmented Connectors	62423	448	1638224160	6.10E-10	78.1%	89.7%
108SEGUP10L3PTNOFRPS1	0	0	0.0253	3.95E+01	-	75.0%
Continuous Connectors	69231	497	1816903289	5.50E-10	80.6%	89.0%
108CON10L3PTNOFRPS1	0	0	0.0095	1.05E+02	-	92.5%
<b>Phase 2.1</b>						
Segmental Connectors	71058	509.7061547	1864847580	5.36237E-10	81.17%	86.2%
	0	7.40706E-09	0.0271	36.900369	-	73.0%
Continuous Connectors	70078	502.6796312	1839139837	5.43732E-10	80.86%	86.3%
	0	3.06122E-09	0.0112	89.28571429	-	90.6%
<b>Phase 2.2</b>						
8" FPCS Scaled						
10" FPCS Scaled	80925	534.4646321	2123791908	4.70856E-10	84%	83.7%
	0	1.34268E-08	0.053354	18.74273719	-	39.7%
<b>Phase 3</b>						
8" FPCS Full Scale						
10" FPCS Full Scale	13331	497.3986997	1965799172	5.08699E-10	82.50%	71.5%

#### 4.6.2 STRAIN DISTRIBUTION METHOD

The solid concrete test panel is considered the reference beam and the fully composite specimen. In that case the strain distribution through the depth of the specimen, normal to the plane of bending, should be completely linear. Likewise the sandwich panels that exhibit full-composite action should also have a strain distribution through depth of the entire specimen from top wythe to bottom wythe with no disconnect at the insulation. In order to determine a consistent DCA for each specimen, the

strain was analyzed at a time when all specimens were subjected to a load that corresponded to an equivalent flexural moment. The following equation was used to determine the degree of composite action of the various specimens based on the strain distribution:

$$DCA = \frac{\Delta x_{Actual} - \Delta x_{0\%}}{\Delta x_{100\%} - \Delta x_{0\%}} (100\%)$$

where  $\Delta x_{0\%}$  represents the change in the calculated strain equation from one wythe to the other in a slab acting with 0% composite action (fully non-composite),  $\Delta x_{actual}$  represents the change in the calculated strain equation from one wythe to the other in a slab from test results based on load and deflection, and  $\Delta x_{actual}$  represents the strain difference calculated for the solid control specimen, which is 100% composite. In the solid slab there is no variation in the strain distribution as can be seen in Figure 100.

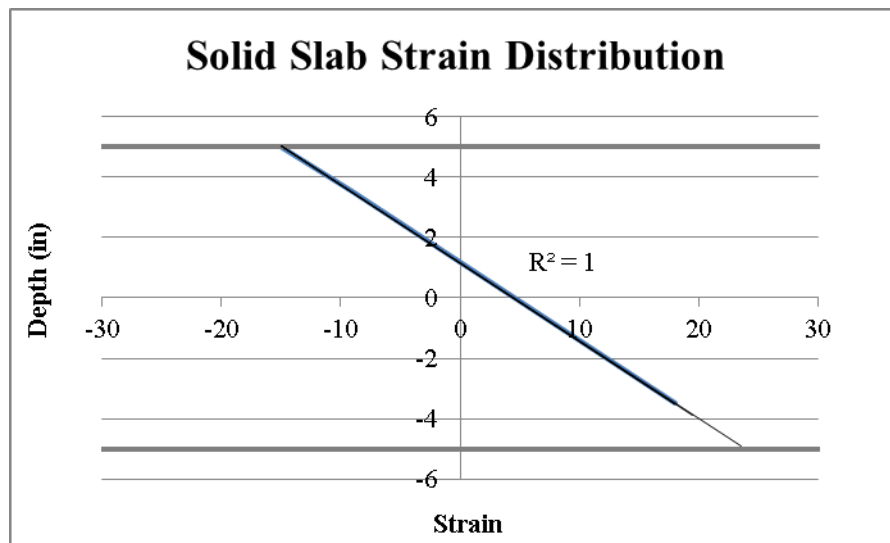


Figure 100 – Solid slab test panel strain distribution

The linear static analysis model was performed in finite element for a load of  $P = 1,400$  lbs to be consistent with the analytical calculations. The contour strain distribution from the finite element analyses is shown in Figure 101.

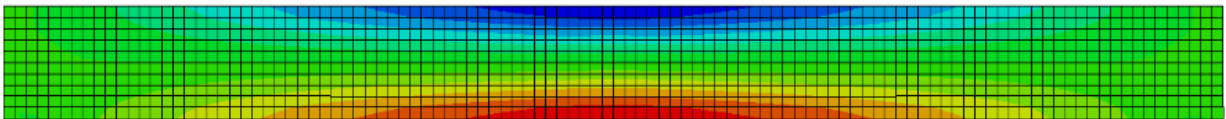


Figure 101 – Solid slab FEA strain distribution ( $\epsilon_{11}$ )

The corresponding values of strain along the x-direction or  $\epsilon_{11}$  are shown in the plot in Figure 102. These values shown in the plot in Figure 102 are taken from nodes in the center of the panel along the vertical direction and this is the typical method for each panel. There is a linear distribution of strain through the section of the concrete panel. The strain does jump a little where the steel reinforcement bars are located.

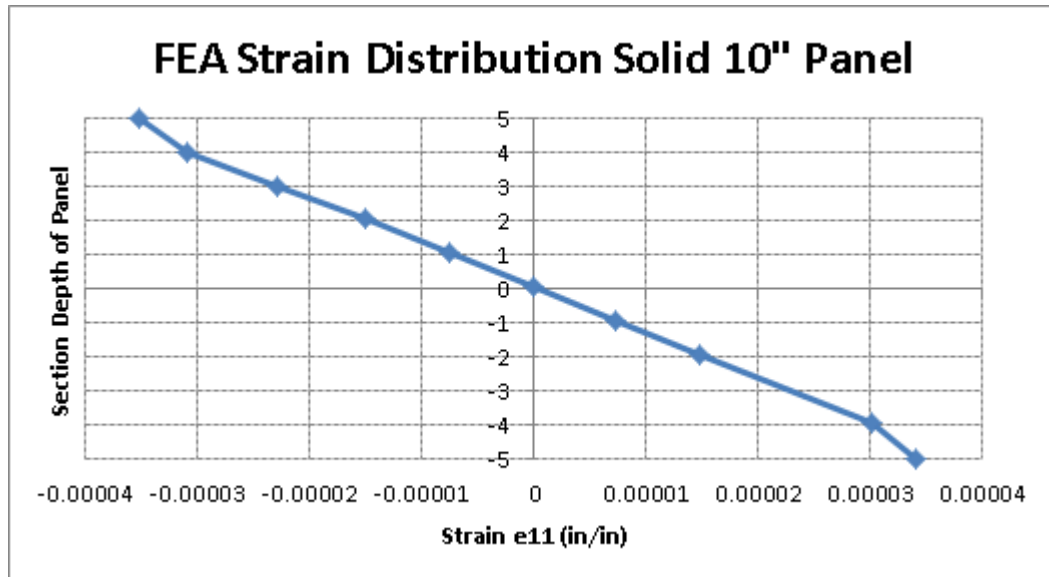


Figure 102 – Solid slab FEA strain distribution plot ( $\epsilon_{11}$ )

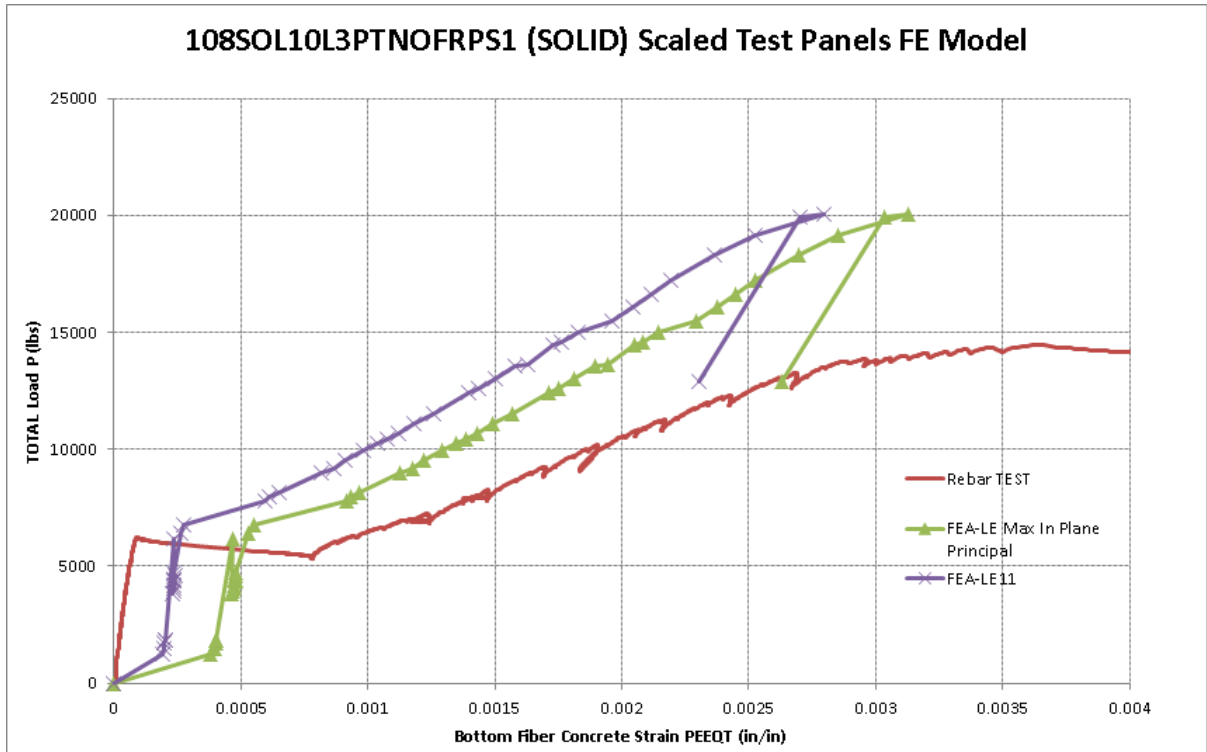


Figure 103 – Solid slab FEA panel rebar strain vs. test results

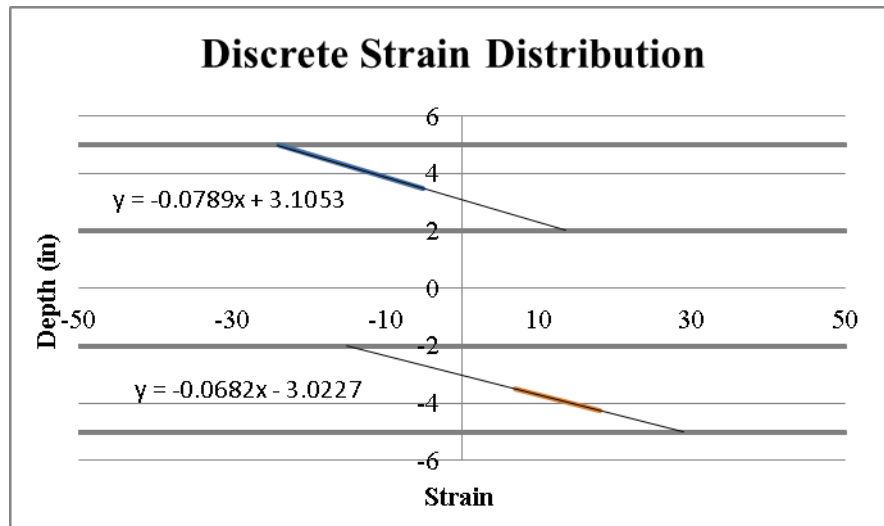


Figure 104 – Discrete connector test panel strain distribution

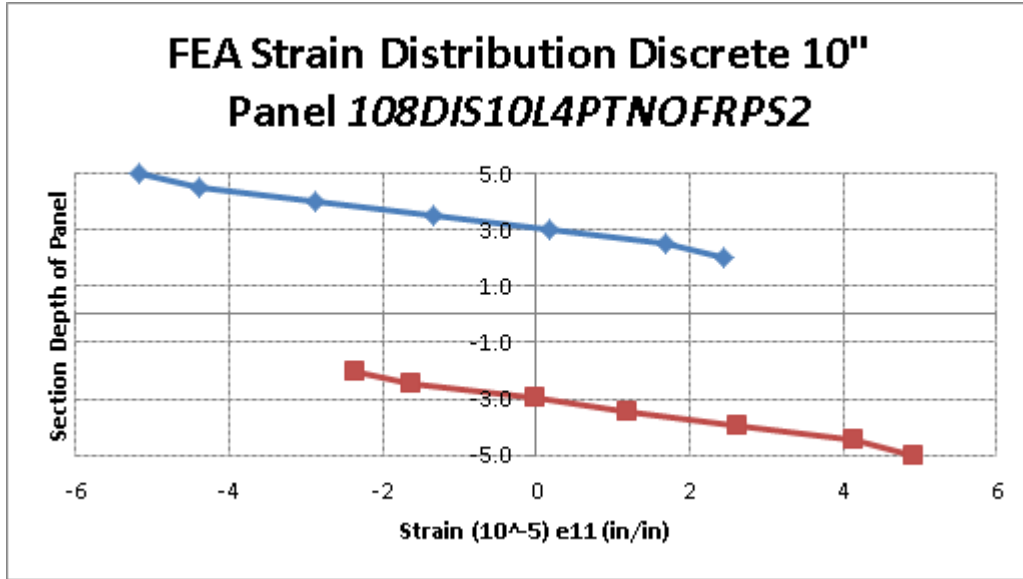


Figure 105 – Discrete connector FEA panel strain distribution

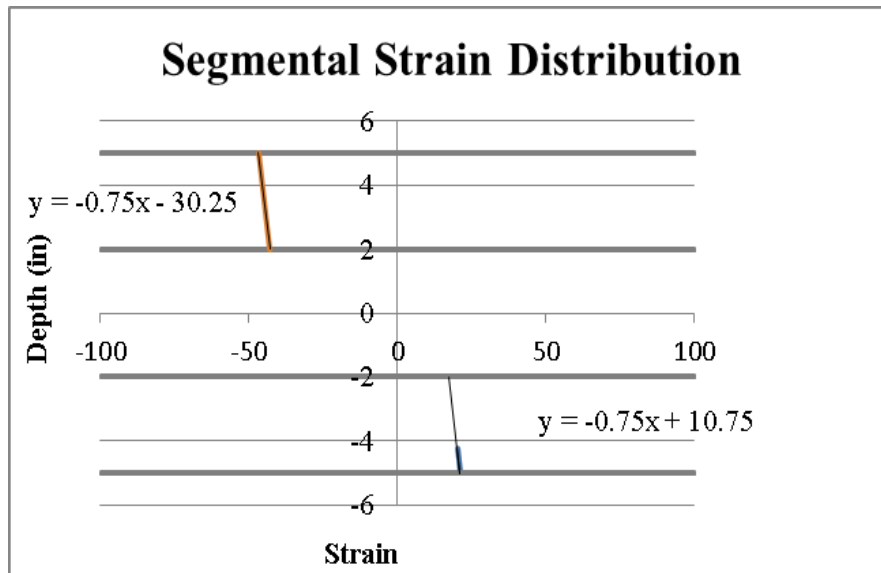


Figure 106 – Segmental connector test panel strain distribution

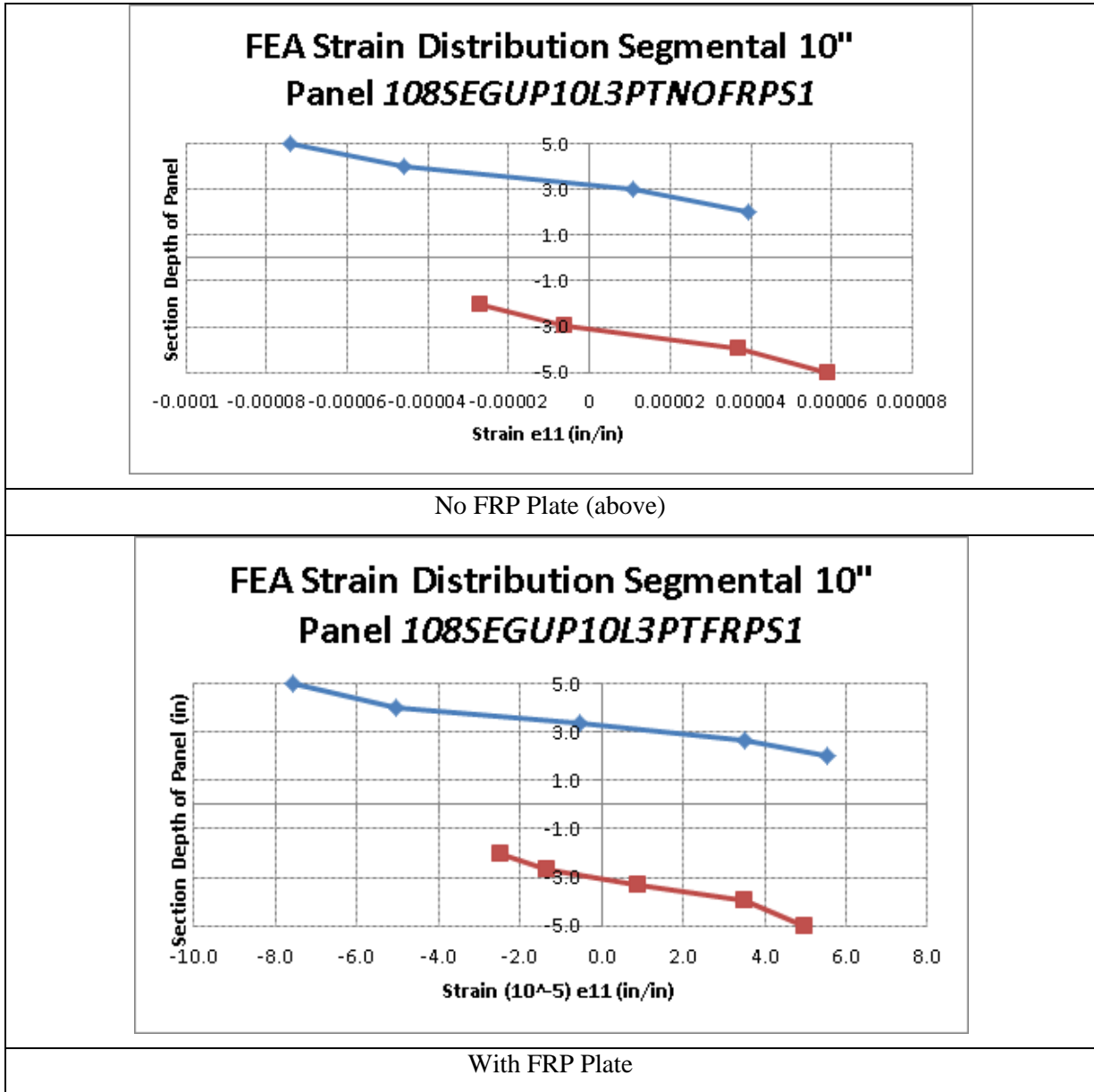


Figure 107 – Segmental connector test panel strain distribution

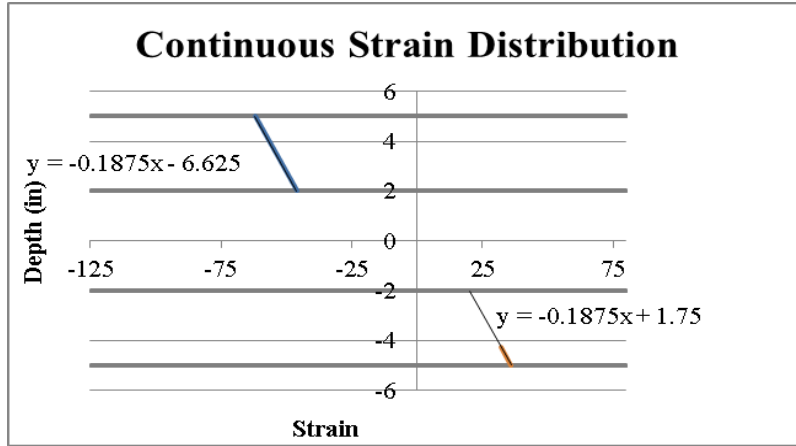
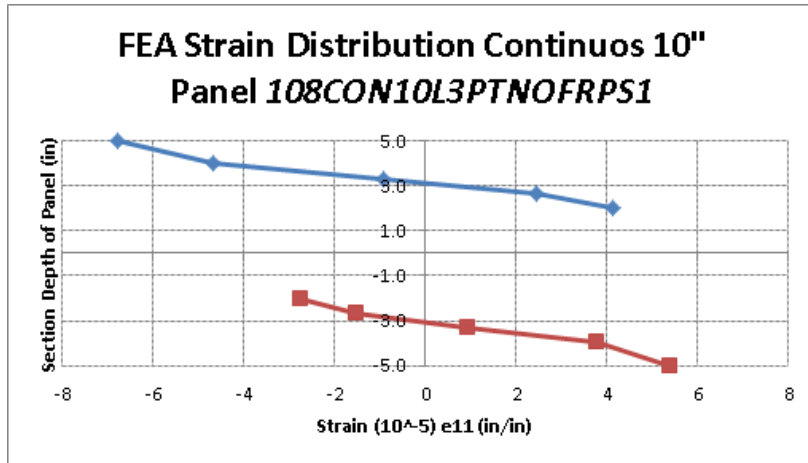
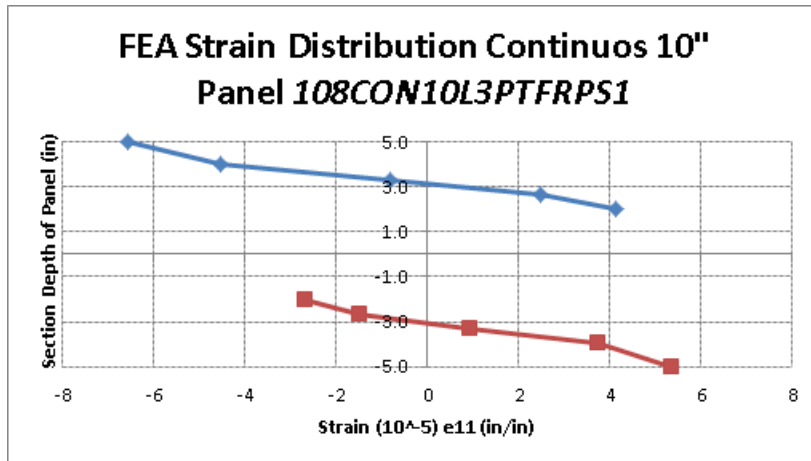


Figure 108 – Continuous connector test panel strain distribution



No FRP Plate (above)



With FRP Plate

Figure 109 – Continuous connector FEA panel strain distribution

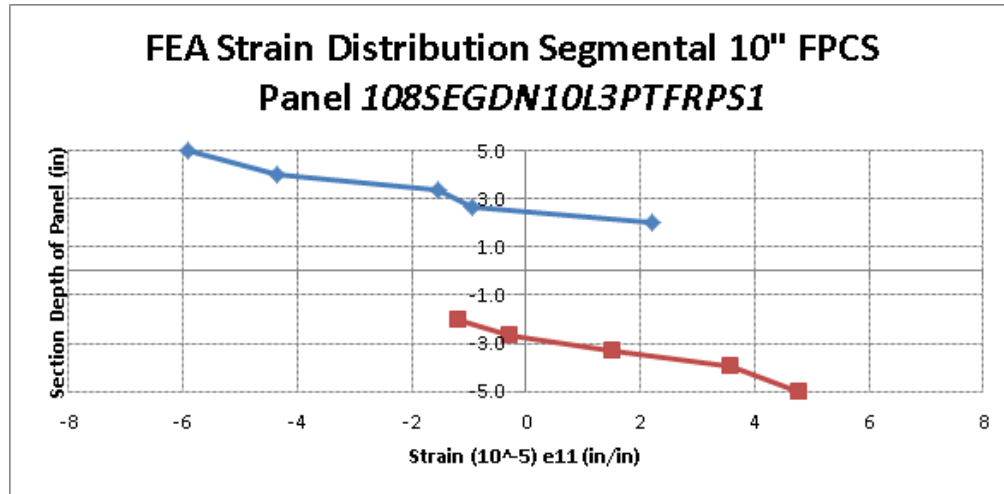


Figure 110 – FPCS Segmental 10'' FEA panel strain distribution

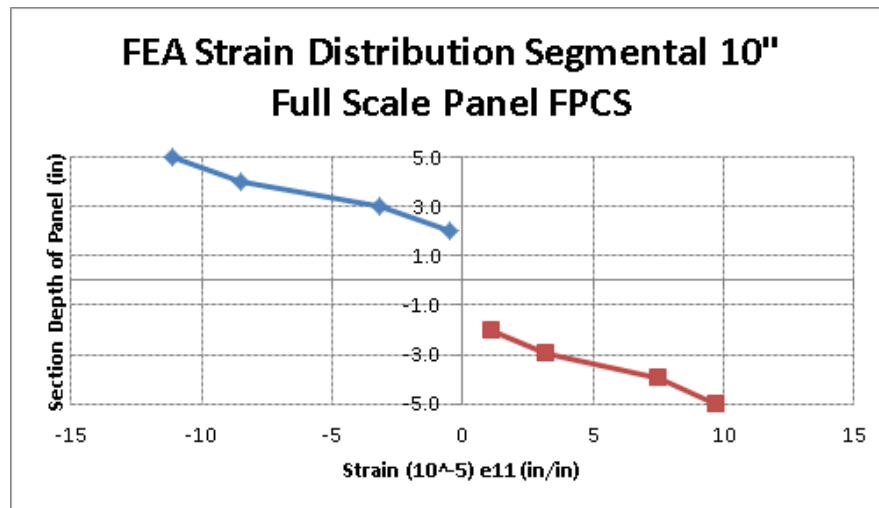
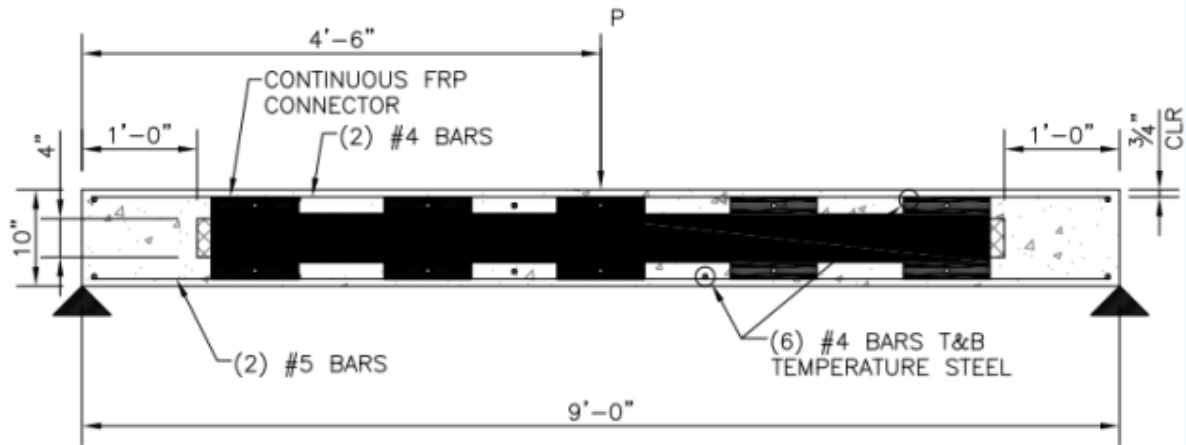


Figure 111 – FPCS Segmental 10'' Full Scale FEA panel Strain Distribution

The test panels with FRP top and side plates were not constructed in a way to allow for the strain data to be collected to establish the DCA by this method.<sup>[44]</sup> The panels with top and side plates shall rely on the load-deflection method in this study. Specimens with top FRP only did provide sufficient data to accurately construct the strain distribution profiles. The following is an example of the calculations used to determine the DCA based on the strain distribution for the phase 1 test panels. Further equations and data can be found in the thesis submitted by Tom Norris<sup>[44]</sup> for the testing of all panels.

### Continuous Shear Connector DCA (Strain-Distribution Method) Calculation:



**108CON10L3PTNOFRPS1**

#### Analysis Information:

Concrete 28 day Compressive Strength:  $f'_c := 4120 \cdot \text{psi}$

Concrete Modulus of Elasticity (ACI 318):  $E_c := 57000 \cdot \sqrt{f'_c \cdot \text{psi}}$   $E_c = (3.659 \cdot 10^3) \text{ ksi}$

Simply Supported Beam Effective Length:  $L := 9 \cdot \text{ft}$

DCA Reference Moment:  $M := 18.9 \cdot \text{kip} \cdot \text{in}$  (Constant)

Panel Width:  $b := 24 \cdot \text{in}$  Wythe Height:  $h := 3 \cdot \text{in}$

Solid Panel Moment of Inertia Transformed considering rebar:  $I_{\text{solid}} := 2101.9 \cdot \text{in}^4$

Distribution Equation:  $y_1 = -0.0625 x + 3.125$   $y_{\text{bar}1} := 1.5 \cdot \text{in}$

$y_2 = -0.0625 x - 0.5625$   $y_{\text{bar}2} := 3 \cdot \text{in}$

$y := 5$

#### Degree of Composite Action:

Determine  $\Delta x_{0\%}$ :

By assuming different values of 'y' and using the following equation, the slope of the strain distribution for a fully non-composite specimen can be calculated. Assuming that this distribution crosses the neutral axis at the center of each wythe, the difference ( $\Delta x_{0\%}$ ) can be calculated:

$$\text{Moment of Inertia of Single Wythe: } I := \frac{b \cdot h^3}{12} \quad I = 54 \text{ in}^4$$

$$\text{Strain at Extreme Fiber: } \varepsilon = \frac{My}{EI}$$

$$\text{Strain at Top Fiber: } \varepsilon_1 := \frac{M \cdot y_{bar1}}{E_c \cdot I} \cdot 10^6 \quad \varepsilon_1 = 143.495$$

$$\text{Strain at Bottom Fiber: } \varepsilon_2 := \frac{M \cdot y_{bar2}}{E_c \cdot I} \cdot 10^6 \quad \varepsilon_2 = 286.989$$

$$\text{Slope of Strain Distribution: } slope := \frac{y_{bar1} - y_{bar2}}{(\varepsilon_1 - \varepsilon_2) \cdot \text{in}} \quad slope = 0.01$$

Assuming the top of the specimen to be the datum, use the distance between the dtop of the specimen and the center of each wythe to determine the values of 'x'.

$$x_1 := \frac{1.5}{slope} \quad x_1 = 143.495 \quad x_2 := \frac{8.5}{slope} \quad x_2 = 813.137$$

$$\text{Fully Non-Composite: } \Delta x_0 := x_2 - x_1 \quad \Delta x_0 = 669.642$$

Using the equations provided by the strain distribution and assuming an arbitrary datum, Dxex can be calculated for the experimental test:

$$x_1 := \left( \frac{y + 0.5625}{-0.0625} \right) \quad x_1 = -89 \quad x_2 := \left( \frac{y - 3.125}{-0.0625} \right) \quad x_2 = -30$$

$$\text{Experimental Panel: } \Delta x_{exper} := x_2 - x_1 \quad \Delta x_{exper} = 59$$

$$\text{Fully Composite: } \Delta x_{100} := 0 \quad (\text{No variance})$$

$$DCA := \left( \frac{\Delta x_{exper} - \Delta x_0}{\Delta x_{100} - \Delta x_0} \right) \cdot 100\% \quad DCA = 91.2\%$$

The results for all of the Phase 1 and Phase 2 test panels using this procedure can be found in Table 25 and just as was the case with the load-displacement method the DCA for the continuous shear connectors exhibited the highest percentage. The test panels with the segmental shear connectors

also produced a relatively high percentage of composite action. This second set of calculations and data for the DCA confirm the previous results from the load distribution method.

**Table 25 – Degree of composite action (DCA) – strain distribution method**

<b>DCA - Strain Distribution Method (TEST)</b>					
<b>Phase 1</b>					
<b>Specimen</b>	<b>X<sub>bot-ext</sub></b>	<b>X<sub>top</sub></b>	<b>X<sub>max</sub></b>	<b>ΔX</b>	<b>DCA</b>
Solid	-	-	-	0	100%
Discrete	-117.6349	-24.015209	669.6419	93.619688	86%
Segmental	7.6666667	-47	669.6419	54.666667	92%
Continuous	-17.333333	-62	669.6419	44.666667	93%
<b>Phase 2.1</b>					
Segmental	-147.64865	-90.09009	669.642	57.558559	91%
Continuous	-89	-30	669.642	59	91%

<b>DCA - Strain Distribution Method - (FEA)</b>					
<b>Phase 1</b>					
<b>Specimen</b>	<b>X<sub>bot-ext</sub></b>	<b>X<sub>top</sub></b>	<b>X<sub>max</sub></b>	<b>ΔX</b>	<b>DCA</b>
Solid	-	-	-	0	100%
Discrete (108DIS10L4PTNOFRPS2)	-20.764232	-5.4680559	669.6419	15.296176	98%
Segmental (108SEGUP10L3PTNOFRPS1)	-24.696528	-7.8376623	669.6419	16.858866	97%
Continuous (108CON10L3PTNOFRPS1)	-24.088359	-7.6048937	669.6419	16.483466	98%
<b>Phase 2.1</b>					
Segmental (108SEGUP10L3PTFRPS1)	-21.992552	-8.5490575	669.642	13.443494	98%
Continuous (108CON10L3PTFRPS1)	-23.728814	-7.391253	669.642	16.337561	98%

The FEA strain distribution method yielded results that were all relatively similar for the 5 test panels analyzed. The reason could be the fidelity of the mesh or disadvantage in using this analysis method for DCA evaluation.

**Table 26 – DCA load displacement vs. strain distribution methods based on test data**

<b>Specimen</b>	<b>DCA LDM</b>	<b>DCA SDM</b>	<b>Difference</b>
Solid	100%	100%	0%
Discrete	76%	86%	12%
Segmental	90%	92%	2%
Continuous	92%	93%	1%

## 4.7 DESIGN CONSIDERATIONS

The test panels in this study have displayed a DCA range from 70%-92% depending on the span, configuration and material properties. The test panels in this study are considered partially composite and therefore normal ACI design equations are used to determine the moment capacity of the panel if it were a solid reinforced concrete beam, then reduced according to the DCA percentage.

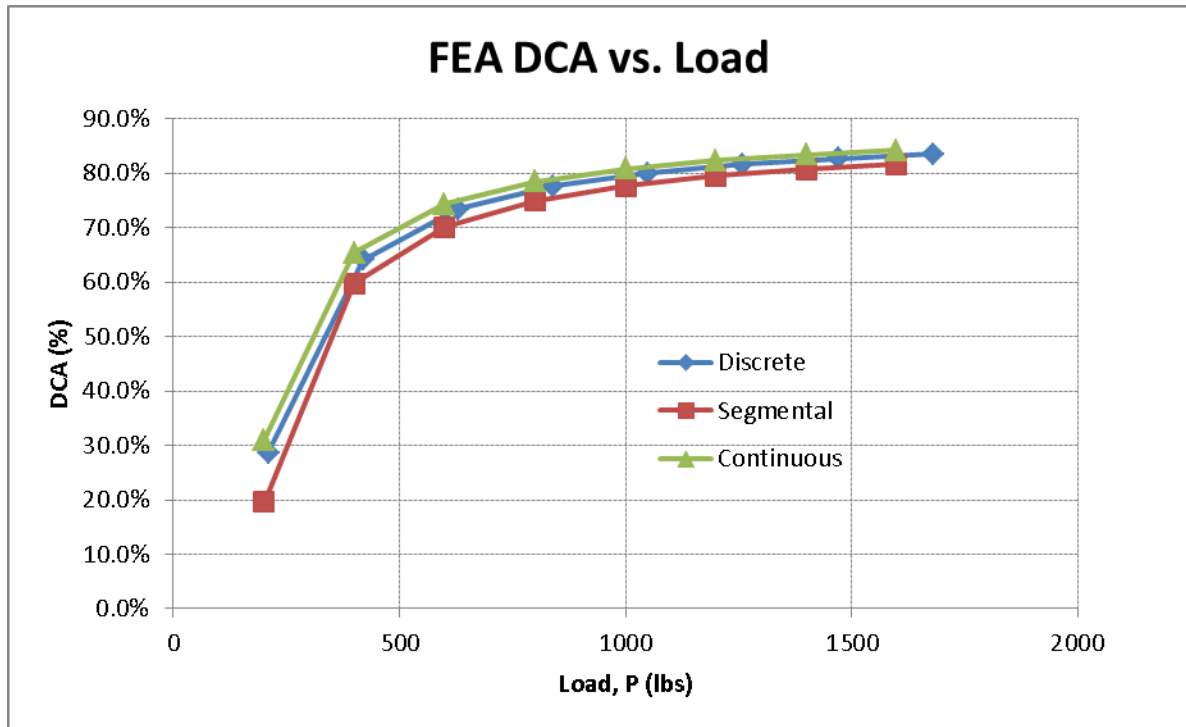
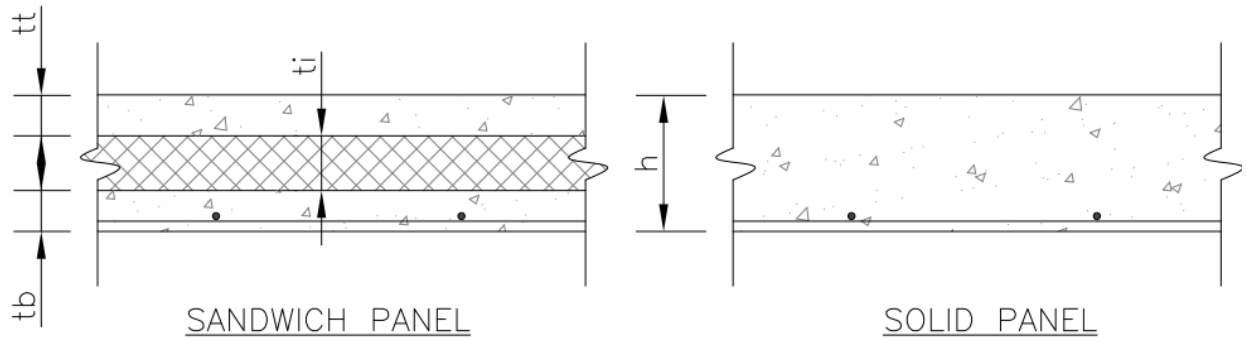


Figure 112 – FEA DCA vs. Load comparison

For varying loads applied to the panel in the finite element model, the DCA was determined for the three-phase one sandwich panels. The DCA versus the load, applied up to 1,600 lbs concentrated in the middle for three-point bending, is shown in Figure 112. It is clear that the DCA changes as the load is applied and seems to hit a maximum around 85-90% DCA.

Some of these panels have reinforcing steel top (compression steel) and bottom (tension steel) and some of the panels have FRP plate on top and reinforcing steel on the bottom only.



**Figure 113 – Partial composite section vs. solid panel section**

For the partial composite panel/beam section shown in Figure 113 the section modulus of elasticity is derived by the following equations in terms of a 12 inch or 1 foot section width. These panels are symmetrical; therefore the section modulus is the same for top and bottom. As measured from the top, the neutral axis distance,  $c$  is calculated:

$$b = 12 \text{ inch}$$

$$A = b(t_b + t_t)$$

$$c = \frac{0.5b(t_t)^2 + bt_b\left(h - \frac{t_b}{2}\right)}{A}$$

$$I = \frac{bt_t^3}{12} + bt\left(c - \frac{t_t}{2}\right)^2 + \frac{bt_b^3}{12} + bt_b\left(h - c - \frac{t_b}{2}\right)^2$$

$$S = \frac{I}{c}$$

However in the case of using these panels tested and designed for out-of-plane loading, flexural and shear capacity can be determined from normal ACI equations and then reduced accordingly to the DCA charts based on span and configuration.

Further design considerations to be used in the application of these panels for residential, commercial and/or industrial construction are listed as follows:

1. Panels when placed in the field will not have solid concrete end zones.
2. FRP top plates adhered to the concrete panels should be used in the form of FPCS panels. Then a membrane sealed over the butting joints.
3. Panels should be designed with normal ACI concrete equations considering bottom steel reinforcement only and treated as a solid section, then flexural and shear capacity should be reduced by the DCA from a chart based on span and configuration.

## 4.8 CONCLUDING REMARKS

Various configurations of precast concrete sandwich panels were tested and reported on in Tom Norris Thesis<sup>[44]</sup>. These panels with and without FRP top plates should good results for strength and deflection when compared to a similar solid concrete panel. Degree of composite action was determined for each panel and the range is from 70-90% DCA.

A finite element analysis model was created to determine the suitability for carry-out future analyses of precast concrete panels based on numerical modeling only. Several FEA models showed good correlation between the test results and the numerical analysis results. A dynamic explicit analysis using ABAQUS Damaged Plasticity model is recommended for future FEA studies as it captures the quasi-static failure of the concrete materials and provides a full solution. Variables that still need some research are the amplitude of loading and the failure mechanisms and bond failure between the constituent materials. A static general or static RIKS models did not perform as well, was actually more time consuming in solving the problem and in many cases prematurely ended before a solution in the nonlinear range of the model.

## **CHAPTER 5: CREEP BEHAVIOR OF FRP-PRECAST CONCRETE SANDWICH PANELS**

### **5.1 INTRODUCTION**

The non-linear effects of concrete cracking, creep and shrinkage, when not understood, qualified, predicted or designed for, can be a common cause of serviceability failure in concrete structures. (Gilbert & Ranzi, 2011). As documented by Gilbert and Ranzi (2011) approximately 50% of the final creep in a concrete structural member is developed in the first 2-3 months. The remaining 90% of the final creep is then estimated to develop in 2-3 years after. The test data and finite element analysis modeling presented here are based on (4) precast concrete panels subjected to creep loading for duration of less than 1 year. The data has many variables; however it does provide some insight to the structural behavior of the sandwich and FPCS panels under sustained loading and sets the stage for further development and creep testing.

Latest research published by Bazant et al.,<sup>[11][12][13]</sup> show that existing creep models, both in software format and analytical models, can underestimate creep effects in concrete structural members, especially over long periods of time. Since there is a lack of published data on long-term creep effects of concrete structures with various types of environmental conditions, loading, material properties and constituent materials, there is a little bit of blind faith in using such models without complete validation.

The creep test data presented in this research has many variables, all four panels are constructed differently and the creep test duration was less than one year. However, there are some useful preliminary insights to the creep behavior of the panels. The panels are expected to be loaded with linear-elastic service loads for the duration of their life; therefore a simplified creep power law model can be presented to make some preliminary predictions, when considering all of the inherent unknown variables such as relative humidity, temperature, aggregate size and type, water cement ratio, etc. No viscoelastic or inelastic creep models are required for this study.

### **5.2 EXPERIMENTAL DATA**

There are three types of analyses and/or data collection that will be considered for the creep behavior. The first will be an analytical model based on theoretical and empirical formulas for

concrete creep and flexural behavior of beams. The second form of analysis will utilize the finite element method with Abaqus© as the solver. These first two methods will be compared with the third form of data collection which will be the creep test panel itself.

There are four different creep test panels considered in this section of the study. They include:

- 1) 8" FPCS panel
- 2) 10" FPCS panel
- 3) 10" sandwich panel with FRP segmental shear connectors (no exterior FRP plate)
- 4) 10" solid panel to act as a baseline analysis.

The first panel is the 8 inch creep test panel with FRP plate as shown in Figure 114. The panel has the segmental FRP shear connector that anchors the top concrete wythe to the bottom concrete wythe. This panel also has an FRP plate bonded to the top and the sides of the panel.

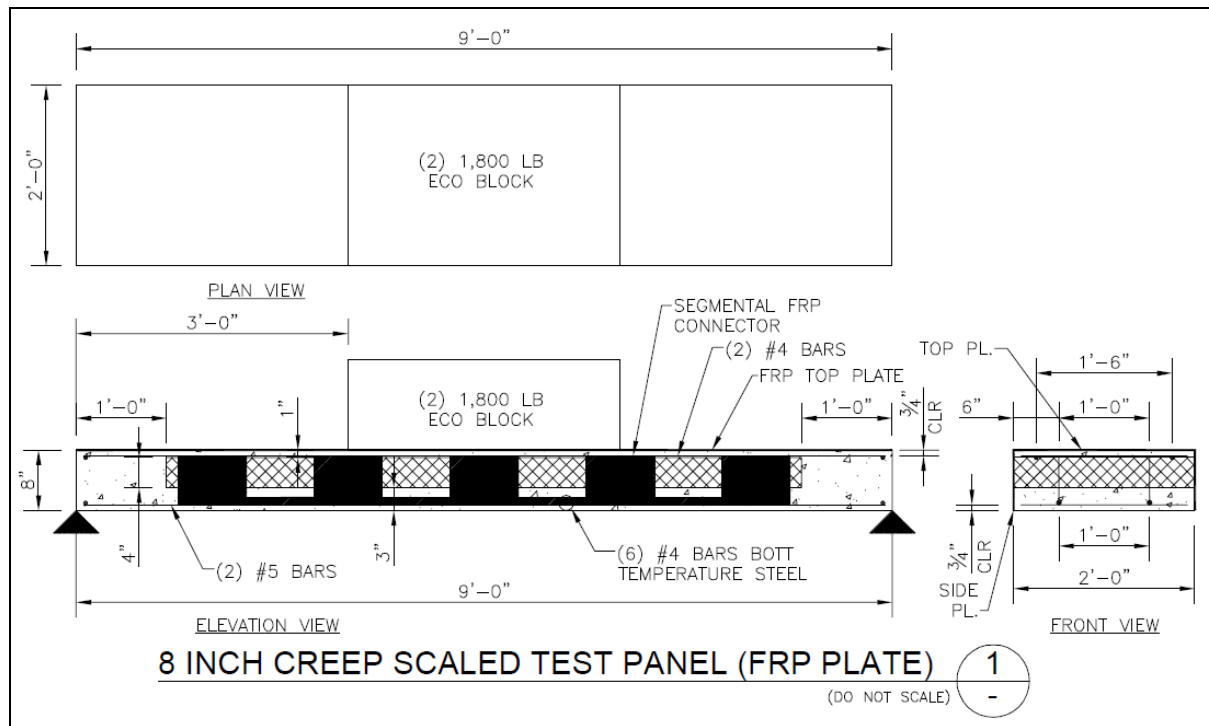


**Figure 114 – 8 inch creep test panel with FRP top & side plates (FPCS)**

The second creep test panel constructed and analyzed is the 10 inch creep test panel with the segmental FRP shear connector and the FRP plate bonded to the sides and tope of the concrete exterior face. This panel is shown in Figure 115. The third creep test panel is the 10 inch sandwich panel with the segmental FRP connectors in the upward orientation and no external FRP plates. Figure 116 shows the construction details of this panel.

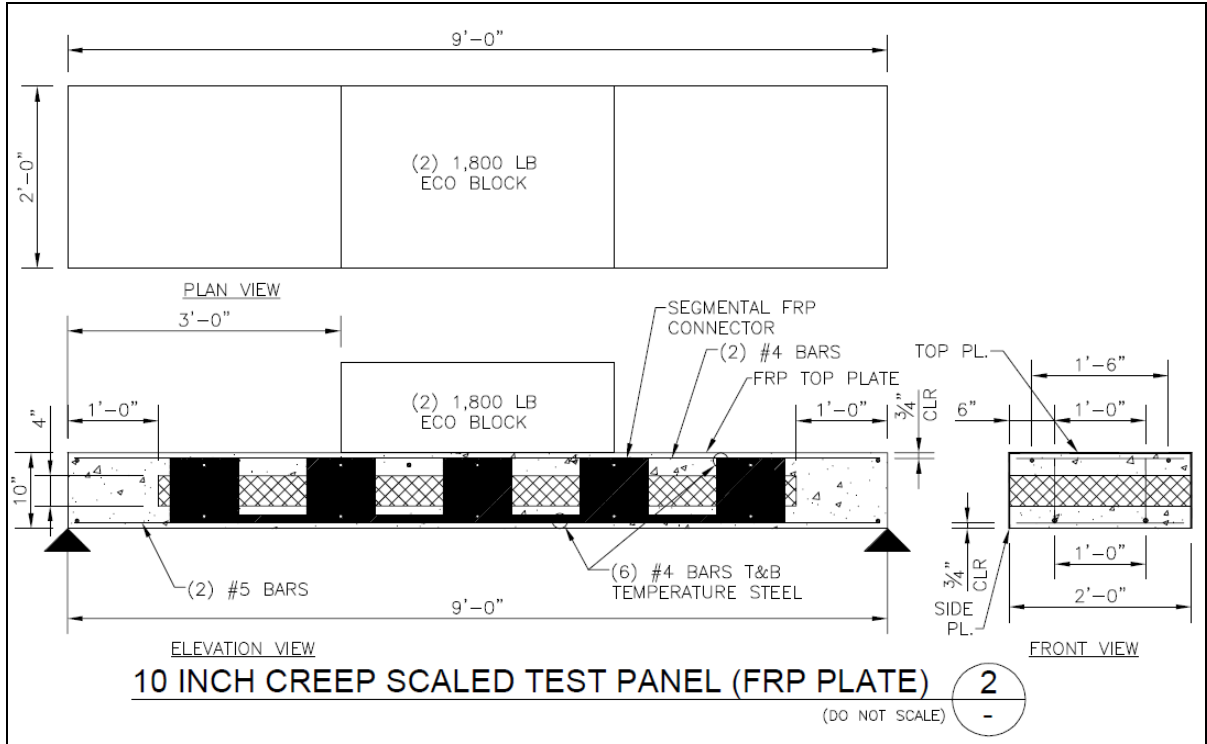


Figure 115 – 10 inch creep test panel with FRP top & side plates (FPCS)

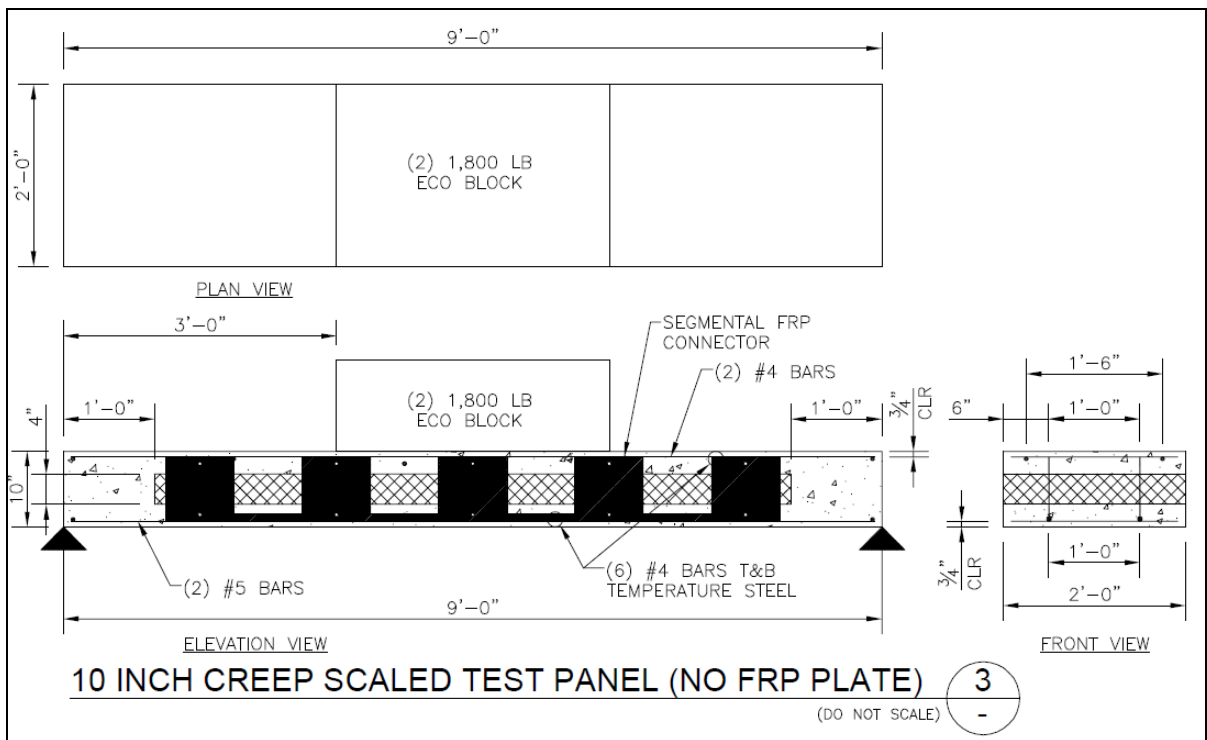
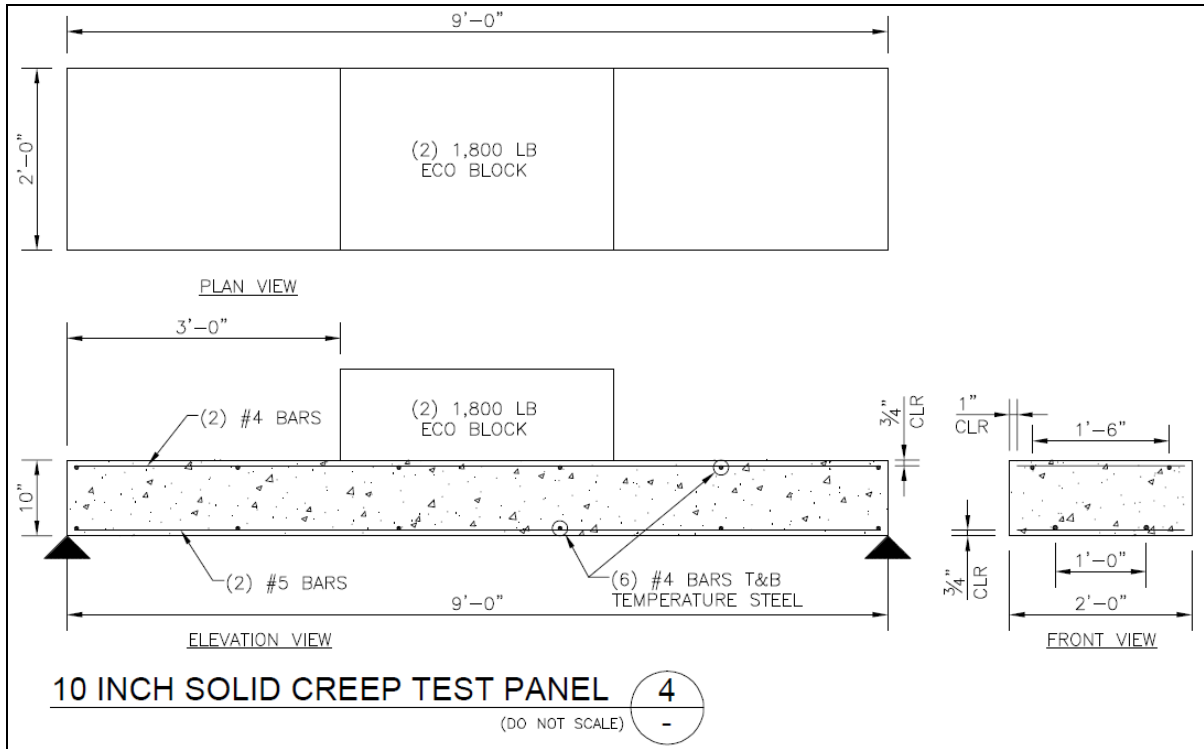


Figure 116 – 10 inch creep test panel with no FRP plate

Finally the 10 inch solid reinforced concrete test panel, used as the benchmark panel, is shown in Figure 117. This panel is also identical to the 10 inch solid concrete test panel used in the previously documented scaled test panel loaded to failure.



**Figure 117 – 10 inch solid creep test panel**

A summary of the panel loading and the actual weights of the blocks on each panel are shown in Table 27.

**Table 27 – Creep test block weights**

Specimen	Weight of Block 1 (lbs)	Weight of Block 2 (lbs)	Total Load (lbs)
Solid Slab	1552	1504	3056
10" Sandwich Panel	1540	1542	3082
8" FPCS Panel	1565	1572	3137
10" FPCS Panel	1598	1576	3174

### 5.3 ANALYTIC MODELS

The ACI 318 code has provisions for immediate deflection requirements and long-term sustained load deflection. These calculations are provided in this report to show the limitations of such models when compared to the test data and the finite element analysis. Sustained loading will create creep strains in the concrete which are additive to the shrinkage strains and the immediate instantaneous loading strain. The sum of the instantaneous deflection due to live loads, the sustained portion of the deflections due to dead load and any sustained live load is provided by the formula in Wight & MacGregor<sup>[55]</sup>;

$$\Delta = \lambda_{t_0, \infty} \Delta_{iD} + \Delta_{iL} + \lambda_{\infty} \Delta_{iLS} \quad (5-1)$$

Where,

Instantaneous deflection due to dead load:	$\Delta_{iD}$
Instantaneous deflection due to live load:	$\Delta_{iL}$
Deflection due to sustained Portion of the Live Load:	$\Delta_{iLS}$
Long term deflection factor for load applied at time $t_0$ :	$\lambda_{t_0, \infty}$
Long term deflection factor for loading > 5 years:	$\lambda_{\infty}$

The initial deflection when the concrete panel is placed on the blocks can be derived by the formula:

$$\Delta_{iD} = \frac{5w_{sw}L^4}{384E_c I_{gt}} \quad (5-2)$$

Where,

ACI 318 Modulus of Elasticity of Concrete:

$$E_c = 57000 * \sqrt{f'_c} = 57000\sqrt{4600} = 3,865,928 \text{ psi} \quad \text{ACI 318 Section 8.5.1} \quad (5-3)$$

Transformed Gross Moment of Inertia:

$$I_{gt} = \frac{b_w h^3}{12} + b_w h \left( \frac{h}{2} - y_t \right)^2 + (n-1)A_s (d - y_t)^2 + (n-1)A'_s (d' - y_t)^2 \quad (5-4)$$

Selfweight of the Concrete Panel:  $w_{sw} = b_w h \gamma = (24 \text{ in})(10 \text{ in})(0.084 \text{ pci}) = 20.139 \frac{\text{lb}}{\text{in}}$

Length of the Panel between supports: L=108 inches

$$\Delta_{iD} = \frac{5w_{sw}L^4}{384E_C I_{gt}} = \frac{5(20.139lb/in)(108^4)}{384(3,865,928psi)(2101.4in^4)} = 0.0044in \quad (5-5)$$

From the FEA model of just the selfweight run the deflection is:  $\Delta_{iD\_FEA} = 0.0047in$

From the FEA model of blocks + selfweight the deflection is:  $\Delta_{iTL\_FEA} = 0.0161in$

The instantaneous live load deflection then becomes:

$$\Delta_{iL} = \Delta_{iTL} - \Delta_{iD} = 0.0172371 - 0.0047 = 0.0125in \quad (5-6)$$

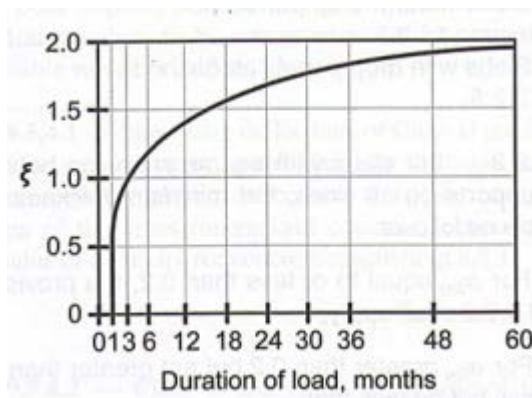


**Figure 118 – ACI multiplier for long term deflection (ACI 318, Figure R9.5.2.5)**

The multipliers for incremental time are shown in Table 28.

**Table 28 – ACI load duration multipliers**

Duration of Load (months/days)	Multitplier (ξ)
1/30	0.5
3/90	1
6/180	1.2
12/365	1.4

The compression steel ratio is:  $\rho' = \frac{2(0.20in^2)}{(10in)(24in)} = 0.0017 \quad (5-7)$

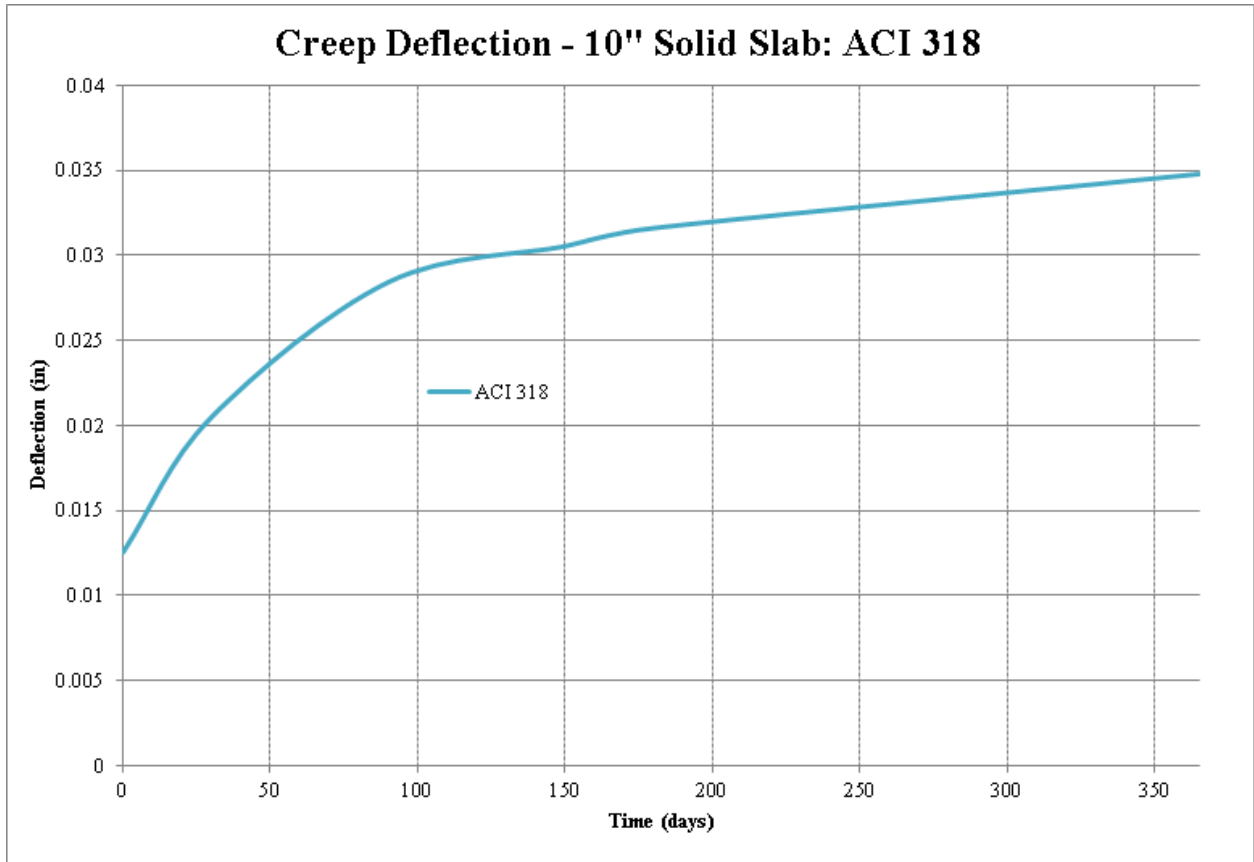
The sustained load multiplier is:  $\lambda_{\Delta} = \frac{\xi}{1 + 50\rho'}$  ACI 318 Eqn (9-11) (5-8)

The sustained load factor ( $\lambda_{\Delta}$ ) from ACI 318 equation 9-11 and the resulting deflections are shown in Table 29.

**Table 29 – ACI sustained load factors and deflections**

Time (days)	Variable ( $\xi$ )	Variable ( $\lambda_{\Delta}$ )	10" Solid	8" Solid	10" Solid		8" Solid	
			(in)	(in)	(in)	(in)		
0	0	0	0.012537	0.023968	$\Delta_{iD} =$	0.0047	$\Delta_{iD} =$	0.007326
30	0.5	0.460829	0.02048	0.038389	$\Delta_{iT_L} =$	0.017237	$\Delta_{iT_L} =$	0.031294
90	1	0.921659	0.028424	0.052811	$\Delta_{iL} =$	0.012537	$\Delta_{iL} =$	0.023968
180	1.2	1.105991	0.031601	0.058579				
365	1.4	1.290323	0.034779	0.064348				

For reference, the plot of the solid slab creep deflection is shown in Figure 119 and the duration was set for 365 days, which is almost twice that of the actual test. This represents the standard code-based analytical method currently available to the engineer. The ACI figure will be compared to the test data and FEA analysis later in this chapter.

**Figure 119 – Analytical creep deflection, ACI 318**

### 5.3 EXPERIMENTAL INVESTIGATION

The four specimens were statically tested with 3-point bending as a simply supported beam and loaded with (2) ecology blocks as shown in Figure 120, Figure 121 and Figure 122. The weights of the ecology blocks were provided in Table 27 and are approximately 1,500 lbs each. Further detail of the test set up is explained in the final Thesis document by Tom Norris<sup>[44]</sup>. Tom had the responsibility for the majority of the test set up and data recording.

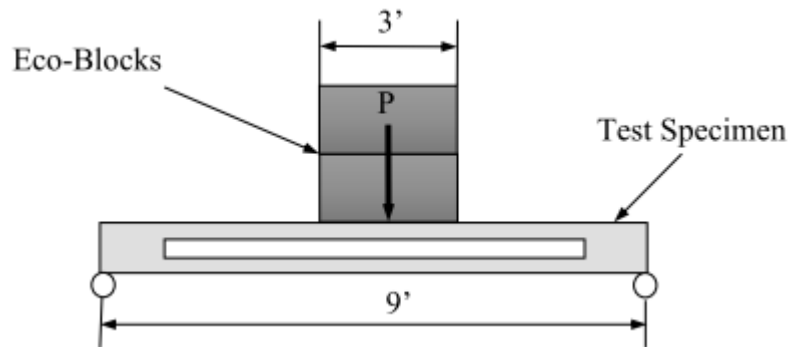


Figure 120 – Creep test loading diagram



Figure 121 – Creep test set up for 10" FPCS panel



**Figure 122 – Creep test panel set up for 8'' FPCS, 10'' sandwich and 10'' solid panel**

As explained in Norris<sup>[44]</sup> thesis document there was a good attempt in capturing more data by applying the high number of the gages, however not all gages were functional, used and/or operational during the test. Furthermore, anomalies and discrepancies in the data collected were commented on and explanations were provided in Norris<sup>[44]</sup> thesis. In Figure 121 the 10'' FPCS panel was placed on the loading dock under the building canopy and therefore never received any direct sunlight. All creep test panels were covered with a tarp, however (3) of the panels were located in the open environment as shown in Figure 122. These three panels that were set up outside in the driveway and are indicated as items 1, 2 and 3 in Figure 123. These three panels also resulted in the highest deflection values which presumably were influenced by shrinkage creep and mechanical breakdown in the interstitial zones due to temperature fluctuations from day to night. In the plot shown in Figure 123, areas are highlighted and numbered with explanations also provided in Norris<sup>[44]</sup> thesis as follows:

1. The dial gages had been moved at this panel such that they no longer recorded any data. For that reason, deflection data acquisition at this panel was halted.
2. At 150 days the load was removed from the panel and the elastic recovery in the sandwich panel is shown.

3. At 150 days the load was removed from the panel and the elastic recovery in the solid panel is shown.

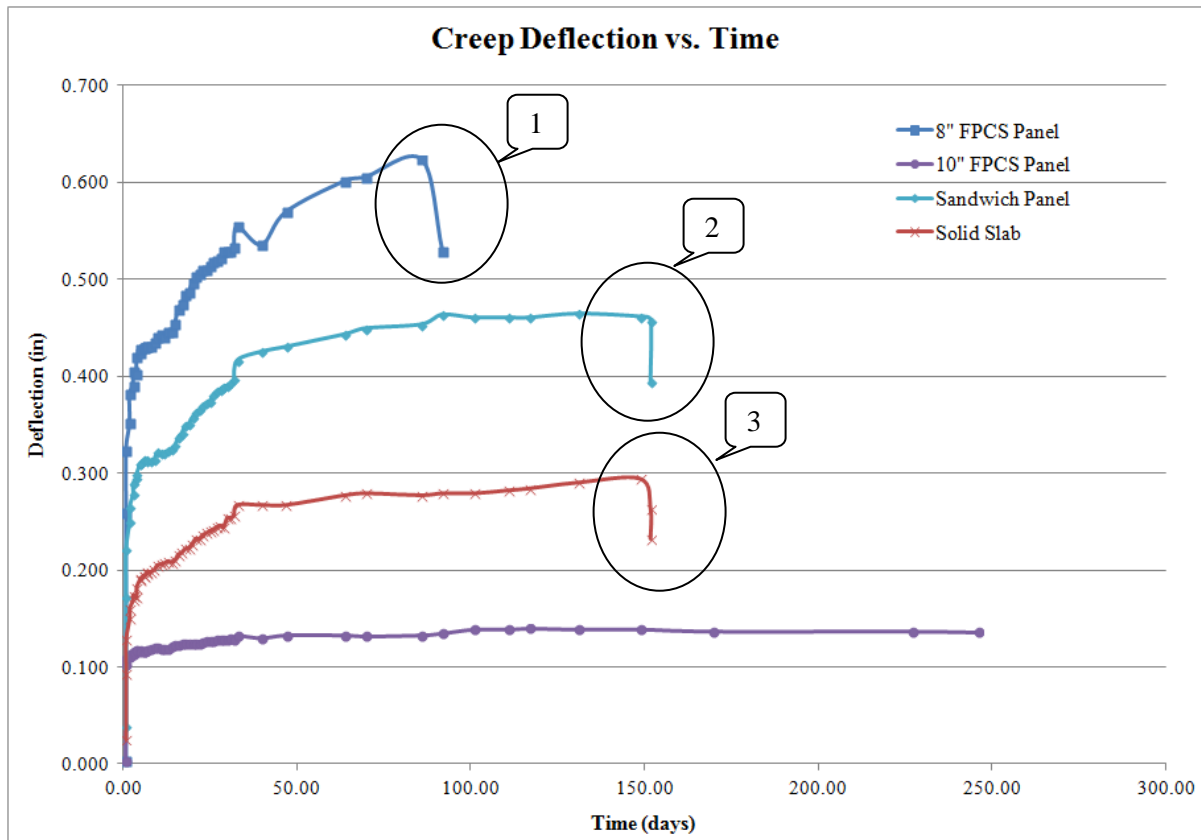


Figure 123 – Creep deflection vs. time, Norris<sup>[44]</sup>

The testing of the (4) panels for creep deflection was performed in an uncontrolled and exterior environment. Notable factors/influences regarding the testing of these panels for the 150 day duration are as follows:

- A. The panels were outside.
- B. The panels were not protected/secured from public or natural disturbances.
- C. The creep deflection of the panels is both influenced by mechanical creep strain along with shrinkage creep strain. Thermal strain cannot be ruled out, however it most likely had less of an effect when compared to the shrinkage creep and the arid climate it was tested.

The mid-span deflection vs. time of the four panels was compared to the quarter point deflections and these deflection plots can be seen in Figure 124. The three exterior panels shown in Figure 122 have the highest initial peak deflection at the placement of the load then the recordings taper off as normal creep deflections occurred over time.

Analytical hand calculations were performed on the solid slab along with finite element analysis and the initial deflection of the solid slab with the (2) ecology blocks should have been around 0.014 inches to 0.031 inches respectively as shown in Table 30. The initial deflection of the solid slab in Figure 124 is 0.124 inches and this is an order of magnitude higher than both of the hand calculation and finite element analysis results. Adjusting for this discrepancy is the quarter point deflection comparison with no initial deflection as shown in Figure 125.

**Table 30 – 10” solid panel deflection calculations**

10” Solid Reinforced Concrete Panel		
Analysis Method	Load	Midspan Deflection (in)
ACI 318	Selfweight + 3,056 lbs	0.014
Finite Element Analysis	Selfweight + 3,056 lbs	0.031

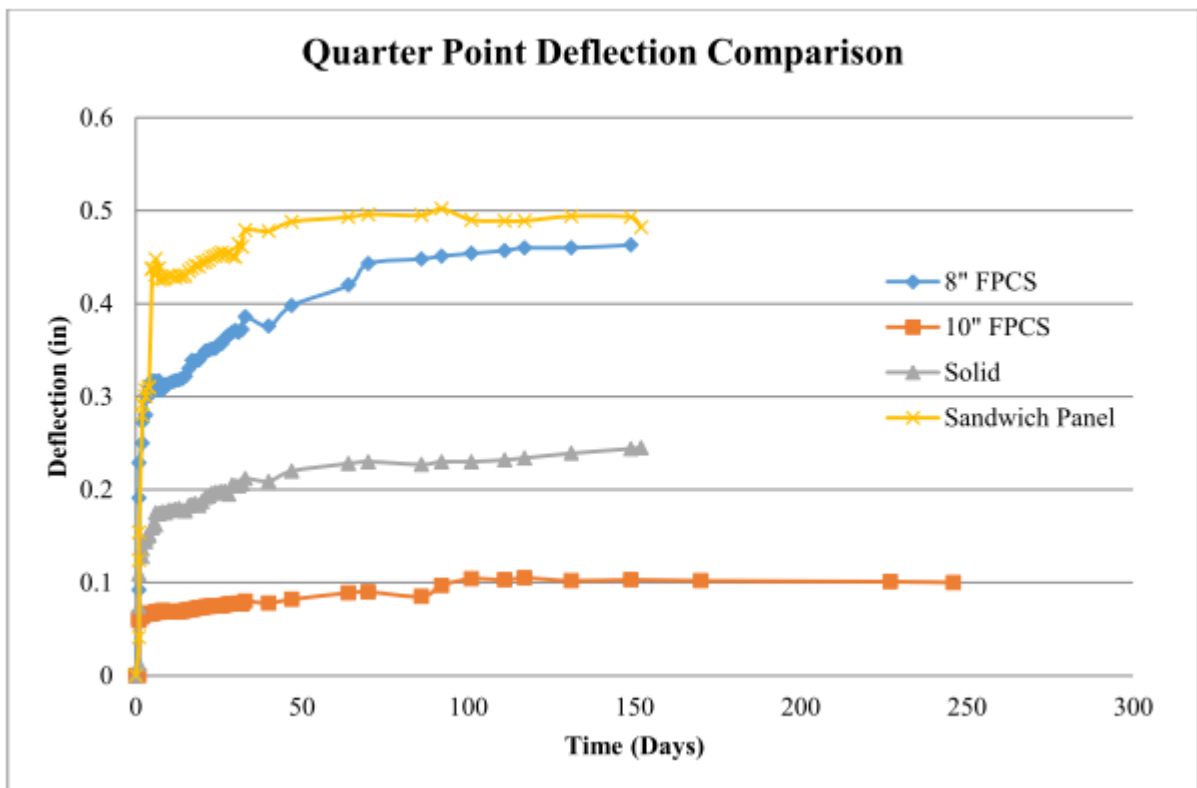


**Figure 124 – Quarter point deflection vs. time, Norris (2014)**

Even with the no initial deflection adjustment, there still remains a sharp increase in deflection at the early stages of the test. Quite possibly the panels had experienced a high level of shrinkage creep

strain and this caused the panels to deflect rapidly in the beginning stages of the test and/or support settlement. The panels were placed on test blocks and loaded in July of 2013 and this is the height of the hot and dry seasonal environment in Moscow, ID, where the panels were located.

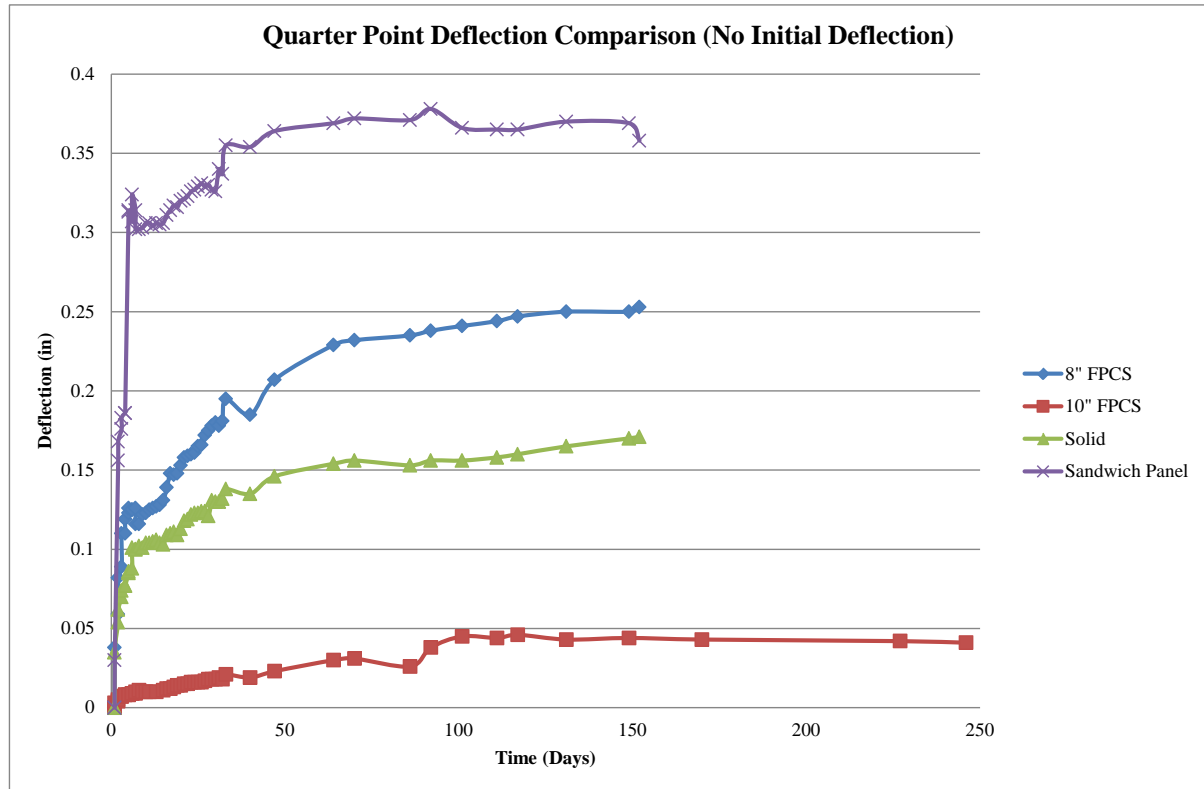


**Figure 125 – Quarter point deflection vs. time, no initial deflection**

From Figure 125, the high initial deflection values remain, even with initial deflection adjustments the reliability of the data of the (3) panels tested outdoors remains questionable.

One piece of data that can be extracted from the four creep test panels is the secondary creep. The primary creep results, which can be influenced by shrinkage, are unlike the secondary creep results which tend to have more of a flat curve and low slope. The secondary creep results along with a linear trendline equation are shown in Figure 126. Included in this plot is the ACI 318 equation which is estimated between 30 and 180 days. The slope of the ACI 318 line, which is the rate of secondary creep, is 0.00007. This is relatively low when compared to the other secondary creep slopes for the test panels.

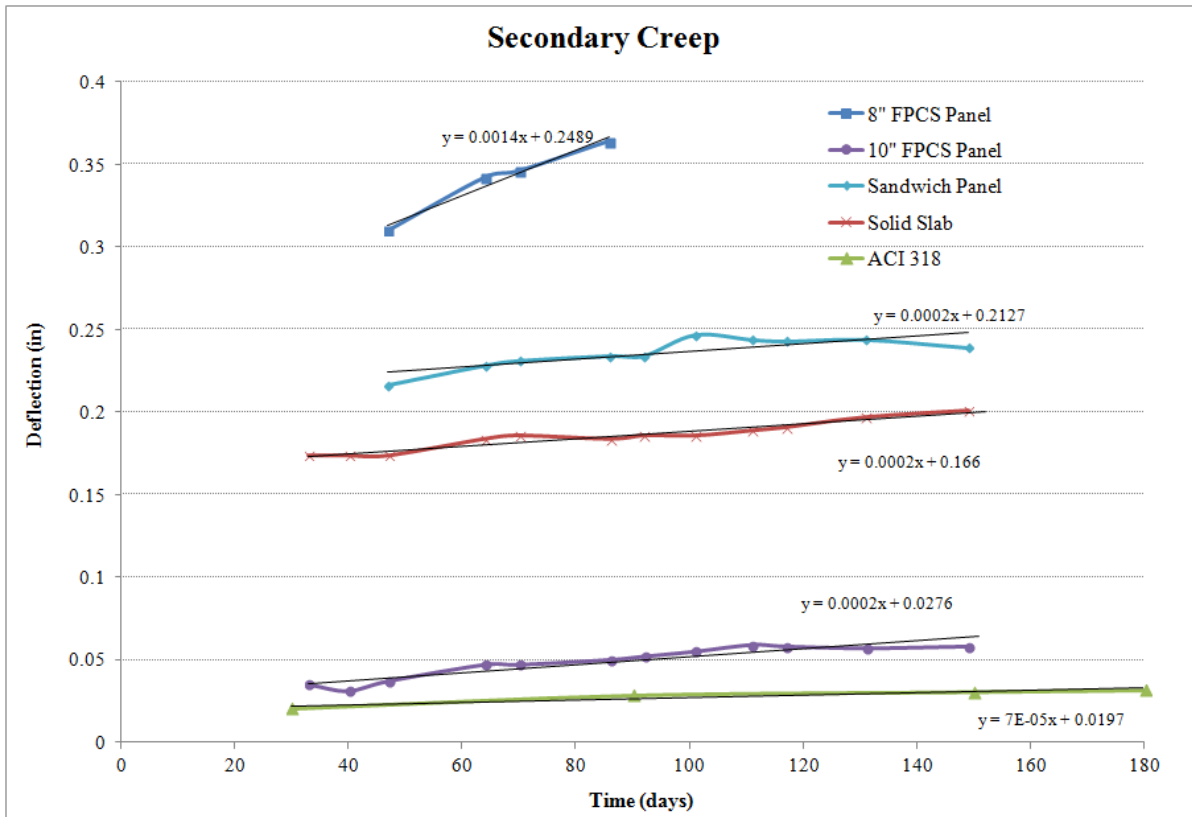


Figure 126 – Secondary creep comparisons

### 5.4 FINITE ELEMENT ANALYSIS

Creep effects in concrete structures has been studied since the 1970’s and many analytical models have been published in codes such as the ACI model, the Comite Euro-Internationale du Beton (CEB), Federation internationale de la precontrainate (FIP) model, the Japan Society of Civil Engineers (JSCE) model, the Gardner and Lockman (GL) model and Model B3. Evaluation of existing commercial software programs and the code-based models themselves, i.e., ACI 209, show that they underestimate the effects of multi-decade creep in large-span prestressed bridges.<sup>[13]</sup> Bazant and others have studied and documented concrete creep models for over 30 years and have shown that a successful concrete creep model is based on many constituent sections and algorithms that account for water-cement ratio, temperature, relative humidity, prestress loss, and sun exposure to name a few. Bazant, et.al., have commented that engineers strive to find a model to predict creep and shrinkage from as few parameter as possible.<sup>[11]</sup> Specifically, they wish to use only the strength of the concrete as the sole design variable to determine the concrete creep strain. A model such as this would be more convenient and user-friendly, however it is not realistic and therefore a rigorous

model, well tested against suitable number of specimen results over a long period of time, should be developed and used.

### **Simple Creep Power Law – Strain Hardening:**

Abaqus© includes in its solver a few different creep models that can be used in lieu of creating a UMAT subroutine. One approach is to create a subroutine that incorporates the engineering properties of the concrete materials. The approach taken here is to use the simplified creep power law function and fit it to the solid panel test data. Next step is to verify the same formula on the FPCS sandwich panel and then extrapolate that out to several years (since the test was only 180 days). From Abaqus User's Manual, Section 23.2.4

The equivalent deviatoric creep strain increment is determined by the following equation:

$$\dot{\varepsilon}_{cr} = \left( A \tilde{q}^n \left[ (m+1) \bar{\varepsilon}^{cr} \right]^m \right)^{\frac{1}{m+1}} \quad (5-9)$$

Where,  $\bar{\varepsilon}^{cr}$  is the equivalent creep strain and  $\tilde{q}$  is the uniaxial deviatoric stress,  $t$  is the total time and  $A$ ,  $n$  and  $m$  are defined constants and functions of temperature. For the 10" solid concrete creep test panel the following values were used for the defined constants:

$$A = 1E-09$$

$$n = 2.25$$

$$m = -0.5$$

These values were obtained through curve fitting functions in excel from the actual creep test data plots.

### **Gilbert Creep Strain:**

The creep strain is determined from Gilbert's AS3600<sup>[22]</sup> equation as follows:

$$\varepsilon_{cc} = \varphi_{cc} \frac{\sigma_o}{E_{c28}} \quad (5-10)$$

Where  $\varphi_{cc}$  is the creep coefficient defined as:

$$\varphi_{cc} = k_2 k_3 k_4 k_5 \varphi_{cc,b} \quad (5-11)$$

From Gilbert's SP-227-2<sup>[22]</sup> model the modification factors for creep and shrinkage were determined as follows;  $\alpha_2 = 1.1468$ ,

$$k_2 = \frac{\alpha 2t^{0.8}}{t^{0.8} + 0.15t_h},$$

$$k_3 = 1,$$

$$k_4 = 0.6,$$

$$k_5 = 1.0,$$

$$\varphi_{ccb} = 3.4$$

The equivalent deviatoric creep strain increment is determined by the following equation:

$$\dot{\varepsilon}_{cr} = A \tilde{q}^n e^{(\varphi_{cc} \varepsilon_{co})} \Delta t \quad (5-12)$$

The derivative of the equivalent deviatoric creep strain increment with respect to von mises stress is:

$$\ddot{\varepsilon}_{cr} = n A \tilde{q}^{(n-1)} e^{(\varphi_{cc} \varepsilon_{co})} \Delta t \quad (5-13)$$

Definitions:

DECRA(1):	Equivalent (uniaxial) deviatoric creep strain increment, $\Delta \varepsilon^{-cr}$
DESWA(1):	Equivalent (volumetric) consolidation creep strain increment, $\Delta \varepsilon^{-sw}$
A	cross-sectional area
$E_{c28}$	elastic modulus of concrete at 28 days
$F^c$	characteristic
$\tilde{q}$	uniaxial deviatoric stress

This Gilbert model has been presented here as an example of a simplified creep power law approach, however results from the model were not compared nor validated.

### **Bazant B3 Model:**

Bazant et al<sup>[11][12][13]</sup> have published a few articles on creep models which can be created and used in ABAQUS for analysis. As shown in their research work, there are several other creep models published, both analytical and numerical (commercial software), that can grossly underestimate the creep deflections in large structures. The basic algorithm from these published models can be used to analyze the creep in the FPCS sandwich panels, however as explained in Bazant's research, each model needs to be configured to the data from the test structure. This in itself is a limitation and leads us to believe that long term creep testing needs to be performed on the FPCS panels researched in this study in order to provide an accurate and reliable creep algorithm.

## 5.5 TEST RESULTS VS. ANALYTICAL AND FE PREDICTIONS

The creep tests in this study provide a preliminary idea of how the sandwich panels, in particular the FPCS sandwich panel, perform over the duration of static linear loading. Considering the data in generalized form and ignoring severable variables and factors, a simple power creep law model can be used to show correlation to the test panels and then provide a generalized and conservative prediction to the long term effects. The 10 inch solid panel, both test data and FEA data, is shown in Figure 127. In the FEA model the initial selfweight of the panel is measured as the first step, and then the applied creep load is incorporated as the subsequent step for the allotted time duration. The power law previously described matches well with the available data. It is interesting to note the ACI 318 creep equation plot is vastly under-conservative.

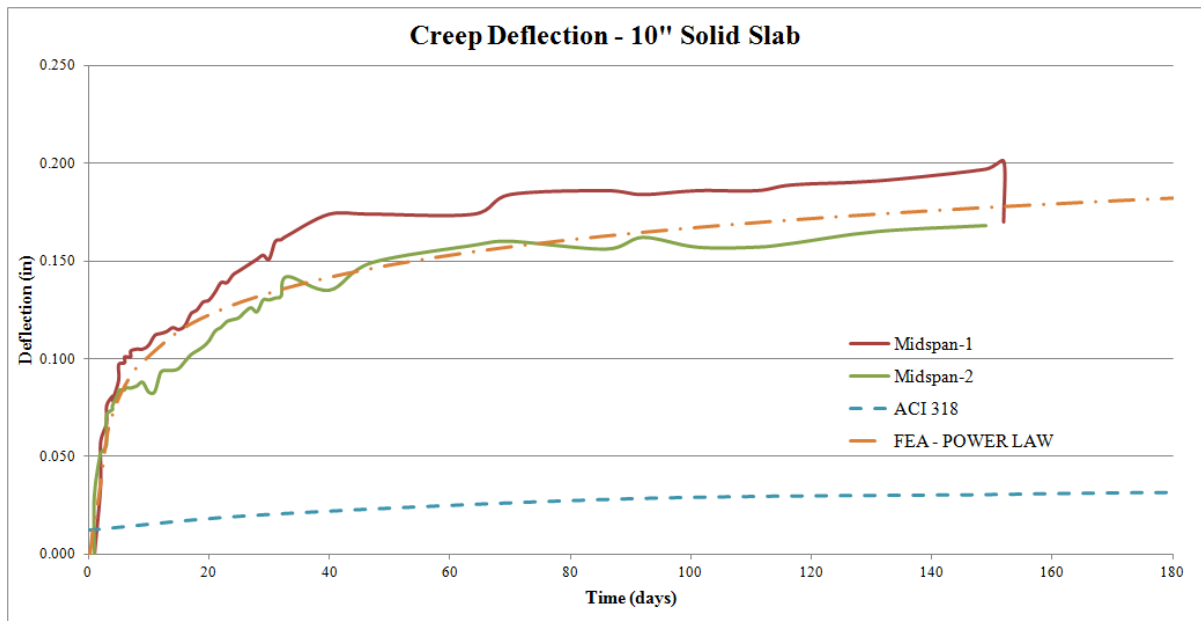
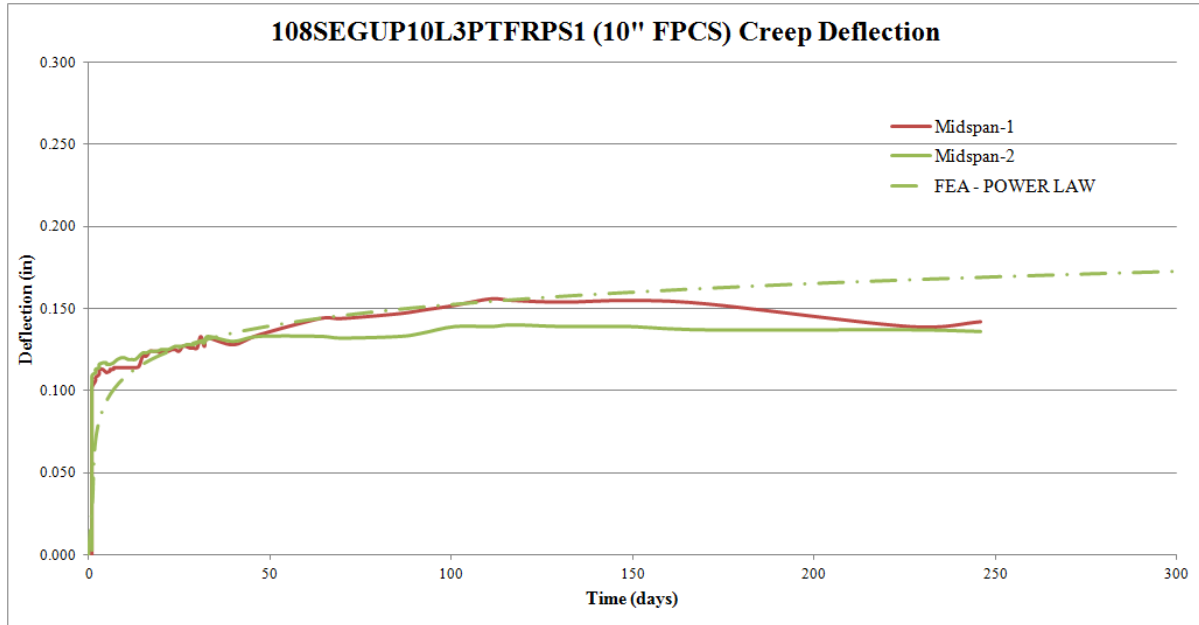


Figure 127 – 10 in. solid concrete creep test panel 4 deflection

With this generalized simple creep power law showing good correlation to the test data, it can then be used for the 10 inch FPCS sandwich panel to see how well it matches that test data. The comparison between the solid panel and the FPCS sandwich panel is shown in Figure 128.



**Figure 128 – 10 in. FPCS sandwich creep test panel 2 deflection**

The power law used for the FPCS sandwich panel is providing conservative results for the 180 day span and that shall be considered the upper limit to this approach. When extrapolating that curve out to 30 years the estimated final creep deflection is less than 0.25 inches which can be seen in Figure 129. For the 9 foot span, the 0.25 inch deflection would constitute a deflection ratio of  $L/432$  which is acceptable per building code and ACI standards. Once again the load on the panel, which distributed into a surface load is:

$$W = (3,174 \text{ lbs}) / (2' \times 9') = 176 \text{ psf} \ggg \text{ than any service live load}$$

The load is not distributed over the surface of the panel, however when considering the total load of the ecology blocks over the area of the panel, the surface live load is far greater than any code specified pressure load such as 20 psf for roofs, or additional dead load material weights or even snow loading. Therefore, considering the estimated 30 year creep deflection of  $L/432$  with this loading is remarkably good and acceptable, however not verifiable at this point.

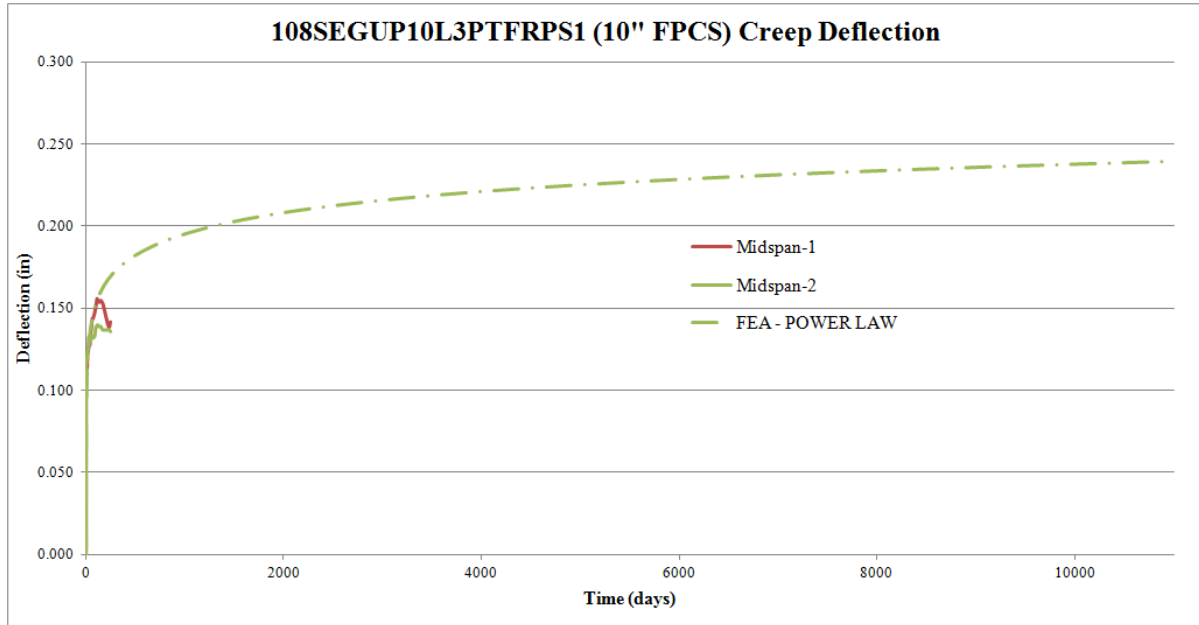


**Figure 129 – Estimated long term creep effects for 10” FPCS panel**

Once again this method is preliminary and cannot be verified with the limited data available and with so many variables. It is recommended that creep test panel be constructed again with fewer variables and loaded for duration of more than 1 year and preferable several years. The finite element analysis model should use one of the published creep subroutine models by Bazant, etal or another accepted constitutive model. Research by Bazant etal<sup>[11][12][13]</sup> shows that by creating a model with limited data and extrapolating that out for 20-30 years can lead to gross underestimation.

## 5.6 CREEP SUMMARY

The (4) panels tested for creep loading in this research all varied in type of construction and in some cases environmental influences. Three of the panels were completely outside and covered with a tarp during the test and one panel was under a building canopy at a loading dock, also covered. Recent research shows that current creep analytical models and FEA software are based on obsolete methods and may even produce unconservative deflection estimates for larger structures with more creep sensitivity<sup>[11][12][13]</sup>. With the variability in the loading and the environmental effects, it may be unreliable to develop a finite element analysis creep model to capture the effects of the test accurately and then to extrapolate that to long-term predictions with any kind of confidence. Future creep testing is desired where (2) of each type of panel is tested, in a controlled temperature and humidity environment. The panels should be tested for at least 365 days and preferably longer and a creep analysis model should be then developed based the algorithms presented in Bazant, etal’s

research<sup>[13]</sup>. These algorithms have several variables in the subroutine that need to be accounted for to provide an accurate creep prediction. If the future FPCS test panels can narrow in on a few variables and correlate a FEA UMAT subroutine model for that test, it should lead to better confidence for extrapolation.

The 10" FPCS panel did show the best creep results, perhaps the FRP enclosure contained more of the moisture and protected the panels from shrinkage creep or perhaps the FRP provided additional strength for the panel. This type of panel should be tested again along with a solid concrete panel to be used as a baseline comparison. The 8" panel should most likely be avoided when performing a creep test as the results for this type of panel showed the highest deflections over the same time period.

## **CHAPTER 6: BLAST RESISTANCE OF FRP-PRECAST CONCRETE SANDWICH PANELS**

### **6.1 INTRODUCTION**

Technical investigations on the study of blast effects have been available for over 60 years. There is little to be found on existing investigative research of precast concrete sandwich panels; however there are resources available for information on reinforced concrete structures subject to blast loading, Hinman<sup>[26]</sup> and McCann<sup>[40]</sup>.

When designing buildings or structures for blast loading, the engineer must prioritize the goals for the building performance, knowing that a “blast-proof” building for a known event may be too expensive to build. “Preventing the building from collapsing is the most important objective”. Hinman<sup>[26]</sup>. This statement is highest priority for structural design for blast loading and following the 1) prevention of the building collapse; an engineer must 2) reduce flying debris and 3) allow for safe evacuation and/or rescue/recovery efforts.

To provide an idea of the likelihood of blast loading to a building, the chart in Figure 130 shows the number terrorist attacks and to which type of building the blast generally occurred.

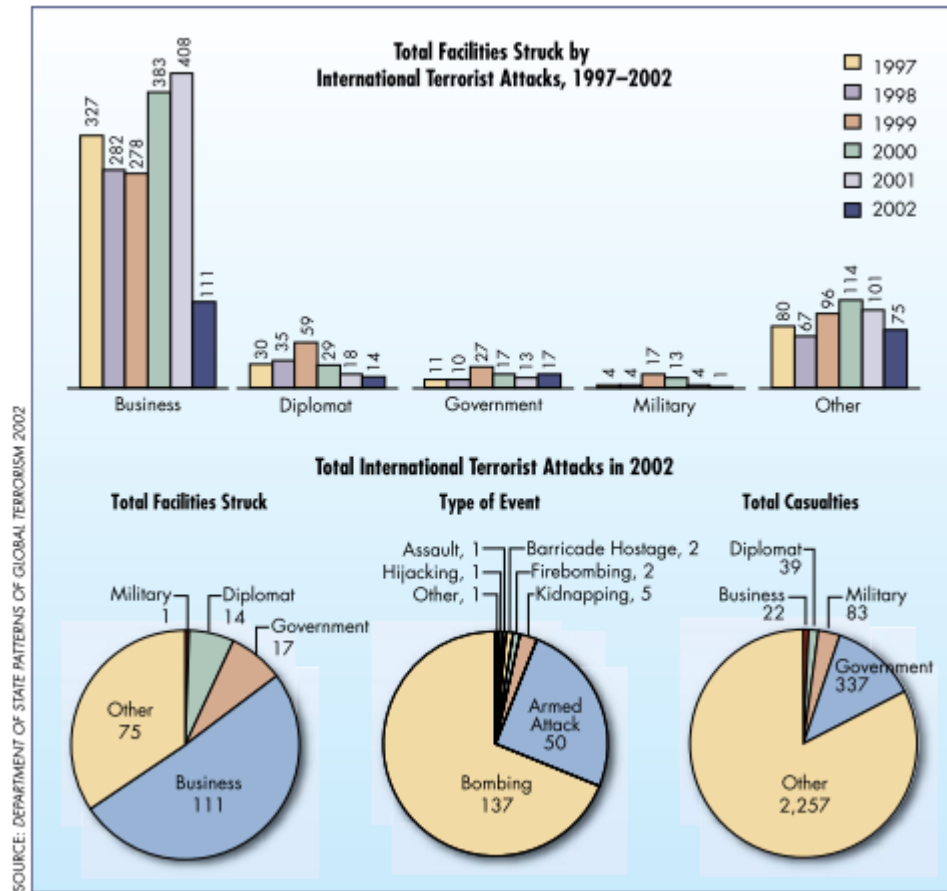


**Figure 130 – Facility terrorist attack, (FEMA 426)**

Blast loading does not always mean a terrorist event, a building at a petrochemical, industrial and/or manufacturing facility can also experience an accidental blast load event. Nevertheless, blast loads do occur, are likely to happen to certain building targets and when required, structural engineers need to understand more about the available materials to design for these events.

## 6.2 BLAST LOADING

Typical blast waves are described as condensed air pressure waves that travel at supersonic speeds from a point explosion source<sup>[6]</sup>. The typical blast pressure versus time plot is shown in Figure 131. The level of peak incident and peak reflected pressure is usually many times more than typical operating and environmental loads that a building would experience, however the phase duration or time is on the order of milliseconds.

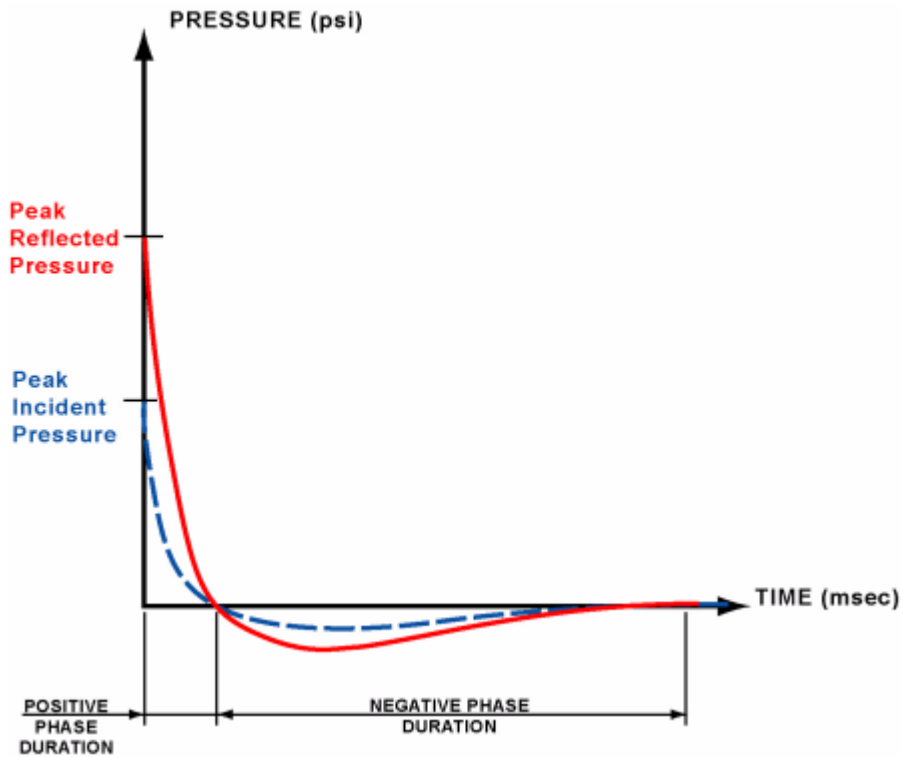


Figure 131 – Typical blast pressure wave (Hinman, 2003)

The structural design should also account for load reversals, unpredictable secondary loads such as loss of elements or falling debris and formation of plastic hinge mechanisms. A simplified version of the blast pressure versus time is shown in Figure 132, where the  $f_0$  sometimes known as  $P_{s0}$  is the peak surface-on pressure or peak intensity. The time duration,  $t_d$  of the blast wave is typically in the range of 0.1-0.001 seconds.

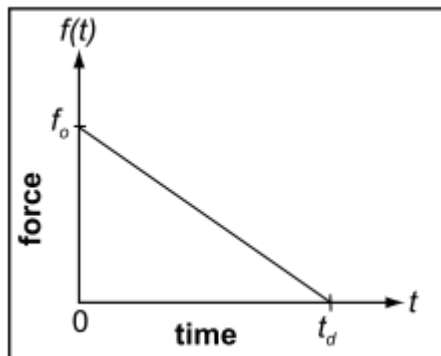


Figure 132 – Idealized blast pulse versus time

The magnitude of the initial velocity,  $v$ , for a single degree of freedom (SDOF) system is characterized by the following equation:

$$v = \frac{f_o t_d}{2m}, \text{ where } m = \text{mass of the structural system.}$$

Concrete has more mass than other conventional building materials and therefore since mass is the only parameter that controls the magnitude of the initial motion, it becomes more advantageous for blast design. McCann (2007). To further develop this thought, a precast concrete sandwich panel, with 40% less mass than a solid concrete panel, will also be a beneficial material for blast resistance even though it has less mass than its solid counterpart. The precast sandwich panel still has more mass than other conventional building materials such as steel with decking or wood.

Kingery<sup>[21]</sup> developed equations and graphical representations to allow an engineer to derive the pressure at surface defined by the standoff distance  $Z$ . The graph in Figure 133 has several parameters that can be defined by locating them on the curves in double logarithmic diagram. The variables in the diagram in Figure 133 are:

Peak Side-On Pressure:	$P_{so}$
Peak normally reflected pressure:	$P_r$
Side-on specific impulse:	$i_s$ which is derived from the value $(i_s/W^{1/3})$
Normally reflected specific impulse:	$i_r$ which is derived from the value $(i_r/W^{1/3})$
Time of arrival:	$t_a$ which is derived from the value $(t_a/W^{1/3})$
Positive phase duration:	$t_d$ which is derived from the value $(t_d/W^{1/3})$
TNT equivalent weight:	$W$
Shock wave velocity:	$U$
Wave length of positive phase:	$L_w$ which is derived from the value $(L_w/W^{1/3})$

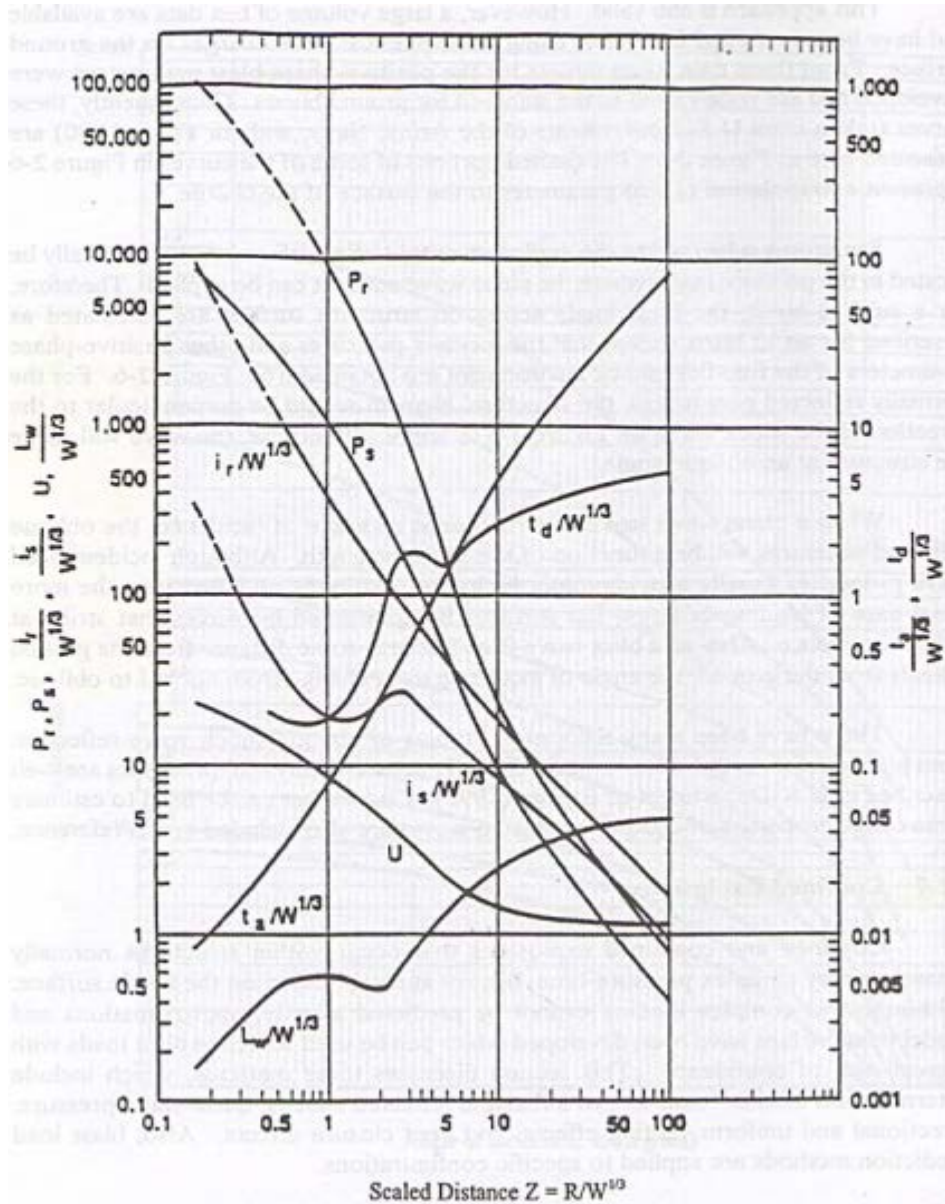


Figure 133 – Positive phase air blast parameters for hemispherical TNT Detonation, Surface

Figure 134 shows a similar double logarithmic diagram for the negative pressure attributes common to the hemi-spherical blast, however for this study only the positive pressures will be accounted for in the analysis. Normally in building design where a larger blast load may occur and the time duration is longer there will be both positive phase blast pressure loading as well as negative phase blast pressure as the blast wave rolls over and around then away from the building.

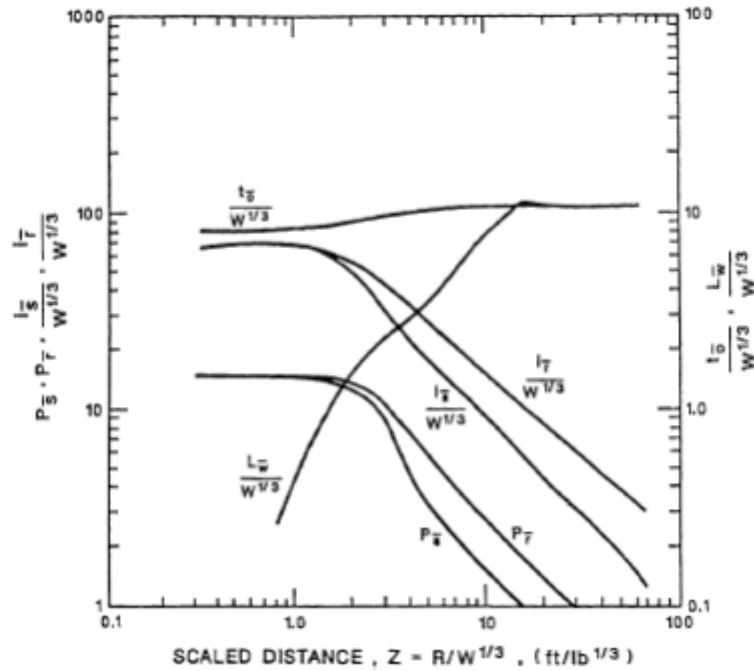


Figure 134 – Negative pressure parameters for hemispherical blast<sup>[26]</sup>

## 6.2.1 COMPUTATION OF BLAST PRESSURE USING HEMISPHERICAL DETONATION GRAPH

TNT weight:  $W = 1 \text{ lbm}$

Distance from target:  $R = 10 \text{ ft}$

$$W^{1/3} = 1^{1/3} = 1$$

$$Z = (R/W^{1/3}) = 10/1 = 10$$

From diagram in Figure 133:

Peak Side-On Pressure:  $P_{so} = 10 \text{ psi}$

Peak normally reflected pressure:  $P_r = 23 \text{ psi}$

Side-on specific impulse:  $(i_s/W^{1/3}) = 8, i_s = 8 \text{ psi-ms}$

Normally reflected specific impulse:  $(i_r/W^{1/3}) = 20, i_r = 20 \text{ psi-ms}$

Time of arrival:  $(t_a/W^{1/3}) = 450, t_a = 450 \text{ ms}$

Positive phase duration:  $(t_d/W^{1/3}) = 2.2, t_d = 2.2 \text{ ms}$

Shock wave velocity:  $U = 3 \text{ ft/ms}$

Wave length of positive phase:  $(L_w/W^{1/3}) = 2.5, L_w = 2.5 \text{ ft}$

## 6.2.2 COMPUTATION USING IDEALIZED BLAST PRESSURE WAVE FORMULAS

The UFC 3-340-02 has created the idealized blast pressure wave as shown on Figure 132 and there are equations that have been created to simplify the procedure for hand calculation purposes.

Peak Reflected Pressure:  $P_r = (2+0.05P_{so})P_{so} = (2+0.05(10))10 = 25 \text{ psi}$  [Eqn 3-3]<sup>[9]</sup>

Dynamic (blast wind) Pressure:  $q_o = (2.5P_{so}^2)/(7P_o + P_{so}) = (2.5 \times 10^2)/(7 \times 14.7 + 10) = 2.21 \text{ psi}$

Where  $P_o$  is atmospheric pressure

Shock wave velocity:  $U = 1130(1+0.058P_{so})^{0.5} = 1130(1+0.058 \times 10)^{0.5} = 1420 \text{ ft/s}$

$U = 1.42 \text{ ft/ms}$  [Eqn 3.5]<sup>[9]</sup>

Blast Wave Length:  $L_w = Ut_d = 1.42 \times 2.2 \text{ ms} = 3.12 \text{ ft}$

Computation of blast pressure positive phase wave length from the hemispherical graphs ( $L=2.5\text{ft}$ ) and from that of the idealized blast pressure wave formulas ( $L=3.12 \text{ ft}$ ) are similar. Similar values can be found when using the ATBlast program as shown in Figure 135.

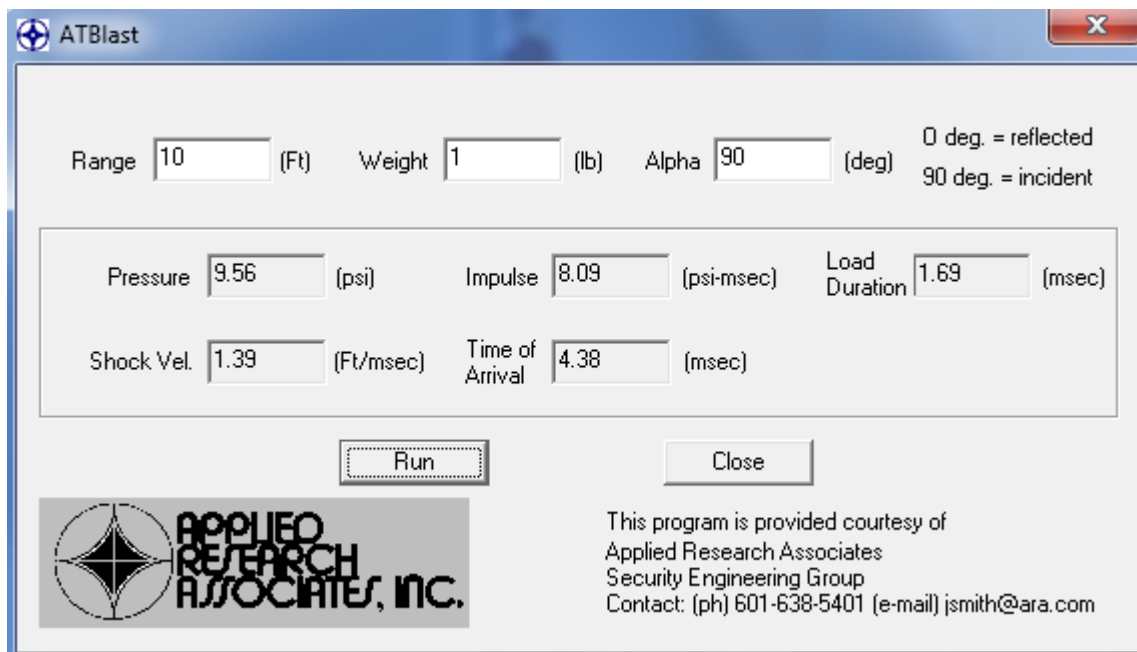


Figure 135 – Blast parameters from ATBlast program

## 6.3 FINITE ELEMENT ANALYSIS

It is difficult to find information on blast effects or blast loading on concrete structures in the public domain, therefore this study will be restricted to performing numerical analysis studies. Abaqus© will be used to model and analyze the blast loading event through its explicit solver and using the CONWEP<sup>[12]</sup> blast loading application. This type of loading is defined as determining the blast effects on a defined surface from a reference point. The distance and angle of the reference point to all nodes on the surface is taken into consideration when determine the blast pressure wave.

### 6.3.1 FEA BLAST LOADING MODEL VALIDATION

The precast concrete sandwich panels built and tested in this study and analyzed using numerical methods were all completed under a static (or equivalent quasi-static) load. The dynamic explicit FEA model was created and validated using the static test load data from the physical specimens. No dynamic blast load was ever applied to this panels, however as mentioned previously, they are considered to be practical and energy efficient solutions to buildings susceptible to blast loading, whether accidental or terroristic. In order to provide some validity to using the dynamic explicit analysis method in ABAQUS© with the Damaged Plasticity model, the author has research other published test articles on blast loading and used that data to provide validity to the modeling techniques used in this study. The published research performed by Thiagarajan et. al.<sup>[51]</sup> and the thesis submitted by Vasudevan<sup>[53]</sup> was used to assist in the validation of the blast research initiated in this study.

In Thiagarajan et. al. research, four doubly reinforced concrete panels were tested at the Army Research Lab under a simulated pressure blast loading event. The panels tested and also analyzed using numerical methods in LS-DYNA© were comprised of reinforcing steel and concrete and the layout and cross section is shown in Figure 136 and Figure 137 respectively.

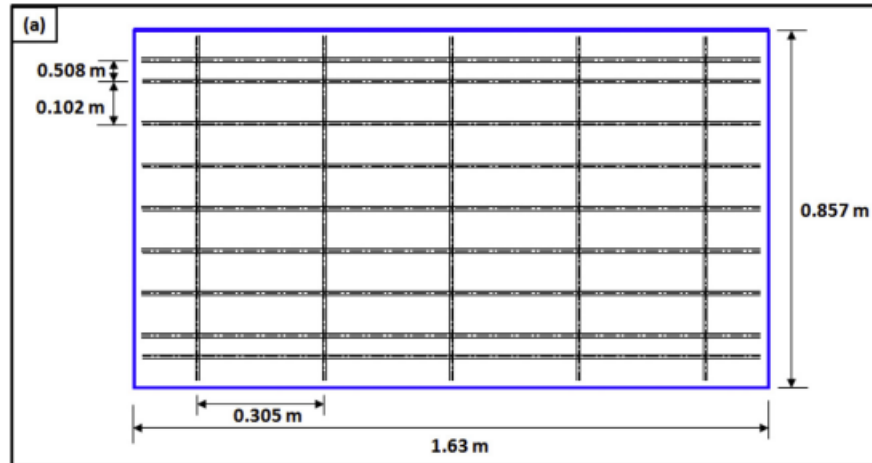


Figure 136 – Reinforcing steel layout in plan view<sup>[51]</sup>

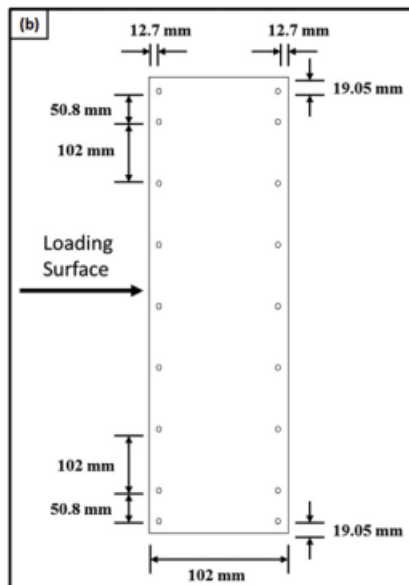


Figure 137 – Cross section of panel and loading direction<sup>[51]</sup>

The replicated panels in this study using ABAQUS were done so in U.S. units consisting of inch-lb. The boundary conditions in the FEA model were applied to best match the test setup and support apparatus and these boundary conditions are shown in Figure 138. The top and bottom surface are provided vertical (y-direction) support. There is a 6 inch (152.4 mm) out-of-plane support provided by the bearing surface on the back face and there is also a 3 inch bearing support on the load face as shown in Figure 138.

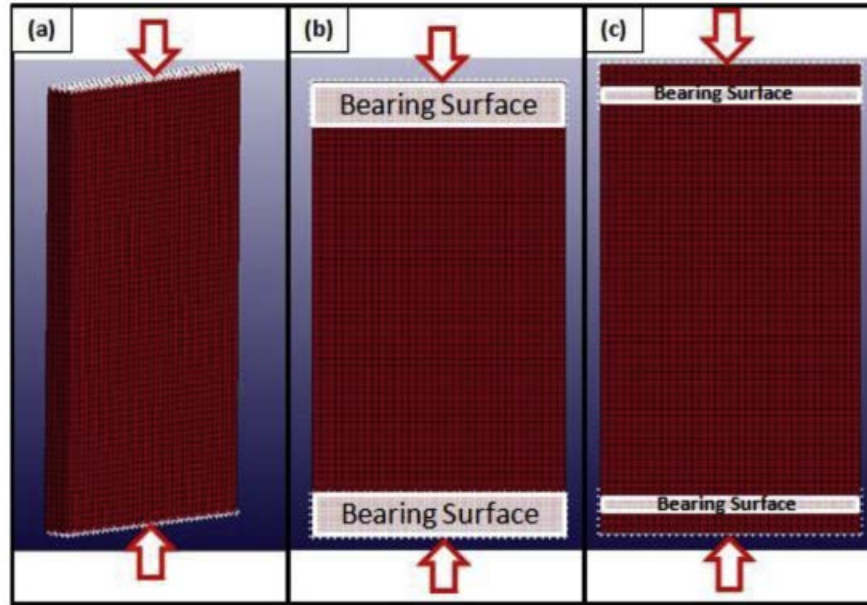
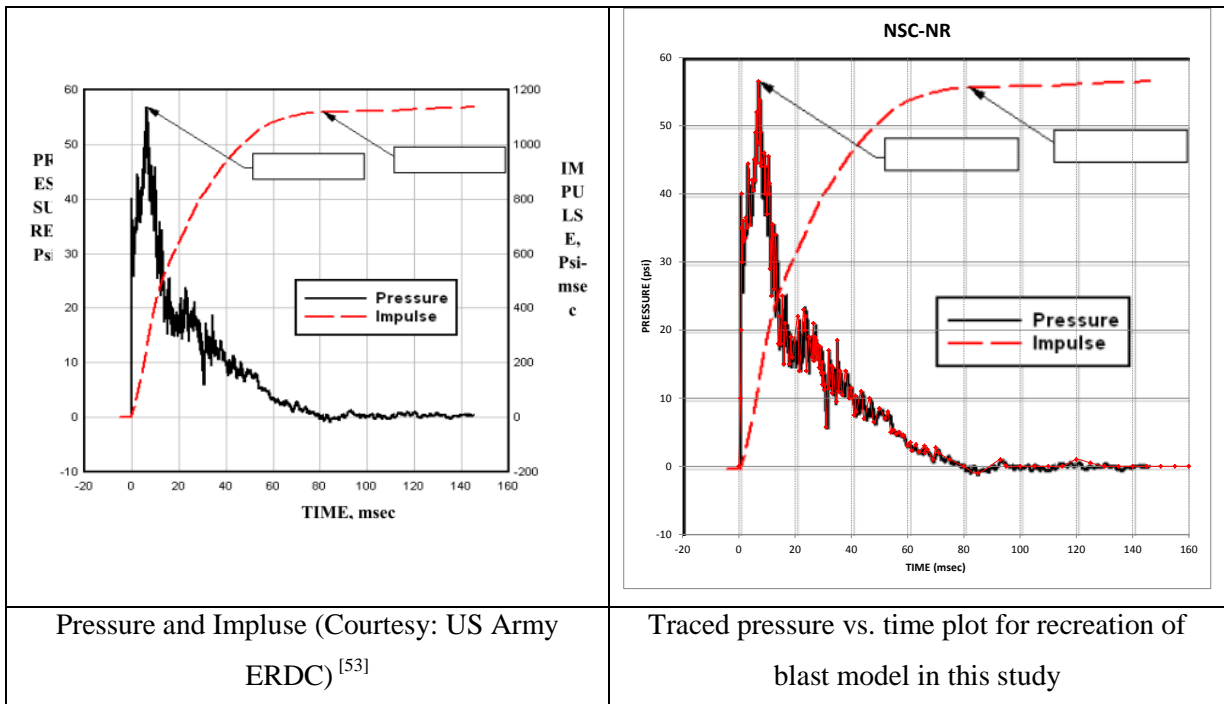


Figure 138 – Boundary conditions of FEA (a) vertical support, (b) back face, (c) pressure loading face<sup>[51]</sup>

The simulated blast pressure load was applied to the panels using a mechanical device owned and operated by the US Army ERDC. The blast pressure wave that was recreated or copied as shown in Figure 139 was the NSC-NR which is the “Normal Strength Concrete – Normal Rebar” model.



Pressure and Impulse (Courtesy: US Army ERDC)<sup>[53]</sup>

Traced pressure vs. time plot for recreation of blast model in this study

Figure 139 – Recreation of blast pressure vs. time plots

The pressure vs. time plot was traced using points in Excel and this was done visually. There is no way to recreate the exact test data used in the Thiagarajan et. al.<sup>[51]</sup>, therefore some variation is to be expected. An assumption was made in both studies in that the pressure distribution is applied to the face of the concrete panel uniformly, which during an actual blast event is not accurate.

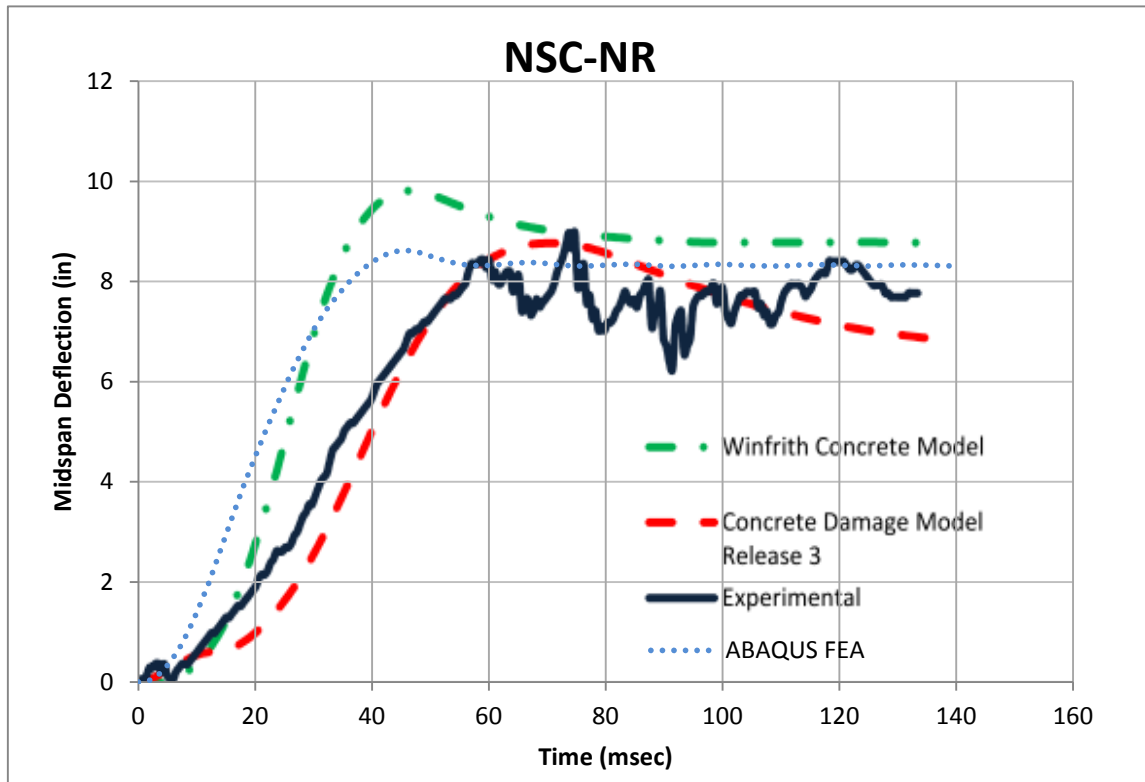


**Figure 140 – FEA comparisons with experimental**

The deflection versus time plot for the ABAQUS© FEA dynamic explicit solver using the Damaged Plasticity model compares well to that of the LS-DYNA© plots and the experimental data as can be seen in Figure 140. The experimental panel damage, the deflection and crack patterns are shown in Figure 141 for the research published by Thiagarajan et. al.<sup>[51]</sup>. The results from the analysis performed in ABAQUS© using the Damaged Plasticity model and the dynamic explicit solver are shown in Figure 142 and there is good comparison between the two. Historically, LS-DYNA© does an excellent job at solving dynamic explicit problems involving damage and loss of elements, however the ABAQUS© bodes well and can be used with confidence for similar studies.

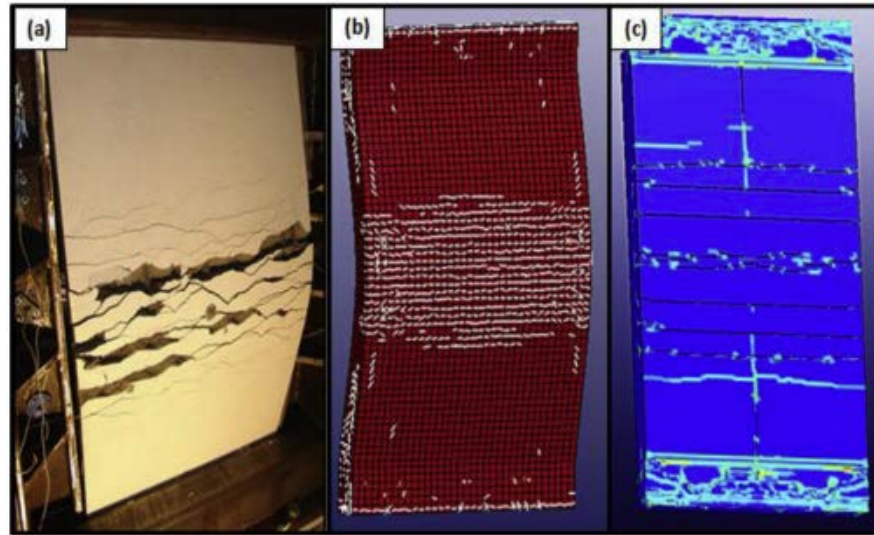


Figure 141 – Experimental and FEA results from Thiagarajan et. al.<sup>[51]</sup>

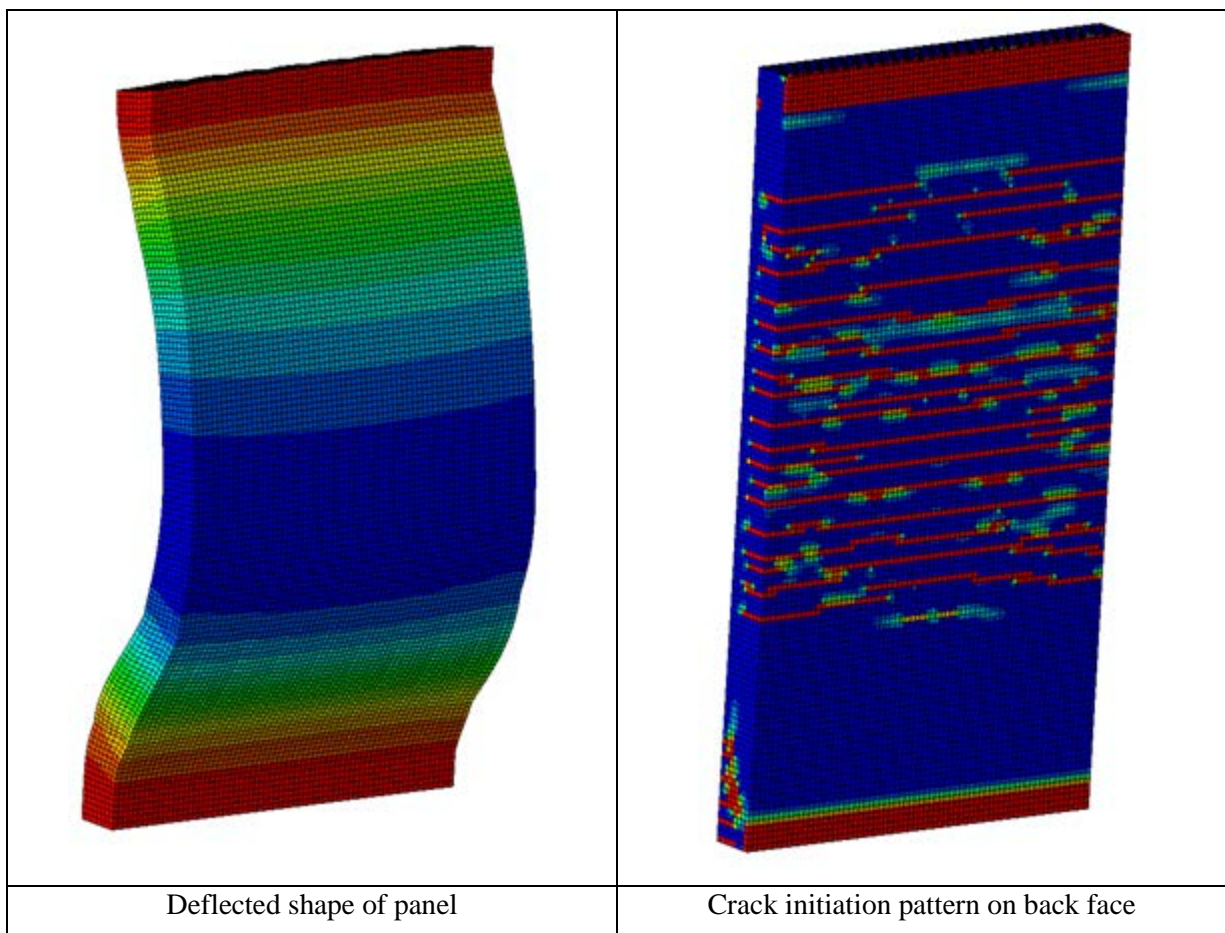


Figure 142 – ABAQUS FEA plots using Damaged Plasticity Model

### 6.3.2 FEA BLAST MODEL FOR FPCS PANEL

The solid reinforced 10" concrete panel shall be loaded with a blast pressure wave and then the same event will be applied to the 10" FPCS panel. The free body diagrams of the two panels are shown in Figure 143 and Figure 145 and the construction diagrams of the panels are shown in Figure 144 and Figure 146. The blast load is a 1 lbm, 2 lbm, 3 lbm and a 5 lbm of equivalent TNT and is placed at the reference point (RP-1) which has a standoff distance of 12 inches and is located at the midspan of the panel. The reference point is shown in Figure 147 along with the boundary conditions.

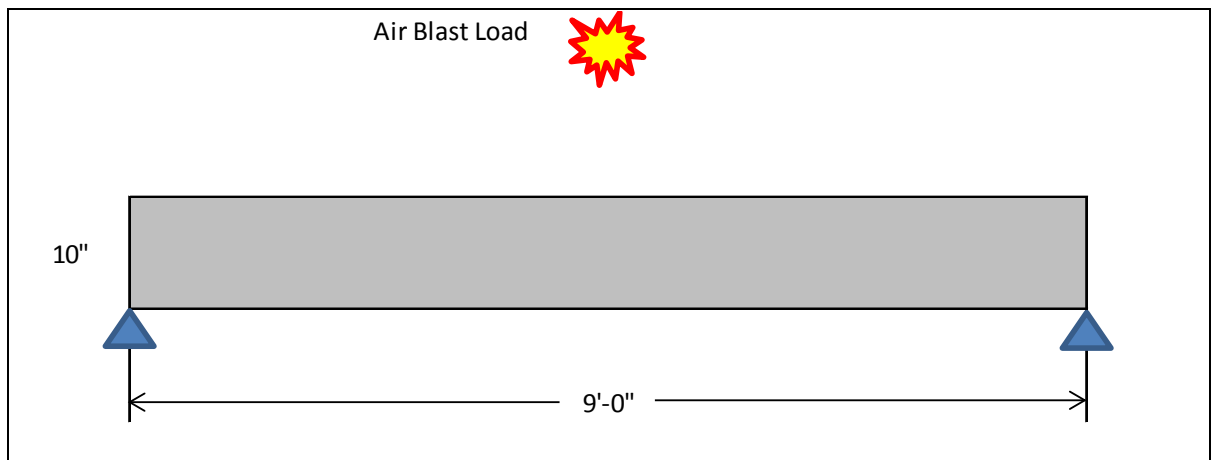


Figure 143 – Blast loading diagram for solid concrete panel

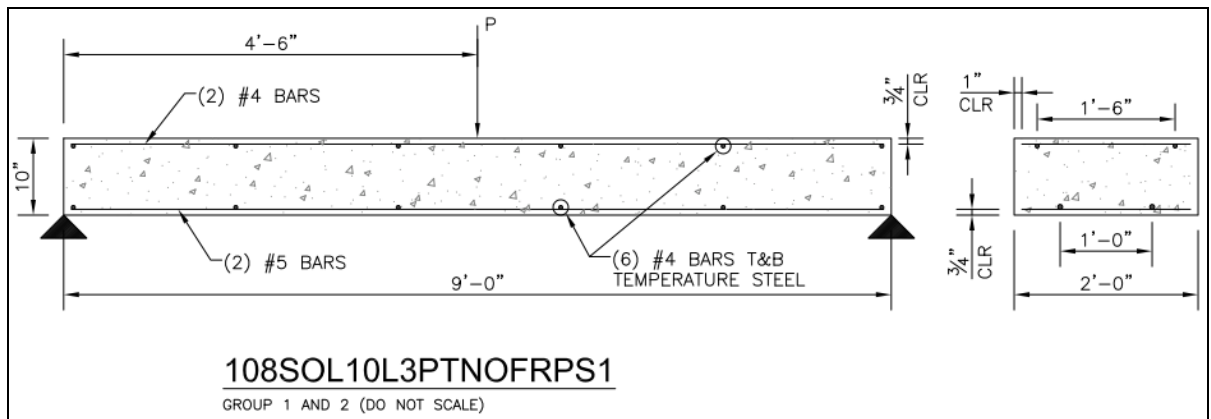


Figure 144 – Solid panel construction details

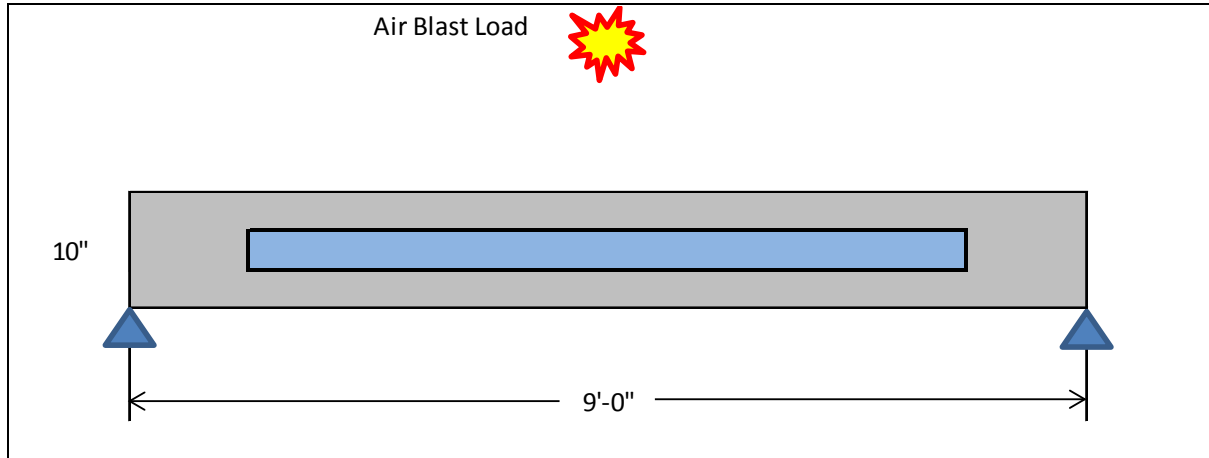


Figure 145 – Blast loading diagram for FPCS panel

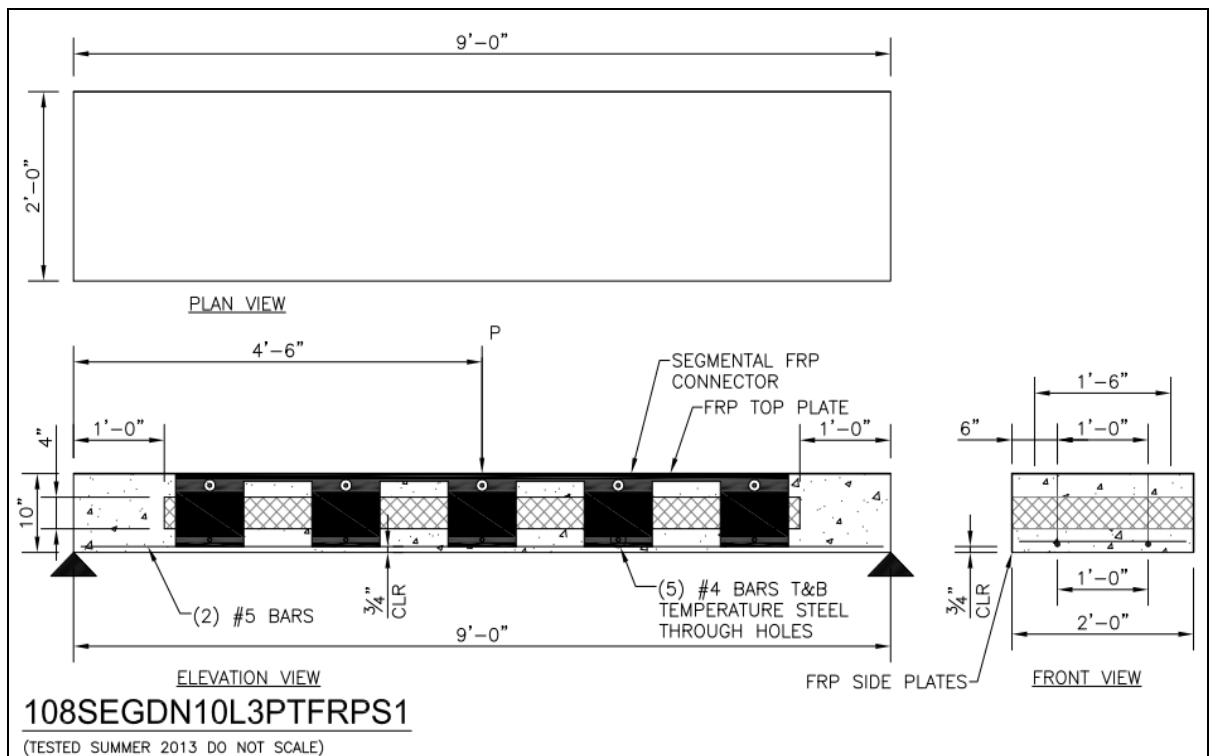
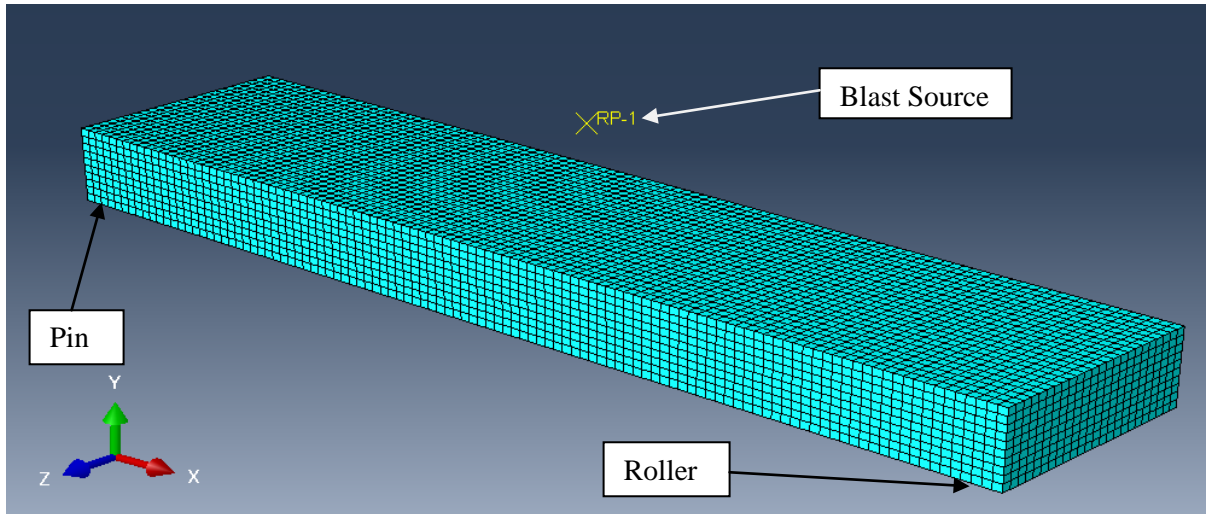


Figure 146 – Segmental FPCS panel construction details

The finite element analysis model is shown in Figure 147 and other than the blast loading; it is similar to previously modeled and analyzed solid concrete panels in this study. The blast source was located at mid-span, mid-panel, and 12 inches above the top of the panel surface.



**Figure 147 – Finite element analysis model of 10” solid panel 108SOL10L3PTNOFRPS1**

The model used C3DR continuum hexahedral elements with embedded stringers to represent the T3D2 truss elements for the reinforcing steel. To accurately apply the blast pressure wave to the surface of the concrete panels the CONWEP function in ABAQUS is used and the parameters for the 1 lbm TNT blast load is shown in Figure 148.

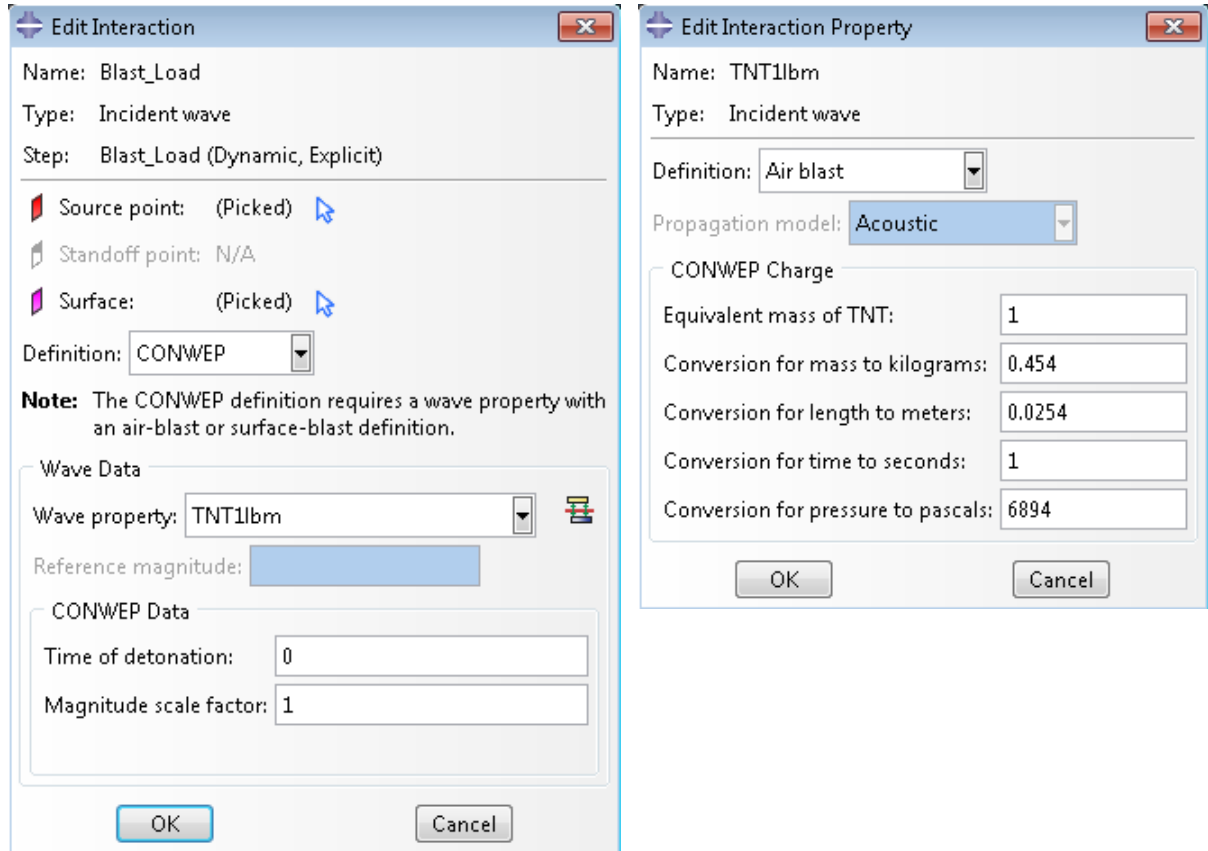


**Figure 148 – Blast interaction properties in Abaqus**

The analyses were executed for 50 ms which was a time where there no more observable oscillation in the solid concrete panel due to the blast loads. In order to quantify the failure of the panels from the blast load Compression Damage and Tension Damage can be plotted to determine the percent damage to the concrete material elements. The strain in the steel rebar could also be plotted to determine the plastic strain and deformation in the steel. Figure 149 shows plots for the (4) loading conditions for the solid concrete panel and as the blast load increase, so does the tension damage in the concrete.

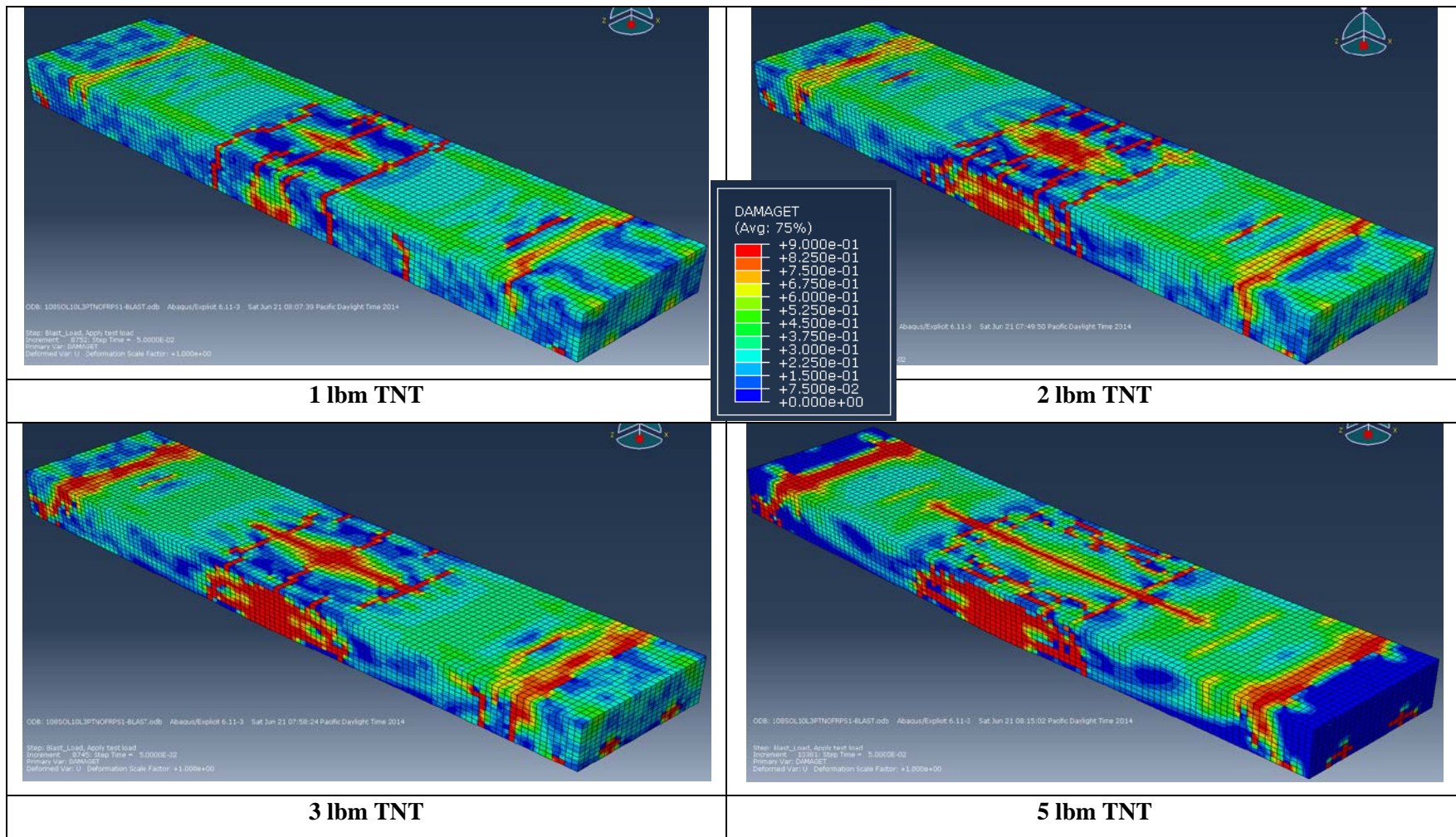
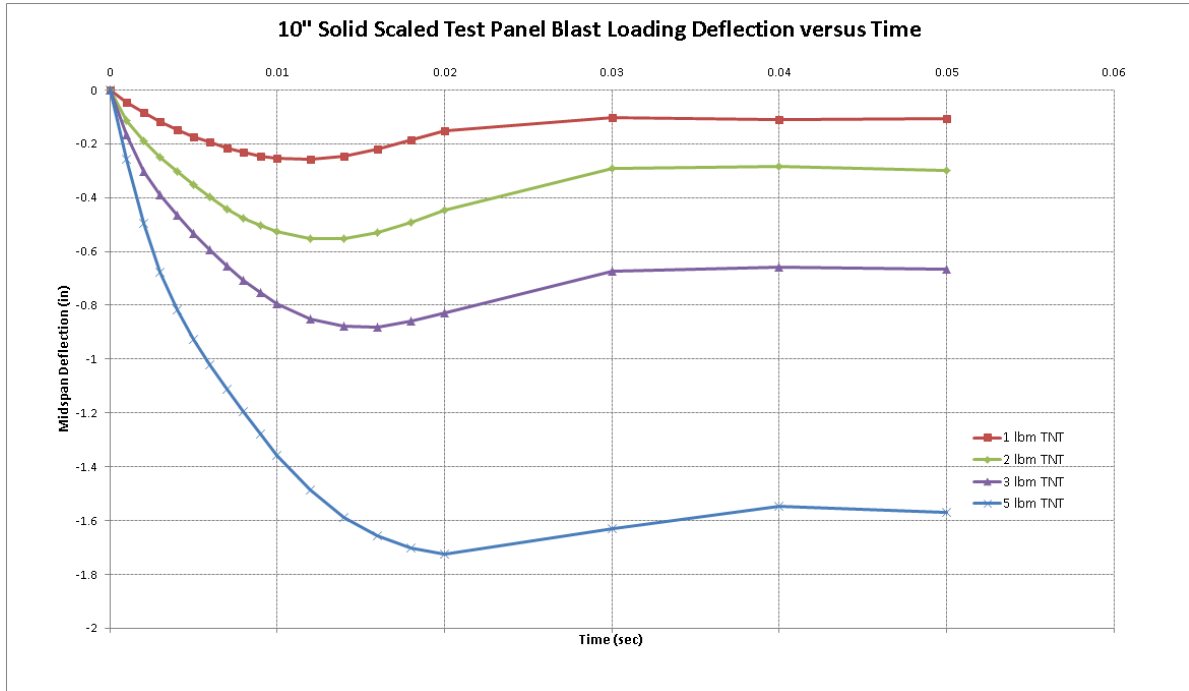


Figure 149 – 10” Solid panel blast loading tension damage



**Figure 150 – Deflection versus time for 10” solid concrete panel under blast loading**

The plotted curves in Figure 150 show the four blast models and midspan deflection responses for the 10” solid concrete panels. The panel that deflected the most had the 5 lbm TNT blast load applied to it and likewise the panel that deflected the least had the 1 lbm TNT blast load or the least load applied. The maximum midspan deflection of the 5 lbm TNT blast load was approximately 1.7 inches. No panels fully regained zero deflection after 50 milliseconds.

Likewise the FPCS sandwich panel was loaded in similar fashion to the 10” solid concrete panel and the tension damage plots for the 1 lbm, 2 lbm, 3 lbm and 5 lbm TNT blast loads are shown in Figure 151.

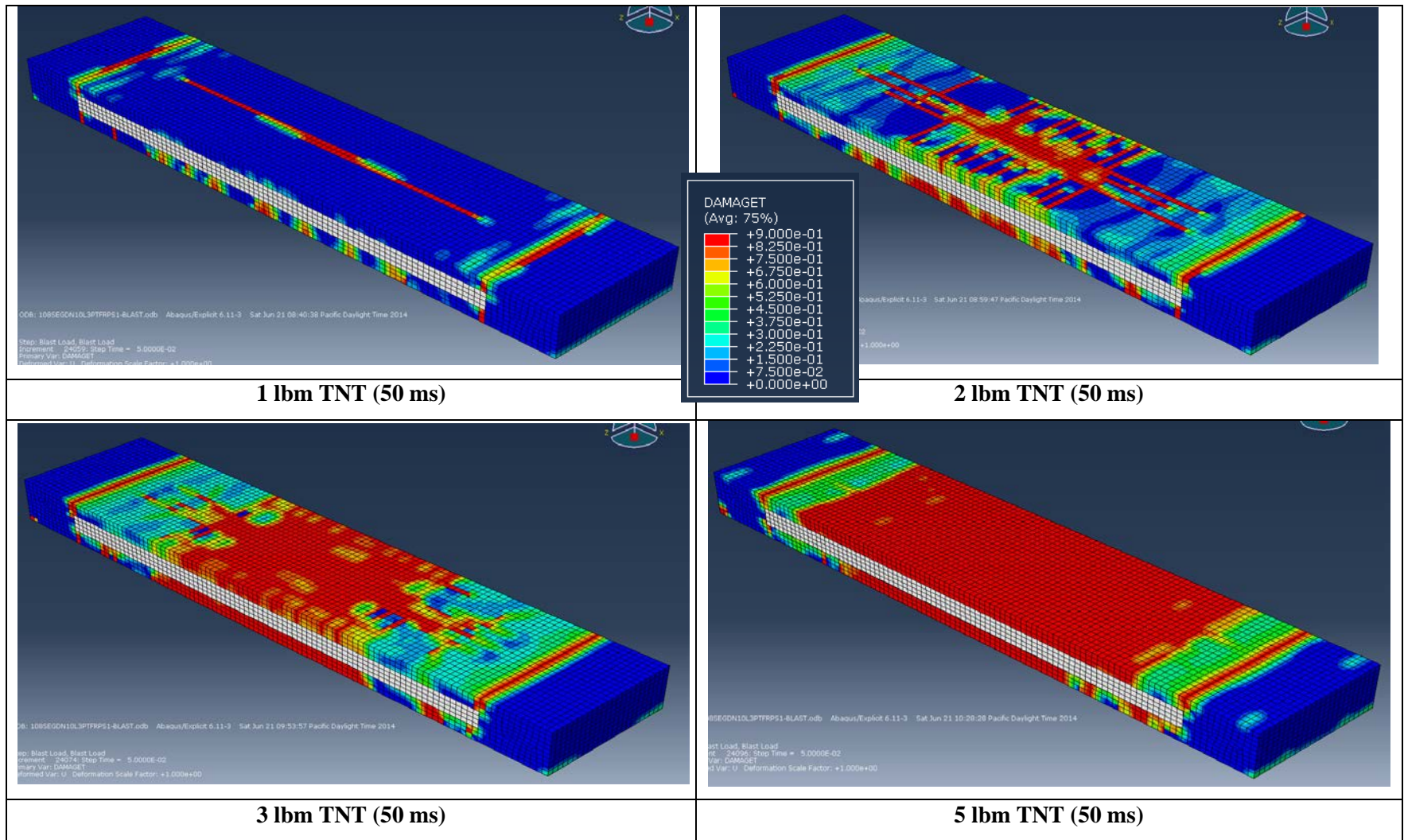
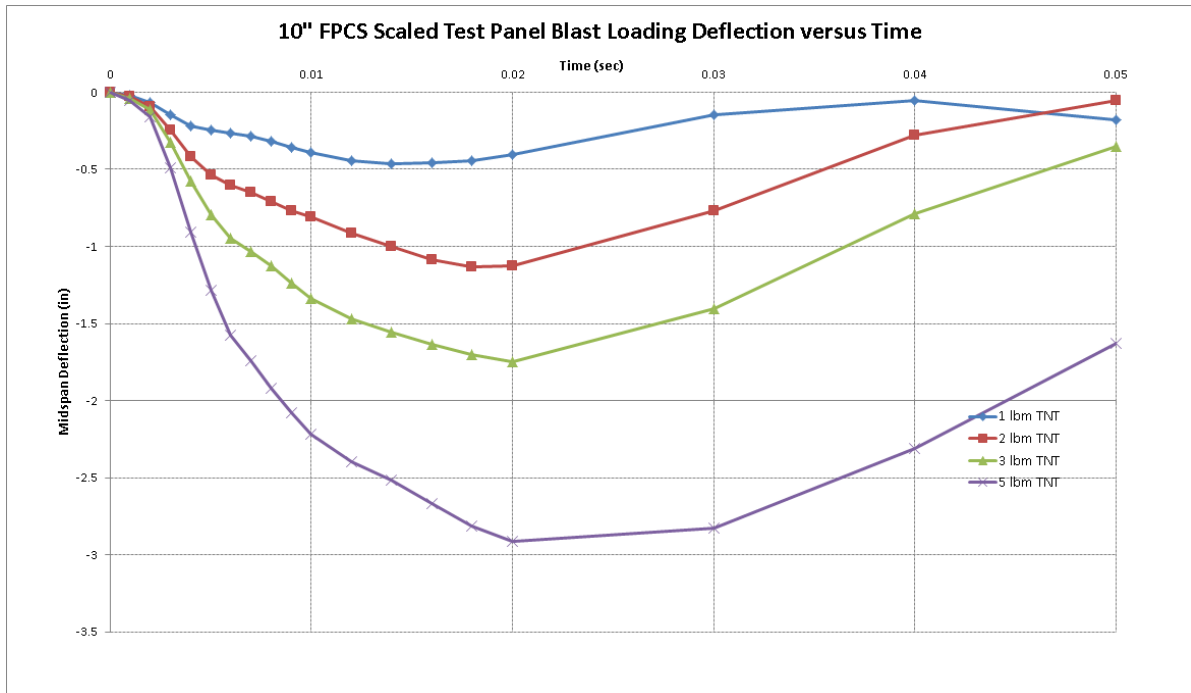


Figure 151 - 10" FPCS panel blast loading tension damage



**Figure 152 - Deflection versus time for 10” FPCS panel under blast loading**

The deflection versus time plot for the 1 lbm, 2lbm, 3lbm and 5 lbm TNT applied as a blast load to the 10” FPCS panel is shown in Figure 152. It’s interesting to note that the panel rebounds much more discretely than the solid concrete panel which tended to dampen once it was deflected. This could be attributed to the fact that the FPCS panel is approximately 40% lighter or has approximately 40% less mass due to the insulation and the connections of the FRP shear connectors. The ABAQUS Damaged Plasticity model is an excellent numerical analysis model to use in capturing the reversing loading or rebounding of the panel. To be consistent with the solid 10” concrete panel the time duration of the blast pressure waves was 50 milliseconds and it can be observed that the loading event does quite dampen out at that time for the FPCS panel.

## 6.4 BLAST ANALYSIS CONCLUSION

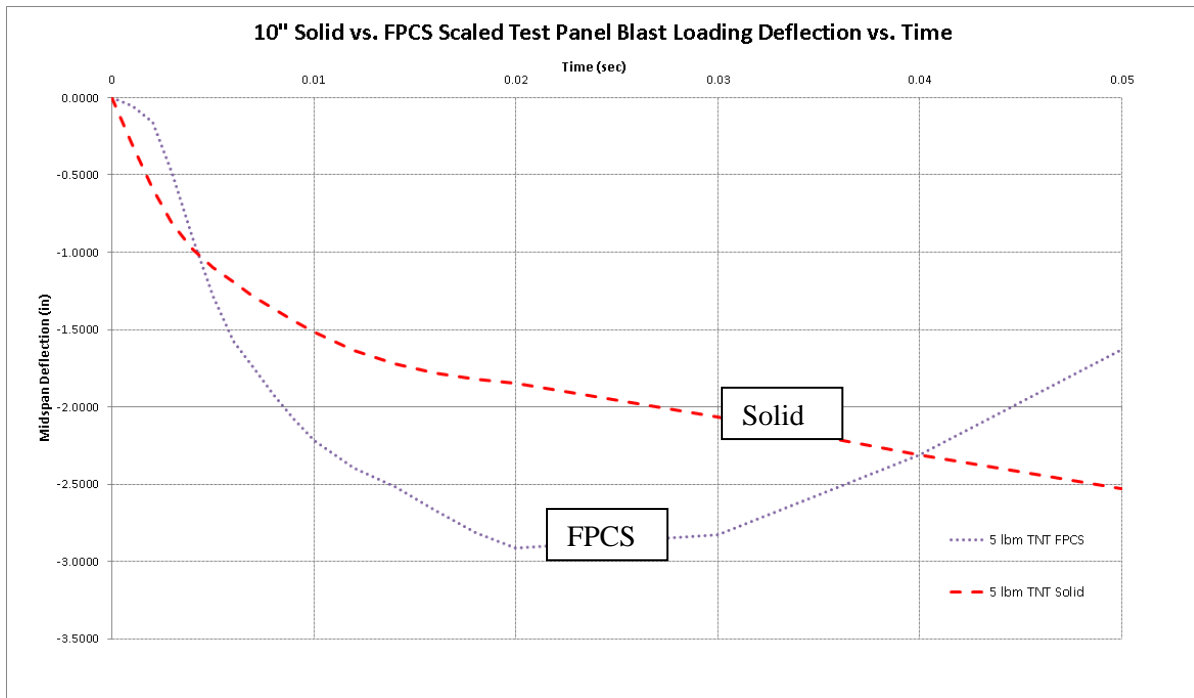


**Figure 153 – Deflection versus time for 10” FPCS panel and 10” solid panel under blast loading**

The comparison of the 5 lbm TNT blast loading for the 10” FPCS and 10” solid concrete panel is shown in Figure 153. The sandwich panel with the confined FRP has a max midspan deflection of approximately 3 inch while the solid concrete panel has a maximum deflection of about 2.5 inches. Although both have high deformations, the FPCS panel appears to have some elastic rebound characteristics and more so, compares well with the solid panel, which is a preferred construction material for blast resistant structures.

Another study was conducted and a comparison between the sandwich panel with no exterior side and top FRP plates to that of the solid reinforced concrete panel. The sandwich panel analyzed under blast load is shown in Figure 154 and the concrete panel was the same 10 inch reinforced concrete panel, however the supports were changed to 8’-0” to match that of the sandwich panel.

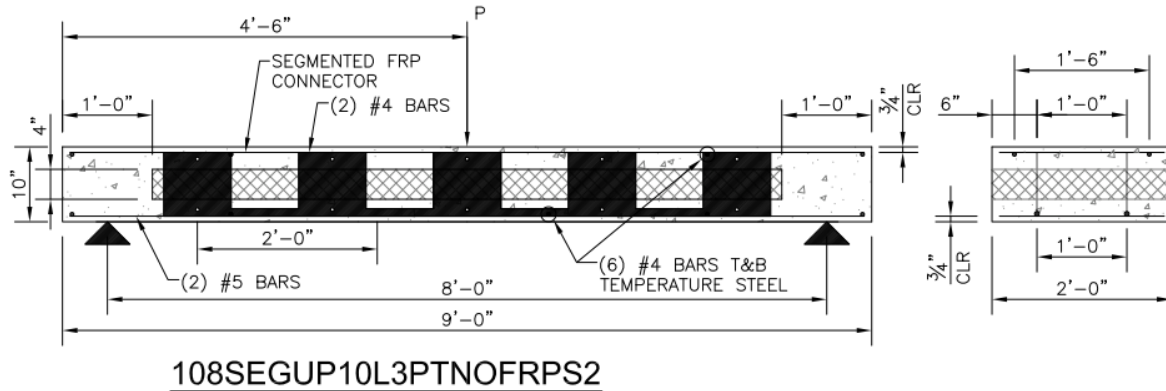


**Figure 154 – Blast load sandwich panel 108SEGUP10L3PTNOFRPS2**

The results are shown in Figure 155 and once again the concrete panel has permanent deformation at around 1.75 inches, whereas the sandwich panel, no exterior FRP plates, has a much larger and permanent deflection of around 5 inches.

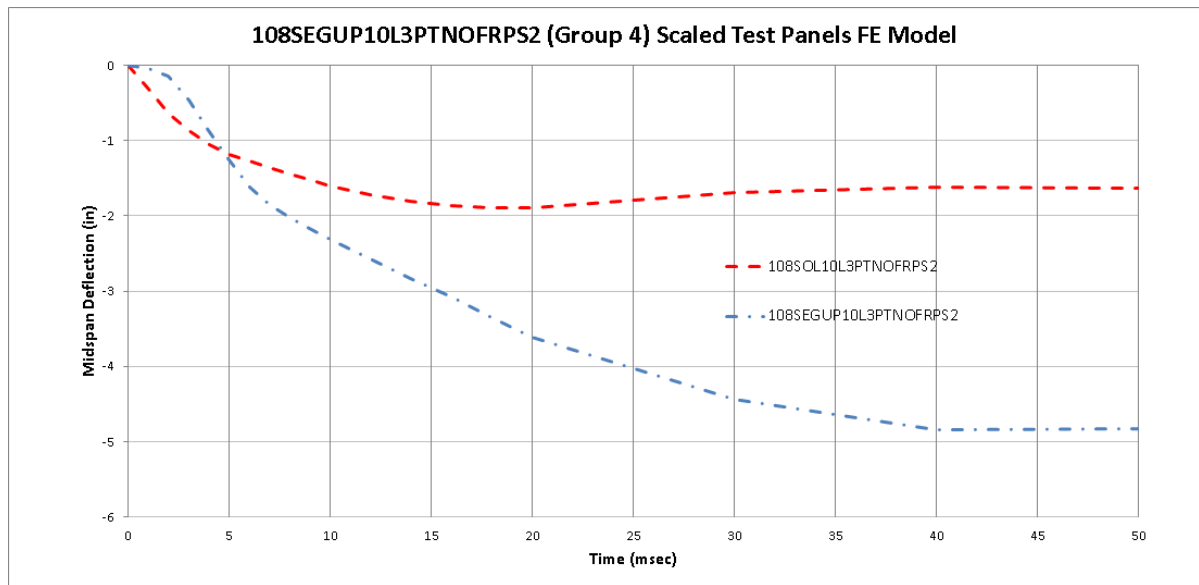


**Figure 155 – Deflection vs. time for 10” sandwich panel and 10” solid panel under blast loading**

When the comparison is made between the results in Figure 155 and Figure 153 it is clear that the FPCS panel performs much better than the plain sandwich panel and is a much better candidate for use as a building material in blast resistant construction.

## **CHAPTER 7: APPLICATION OF FRP-PRECAST CONCRETE SANDWICH ROOF PANELS**

Provided here are three brief application examples where the panels presented in this research study could have immediate and beneficial impacts to the construction sector. This is not meant to be a thorough market analysis study, but rather a brief overview on the advantages of precast sandwich panel construction and how it can be readily applied to construction markets that would have such a need for it.

### **7.1 RESIDENTIAL**

Precast concrete and cast-in-place residential construction is a growing trend in the United States. Building codes require more energy efficiency and more durability against damages due to coastal storms and inland tornadoes. Major coastal storms in the United States have become more frequent as was the case of Hurricane Katrina (2005, \$108B damage) and the 100 year storm Hurricane Sandy (2012, \$68B damage), both of which had devastating results with respect to life and property. Utilizing more durable construction such as concrete, masonry and precast concrete allows for lower life-cycle costs, reduction in losses and better insurance premiums. This was shown to be true with the Sunberg reinforced concrete home shown in Figure 156, which was a lone structural survivor of Hurricane Katrina in a particular coastal neighborhood. All other homes around this particular home were built of standard timber residential construction.



**Figure 156 – Sunberg house, Pass Christian, Mississippi (Hurricane Katrina)**

Although wood is an appropriate and sustainable building material for residential construction, it does not perform as well along coastal regions and is inferior to hurricane and tornado type wind

forces. Precast concrete sandwich panels provide the required insulation, strength and durability and with proper connections and membranes can be an exceptional residential building material. Furthermore, with precast construction, the need for formwork and pump trucks is eliminated as would be necessary for cast-in-place construction.

## **7.2 INDUSTRIAL & COMMERCIAL**

Insulated precast wall panel and roof double tee precast insulated panel construction is a readily used building construction type for storage warehouses and wide open facilities. Typically the walls have a concrete outer and inner wythe, of which the inner wythe is considered structural and the outer wythe considered architectural. In normal construction cases, the walls are the precast sandwich panels and the roof members are either double tee sections, hollow core sections, trusses or some other form of roof structure. If the open spans can be minimized to approximately 20 feet, insulated precast sandwich panels could be used for both the walls and the roof structure. This would provide a faster construction system and allow for more floor-to-ceiling height.

Likewise industrial plants could benefit from the durable construction and insulation value of the precast sandwich panel wall and roof system and the system could potentially provide protection against accidental chemical blast explosion. Preliminary FEA models should good results with the FPCS panels being used as blast resistant structures; however this should be further tested and developed.

## **7.3 MILITARY**

Government buildings require, generally, higher design criteria for seismic, wind and ballistic events. Most military buildings are design per the Unified Facilities Criteria (UFC) documents for structural loading, accidental explosions and progressive collapse. Many times buildings are designed with strong concrete or masonry walls; however the roof structures use steel or wood trusses which then have to be reinforced. Furthermore, due to budget constraints, the roof cavities are not always insulated and mechanical systems are a luxury.

The FPCS panels can provide the strength, durability and energy efficiency to military buildings both domestic and abroad and may have good capabilities to provided desired blast resistance.

## CHAPTER 8: CONCLUSIONS AND RECOMMENDATIONS

Preliminary testing of a typical precast concrete wall sandwich panel at the Central Pre-Mix Prestress Co. Spokane, WA plant showed adequate strength for out-of-plane flexural loading, although the panel was originally designed as a vertical building element. The shear connectors in that panel were proprietary and other than the test results and preliminary development of finite element analysis models, no further research was performed. From that point forward new panels were developed and tested at the University of Idaho consisting of various types and configurations of FRP shear connectors as documented in a previous study by Tom Norris<sup>[44]</sup>. This research study concludes on the non-linear finite element analysis of these panels and offers recommendations into the future development of the panels for both conventional construction and possibly blast resistant structures.

### 8.1 ABBREVIATED SUMMARY

1. These FRP precast concrete sandwich panels are built from readily available materials using standard and existing construction practices.
2. The panels have been tested with different configurations of shear connectors and exterior FRP plates and have produced up to 90% of the strength of a same-sized solid reinforced concrete panel with 40% less weight.
3. Panels using a segmental or continuous FRP shear connector provided the highest strength and stiffness.
4. In order to analyze the panels using a finite element analysis program, it's recommended to do a nonlinear explicit analysis as the failure mechanisms of the concrete cracking is a quasi-static phenomenon and a linear static analysis model does not fully capture this.
5. The panels with the fully enclosed FRP plate system (FPCS) performed better under creep loading than did the standard precast sandwich panel.
6. The FPCS panels based on numerical analysis only, performed well under blast loading when compared to the same load on a solid reinforced concrete slab.

## 8.2 DETAILED SUMMARY

These FRP precast concrete sandwich panels used readily available materials and solid FRP shear connectors were cut from standard rolls to determine the best application for their use in developing the highest degree of composite action and flexural strength possible. It was determined that panels with a segmental or continuous FRP shear connector provide the highest DCA with the most comparable strength to that of a solid reinforced concrete slab. The benefit being that the sandwich panel has 40% less weight and added thermal insulation value.

Testing these panels is time consuming and costly, therefore other means of predicting strength, deflection and failure is desired in lieu of testing. Analytical calculations are difficult to perform for such panels due to the number of constituent materials in the panel such as the insulation, reinforcing steel, concrete, and FRP shear connectors. The panels do exhibit a linear elastic response to a certain point then quickly begin showing non-linear interaction as the bond between the insulation and concrete breaks, the concrete begins to crack and the FRP shear connectors begin to engage. Such a nonlinear problem is best solved with a finite element analysis numerical approach. The difficulty however in using finite element analysis is the quickest solution model consists of a static analysis model with non-linear geometry and non-linear material properties. These numerical solutions have difficulty in solving the complex non-linear response and diverge once the panel gets just beyond the linear elastic response. Therefore a new approach was used in this research study in using a dynamic explicit analysis which captures the quasi-static response of the panel once the concrete begins to crack and the insulation no longer contributes to any flexural strength. This quasi-static analysis captures the full loading response of the sandwich panel to ultimate failure. Since the approach is dynamic, the FEA results display a lot of variation in the loading and response during the early stages of loading. If one to superimpose the non-linear static analysis model with that of the quasi-static dynamic analysis model, the curve will be more smooth and show good correlation to the test results.

These panels are intended to be in the horizontal application and therefore long term creep effects are desired for design understanding. Four panels were tested for approximately 180 with static loads and creep results were extracted from the data. The panels provided good creep test data, but there still are a lot of variables to account for in their future development. For example the panels were outside, day and night and subjected to an arid climate during summer. The panels were also

subjected to temperature variations and finally they were left in unsecured locations where the test gages were either tampered with by pedestrians or from wind.

Finally, this research study showed that based on FEA only these FPCS panels are capable of blast resistance and perform better than comparable solid reinforced concrete slabs. These quick analyses show promise that they could be used for buildings that require protection for terrorist or accidental blast events while providing the desired insulation and environmental protection needed. This study could even be extrapolated that the FPCS panels would be good candidates for building construction along coastal regions susceptible to hurricanes.

Future research for these types of panels should include controlled environment and controlled variable creep testing. This will provide a better understanding of the creep strength of the concrete, shear connectors and rebar and insulation while eliminating shrinkage and thermal creep. Those can also be checked later. The panels should be tested for wind loading or cyclic loading to show strength for long term building application effects. Blast testing of the panels would also be warranted and beneficial if the panels were to be used for protection to accidental and terrorist blast loading events. The groundwork presented here for the finite element analysis approach using a quasi-static model should be continued and methods to capture more accurate results and smoother curves should be investigated further. Finally a better understanding of the microscopic interaction of the shear connectors and the concrete is desired as the FEA models assume the shear connectors are fully tied to the concrete where physically that is not entirely the case. Locking in the shear connectors to the concrete with transverse reinforcing steel certainly justifies this assumption; however more will need to be understood about this bond so that the panels can be further developed.

## REFERENCES

1. Abaqus, Inc., ABAQUS User Manual, V6.11-1, 2011
2. ACI Committee 209, 2008. *Prediction of Creep, Shrinkage and Temperature Effects in Concrete Structures* (ACI 209R-92). Farmington Hills, MI: American Concrete Institute (ACI).
3. ACI Committee 209, 2008. *Guide for Modeling and Calculating Shrinkage and Creep in Hardened Concrete*. (ACI 209.2R-08). Farmington Hills, MI: American Concrete Institute (ACI).
4. ACI Committee 318, 2011. *Building Code Requirements for Structural Concrete* (ACI 318-11) and *Commentary* (ACI 318R-11). Farmington Hills, MI: American Concrete Institute (ACI).
5. ACI Committee 533R, 2011. *Guide for Precast Concrete Wall Panels* (ACI 533R-11). Farmington Hills, MI: American Concrete Institute (ACI).
6. Agnew, E., Marjanishvili, S., & Gallant, S. (2007, January). "Concrete Detailing for Blast." *Structure Magazine*, pp. 26-28
7. Al Chami, G., M. Theriault and K.W. Neale. "Creep Behavior of CFRP-strengthened reinforced concrete beams." *Construction and Building Materials*. 23 (2009): 1640-1652. Print.
8. Al-Salloum, Yousef A. and Tarek H. Almusallam. "Creep effect on the behavior of concrete beams reinforced with GFRP bars subjected to different environments." *Construction and Building Materials*. 21. (2007): 1510-1519. Print.
9. ASCE Task Committee on Blast-Resistant Design of the Petrochemical Committee of the Energy Division of the American Society of Civil Engineers. "Design of Blast-Resistant Buildings in Petrochemical Facilities", 2<sup>nd</sup> Edition. (2010), ASCE.
10. ASCE Task Committee. "Structural Design for Physical Security, State of the Practice". (1999), ASCE/SEI.
11. Bazant, Z. P., Yu, Q. and Li, G.-H., "Excessive Long-Time Deflections of Prestressed Box Girders: I. Record-Span Bridge in Palau and Other Paradigms," *Journal of Structural Engineering*, ASCE, V. 138, No. 6, 2012, pp. 676-686.
12. Bazant, Z. P., Yu, Q. and Li, G.-H., "Excessive Long-Time Deflections of Prestressed Box Girders: II. Numerical Analysis and Lessons Learned," *Journal of Structural Engineering*, ASCE, V. 138, No. 6, 2012, pp. 687-696.
13. Bazant, Z. P., Yu, Q. and Wendner, R., "Improved Algorithm for Efficient and Realistic Creep Analysis of Large Creep-Sensitive Concrete Structures," *ACI Structural Journal*, V. 109, No. 5, September-October 2012, pp. 665-675.

14. Benayoune, A., Abdul Samad, A.A., Trikha, D.N., Abang Ali, A.A., & Ellinna, S.H.M. "Flexural behavior of pre-cast concrete sandwich composite panel-Experimental and theoretical investigations." 2007, *Construction and Building Materials*, Volume 22 (2008) pp. 580-592.
15. Bush, T.D. and Wu, Z., 1998. Flexural Analysis of Prestressed Concrete Sandwich Panels with Truss Connectors, *PCI Journal*, (September-October): pp. 76-86
16. Bush, T.D. and Stine, G., 1994. Flexural Behavior of Composite Precast Sandwich Panels with Continuous Truss, *PCI Journal*, V. 39, No. 2, (March-April): pp. 112-121.
17. Chipley, M., Kaminskas, M., etal. (2003) "Risk Management Series, Reference Manual to Mitigate Potential Terrorist Attacks Against Buildings." FEMA 426.
18. Conventional Weapons Effects ("ConWep", 1991), is a computer program, based on the content of technical manual TM 5-855-1 (1986). Fundamentals of protective design for conventional weapons, Structural Laboratory, Waterways, Experimental Station, for the Department of the Army, US Army Corps of Engineers.
19. Crisfield, M.A., "Snap-Through and Snap-Back Response in Concrete Structures and the Dangers of Under-Integration," *International Journal for Numerical Methods in Engineering*, vol. 22, pp. 751-767, 1986.
20. Davalos, J.F., Qiao, P., Xu, X.F., Robinson, J. and Barth, K.E., 2001. Modeling and characterization of fiber-reinforced plastic honeycomb sandwich panels for highway bridge applications. *Composite Structures*, V. 52: pp. 441-452.
21. Frankl, B.A., Lucier, G. W., Hassan, T.K. and Rizkalla, S.H., 2011. Behavior of Precast Prestressed Concrete Sandwich Panels Reinforced with CFRP Shear Grid, *PCI Journal*, (July-August): pp. 42-54.
22. Gilbert, R.I. and Ranzi G., 2011, *Time-Dependent Behaviour of Concrete Structures*, Spon Press.
23. Gilbert, R.I. and Warner, R. F., 1978, Tension Stiffening in Reinforced Concrete Slabs, *Journal of the Structural Division, American Society of Civil Engineers*, Vol. 104, ST12: pp. 1885-1900.
24. Henin, E., Morcous, G. and Tadros, M.K., "Precast concrete sandwich panels for floor and roof applications." 2011. *PCI Structural Journal*.
25. Hillerborg, A., M. Modeer, and P.E. Petersson, "Analysis of Crack Formation and Crack Growth in Concrete by Means of Fracture Mechanics and Finite Elements," *Cement and Concrete Research*, vol. 6, pp. 773-782, 1976.
26. Hinman, E. (2003), "Primer for Design of Commercial Buildings to Mitigate Terrorist Attacks." FEMA 427.
27. Hopkins, P.M. & Brown, K.M., "Modeling and Testing of Full-size Carboncast Wall Panel." SEA NW Conference Presentation, September 2011.

28. Hsu, L.S., & Hsu, C.-T.T. (1994) "Complete stress-strain behavior of high-strength concrete under compression." *Magazine of Concrete Research*, 46(169), 301-312
29. Jefferson AD. "Finite element analysis of concrete structures", PhD Thesis, University of Wales, Cardiff, UK, 1998.
30. Kingery, C.N. and Bulmash, G. "Airblast Parameters from TNT Spherical Air Burst and Hemispherical Surface Burst;" Technical Report ARBRL-TR-02555, U.S. Army ARDC-BRL, Aberdeen Proving Ground, MD, April 1984.
31. Kinney, G.F., Graham, K.J. (1985) "Explosive Shocks in Air", Springer, Berlin.
32. Kupfer, H.B., and K.H. Gerstle, "Behavior of Concrete Under Biaxial Stresses," *Journal of Engineering Mechanics Division*, ASCE, vol. 99 853, 1973.
33. Lee, J., and G.L. Fenves, "Plastic-Damage Model for Cyclic Loading of Concrete Structures," *Journal of Engineering Mechanics*, vol. 124, no. 8, pp. 892-900, 1998.
34. Lee, B., and S. Pessiki, 2007. Design and Analysis of Precast, Prestressed Concrete Three-Wythe Sandwich Wall Panels. *PCI Journal*, V. 52, No. 4 (July-August): pp. 70-83.
35. Lee, B., and S. Pessiki, 2008. Experimental Evaluation of Precast, Prestressed Concrete Three-Wythe Sandwich Wall Panels. *PCI Journal*, V. 53, No. 2 (March-April): pp. 95-115.
36. Lee, B. and S. Pessicki, 2008. Revised Zone Method R-Value Calculation for Precast Concrete Sandwich Panels Containing Metal Wire Connectors. *PCI Journal*, V. 53, No. 5 (September-October): pp. 86-100.
37. Lowes, L. (1995). "Finite element modeling of reinforced concrete beam-column bridge connections." A dissertation submitted to the office of graduate studies of University of California, Berkeley, CA.
38. Lubliner, J., J. Oliver, S. Oller, and E. Onate, "A Plastic-Damage Model for Concrete," *International Journal of Solids and Structures*, vol. 25, pp. 299-329, 1989.
39. Mander, J.B., Priestley, M.J.N., and Park, R. (1988). "Theoretical stress-strain model for confined concrete." *Journal of Structural Engineering*, 114(8), 1804-1826.
40. McCann, D.M., & Smith, S.J. (2007, April). "Blast Resistant Design of Reinforced Concrete Structures." *Structure Magazine*, pp. 22-26
41. McNeely, D.J. and Lash, S.D., (1963). "Tensile Strength of Concrete," *Journal of the American Concrete Institute, Proceedings*. Vol. 60, No. 6, June 1963, pp. 751-761.
42. Menegotto, M., and Pinto, P.E. (1973). "Method of analysis for cyclically loaded reinforced concrete plane frames including changes in geometry and non-elastic behavior of elements under combined normal force and bending." *IABSE Symposium on the Resistance and Ultimate Deformability of Structures Acted on by Well-Defined Repeated Loads*, Lisbon, Portugal, 15-22.

43. Nayal, R., & Rasheed, H.A. (2006). "Tension stiffening model for concrete beams reinforced with steel and FRP bars." *Journal of Materials in Civil Engineering*, 18(6), 831-841.
44. Norris, T.G. (2014). "Bending Behavior of Insulated FRP-Confined Concrete Sandwich Panels with FRP Plate Shear Connectors." A thesis submitted to the office of graduate studies of the University of Idaho, Moscow, ID.
45. PCI Committee on Precast Sandwich Wall Panels. 2011. State-of-the-Art of Precast/Prestressed Sandwich Wall Panels. *PCI Journal*, V. 60, No. 2 (March-April): pp. 131-176.
46. PCI Committee on Precast Sandwich Wall Panels. 1997. State-of-the-Art of Precast/Prestressed Sandwich Wall Panels. *PCI Journal*, V. 42, No. 2 (March-April): pp. 92-134.
47. Pessiki, S., and A. Mlynarczyk, 2003. Experimental Evaluation of Composite Behavior of Precast Concrete Sandwich Wall Panels. *PCI Journal*, V. 48, No. 2 (March-April): pp. 54-71.
48. Raphael, J.M., 1984. Tensile Strength of Concrete. *ACI Journal, Proceedings*, Vol. 81, No. 2, March-April, pp. 158-165
49. Salmon, D., Einea, A., Tadros, M. and Culp, T., 1997. Full-Scale Testing of Precast Concrete Sandwich Panels. *ACI Structural Journal*, V. 96 No. 4, (July-August): pp. 354-362.
50. Shastri, A.S., 2010 "Computational Modeling of Conventionally Reinforced Concrete Coupling Beams", A thesis submitted to the office of graduate studies of Texas A&M University.
51. Thiagarajan, G., Kadambi, A. V., Robert, S., and Johnson, C.F., 2015. "Experimental and finite element analysis of doubly reinforced concrete slabs subjected to blast loads.", *International Journal of Impact Engineering*. V. 75, pp. 162-173.
52. U.S. Army Corps of Engineers (1990) TM 5-1300, "Structures to Resist the Effects of Accidental Explosions", U.S. Army Corps of Engineers, Washington, D.D. (also Navy NAVFAC P-397 or Air Force AFR 88-22).
53. Vasudevan, A.K., 2013. "Finite Element Analysis and Experimental Comparison of Doubly Reinforced Concrete Slabs Subjected to Blast Loads.", A thesis submitted to the Faculty of The University of Missouri-Kansas City in partial fulfillment of the requirements for the degree of Master of Science. University of Missouri-Kansas City.
54. Wahalathantri, B.L., Thambiratnam, D.P., Chan, T.H.T. & Fawzia, S. (2011). "A material model for flexural crack simulations in reinforced concrete elements using abaqus." *Proceedings of the First International Conference on Engineering, Designing and Developing the Built Environment for Sustainable Wellbeing*. pp. 260-264.
55. Wight, J.K. and MacGregro, J.G., 2012. "Reinforced Concrete Mechanics & Design, 6<sup>th</sup> Edition." Pearson Education, Inc.

## **APPENDIX**

### **APPENDIX A – EPS INSULATION**

The insulation used in the construction of the sandwich panels came from FMI EPS, LLC and the type that was used was the Type II EPS and the modulus of elasticity is shown as 320-360 psi, which the FEA model used 340 psi.



TYPICAL PHYSICAL PROPERTIES OF EXPANDED POLYSTYRENE								
Specification reference: ASTM C578			Type XI	Type I	Type VIII	Type II	Type IX	
Property	Units	ASTM Test						
Density, Minimum	pcf	D1622	.70	.90	1.15	1.35	1.80	
Density Range	pcf		.70-.89	.90-1.14	1.15-1.34	1.35-1.79	1.80-2.20	
Thermal Conductivity (k Factor)	at 40°F at 75°F	BTU/ hr. (sq.ft.)(F/in.)	C518	0.28 0.30	0.24 0.26	0.23 0.25	0.22 0.24	0.21 0.23
Thermal Resistance (R Value)	at 40°F at 75°F	at 1" thickness		3.6 3.3	4.17 3.85	4.25 3.92	4.55 4.17	4.76 4.35
<b>Strength Properties</b>								
Compressive 10% Deformation	psi	D1621	5-9	10-14	13-18	15-21	25-33	
Flexural	psi	C203	10-18	25-30	32-38	40-50	55-75	
Tensile	psi	D1623	14-18	16-20	17-21	18-22	23-27	
Shear	psi	D732	11-13	18-22	23-25	26-32	33-37	
Shear Modulus	psi	----	190-230	280-320	370-410	460-500	600-640	
Modulus of Elasticity	psi	----	110-150	180-220	250-310	320-360	460-500	
<b>Moisture Resistance</b>								
WVT	perm. in.	E96(Proc A)	1.9-3.9	1.2-3.0	1.1-2.8	0.9-2.5	0.6-1.5	
Absorption (vol.)	%	C272	<4.0	<3.5	<3.0	<3.0	<2.0	
Capillarity	----	----	none	none	none	none	none	
Coefficient of Thermal Expansion	in./in. (F)	D696	0.000035	0.000035	0.000035	0.000035	0.000035	
<b>Maximum Service Temperature</b>								
Long-term	°F	----	167	167	167	167	167	
Intermittent			180	180	180	180	180	
Oxygen Index	%	D2863	24	24	24	24	24	
Dimensional Stability	% Change	D2126 (Proc C & E)	max 2.0	max 2.0	max 2.0	max 2.0	max 2.0	



When you choose EPS Insulation manufactured by FMI-EPS, you're working with a team of friendly professionals, dedicated to providing you with the best service and EPS Insulation possible.

We're here to answer your questions, solve your problems and do everything we can to make sure your project goes together smoothly and ends successfully.

**We're small enough to know you, large enough to serve you.**

Technical Data EPS Insulation meets or exceeds physical and thermal property standards as established in ASTM C 578

Physical Properties	Units	ASTM Test	Type XI	Type I	Type VIII	Type II	Type IX	Type XIV	Type XV
Compressive Resistance at 10% Strain Deformation (2" cube)	Min psi (kPa)	D 1621, C 165	5.0 (35)	10.0 (69)	13.0 (90)	15.0 (104)	25.0 (173)	40.0 (276)	60.0 (414)
Flexural Strength	Min psi (kPa)	C 203	10.0 (69)	25.0 (173)	30.0 (208)	35.0 (240)	60.0 (414)	60.0 (414)	75.0 (517)
Thermal Resistance (R-Value)* 75 ± 2° F (24 ± 1° C) 40 ± 2° F (4.4 ± 1° C)	Min R* for 1" thickness	C 177, C518	3.22 (0.57) 3.43 (0.80)	3.85 (0.67) 4.17 (0.73)	3.92 (0.69) 4.25 (0.75)	4.17 (0.73) 4.55 (0.80)	4.35 (0.77) 4.76 (0.84)	4.35 (0.77) 4.76 (0.84)	4.45 (0.78) 4.85 (0.85)
Thermal Conductivity (K-Value)* 75 ± 2° F (24 ± 1° C) 40 ± 2° F (4.4 ± 1° C)	BTU/(hr)(Sq.Ft.)(F/in.)	C 177, C518	0.310 (1.76) 0.292 (1.67)	0.260 (1.48) 0.240 (1.37)	0.255 (1.46) 0.235 (1.35)	0.240 (1.37) 0.220 (1.26)	0.230 (1.31) 0.210 (1.20)	0.230 (1.31) 0.210 (1.20)	0.225 (1.28) 0.206 (1.18)
Coefficient of Thermal Expansion	in./in./F	D 696	0.000035	0.000035	0.000035	0.000035	0.000035	0.000035	0.000035
Moisture Resistance Water Absorption by total immersion	% by volume Max	C 272	<4.0	<4.0	<3.0	<3.0	<2.0	<2.0	<2.0
Water Vapor Permeability of 1" (25.4 mm) thickness max perm	Max perm/in (ng/PA*s*m²)	E 96	5.0 (287)	5.0 (287)	3.5 (201)	3.5 (201)	2.5 (143)	2.5 (143)	2.5 (143)
Oxygen Index	Min Volume %	D 2863	24.0	24.0	24.0	24.0	24.0	24.0	24.0
Dimensional Stability (Change in dimensions)	Max %	D 2126	2.0	2.0	2.0	2.0	2.0	2.0	2.0
Max. Service Temperature Long Term / Intermittent	F		167 / 180	167 / 180	167 / 180	167 / 180	167 / 180	167 / 180	167 / 180
Density, minimum Density, nominal	Min lb/ft³ (kg/m³) lb/ft³	C 303	0.70 (12) 0.75	0.90 (15) 1.00	1.15 (18) 1.25	1.35 (22) 1.50	1.80 (29) 2.00	2.40 (38) 2.50	2.85 (46) 3.00

\*R means resistance to heat flow. The higher the R-value, the greater the insulating power.

Federal Trade Commission requires using the R-Value publication at 75°F temperature when calculating R-Values of all insulations

Aged R-Values of alternative products should be

compared to determine long-term benefit. Some types of insulation lose their R-Value over time.

FMI-EPS has a flame spread index of 20 and a smoke developed index of 150-300 when tested in accordance with ASTM E84/UL 723 for densities from 0.7 - 3.0 lb/ft³.

#### Insulation Consideration:

- **DO NOT COMPARE** polyisocyanurate conditioned R-Values by RIC-TIMA and PIMA to EPS R-Values as per ASTM C-578.
- Ask for a **20 year 100% R-Value Warranty**.
- EPS Insulation offers the **Best Insulating Value Per Dollar** than any material available today.

#### Features:

- **Low Moisture Absorption:** EPS insulations closed cell structure prevents capillary absorption of water and moisture. As density is increased, moisture resistance decreases, but it is still minimal.
- **Permeability:** EPS has a low permeability, but is not considered a vapor barrier.
- **Inert:** EPS experiences no physical or chemical breakdowns over time. No nutrient value to animals, insects, or organisms. No nutrient value to bacterial growth including mold.
- **No Leachates:** EPS will not contaminate the surrounding environment.
- **Design Flexibility:** EPS can be fabricated into various shapes and sizes as needed.

#### Design Cautions:

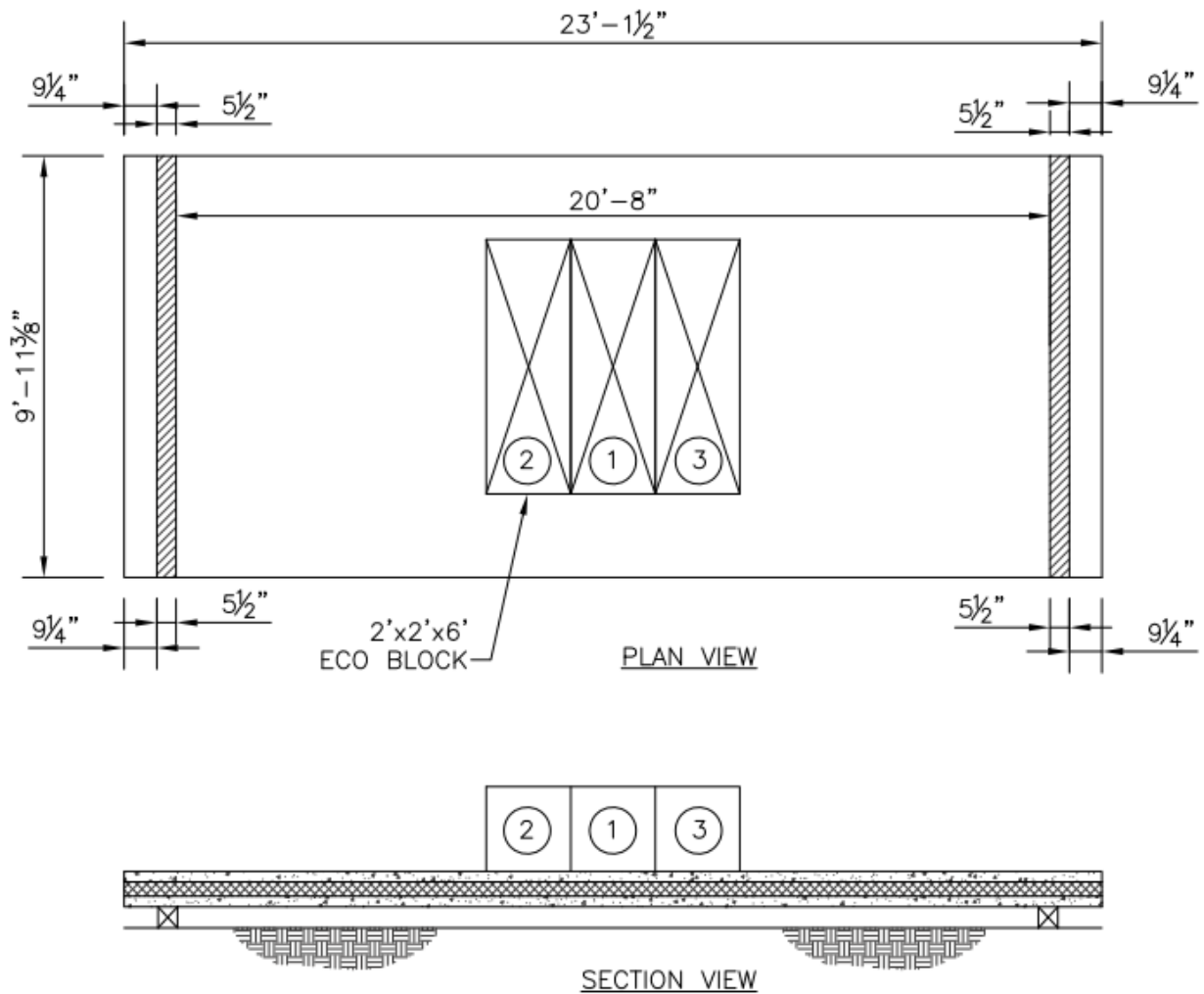
- **Flammability:** EPS is combustible and should not be exposed to flame or other ignition sources. EPS should be covered with a thermal barrier or otherwise installed in accordance with applicable code requirements.
- **Solvent Damage:** EPS is susceptible to damage by petroleum based solvents and their vapors. Protect with vapor barrier covering and or use compatible adhesives when applicable.



The information in this bulletin is presented in good faith, and is believed to be accurate. All statements

## APPENDIX B – ANALYTICAL CALCULATIONS FOR FULL SCALE PANEL

These equations are for the determination of the critical cracking moment and the critical cracking service load for the linear-elastic region of the precast concrete sandwich panel. The panel test set up and boundary conditions are shown below and during the test there were a total of 7 blocks added to the panel, whereas the linear elastic portion is approximately up to block 2-3.



**Deflection Analysis:**

Total Panel Depth:  $h := h_{\text{top}} + h_{\text{insul}} + h_{\text{bot}} \quad h = 10 \text{ in}$

Transformation Ratio:  $n := \frac{E_s}{E_c} \quad n = 5.416$

Distance to Compression Steel:  $d_{\text{prime}} := \frac{h_{\text{top}}}{2} \quad d_{\text{prime}} = 1.5 \cdot \text{in}$

Distance to Tension Steel:  $d := h_{\text{top}} + h_{\text{insul}} + \frac{h_{\text{bot}}}{2} \quad d = 8.5 \cdot \text{in}$

Centroidal Distance:  
(Taken from Top)

$$y_t := \frac{\left[ b_w \cdot h_{\text{top}} \cdot \frac{h_{\text{top}}}{2} + b_w \cdot h_{\text{bot}} \cdot \left( h_{\text{top}} + h_{\text{insul}} + \frac{h_{\text{bot}}}{2} \right) + b_w \cdot A_s \cdot (n-1) \cdot d_{\text{prime}} \dots \right]}{2 \cdot A_s \cdot (n-1) \cdot b_w + 2 \cdot h_{\text{top}} \cdot b_w}$$

$$y_t = 5 \cdot \text{in}$$

Transformed Gross Moment of Inertia:

$$I_{gt} := \frac{b_w \cdot h^3}{12} + b_w \cdot h \cdot \left( \frac{h}{2} - y_t \right)^2 + \left[ (n-1) \cdot A_s \cdot b_w \cdot (d_{\text{prime}} - y_t)^2 \right] \dots$$

$$+ (n-1) \cdot A_s \cdot b_w \cdot (d - y_t)^2$$

$$I_{gt} = 1.007 \times 10^4 \cdot \text{in}^4$$

Cracked Moment of Inertia:

Top Steel:  $A_{stop} := (n - 1) \cdot b_w \cdot A_s$        $A_{stop} = 2.738 \cdot \text{in}^2$

Bottom Steel:  $A_{sbot} := n \cdot b_w \cdot A_s$        $A_{sbot} = 3.358 \cdot \text{in}^2$

$$f(c) := \frac{b_w \cdot c^2}{2} + A_{stop} \cdot (c - d_{prime}) + A_{sbot} \cdot (c - d)$$

guess:  $c := 0.689 \cdot \text{in}$

$c := \text{root}(f(c), c)$        $c = 0.689 \cdot \text{in}$

Moment of Inertia of Cracked Transformed Section:

$$I_{cr} := b_w \cdot c \cdot \left(\frac{c}{2}\right)^2 + \frac{b_w \cdot c^3}{12} + (n - 1) \cdot A_s \cdot b_w \cdot (c - d_{prime})^2 + n \cdot A_s \cdot b_w \cdot (c - d)^2$$

$$I_{cr} = 219.767 \cdot \text{in}^4$$

Modulus of Rupture:  $f_r := 7.5 \cdot \lambda \cdot \sqrt{f_c} \cdot \text{psi}$        $f_r = 662.382 \cdot \text{psi}$

Cracking Moment:  
(ACI Eqn 9-9)  $M_{cr} := \frac{f_r \cdot I_{gt}}{h - y_t}$        $M_{cr} = 111.1 \cdot \text{kip} \cdot \text{ft}$

Service Load Moment:  $M_a := \frac{P_{TL} \cdot l_{span}}{4} + \frac{[w_{TL} + (b_w \cdot h \cdot \gamma_c)] \cdot l_{span}^2}{8}$        $M_a = 111.8 \cdot \text{kip} \cdot \text{ft}$

Effective Moment of Inertia:  $I_e := I_{cr} + (I_{gt} - I_{cr}) \cdot \left(\frac{M_{cr}}{M_a}\right)^3$        $I_e = 9.896 \times 10^3 \cdot \text{in}^4$

Service Load Deflection:  $\Delta_{TL} := \frac{P_{TL} \cdot l_{span}^3}{48 \cdot E_c \cdot I_e} + \frac{5 \cdot [w_{TL} + (b_w \cdot h \cdot \gamma_c)] \cdot l_{span}^4}{384 \cdot E_c \cdot I_e}$        $\Delta_{TL} = 0.146 \cdot \text{in}$

$$\text{check} := \text{if} \left( \Delta_{TL} < \frac{l_{span}}{240}, \text{OK}, \text{NG} \right)$$

check = "OK"      for total load deflection

Total Applied Load:  $P_{TL} = 9 \text{ kips}$

Critical Cracking Load: 
$$P_{cr} := \frac{4}{l_{span}} \cdot \left[ M_{cr} - \frac{[w_{TL} + (b_w \cdot h \cdot \gamma_c)] \cdot l_{span}^2}{8} \right]$$

$$P_{cr} = 8.9 \cdot \text{kips}$$

The cracking moment is calculated to be  **$M_{cr} = 111.1 \text{ kip-ft}$**  and this corresponds to a cracking service load of  **$P_{cr} = 8.9 \text{ kips}$** .

## APPENDIX C – C-GRID© INFORMATION FROM MANUFACTURER

Paul,

Sorry for the slow response. I have been away for a couple of days. Part of the delay in making a response is that there is not a direct answer to your request for properties that is amenable to a direct FE analysis. Design values for C-grid in composite panels have been established through a large number of tests with varying spacing and different types and thickness of rigid insulation. The designs consider the influence that the rigid insulation has in resisting shear in the overall composite behavior. Considering the properties of C-grid alone will not give you results that a producer member of the Altus Group will find when they provide design in response to performance requirements. I have attached a table of the mechanical properties of the carbon strand, and you might find those useful in modeling C-Grid mesh with orthogonal weave and rotation to 45 degrees as shear grid is applied. This is not, however, going to provide an accurate prediction of the total system response.

I have a lot of technical data, but it is difficult to know how to provide specific guidance without knowing more about the details of your problem.

Ned M. Cleland, Ph.D., P.E.

Blue Ridge Design, Inc.

19. W. Cork St., Suite 300

Winchester, VA 22601

540-723-0900

540-664-1405 (cell)

540-723-0901 (fax)



## Index of Carbon Grids

Carbon Fiber Reinforcing Grids for Concrete Structures



**DESCRIPTION** C-GRID® is an intermediate to high strength carbon fiber grid for reinforcing concrete structures.

### FEATURES

Non-corrosive; can be used with as little as 1/4" (6 mm) of cover

Requires less concrete cover leading to lighter structures

Lightweight, easy to handle and use; can be cut to fit using conventional tin snips

High tensile strength and modulus

### APPLICATIONS

Slabs-on-grade and overlays

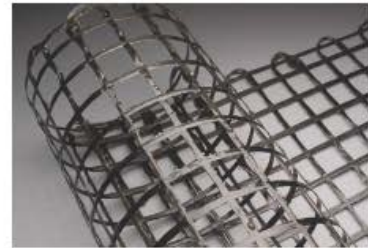
Precast concrete

Concrete repair and shotcrete

Ferrocement

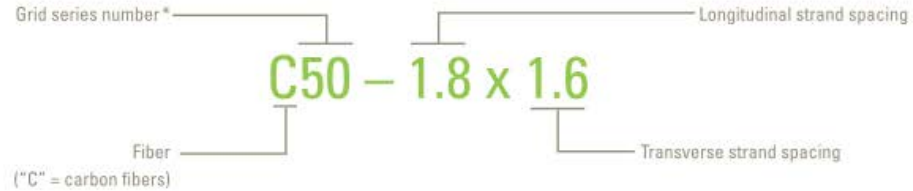
Silos and concrete storage tanks

Decorative concrete



### NOMENCLATURE

C-GRID® nomenclature is unique to carbon fiber grids and should not be confused with the nomenclature for welded wire mesh (WWM). Nomenclature is described below. Additional information may be included in the form of grid "Type" or "Grade" when applicable. Individual data sheets for each product should be consulted for the most up-to-date and comprehensive properties.



\* The grid series number indicates the relative size of the carbon strands for both the longitudinal and transverse directions. For grids with different size carbon strands in each direction, the series number will show both sizes, with the first number representing the relative size of the strands in the longitudinal direction, followed by the transverse direction (e.g. C50/100 – 1.8 x 1.6 grids have carbon strands that are approximately twice as large as in the transverse direction).

### CONSTRUCTION NOTES

- Detailed product data sheets for each product are available online and should be consulted for design purposes.
- For product availability or custom products, contact Chomarat.
- A C-GRID® chemical resistance guide is available upon request.
- C-GRID® products are produced with loops on the transverse strands. Roll width is measured out-to-out of the loops.
- C-GRID® may be spliced by overlapping in concrete. Splice length depends on concrete strength and grid type. For a table of acceptable splice lengths, contact Chomarat North America.
- C-GRID® carbon grids should be handled using gloves and stored in a sheltered area. C-GRID® may be cut using tin snips or other suitable means.



**PHYSICAL & MECHANICAL PROPERTIES**

Composition	carbon fiber and epoxy resin
Color	black
Tensile modulus of elasticity	34,000 ksi (234,500 MPa)
Supply form (custom widths and lengths also available) (Shorter quantities may be available in pre-packaged kits)	47.5" or 95" (1.2 m or 2.4 m) wide rolls with roll lengths up to 500 yds (450 m)

**TYPICAL GRID PROPERTIES (C100 Series Grids)**

GRID DESIGNATION		LONGITUDINAL PROPERTIES		TRANSVERSE PROPERTIES	
English Designation	Metric Designation	Strand Spacing (inch)	Grid Strength (kips/ft) (kN/m)	Strand Spacing (inch)	Grid Strength (kips/ft) (kN/m)
C100 – 3.54 x 3.54	C100 – 90 x 90	3.54	(90) 5.63 (82)	3.54	(90) 5.63 (82)

Note: Actual clear spacing between strands is approximately 0.30" (8 mm) less than the center-to-center spacing.

**TYPICAL GRID PROPERTIES (C50 Series Grids)**

GRID DESIGNATION		LONGITUDINAL PROPERTIES		TRANSVERSE PROPERTIES	
English Designation	Metric Designation	Strand Spacing (inch)	Grid Strength (kips/ft) (kN/m)	Strand Spacing (inch)	Grid Strength (kips/ft) (kN/m)
C50 – 1.8 x 1.6	C50 – 46 x 41	1.8	(46) 6.67 (97)	1.6	(41) 7.50 (109)
C50 – 2.36 x 2.36	C50 – 60 x 60	2.36	(60) 5.08 (74)	2.36	(60) 5.08 (74)
C50 – 2.95 x 2.95	C50 – 75 x 75	2.95	(75) 4.07 (59)	2.95	(75) 4.07 (59)
C50 – 3.54 x 4.0	C50 – 90 x 102	3.54	(90) 3.39 (49)	4.00	(102) 3.00 (44)
C50 – 2.36 x 4.0	C50 – 60 x 102	2.36	(60) 5.08 (74)	4.00	(102) 3.00 (44)
C50 – $\emptyset$ x 2.7	C50 – $\emptyset$ x 69	$\emptyset$	( $\emptyset$ ) $\emptyset$ ( $\emptyset$ )	2.70	(69) 4.44 (65)
C50 – $\emptyset$ x 4.0	C50 – $\emptyset$ x 102	$\emptyset$	( $\emptyset$ ) $\emptyset$ ( $\emptyset$ )	4.00	(102) 3.00 (44)

Note: Actual clear spacing between strands is approximately 0.30" (8 mm) less than the center-to-center spacing.

**TYPICAL GRID PROPERTIES (C25 Series Grids)**

GRID DESIGNATION		LONGITUDINAL PROPERTIES		TRANSVERSE PROPERTIES	
English Designation	Metric Designation	Strand Spacing (inch)	Grid Strength (kips/ft) (kN/m)	Strand Spacing (inch)	Grid Strength (kips/ft) (kN/m)
C25 – $\emptyset$ x 2.3	C25 – $\emptyset$ x 58	$\emptyset$	( $\emptyset$ ) $\emptyset$ ( $\emptyset$ )	2.3	(58) 2.43 (35)

Note: Actual clear spacing between strands is approximately 0.20" (5 mm) less than the center-to-center spacing.

**TYPICAL GRID PROPERTIES (C12 Series Grids)**

GRID DESIGNATION		LONGITUDINAL PROPERTIES		TRANSVERSE PROPERTIES	
English Designation	Metric Designation	Strand Spacing (inch)	Grid Strength (kips/ft) (kN/m)	Strand Spacing (inch)	Grid Strength (kips/ft) (kN/m)
C12 – 1.5 x 1.5	C12 – 38 x 38	1.50	(38) 1.86 (27)	1.50	(38) 1.86 (27)

Note: Actual clear spacing between strands is approximately 0.10" (3 mm) less than the center-to-center spacing.

Application Use Note: C-GRID® remains a relatively novel material without the extensive performance history of traditional construction materials. Reported properties are average values, not design values. Structures and applications using C-GRID® should be designed using appropriate safety factors or load and strength reduction factors. All applications utilizing C-GRID®, including critical life safety and fire rated structures, should be designed and reviewed by a licensed engineer experienced with FRP materials. The data expressed herein is believed to be accurate at the time of publication; however, it is subject to change without notice.

**Notes:**

- Centerline-to-centerline spacing between strands is nominal and based on the average number of strands per unit width. Actual spacing may vary slightly.
- Individual strand cross-sectional area is normalized to the cross-sectional area of the fibers in accordance with ACI 440.2R. The actual measured thickness and width are larger and shall not be used for design purposes.
- The longitudinal direction is in the direction of the roll, and the transverse direction is across the width of the roll. For example, if a roll of C-GRID® is 47.5" wide, the carbon strands in the transverse direction are 47.5" in length. If a roll of C-GRID® is 500 yards long, the longitudinal strands are 500 yards in length.
- Reported tensile strengths are typical values from testing. These values should not be used for design purposes. The individual product data sheets should be consulted for design values that have been statistically adjusted.
- Tensile modulus values are based on properties reported by the carbon fiber supplier. C-GRID® exhibits linear elastic behavior, so failure strains are estimated using Hooke's Law.
- Individual product data sheets should be consulted for a complete list of mechanical and physical properties.

# CHOMARAT

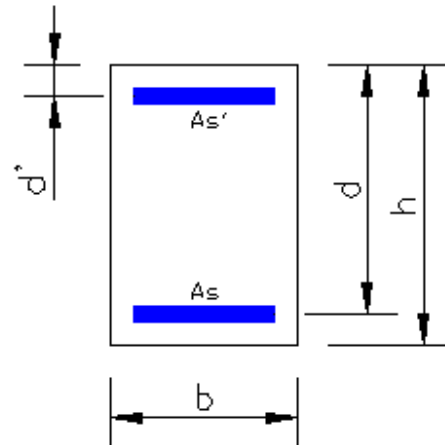
Our world is textile

Chomarar North America  
2901 New Pond Road  
Anderson, SC 29624 - USA

+1 864 328 1700 tel. info@chomarar.com  
+1 864 260 3364 fax. www.chomarar.com

## APPENDIX D – ANALYTICAL CALCULATIONS SOLID 10” CONCRETE PANEL

### Reinforced Concrete Rectangular Beam Design w/ Compression Steel



#### Design Information:

Slab Thickness:	$t_{slab} := 0 \cdot \text{in}$	Span:	$l_{span} := 9 \cdot \text{ft}$
Concrete Compressive Strength:	$f_c := 4120 \cdot \text{psi}$	Modulus of Elasticity:	$E_c := 29000 \cdot \text{ksi}$
Tensile Strength of Reinforcing Steel:	$f_y := 60 \cdot \text{ksi}$	Concrete Strain:	$\epsilon_{cu} := 0.003$
Concrete Unit Weight:	$\gamma_c := 150 \cdot \text{pcf}$	Modulus of Elasticity of Concrete:	$E_c := \left(\frac{\gamma_c}{\text{pcf}}\right)^{1.5} \cdot 33 \cdot \sqrt{f_c \cdot \text{psi}}$
Lightweight Concrete:	$\lambda := 1.0$		

$$\beta_1 := \text{if} \left[ f_c \leq 4000 \cdot \text{psi}, 0.85, \text{if} \left[ f_c > 4000 \cdot \text{psi} \wedge f_c < 8000 \cdot \text{psi}, 0.85 - 0.05 \cdot \frac{(f_c - 4000 \cdot \text{psi})}{1000 \cdot \text{psi}}, 0.65 \right] \right]$$

Top Clearance (To Primary Steel):  $t_{cr} := 0.75 \cdot \text{in}$   $\beta_1 = 0.844$

Bottom Clearance (To Primary Steel):  $b_{cr} := 0.75 \cdot \text{in}$

#### Concrete Reduction Factors:

Bending/Tension:	$\phi_t := 0.9$	Shear:	$\phi_s := 0.75$
Compression:	$\phi_c := 0.65$	Bearing:	$\phi_b := 0.70$

**Factored Loads:**

Service Point Load:	$P_D := 0 \cdot \text{kips}$	Service Uniform Load:	$w_D := 0 \cdot \text{kif}$
	$P_L := 20 \cdot \text{kips}$		$w_L := 0 \cdot \text{kif}$
	$P_{TL} := P_D + P_L$		$w_{TL} := w_D + w_L$
Factored Point Load:	$P_u := 1.2 \cdot P_D + 1.6 \cdot P_L$	Factored Uniform Load:	$w_u := 1.2w_D + 1.6w_L$
Factored Moment:	$M_u := \frac{P_u \cdot l_{span}}{4} + \frac{w_u \cdot l_{span}^2}{8}$		$M_u = 72 \cdot \text{kip} \cdot \text{ft}$
Factored Shear:	$V_u := \frac{P_u}{2} + \frac{w_u \cdot l_{span}}{2}$		$V_u = 16 \cdot \text{kips}$

**Design Tee-Beam for Negative Moment:**

Assumed Tension Strain in Extreme Layer of tension Reinforcement:		$\epsilon_t := 0.0075$
Initial Reinforcement Ratio:	$\rho_i := 0.85 \cdot \left( \frac{0.003}{0.003 + \epsilon_t} \right) \cdot \frac{\beta_1 \cdot f_c}{f_y}$	$\rho_i = 0.014$
Reinforcement Index:	$\omega := \rho_i \cdot \frac{f_y}{f_c}$	$\omega = 0.205$
Flexural Resistance Factor:	$R := \omega \cdot f_c \cdot (1 - 0.59 \cdot \omega)$	$R = 0.742 \cdot \text{ksi}$
Ratio of b to d:	$\alpha := 0.7$	
Distance to Tension Steel:	$d := \sqrt[3]{\left( \frac{M_u}{\alpha \cdot \phi_t \cdot R} \right)}$	$d = 12.27 \cdot \text{in}$
Minimum Depth of Beam:	$h_{min} := \frac{l_{span}}{18.5}$	$h_{min} = 5.838 \cdot \text{in}$
Set Dimensions of Beam:	$h := 10 \cdot \text{in}$	$b_w := 24 \cdot \text{in}$
Factored Moment Adjusted for Dimensions:	$M_u := M_u + 1.2 \cdot \left( \frac{h \cdot b_w \cdot \gamma_c \cdot l_{span}^2}{8} \right)$	
		$M_u = 75.037 \cdot \text{kip} \cdot \text{ft}$

Stress in Compression Reinforcement:  $f_{sprime}(c) := \min(E_s \cdot \epsilon_{sprime}(c), 60 \cdot \text{ksi})$   $f_{sprime}(c) = -31.056 \cdot \text{ksi}$

Force in Compression Reinforcement:  $C_s(c) := A_{sprime} \cdot (f_{sprime}(c) - 0.85 \cdot f_c)$   $C_s(c) = -13.823 \cdot \text{kips}$

Concrete Compression Force:  $C_c(c) := 0.85 \cdot f_c \cdot b_w \cdot \beta_1 \cdot c$   $C_c(c) = 55.543 \cdot \text{kips}$

Tension Reinforcement Force:  $T(c) := A_{sbot} \cdot f_y$   $T(c) = 37.2 \cdot \text{kips}$

Find Exact Value of "c" for Equilibrium:  $f(c) := T(c) - C_c(c) - C_s(c)$

$$c := \text{root}(f(c), c) \quad \boxed{c = 0.749 \cdot \text{in}}$$

Confirm That Tension Steel is Yielding:  $\epsilon_s := \frac{d - c}{c} \cdot \epsilon_{cu}$

$$\text{Check} := \text{if} \left( \epsilon_s > \frac{f_y}{E_s}, \text{yielding}, \text{notyielding} \right) \quad \boxed{\text{Check} = \text{"Tension Steel Is Yielding"}}$$

### **Calculate the Nominal Strength:**

Compression Block:  $a := \beta_1 \cdot c$   $a = 0.632 \cdot \text{in}$

Strain at Tension Fiber:  $\epsilon_t := \frac{d_t - c}{c} \cdot 0.003$   $\epsilon_t = 0.03279$

Strength Reduction:  $\phi_t := \max \left[ 0.65, \text{if} \left[ \epsilon_t \geq 0.005, 0.9, 0.65 + (\epsilon_t - 0.002) \cdot \frac{250}{3} \right] \right]$   $\boxed{\phi_t = 0.9}$

Nominal Moment Strength:

$$\phi M_n := \phi_t \cdot \left[ C_c(c) \cdot \left( d_t - \frac{a}{2} \right) + C_s(c) \cdot (d_t - d_{sprime}) \right] \quad \boxed{\phi M_n = 24.9 \cdot \text{kip} \cdot \text{ft}}$$

Check := if( $\phi M_n > M_u$ , OK, NG) Check = "NG" *for flexural strength*

Minimum Area of Steel:  $A_{s_{min}} := \max\left(\frac{3 \cdot \sqrt{f_c} \cdot \text{psi} \cdot b_w \cdot d}{f_y}, \frac{200 \cdot \text{psi} \cdot b_w \cdot d}{f_y}\right) \quad A_{s_{min}} = 0.715 \cdot \text{in}^2$

Check := if $\left[(A_{s_{bot}} + A_{s_{prime}}) > A_{s_{min}}, \text{OK}, \text{NG}\right]$  Check = "OK" *for minimum steel*

Rho Balanced:  $\rho_b := 0.85 \cdot \left[ \frac{87000 \cdot \beta_1 \cdot f_c}{f_y \cdot \left(87000 + \frac{f_y}{\text{psi}}\right)} \right] \quad \rho_b = 0.0292$

$\rho_w := \frac{A_{s_{bot}}}{d \cdot b_w} = 0.0029$       check := if $\left(\rho_w < 0.75 \cdot \rho_b, \text{OK}, \text{NG}\right)$       check = "OK" *for balanced strain condition*

## **APPENDIX E – FINITE ELEMENT ANALYSIS PROCEDURE**

Provided herein is the step-by-step procedure for creating the finite element model of a precast concrete sandwich panel and performing the dynamic explicit analysis. At the time of the analysis and research, ABAQUS© V6.11-3 was used for the nonlinear numerical solver. Specifically a dynamic explicit solver was used to capture the quasi-static phenomenon of the cracking of the concrete and the load transfer to the reinforcing steel. The procedure is provided herein with pertinent steps and procedures. It is expected anyone using this procedure to be at least knowledgeable and able to use ABAQUS for both pre- and post-processing.

The user should start at the top of the model tree in ABAQUS CAE as shown in Figure 157 and work their way down as each step is completed. The summary of the steps is as follows:

1. Modeling of Parts
2. Materials
3. Creation of Sections
4. Assembly and Set Definitions
5. Steps
6. Interactions
7. Tie Constraints
8. Amplitudes
9. Loading
10. Mesh

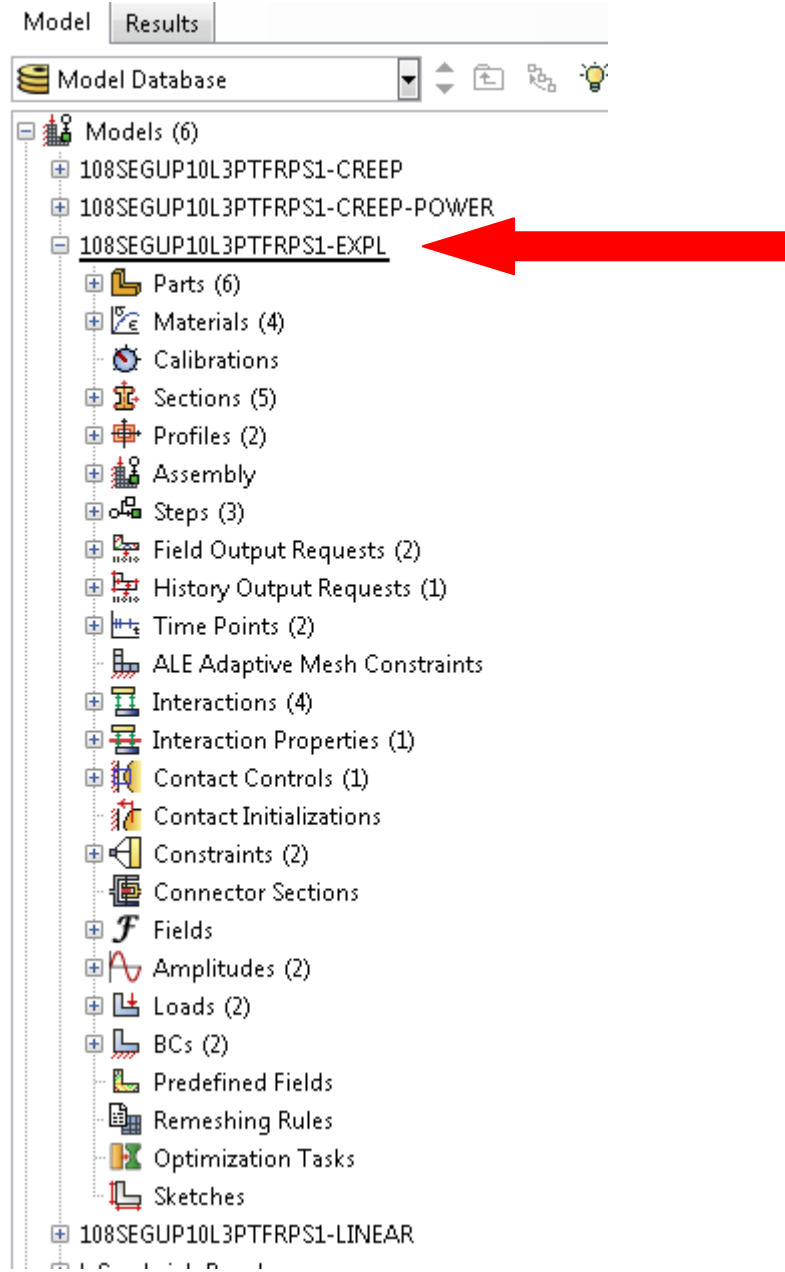
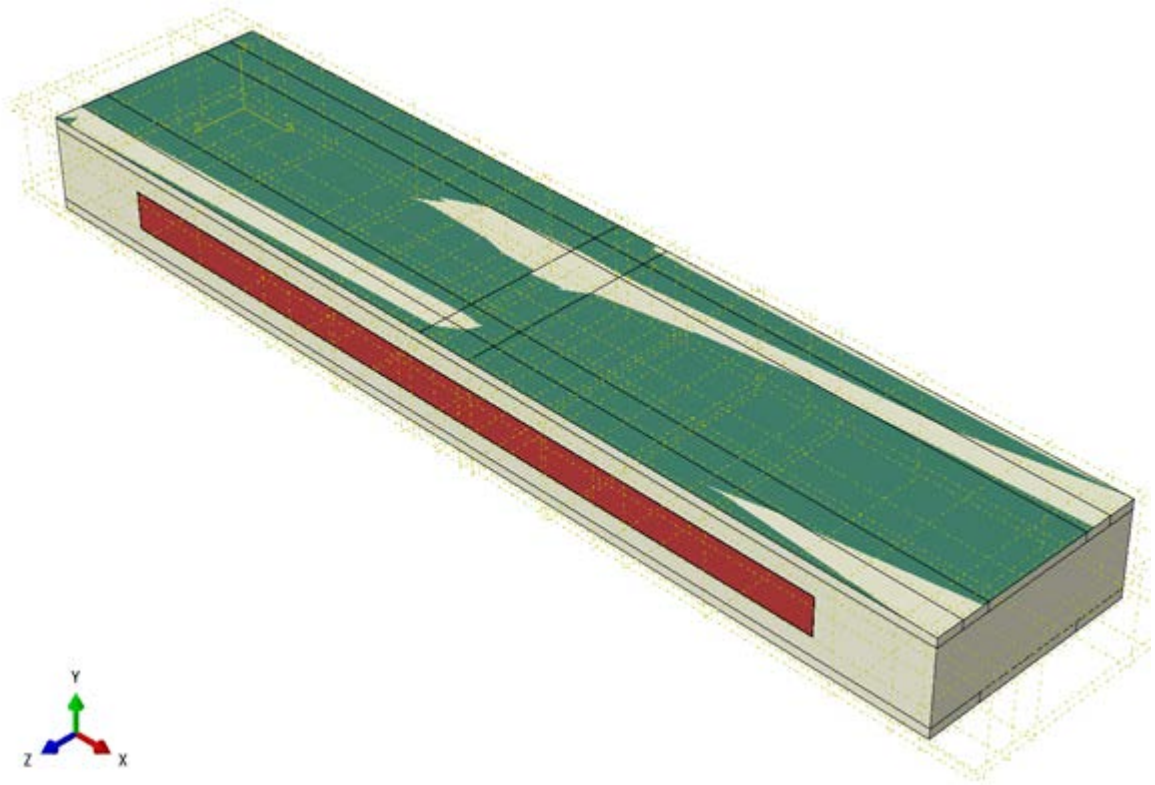


Figure 157 – Abaqus CAE model tree

**STEP 1: Modeling of Parts**

**Figure 158 – Entire assembly modeled in Abaqus**

Each part or component must be created at least one time in the CAE part module or can be imported from another software program such as Solidworks. The parts are then assembled in the assembly as an instance and a single part can be instanced an infinite number of times. The four major parts in the assembly are shown in Figure 159.

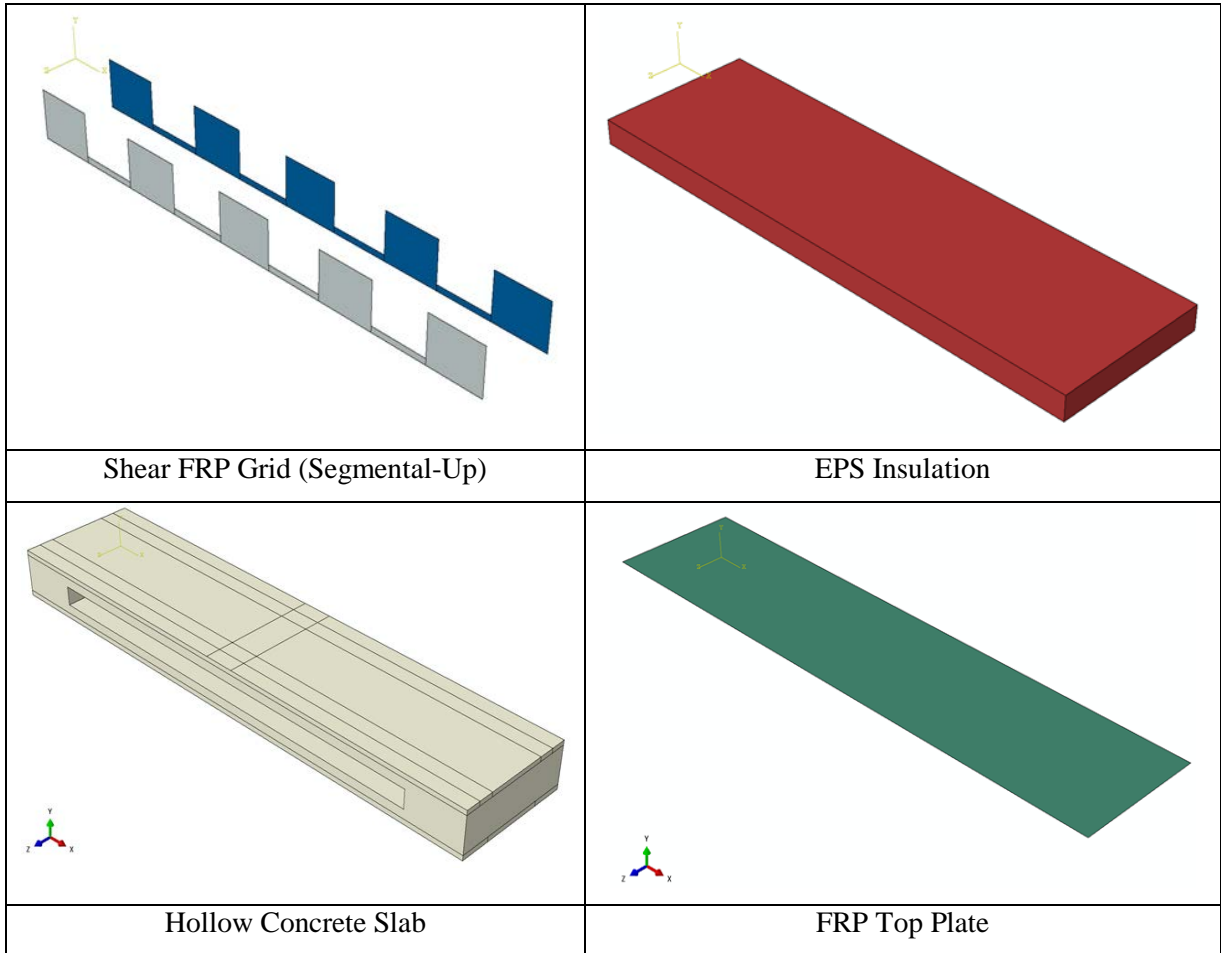
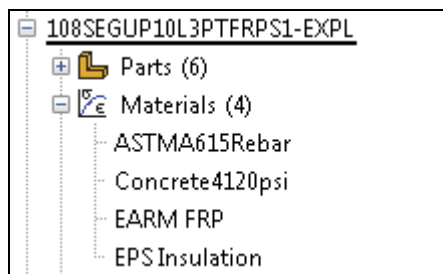


Figure 159 – 108SEGUP10L3PTFRPS1 Parts

## **STEP 2: Materials**

In Abaqus, following the creation of the parts, the materials need to be defined.



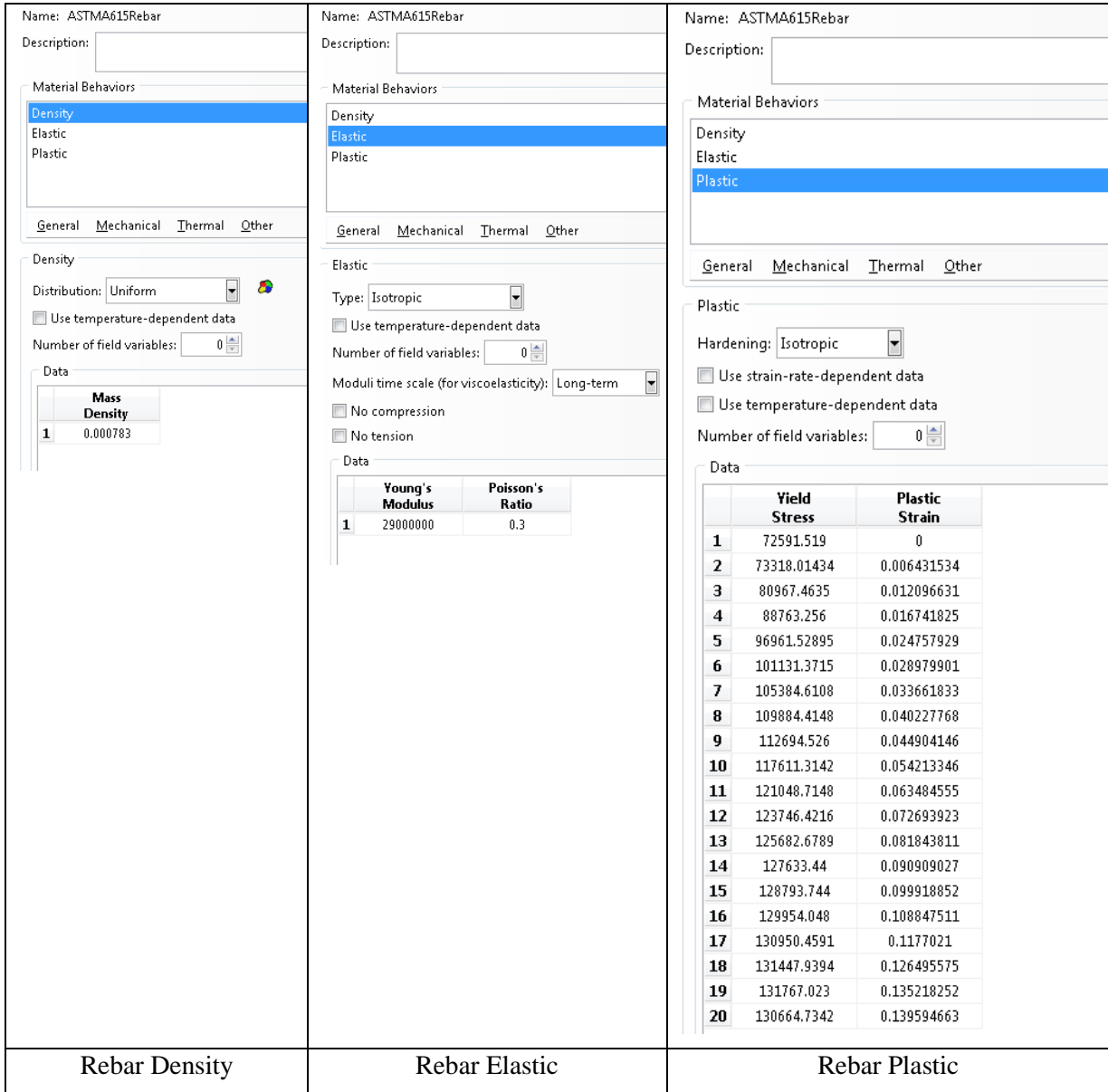


Figure 160 – ASTM A615 reinforcing steel material properties

**Edit Material**

Name: Concrete4120psi

Description:

Material Behaviors

- Density
- Elastic
- Concrete Damaged Plasticity
- Concrete Compression Damage
- Concrete Tension Damage

General Mechanical Thermal Other

Density

Distribution:

Use temperature-dependent data

Number of field variables:

Data

Mass Density	
1	0.000225

**Edit Material**

Name: Concrete4120psi

Description:

Material Behaviors

- Density
- Elastic
- Concrete Damaged Plasticity
- Concrete Compression Damage
- Concrete Tension Damage

General Mechanical Thermal Other

Elastic

Type:

Use temperature-dependent data

Number of field variables:

Moduli time scale (for viscoelasticity):

No compression

No tension

Data

	Young's Modulus	Poisson's Ratio
1	3795277	0.15

Concrete Density

Concrete Elastic

**Figure 161 – Concrete 4,120 psi material properties**

 Edit Material

Name: Concrete4120psi

Description:

Material Behaviors

- Density
- Elastic
- Concrete Damaged Plasticity**
- Concrete Compression Damage
- Concrete Tension Damage

General Mechanical Thermal Other

Concrete Damaged Plasticity

Plasticity  Compressive Behavior  Tensile Behavior

Use temperature-dependent data

Number of field variables:

Data

	Dilation Angle	Eccentricity	fb0/fc0	K	Viscosity Parameter
<b>1</b>	40	0.1	1.16	0.66	0

Figure 162 – Concrete Damaged Plasticity constants

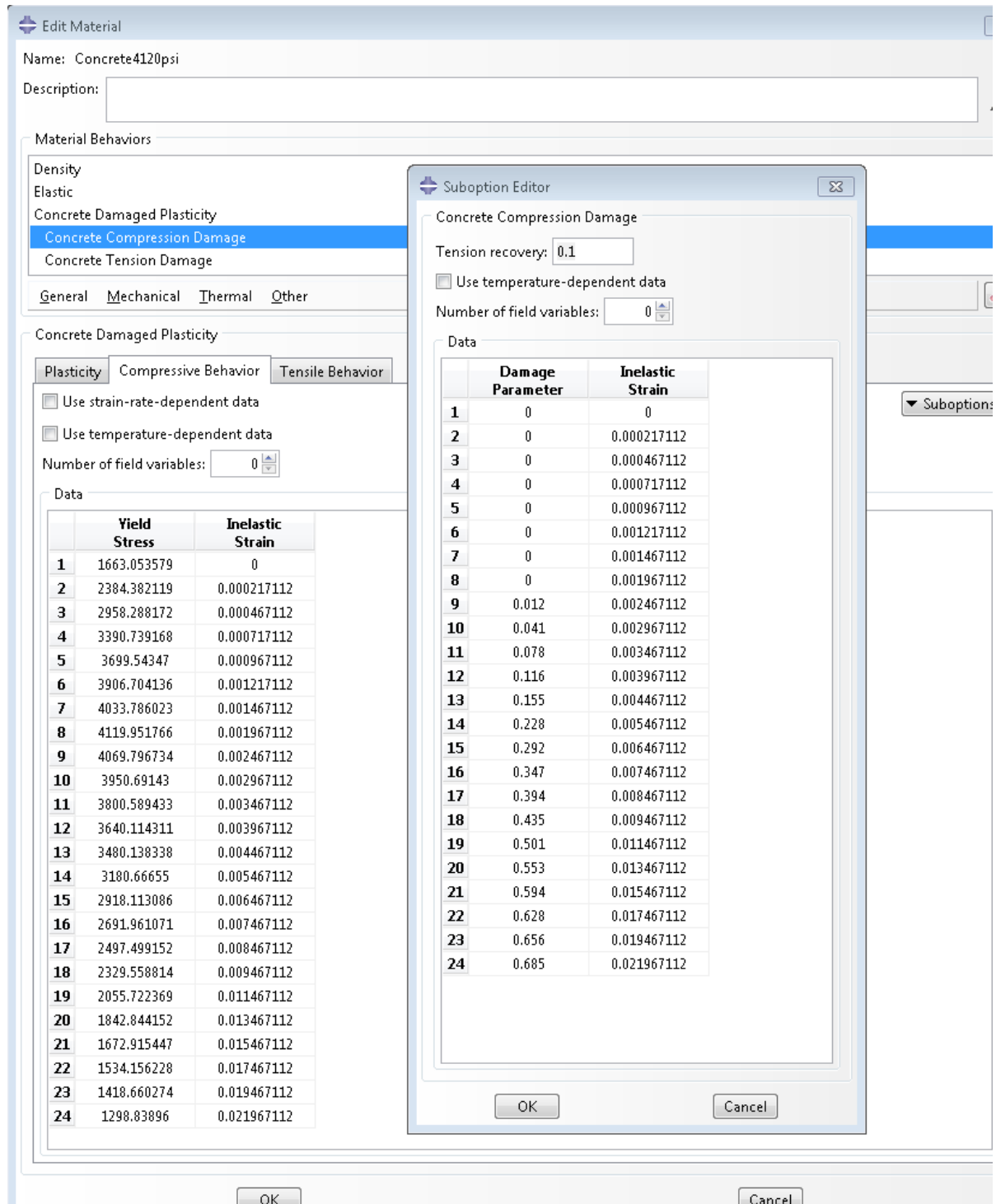


Figure 163 – Concrete compression damage

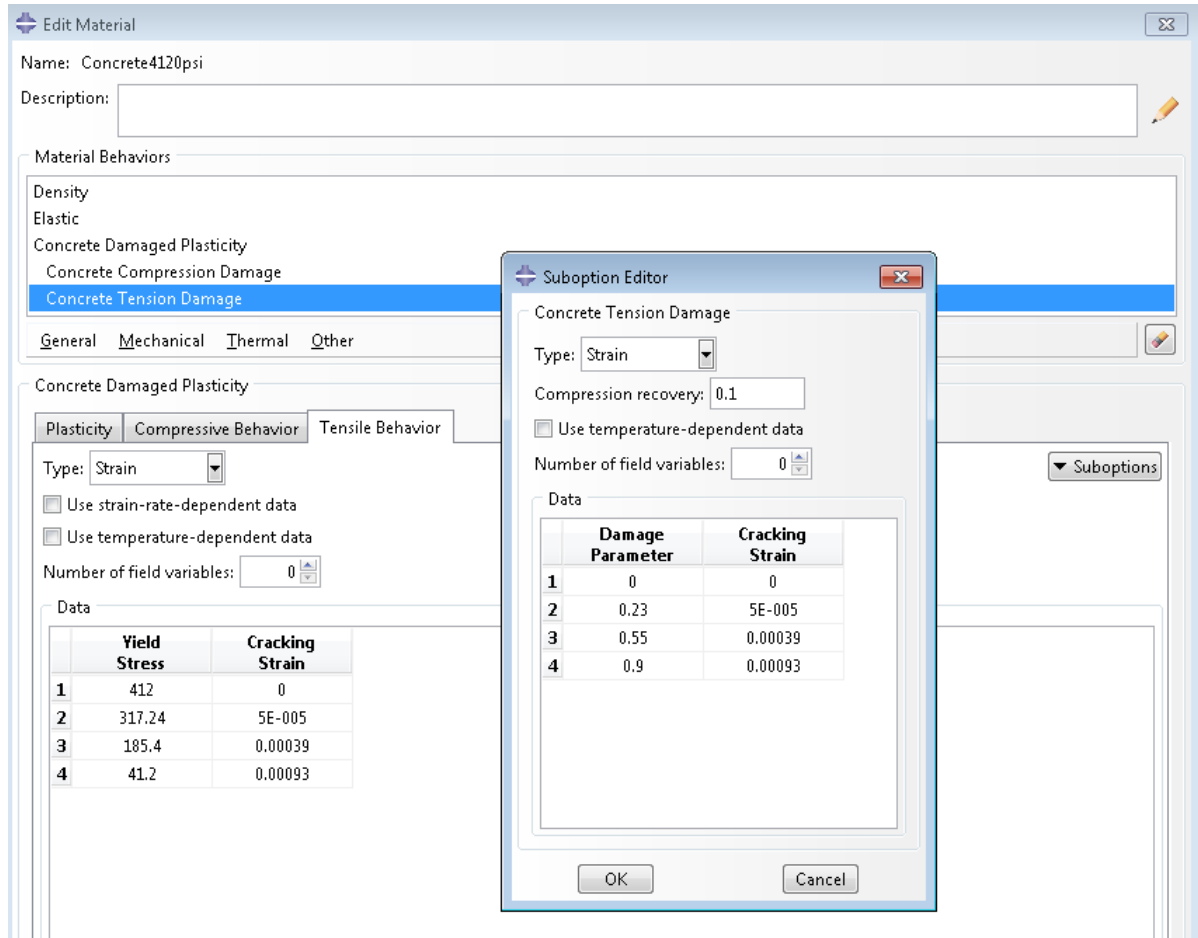


Figure 164 – Concrete tension damage

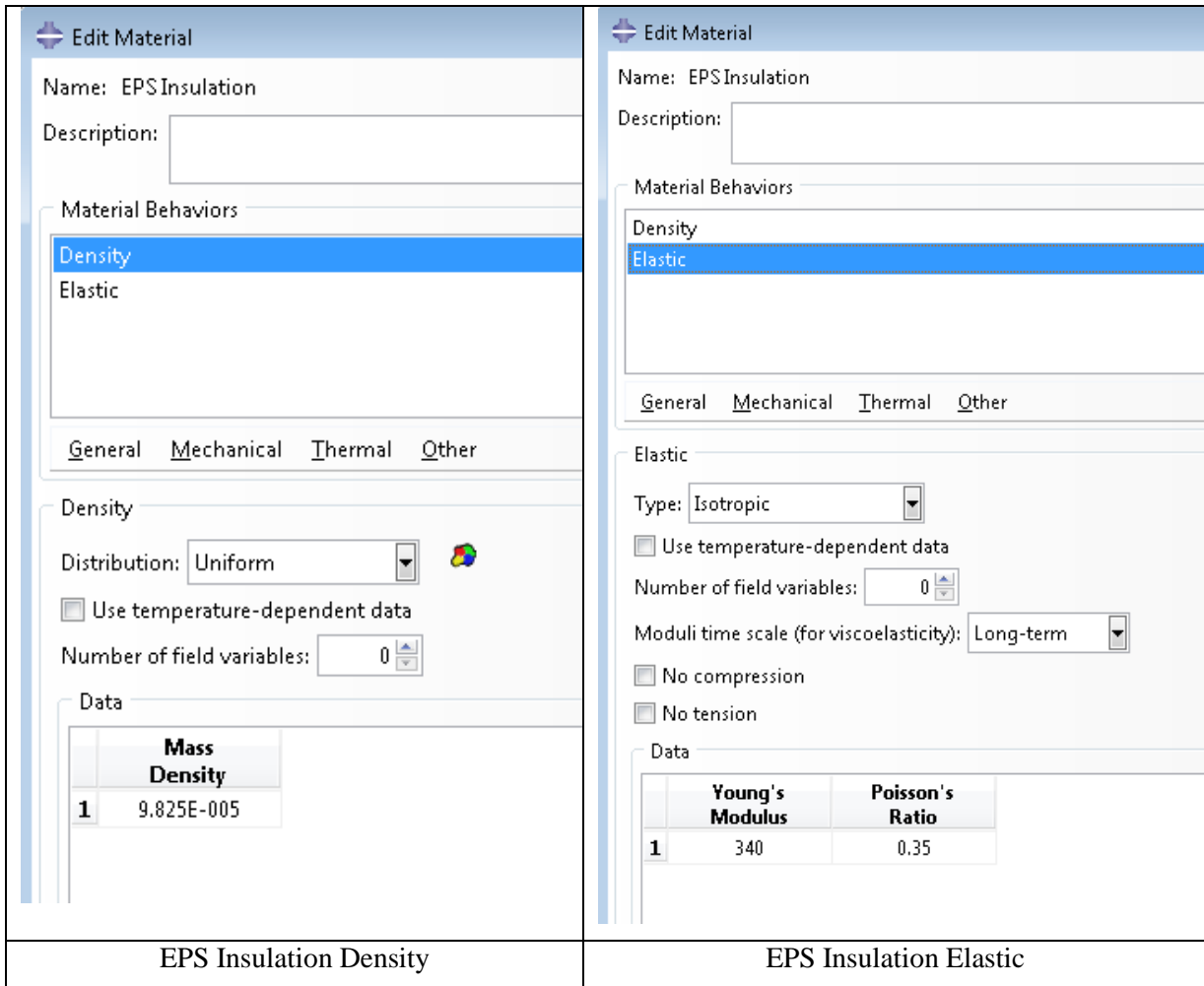
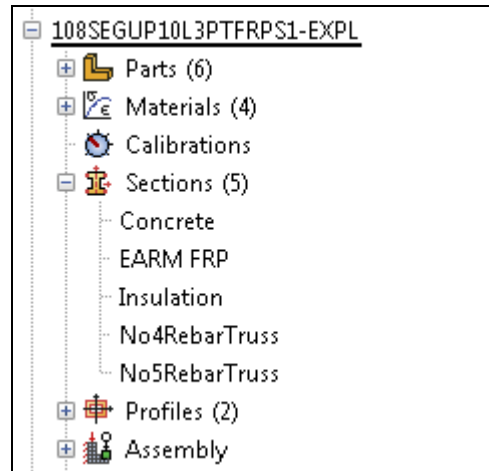


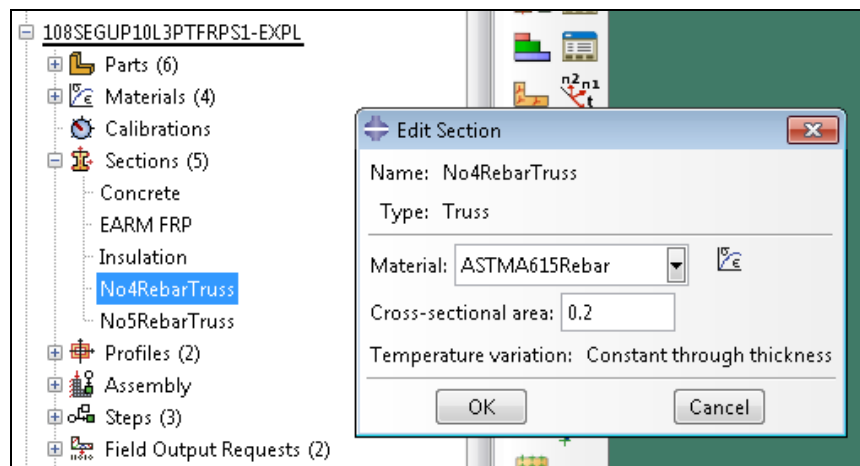
Figure 165 – EPS Insulation material properties

### **STEP 3: Creation of Sections**

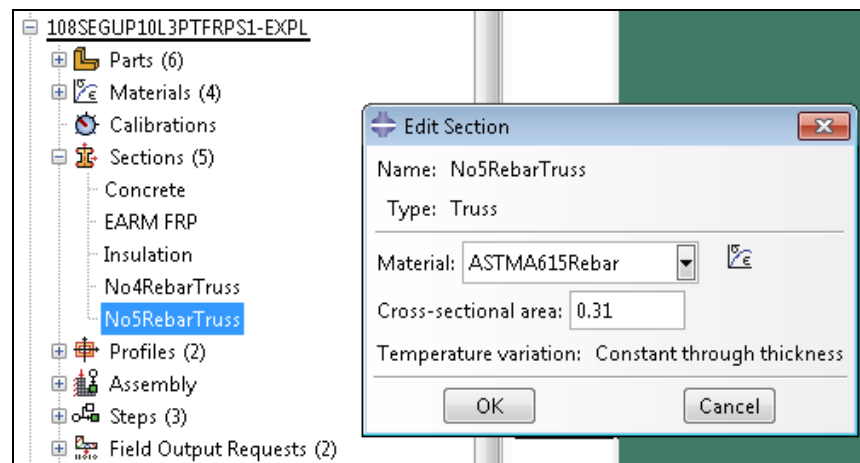
Now that the material properties have been defined and the parts created, sections must be created that align the material property with the appropriate part. The ABAQUS model tree is shown below where the sections tab is defined.



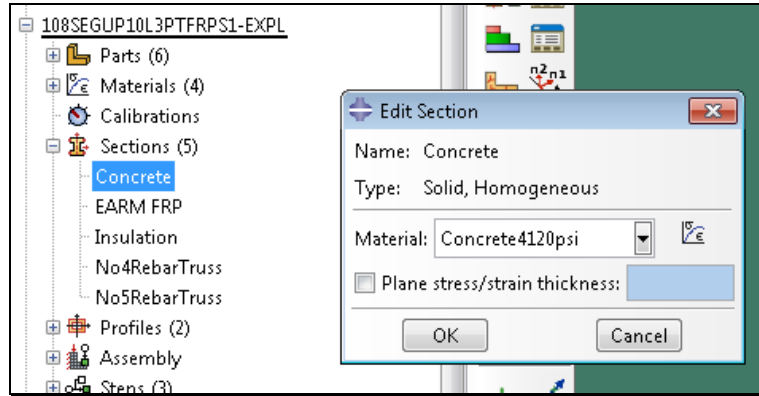
**ABAQUS Model Tree**



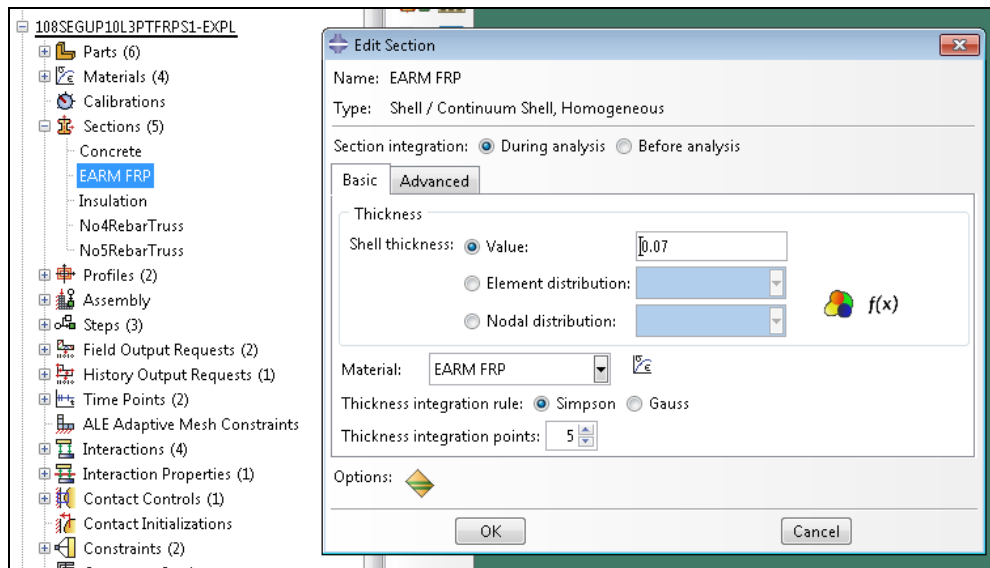
**No. 4 Rebar Truss**



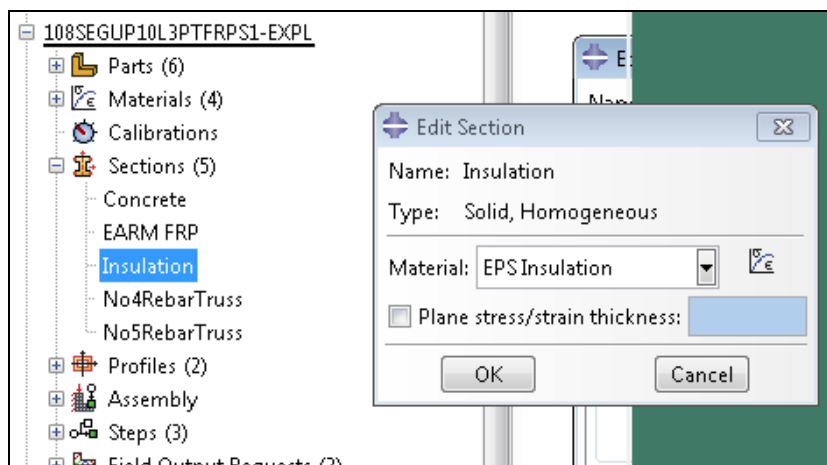
**No. 5 Rebar Truss**



**Concrete Solid**



**FRP Shell**



**EPS Insulation Solid**

The concrete panel must be divided or segmented so that a line exists where the reinforcing steel bars are to be located. Then stringers are assigned to these locations and the sections are associated with those stringers as shown in Figure 166.

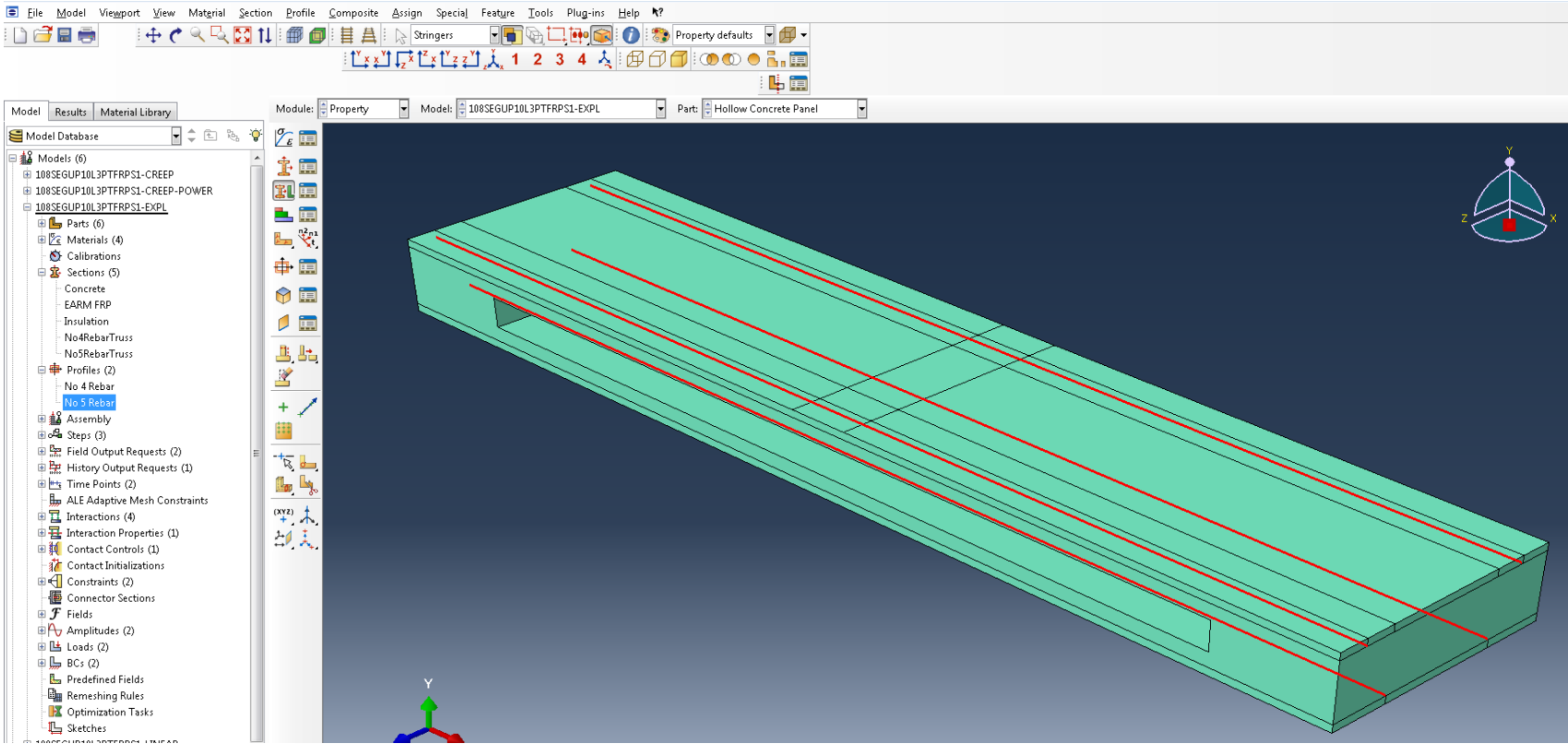
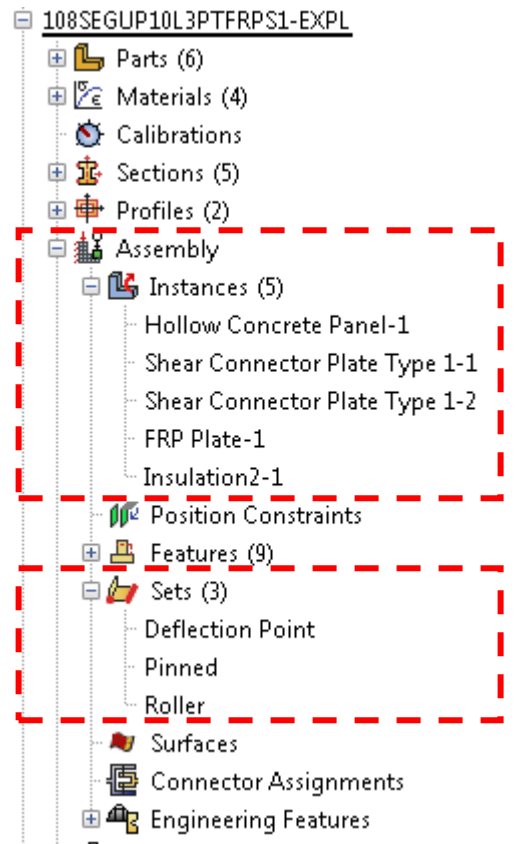


Figure 166 – Rebar sections are assigned as stringers

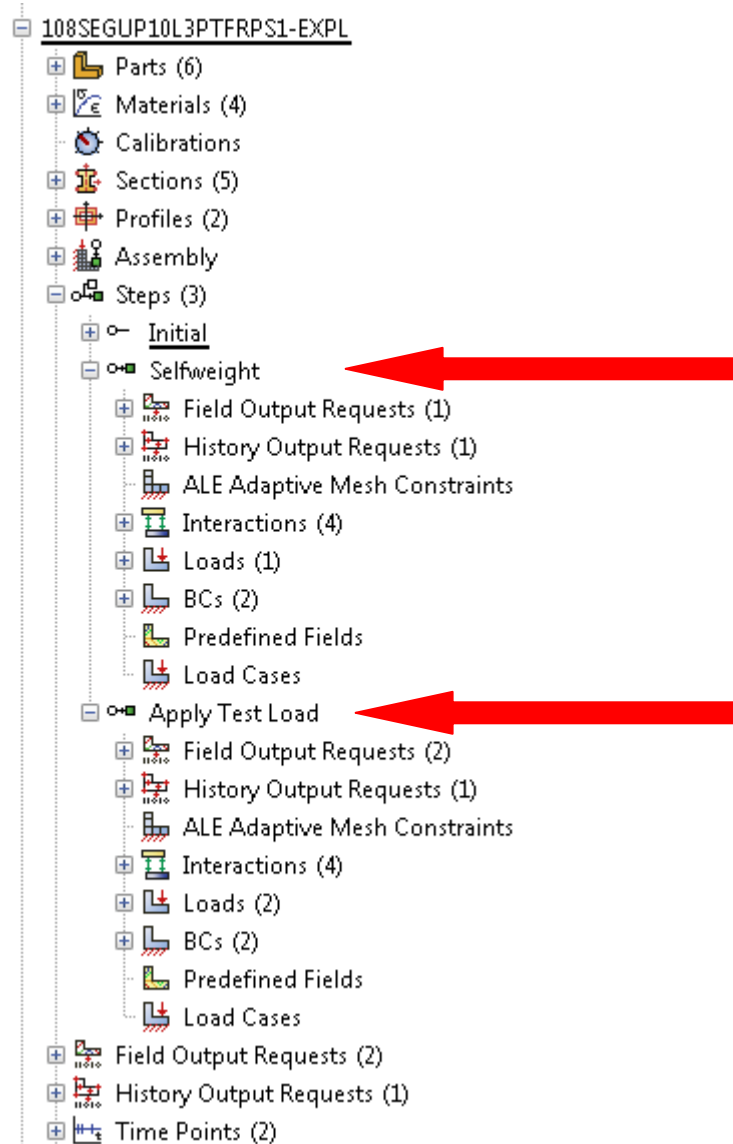
#### **STEP 4: Assembly & Set Definitions**



There are (5) instances in the assembly as shown in the model tree above. They include the insulation, the concrete panel, the FRP top plate and the (2) shear grid connectors. Each instance is positioned as shown in the construction diagram, see Figure 89. There is also a set defined for the pinned reaction/support and the roller reaction/support as well as the mid-span bottom node set for defining the deflection results. These sets are created for post-processing the results.

### **STEP 5: Steps**

ABAQUS uses what's called a "step" to define the type of analysis that will be performed. There is a Static-General, Static-Riks and Explicit analysis among lots others.



There are two steps in this analysis, the selfweight step which allows for the concrete panel to be placed on the supports and includes gravity loading. The second step is the test load. Both are a dynamic, explicit step type.

<p><b>Edit Step</b></p> <p>Name: Selfweight</p> <p>Type: Dynamic, Explicit</p> <p>Basic Incrementation Mass scaling Other</p> <p>Description: Selfweight</p> <p>Time period: 1</p> <p>Nlgeom: On</p> <p><input type="checkbox"/> Include adiabatic heating effects</p>	<p><b>Edit Step</b></p> <p>Name: Apply Test Load</p> <p>Type: Dynamic, Explicit</p> <p>Basic Incrementation Mass scaling Other</p> <p>Description: Apply Test Load</p> <p>Time period: 1</p> <p>Nlgeom: On</p> <p><input type="checkbox"/> Include adiabatic heating effects</p>
<b>Step 1: Selfweight</b>	<b>Step 2: Apply Test Load</b>

**Edit Step**

Name: Apply Test Load

Type: Dynamic, Explicit

Basic Incrementation Mass scaling Other

Type:  Automatic  Fixed

Stable increment estimator:  Global  Element-by-element

Max. time increment:  Unlimited  Value:

Time scaling factor:

**Edit Step**

Name: Apply Test Load

Type: Dynamic, Explicit

Basic Incrementation Mass scaling Other

Use scaled mass and "throughout step" definitions from the previous step

Use scaling definitions below

Data

Region	Type	Frequency/Interval	Factor	Target Time Increment

**Edit Step**

Name: Apply Test Load

Type: Dynamic, Explicit

Basic Incrementation Mass scaling Other

Linear bulk viscosity parameter:

Quadratic bulk viscosity parameter:

**Dynamic Step Load Properties**

**Edit Field Output Request**

Name: F-Output-1  
Step: Selfweight  
Procedure: Dynamic, Explicit

---

Domain: Whole model

Frequency: From time points    Name: Selfweight

Timing: Output at approximate times

Output Variables

Select from list below     Preselected defaults     All     Edit variables

A,CSTRESS,DAMAGEC,DAMAGET,EVF,GRAV,LE,PE,PEEQ,PEEQVAVG,PEVAVG,RF,S,SVAVG,U,V,

- Stresses
- Strains
- Displacement/Velocity/Acceleration
- Forces/Reactions
- Contact
- Energy
- Failure/Fracture
- Thermal
- Porous media/Fluids
- Acoustics
- Volume/Thickness/Coordinates

Output for rebar

Output at shell, beam, and layered section points:

Use defaults     Specify:

Include local coordinate directions when available

Apply filter: Antialiasing

OK    Cancel

### Step 1: Selfweight Fieldoutput Requests

**Edit Field Output Request**

Name: F-Output-2  
 Step: Apply Test Load  
 Procedure: Dynamic, Explicit

---

Domain: Whole model

Frequency: From time points    Name: Test Load

Timing: Output at approximate times

Output Variables

Select from list below     Preselected defaults     All     Edit variables

A,CSTRESS,DAMAGEC,DAMAGET,EVF,GRAV,LE,PE,PEEQ,PEEQVAVG,PEVAVG,RF,S,SVAVG,U,V,

- Stresses
- Strains
- Displacement/Velocity/Acceleration
- Forces/Reactions
- Contact
- Energy
- Failure/Fracture
- Thermal
- Porous media/Fluids
- Acoustics
- Volume/Thickness/Coordinates

Output for rebar:  Include     Only

Output at shell, beam, and layered section points:

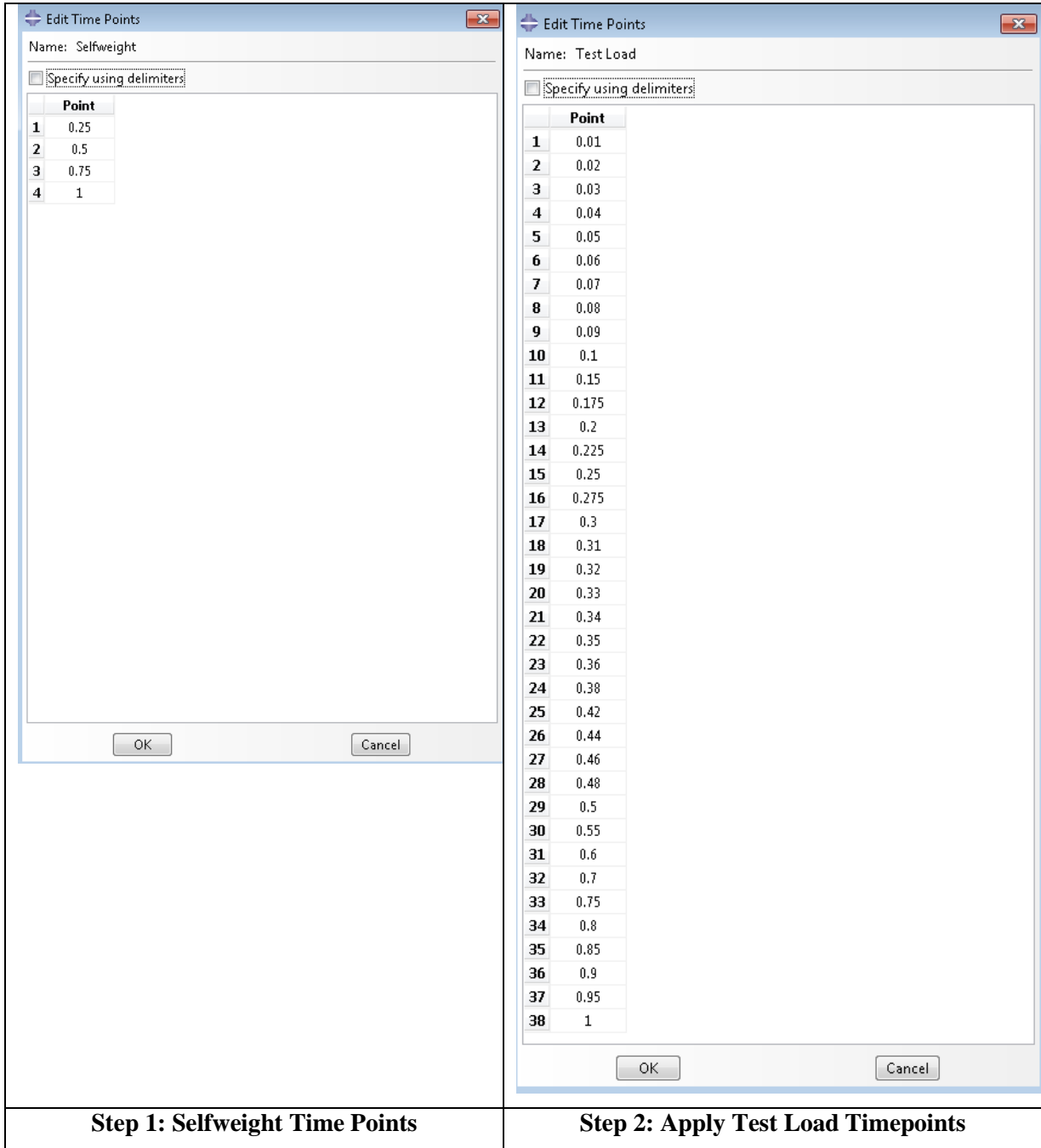
Use defaults     Specify:

Include local coordinate directions when available

Apply filter: Antialiasing

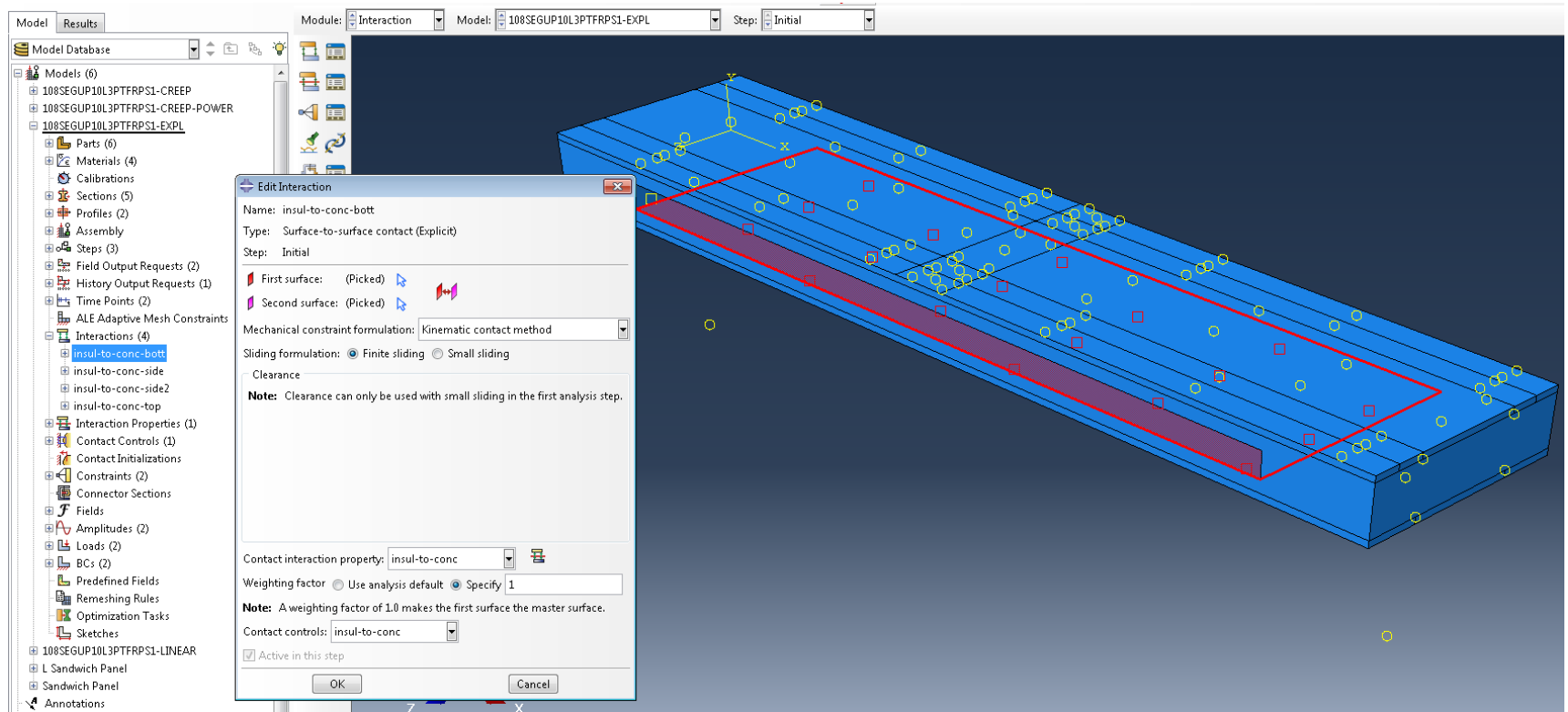
OK    Cancel

### Step 2: Apply Test Load Field Output Requests

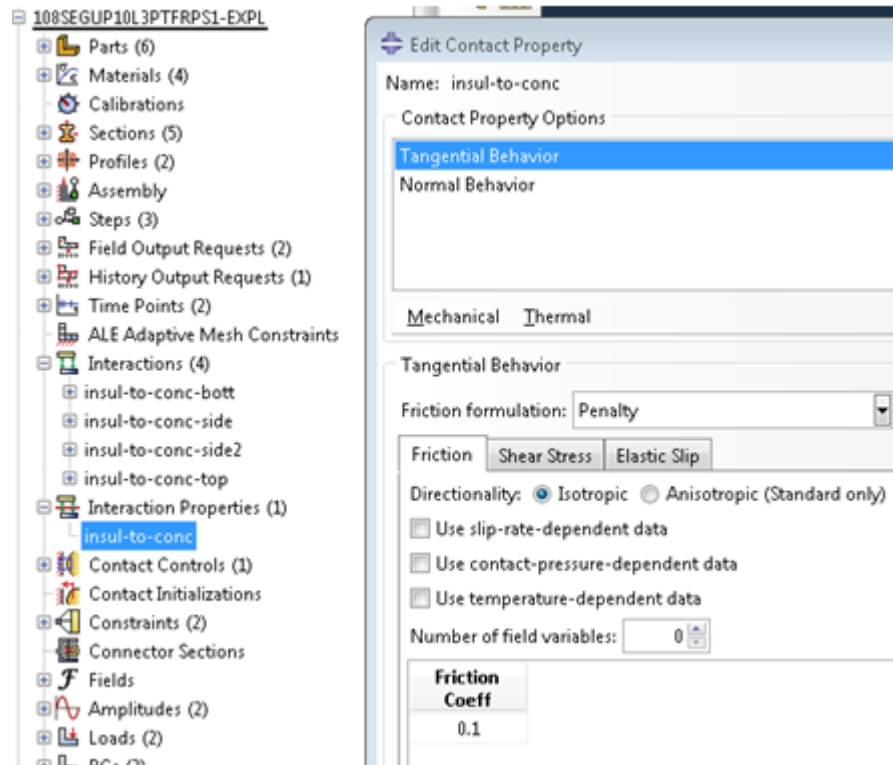


For the Field Output requests ABAQUS allows the user to extract results at certain intervals. It may be only the last interval, no intervals, all intervals or specific time steps. In this case we used specific time steps to extract data from ABAQUS that works well with the anticipated curves we were seeing. Requesting too many points will drive up the size of the files and the run time. Requesting too few data points will provide for choppy curves.

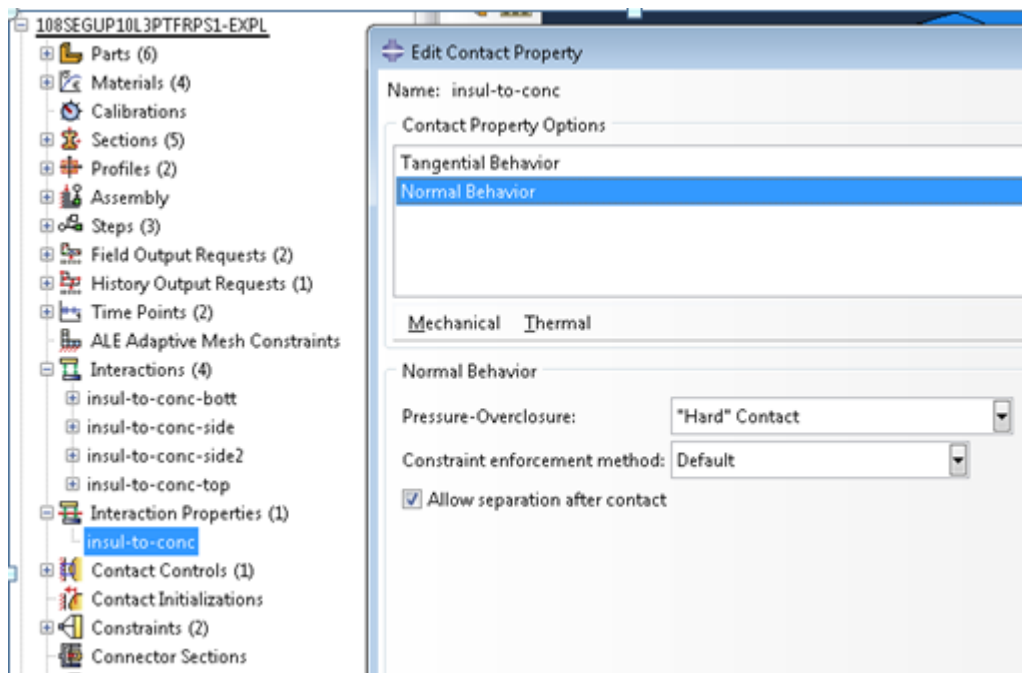
## Step 6: Interactions



In this particular model and test panel there were (4) interactions created. The insulation-to-concrete on the bottom, the top and the two sides. The type of interaction used is the surface-to-surface contact (Explicit) and the Kinematic contact method. Finite sliding was also used as the default. Finite sliding allows the objects in contact to slide pass one another where as the small sliding locks nodes and then the objects slide node for node, which is not accurate.

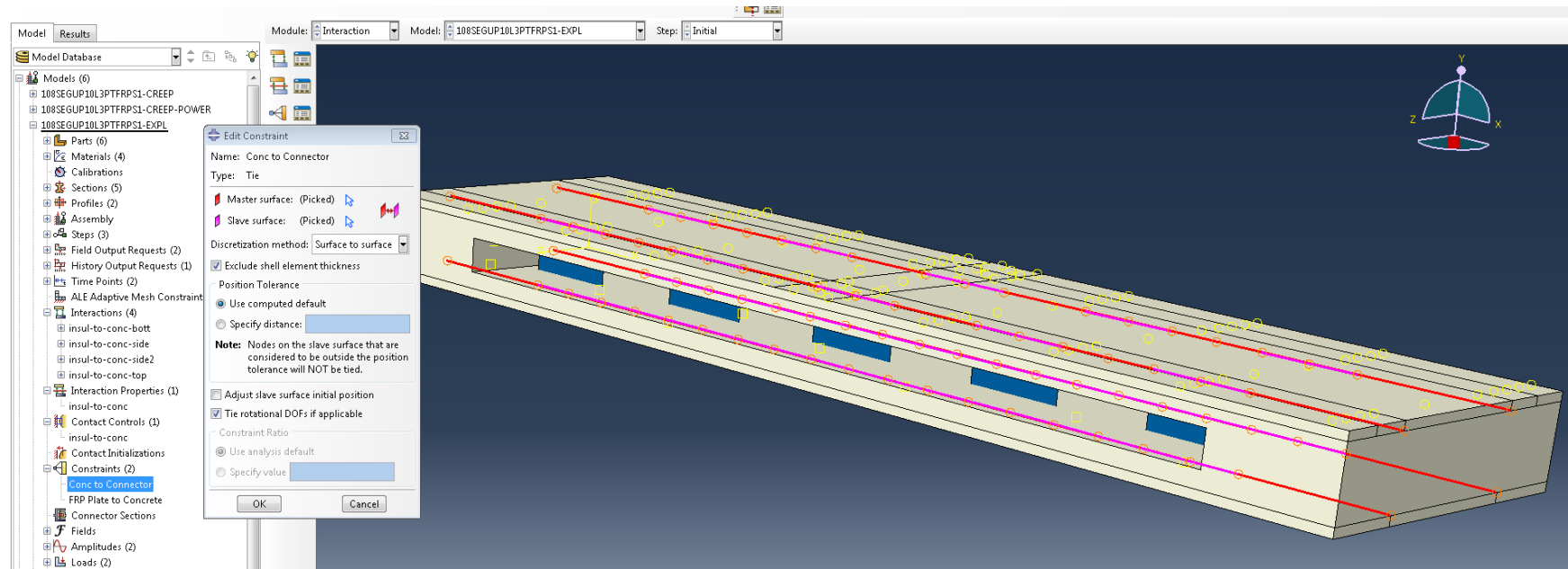


**Insul-to-conc property tangential behavior**

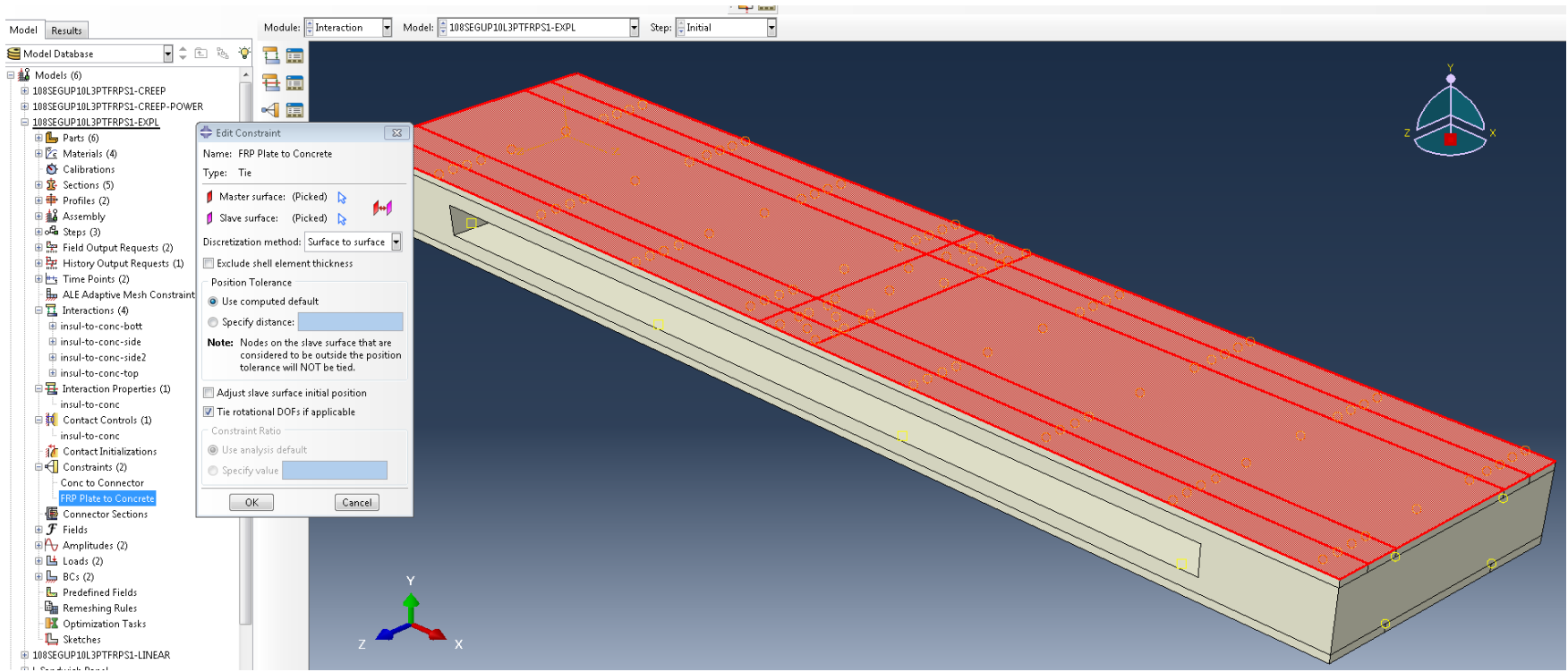


**Insul-to-conc property normal behavior**

## Step 7: Tie Constraints



The shear grid web connectors are tied to the concrete nodes at the locations shown in the figure above. Once again the concrete must be partitioned at these locations so that we have a point to match the components. Furthermore the FRP top plate was also tied to the concrete top surface as shown in the figure below. Neither one of these is entirely accurate as the parts are never completely tied to one another during the full duration of the loading event, however for simplicity this is how they were modeled. Until we have a better understanding of the bond failure properties and strength, we will model it this way.



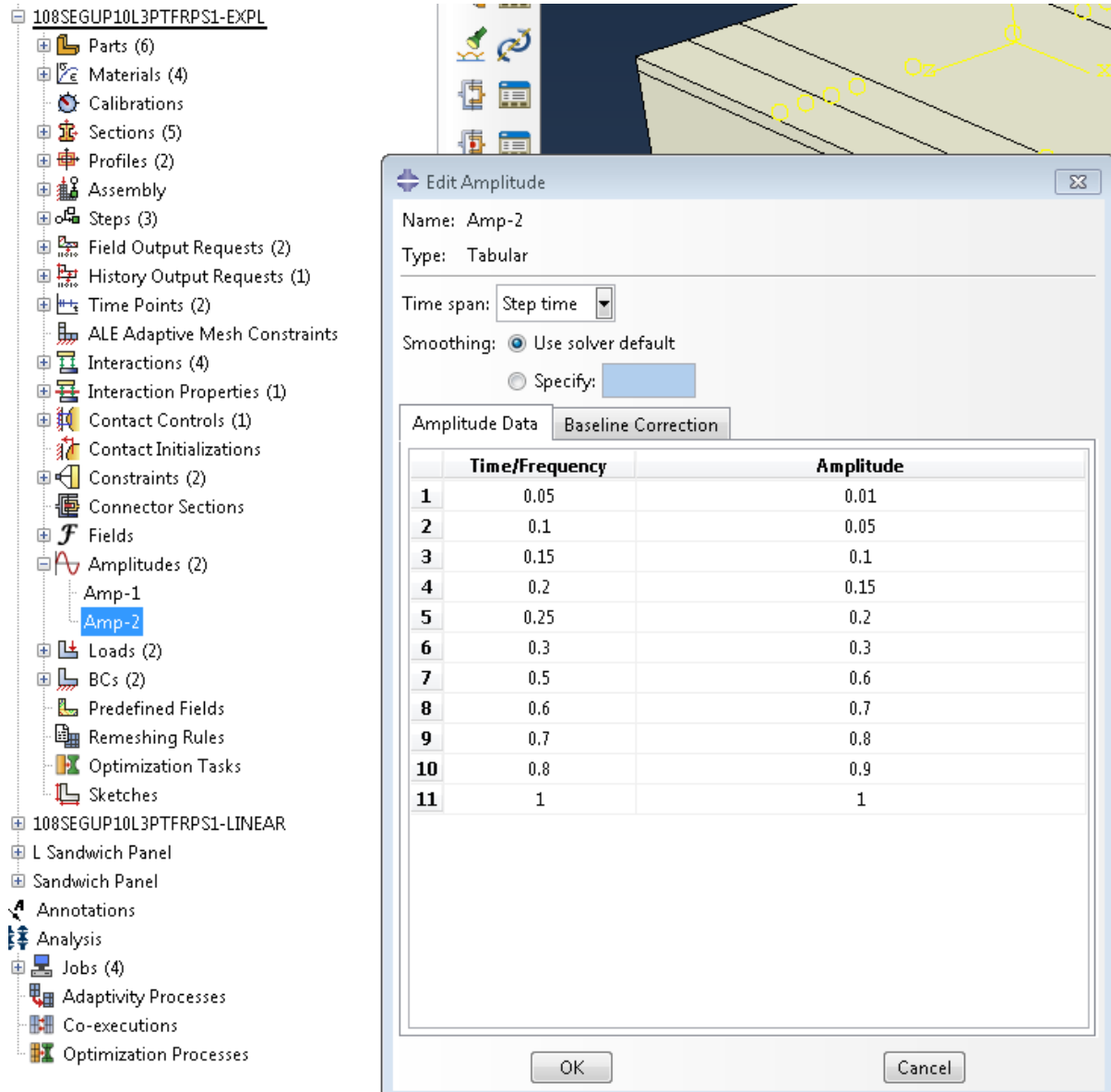
## STEP 8: Amplitudes

The dynamic explicit model needs to have the load controlled in such a way that it turns into a quasistatic or static analysis model. This is accomplished by setting defined amplitude to the loading events in Step 1 and Step 2 loading.

The screenshot shows the 'Edit Amplitude' dialog box for 'Amp-1'. The dialog is open over a 3D model of a mechanical part. The 'Amplitude Data' tab is active, showing a table with two rows: Row 1 (Time/Frequency 0, Amplitude 0) and Row 2 (Time/Frequency 1, Amplitude 1). The 'Time span' is set to 'Step time' and 'Smoothing' is set to 'Use solver default'.

	Time/Frequency	Amplitude
1	0	0
2	1	1

Step 1: Selfweight Loading Amplitude



The screenshot shows a software interface with a tree view on the left and an "Edit Amplitude" dialog box on the right. The tree view lists various models and analysis steps, with "Amp-2" selected under "Amplitudes (2)". The dialog box contains the following settings:

- Name: Amp-2
- Type: Tabular
- Time span: Step time
- Smoothing:  Use solver default
- Specify: [ ]

The "Amplitude Data" table is as follows:

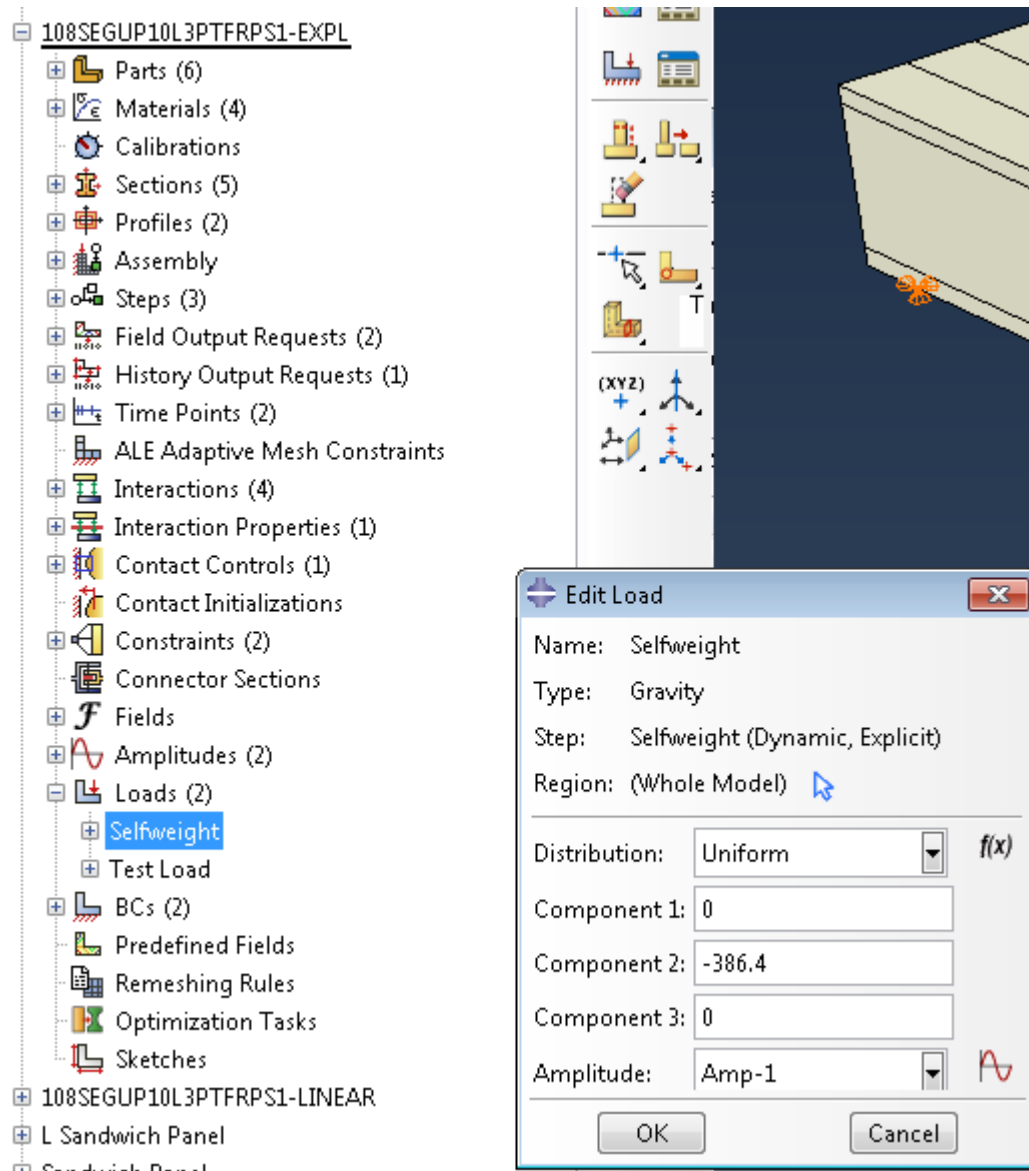
	Time/Frequency	Amplitude
1	0.05	0.01
2	0.1	0.05
3	0.15	0.1
4	0.2	0.15
5	0.25	0.2
6	0.3	0.3
7	0.5	0.6
8	0.6	0.7
9	0.7	0.8
10	0.8	0.9
11	1	1

### Step 2: Apply Test Load Amplitude

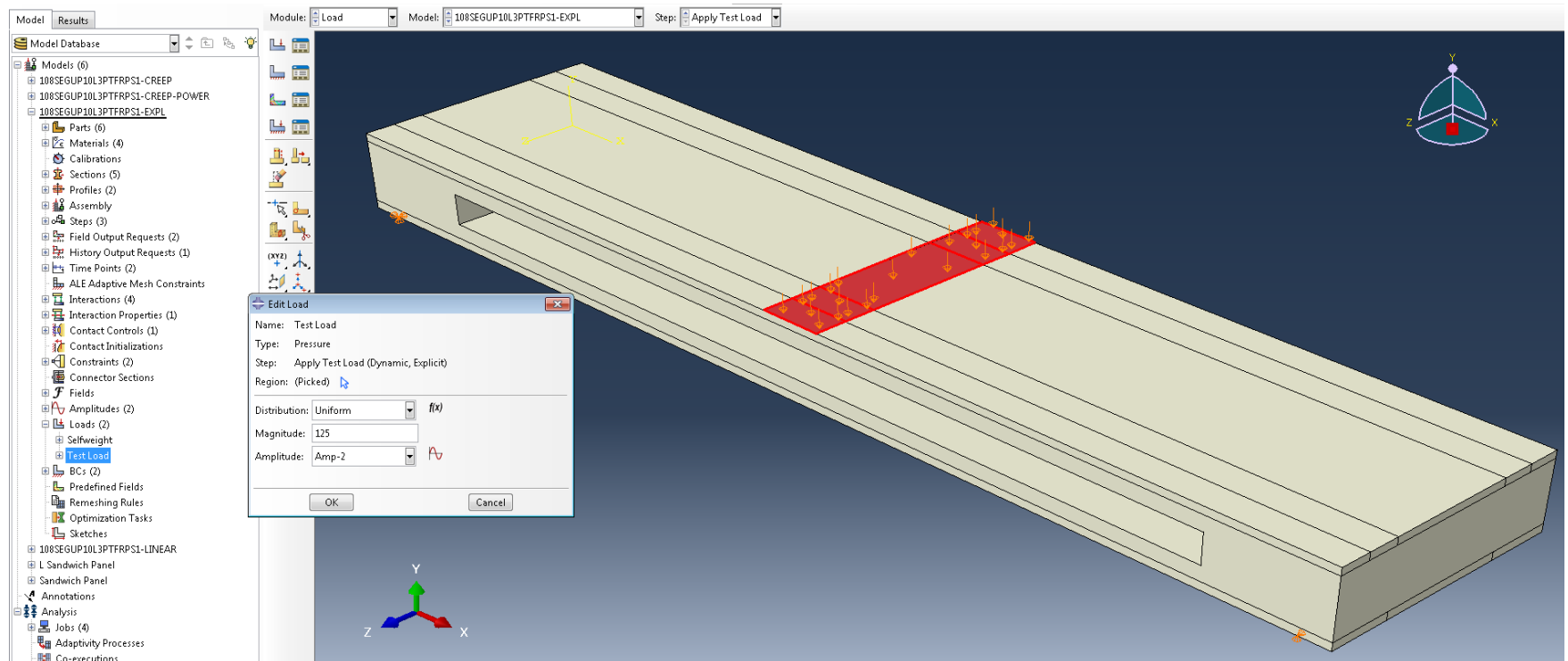
In the case of the applied test load, the amplitude was adjusted to allow for as much of a static load as possible without delaying the problem or influencing the problem too much. If we slow the amplitude down too much it takes a long time to solve and won't fully apply the load. If we put the load on too quickly we have too much dynamic response. Our findings show that the linear solver (Static General or Static RIKS) does well in the elastic range so no need to worry about that part of the amplitude. Then we can focus on the nonlinear range of the response and step up the loading accordingly.

### STEP 9: Loading

There are two types of loading, gravity and the applied test load. ABAQUS is a unit-less solver so the user must take care in assigning the gravity value, and it should be checked.

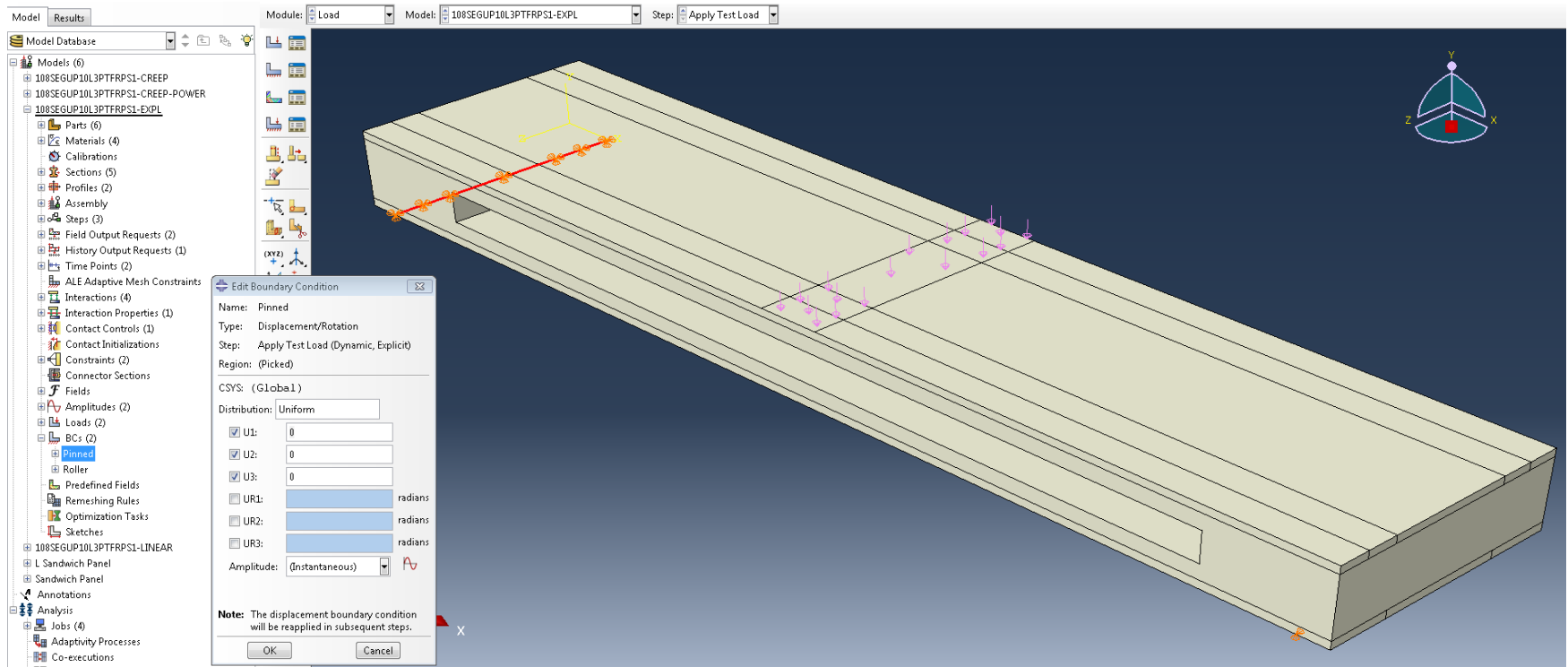


**Selfweight gravity loading**

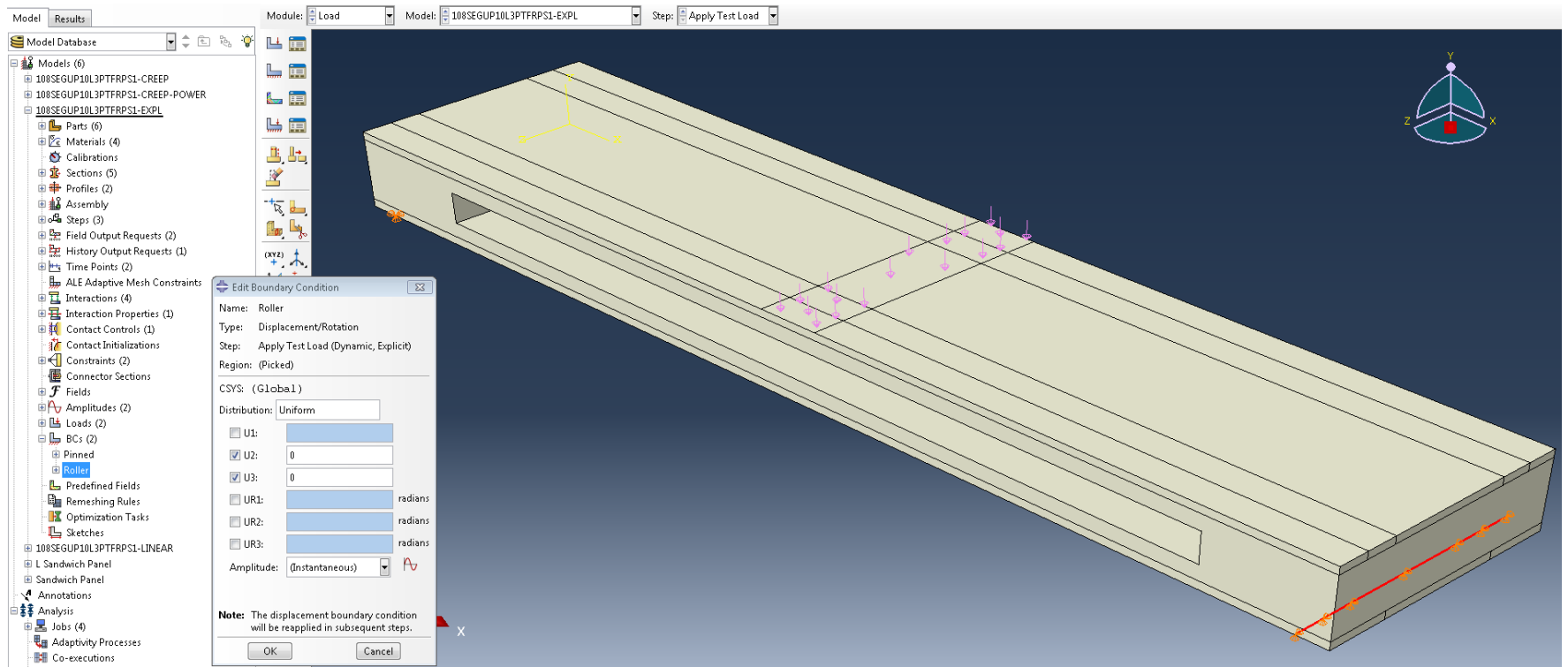


**Test Load applied as a pressure**

The applied test load is assigned as a pressure load over an area that represents the actual applied loading area of the hydraulic cell. This is shown in the figure above. Once again, the user should check that the correct resulting load is applied.

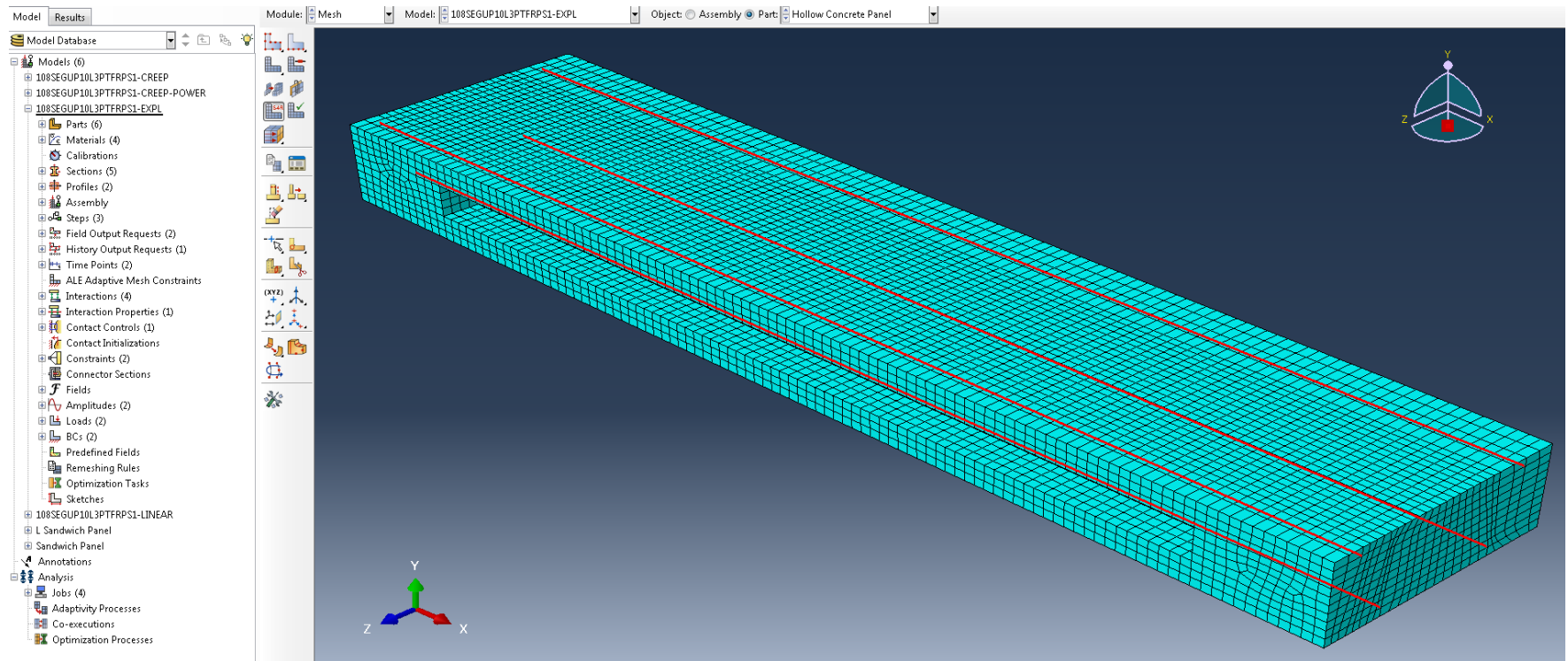


**Pinned Support Boundary Condition**

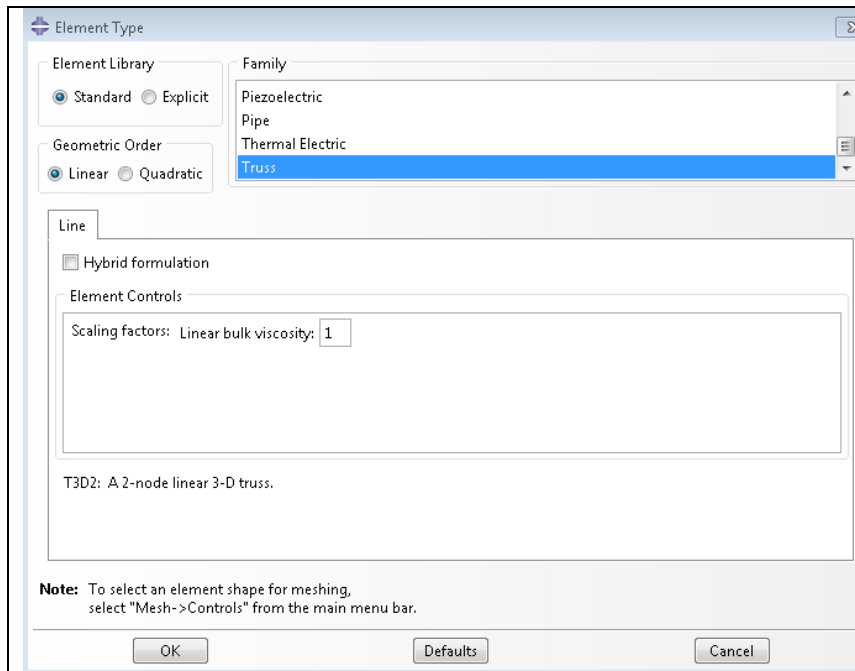


**Roller Support Boundary Condition**

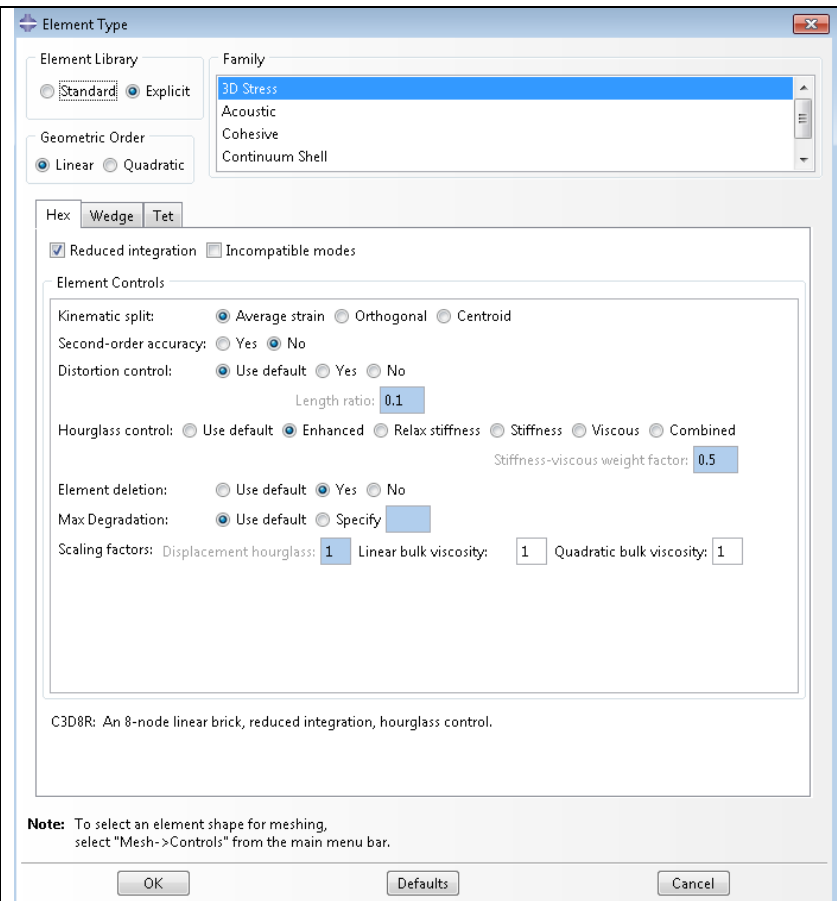
## STEP 10: Mesh



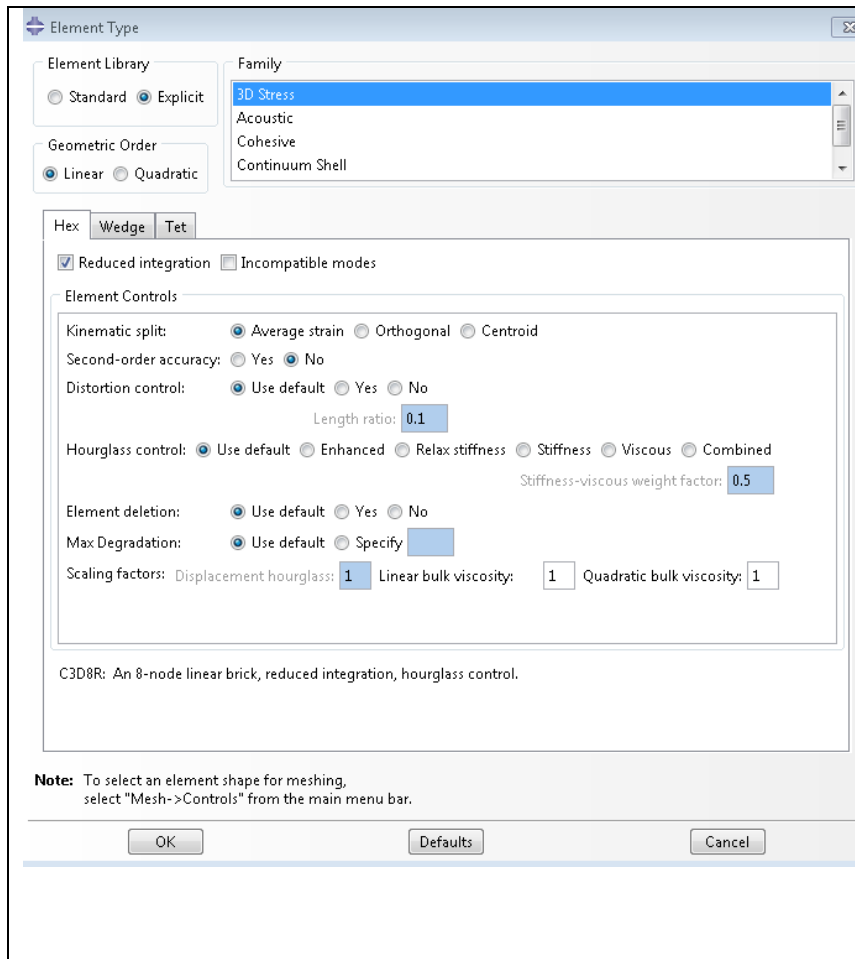
From the resources at the time of this research we were limited to a 1” mesh as the smallest we could implement. The model ran well with 2” or even 3” element mesh to get started. The solid continuum elements used a C3D8R which is a linear brick element with reduced integration techniques and enhanced hourglass control as shown in the figures below. The rebar used truss elements and the FRP shear grid and plates used shell elements.



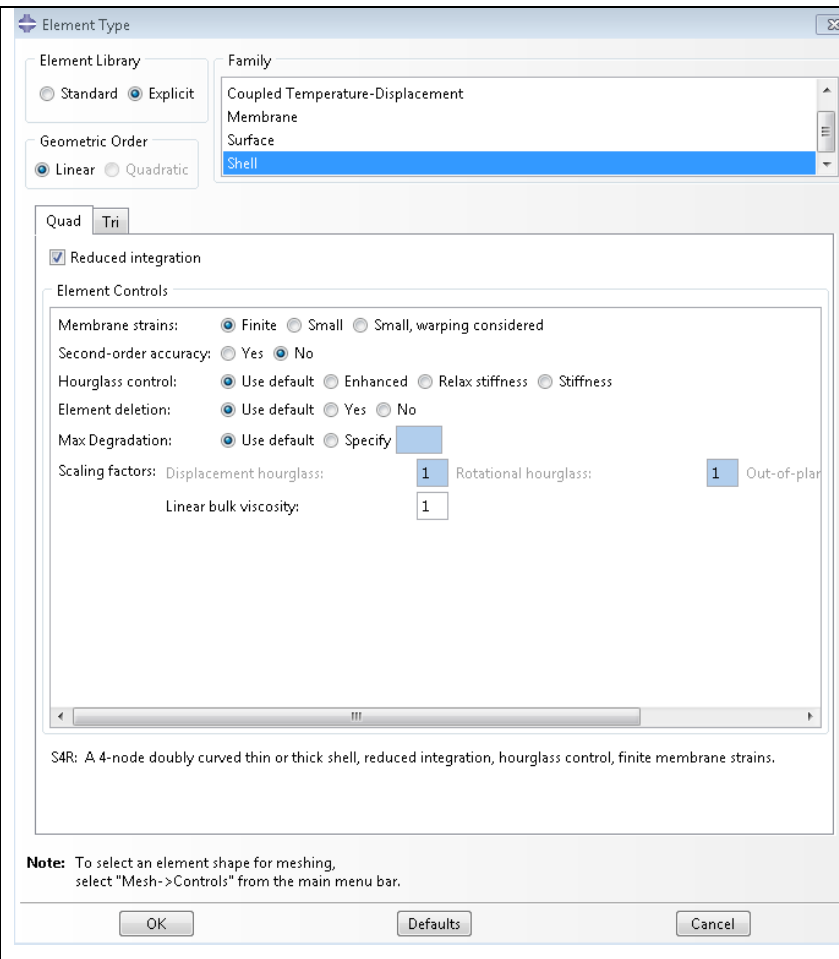
**T3D2 - Rebar**



**C3D8R - Concrete**



**C3D8R - Insulation**



**S4R – FRP Shear Grid and Top Plate**

After all of this has been set up, a job must be created and then executed. The results are post-processed from the \*.odb file and the appropriate values extracted.